THE ASTROPHYSICAL JOURNAL

AN INTERNATIONAL REVIEW OF SPECTROSCOPY AND ASTRONOMICAL PHYSICS

VOLUME 94 NOVEMBER 1941 NUMBER 3

ON THE CLUSTERING TENDENCIES AMONG THE NEBULAE

II. A STUDY OF ENCOUNTERS BETWEEN LABORATORY MODELS OF STELLAR SYSTEMS BY A NEW INTEGRATION PROCEDURE

ERIK HOLMBERG

ABSTRACT

In a previous paper[1] the writer discussed the possibility of explaining the observed clustering effects among extragalactic nebulae as a result of captures. The present investigation deals with the important problem of whether the loss of energy resulting from the tidal disturbances at a close encounter between two nebulae is large enough to effect a capture. The tidal deformations of two models of stellar systems, passing each other at a small distance, are studied by reconstructing, piece by piece, the orbits described by the individual mass elements. The difficulty of integrating the total gravitational force acting upon a certain element at a certain point of time is solved by replacing gravitation by light. The mass elements are represented by light-bulbs, the candle power being proportional to mass, and the total light is measured by a photocell (Fig. 1). The nebulae are assumed to have a flattened shape, and each is represented by 37 light-bulbs. It is found that the tidal deformations cause an increase in the attraction between the two objects, the increase reaching its maximum value when the nebulae are separating, i.e., after the passage. The resulting loss of energy (Fig. 6) is comparatively large and may, in favorable cases, effect a capture. The spiral arms developing during the encounter (Figs. 4) represent an interesting by-product of the investigation. The direction of the arms depends on the direction of rotation of the nebulae with respect to the direction of their space motions.

I. THE EXPERIMENTAL ARRANGEMENTS

The present paper is a study of the tidal disturbances appearing in stellar systems which pass one another at small distances. These tidal disturbances are of some importance since they are accompanied by a loss of energy which may result in a capture between the two objects. In a previous paper[1] the writer discussed the clustering tendencies among extragalactic nebulae. A theory was put forth that the observed clustering effects are the result of captures between individual nebulae. The capture theory seems to be able to account not only for double and multiple nebulae but also for the large extragalactic clusters. The present investigation tries to give an answer to the important question of whether the loss of energy accompanying a close encounter between two nebulae is large enough to effect a capture.

A study of tidal disturbances is greatly facilitated if it can be restricted to only two dimensions, i.e., to nebulae of a flattened shape, the principal planes of which coincide with the plane of their hyperbolic orbits. In order to reconstruct the orbit described by

[1] *Mt. W. Contr.*, No. 633; *Ap. J.*, **92**, 200, 1940.

a certain mass element belonging to one of the two nebulae, we must first derive as a function of the time the x and y components of the total gravitational force acting upon the element. Starting from a certain distribution of mass in the nebulae, we may find the total gravitation by a purely numerical integration. However, such an integration is impracticable on account of the large amount of work involved. In the present case a solution has been found by replacing gravitation by light. Every mass element is represented by a small light-bulb, the light being proportional to the mass, and the total light along the x and y axes is measured by a combination of a photocell and a galvanometer. The measured values represent the components of the gravitational force. The latter components are obtained by adding up the attractions due to individual mass elements, each multiplied by the cosine of the corresponding projection angle. Consequently, the photocell must obey the cosine law as far as the angle of incidence of the light is concerned. If the photocell obeys the cosine law and if the combination of photocell and galvanometer gives a linear relation between light and scale reading, the galvanometer deflection will be proportional to the total gravitational force or, more correctly, to the total acceleration. A detailed account of the instrumental arrangement is given below.

The light-bulbs, which represent the individual mass elements, must fulfil three different requirements. Their candle powers must be the same within certain limits. Furthermore, the candle power must not change when the light-bulb is rotated about its axis of symmetry. The third condition is that the light must not show any appreciable decrease with time. The light-bulbs used in the present case were designed and manufactured by the Luma Factory, Stockholm, Sweden. Figure 1 shows a cross-section of the lamp. The vertical spiral filament is situated at the center of a spherical glass bulb with a rough inner surface. For 100 light-bulbs the difference in candle power is found to be within 10 per cent, whereas the deviations corresponding to rotation about the axis of symmetry average ± 2.1 per cent. Since differences of the first kind can be largely eliminated by using various resistances, the above results are quite satisfactory. The spiral filament was designed for a current of 3.8 volts and 0.3 amperes. The use of a voltage of less than 2 volts insures constancy of the light over a long period.

Each light-bulb is mounted on a steel needle as shown in Figure 1. The plane surface on which the experiments are performed consists of a layer of cardboard covered by a layer of brass plate (thickness, 0.05 mm) and a layer of thin black paper. The brass plate is connected to one pole of the battery, the other pole being connected with a single, isolated wire leading to each light-bulb. In this way the number of wires connected with each lamp is reduced from two to one, which greatly facilitates the shifting of the lamps during the measurements. The black paper, which was especially made for this investigation, is covered by a co-ordinate system of faint gray lines. The reflection coefficient is small and will be further discussed below.

The photocell that is used for the measurements is shown in half-size in Figure 1. The cell is of the special type called "Sperrschichtphotometer." The incident light penetrates a thin layer of *Cu* and is then absorbed in a thick layer of Cu_2O mounted on a *Cu*-plate.[2] The latter plate forms the positive pole of the element, while the negative pole is represented by the thin *Cu*-layer. It was pointed out above that the photocell must obey the cosine law with regard to the angle of incidence of the light. In Figure 2 the full curve gives the measured values, while the dotted line represents the theoretical cosine law. The agreement is quite satisfactory for the present purpose.

The galvanometer was manufactured by the Leeds and Northrup Company of Philadelphia. The instrument is of the light-pointer type and has a sensitivity of about 0.025 microampere per millimeter scale division. The moving coil has a resistance of 1000 ohms. During the measurements the galvanometer is connected with the photocell through a variable resistance of 10,000 ohms. Figure 2 shows the relation between light-

[2] Cf. R. Sewig, *Objective Photometrie*, p. 28, 1935.

intensity and galvanometer deflection. The two lines correspond, respectively, to the limiting cases of 0 and 10,000 ohms of additional resistance. The deviations from straight-line relations are insignificant.

Before proceeding further we will call attention to some disturbing reflection and obscuration effects that affect the measurements. Light from each lamp is reflected by the black-paper surface and by other lamps. On the other hand, part of the light may be cut off from the photocell by other lamps. The proportion of light reflected by the black-paper surface is found by experiment to be approximately independent of the distance between light-bulb and photocell and to amount to about 5 per cent. The constancy of the reflection effect is nicely demonstrated by the relations between light-intensity and galvanometer deflection that are given in Figure 2. The different light-intensities are obtained by placing the same light-bulb at different distances from the photocell, the distance ranging from 30 to 120 cm. Although the reflections are included in the corresponding light-intensities, the deviations from a straight-line relation are very small.

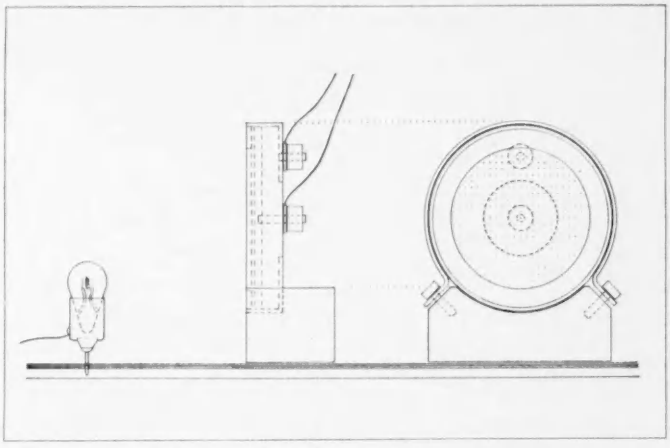

FIG. 1.—Cross-section of light-bulb and photocell (half-size)

Similarly, the reflections by the other lamps will not cause any appreciable disturbance. The diameter of a light-bulb is 8 mm, a small value compared with the distances between the different lamps, which range from 10 to 20 cm. The obscuration effect is largely eliminated by mounting the photocell as shown in Figure 1. The center of the sensitive surface is raised 2 cm above the lamp centers. The maximum obscuration should amount to only a few per cent.

A schematic picture of the arrangement of light bulbs, batteries, and other accessories is given in Figure 3. The lamps are arranged in two groups, *A* and *B*, each containing 37 lamps and having a diameter of 80 cm. Each group represents a nebula. By using three or more different voltages it is possible to reproduce, within certain limits, any desired distribution of mass. In order to obtain more complicated distributions it may be necessary to use a larger number of lamps. In the present case, however, the simplest possible assumption of the internal mass distribution is made. For practical reasons the number of light-bulbs should be kept as small as possible. The battery is composed of thirty 2-volt accumulators, connected in parallel. For a total of 74 lamps, arranged in parallel, the discharge amounts to about 12 amperes. In order to stabilize the voltage, the battery is continuously recharged by about 6 amperes from the municipal-power network of 120 volts. Since the candle power of a light-bulb is approximately proportional to the third power of the voltage, it is important to keep the voltage as constant as possible. In

order to calibrate the photocell and to check minor variations of the voltage, a control device consisting of 5 additional light-bulbs was constructed. To make sure of the same temperature and the same external conditions, the control device is kept in the room where the measurements are made. A possible decrease of light with time is neutralized by always having the control lamps burning simultaneously with the other 74 lamps. Checks are frequently made by placing the photocell in a special mounting at a fixed distance from the 5 control lamps. Minor deviations in the control reading of the galvanometer are neutralized by changing the variable resistance connecting the photocell and galvanometer.

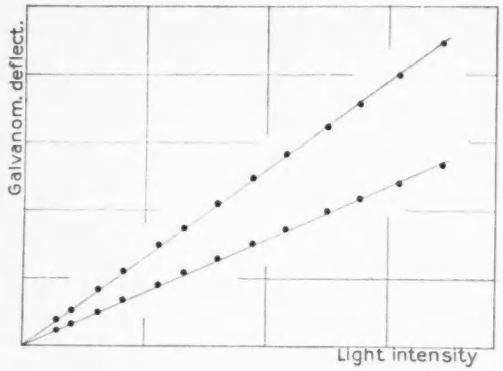

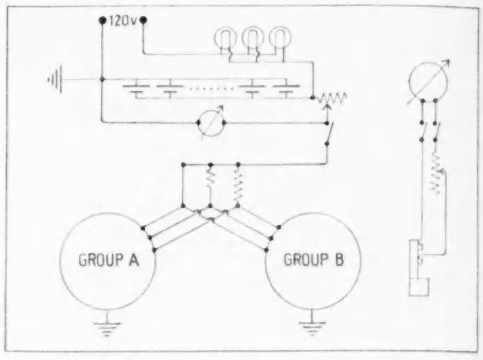

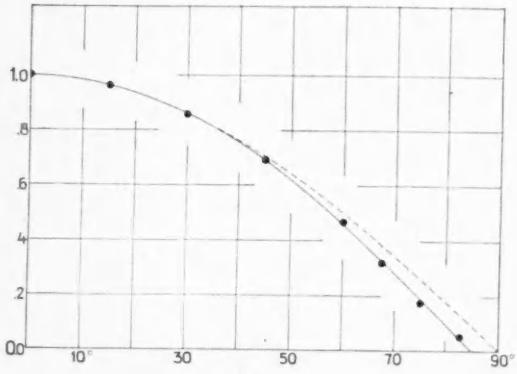

FIG. 2

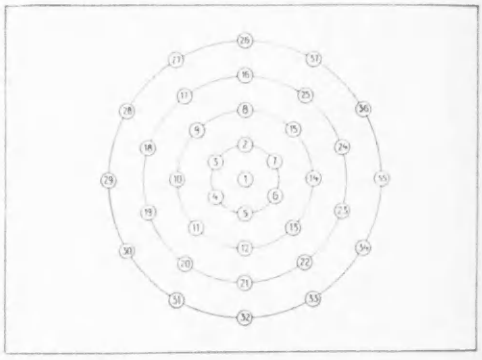

FIG. 3

FIG. 2.—(*a*) Relation between galvanometer deflection and light-intensity (resistance of 0 and 10,000 ohms). (*b*) Relation between galvanometer deflection and angle of incidence of light (*dotted line* = theoretical cosine law).

FIG. 3.—(*a*) Coupling scheme. (*b*) Arrangement of the 37 light-bulbs in groups A and B

II. THE MEASUREMENTS

Before starting the measurements, we must make some assumption regarding the internal distribution of mass in the nebulae. An indication of the mass distribution is obtained from studies of the distribution of light in nebulae, which show that the surface brightness increases rapidly toward the center. Although the assumption of a strict proportionality between mass and light may not be justified,[3] it seems permissible to con-

[3] Cf. H. W. Babcock, *Lick Obs. Bull.*, **19**, 41, 1939.

clude that the density of mass generally increases toward the center of a nebula. In the absence of any detailed knowledge the simplest assumption with regard to mass distribution is probably a normal error-curve. In the present case the mass distribution will enter the problem mainly as a statistical quantity, and certain deviations from the assumed distribution will not materially change the final results. A normal distribution of light is obtained by giving lamps 1–15 (see Fig. 3) a relative candle power of 1.0, lamps 16–25 a power of 0.7, and lamps 26–37 a power of 0.3.

It should be pointed out that the numerical values adopted for the total mass and the absolute diameter of the nebulae are of comparatively small importance in the determination of tidal deformations. In the case of parabolic motions the space velocities and internal rotational velocities will both be proportional to the square root of the mass. Thus a change in mass will have the same effect as a change in the unit of time. This is approximately true even for hyperbolic motions, if the initial space velocities are not too large. Similarly, the parabolic and the rotational velocities are inversely proportional to the square root of the diameter, if the diameter is used as a unit of distance. In the cases where numerical values are desirable, the mass has been put equal to 10^{11} solar units and the diameter of 2500 parsecs.[4] However, only the ratio between the two values needs to be fixed.

As has been pointed out above, the measurements are performed on a plane surface covered by a layer of black paper with an imprinted co-ordinate system. The dimensions of the surface are about 300×400 cm. At the beginning the two groups of lamps, each representing a nebula, are assembled at either end of the surface. The diameter of each group is 80 cm. By means of different resistances, the candle powers of the light-bulbs are adjusted in order to fit a normal distribution of light, as has been described above. The different lamps are then moved step by step, their orbits describing the space motion of the nebula combined with the internal rotation. The two rotating systems will gradually approach each other. As to the rotation, the mass elements are supposed to move in the same direction in circular orbits about the center of the nebula. The space motions depend on the initial velocities (at infinite distance) of the two objects and on the distance of closest approach. All motions are assumed to be undisturbed by possible clouds of dark material inside or outside the nebulae. In order to obtain a complete picture of the tidal disturbances accompanying a close encounter, we must make different assumptions concerning the three parameters represented by (1) the direction of rotation, (2) the initial velocity, and (3) the distance of closest approach. The dependence on the first parameter has been studied by undertaking two series of measurements corresponding to clockwise and counterclockwise rotations, respectively. With regard to initial velocity, two different values have been selected, namely, 0 (parabolic motion) and 450 km/sec. In view of the fact that the average space velocity of nebulae outside the large clusters amounts to about 300 km/sec, as indicated by observed radial motions, these values may represent limiting cases.[5] Finally, the distance of closest approach has been varied. The main efforts, however, have been concentrated on the case where the

[4] By using the apparent major diameters and magnitudes given in the Shapley-Ames catalogue of bright nebulae and by adopting an average, absolute magnitude, $\overline{M}_m$, equal to -15.2 (cf. Hubble, *Mt. W. Contr.*, No. 548; *Ap. J.*, **84**, 158, 1936), we derive the following average values of $\log D$ (D=absolute diameter): 3.01 (type E), 3.25 (type Sa), 3.37 (type Sb), and 3.40 (type Sc). Thus a diameter of about 2500 parsecs is obtained for the intermediate and late-type spirals. It may be remarked that the diameters to be used in the present case should refer to the main body of the nebulae, since the faint, outermost parts have a small mass density.

[5] If there were no selection effects, the average value of the initial velocity, V_0, would be equal to about two-thirds of the average space velocity. However, the frequency of encounters between a certain nebula and other objects is proportional to the relative velocity of this nebula with respect to the others. Owing to this selection effect, the average value of V_0 will amount to about 75 per cent of the average space velocity, or approximately 225 km/sec.

two nebulae pass each other edge to edge (closest distance between centers = diameter of nebula).

The orbits of individual mass elements, i.e., lamps, are constructed piece by piece, by joining the orbital elements, each corresponding to a certain interval of time. For practical reasons the elements should have a certain length, neither too small nor too large, which necessitates the definition of a proper unit of time. It is found that the interval of time corresponding to a rotational motion at the edge of a nebula of 12 cm would be a suitable unit. Knowing the motion of a mass element up to a certain point of time, we are able to construct the piece of orbit corresponding to the subsequent unit of time if the x and y components of the acceleration caused by the total gravitational force acting upon the element can be determined. The accelerations are measured by the photocell. The lamp is removed and replaced by the photocell, which is turned successively in the directions $+x$, $-x$, $+y$, and $-y$. The galvanometer is calibrated by comparing the computed centripetal accelerations in one of the nebulae with the corresponding measured values. The resistance connecting the photocell and the galvanometer is adjusted in such a way as to make the galvanometer reading equal to the acceleration in millimeters (per square unit of time).

The constructions and drawings of the orbits of the individual mass elements are made on large sheets of graph paper. Since the two nebulae are identical, it is necessary to consider only one of the objects. The center of the nebula is kept fixed. Instead, the point representing the center of mass of the two objects is moved in a parabolic, or hyperbolic, orbit. The greatest possible care is exercised in drawing the tangents of the individual curves and in giving the proper curvature to every additional piece of orbit. A set of French curves is used for this purpose. Despite the care taken, the derived orbits will, of course, give only an approximate picture of the real motions inside the nebula. However, the accuracy ought to be sufficient to give a fair idea of the general tidal deformations and the loss of energy accompanying a close encounter.

III. THE RESULTS

Regarding the tidal deformations of the two nebulae, we refer at once to Figures 4*a* and 4*b*, which give a good illustration of the average tidal disturbances. The figures correspond to the case where the objects meet edge to edge, i.e., the distance of closest approach equals the diameter of the nebulae. In Figure 4*a* the objects have a clockwise rotation, whereas Figure 4*b* corresponds to rotations in the opposite direction. In both cases the motions are parabolic, i.e., the initial space velocities are equal to zero. However the figures also represent the deformations of nebulae moving in hyperbolas with small eccentricities, since the changes corresponding to initial velocities of 100–200 km/sec are rather small. The common mass center is denoted by a cross. It appears that the deformations are rather small before the nebulae have reached the distance of closest approach. The maximum deformation occurs after the passage. Thus the tidal deformation, if expressed as a function of time, is an asymmetrical effect. Furthermore, the tidal effects are asymmetrical in space, the deformations being larger on those sides of the nebulae that are turned toward one another. These asymmetries in time and space, which are further discussed below, represent two conditions which must be fulfilled in order that a capture may take place.

The most striking features of Figures 4 are the spiral arms which gradually develop during and after the passage. In the case of clockwise rotations the arms point in the direction of rotation, whereas the opposite is true when the rotations are counterclockwise. This result is very interesting in the light of past and present discussions about the direction of spiral arms. Arguments, theoretical and observational, have been put forth for arms pointing in both directions. The above mechanism for the "ejection" of spiral arms suggests that their direction depends on the direction of rotation of the nebulae compared to the direction of the relative space velocity. It should be pointed out that,

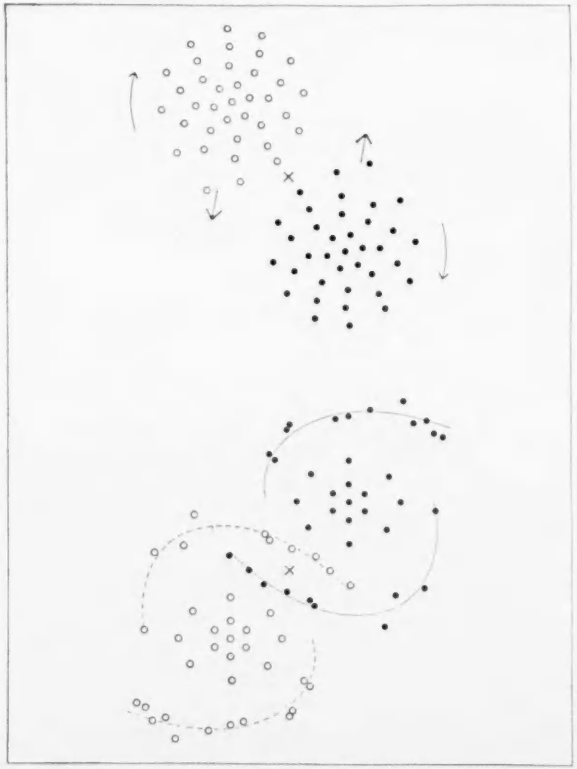

FIG. 4*a*

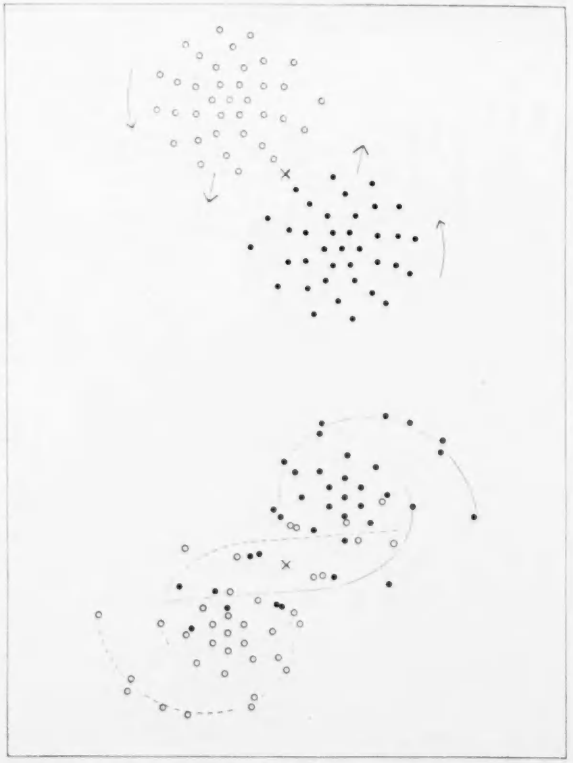

FIG. 4*b*

FIG. 4*a*.—Tidal deformations corresponding to parabolic motions, clockwise rotations, and a distance of closest approach equal to the diameters of the nebulae. The spiral arms point in the direction of the rotation.

FIG. 4*b*.—Same as above, with the exception of counterclockwise rotations. The spiral arms point in the direction opposite to the rotation.

whatever the direction of the arms, the ejected matter rotates in the same direction as the main body of the nebula. The observed spiral arm represents merely the distribution in space of this material. On account of the approximations and the small number of mass elements used, it is not possible in the present case to obtain any conclusive evidence with regard to the form of the arms and the distribution of matter within them. According to observations, most spiral arms seem to have the approximate form of a logarithmic spiral. The position of the points of ejection represents another important

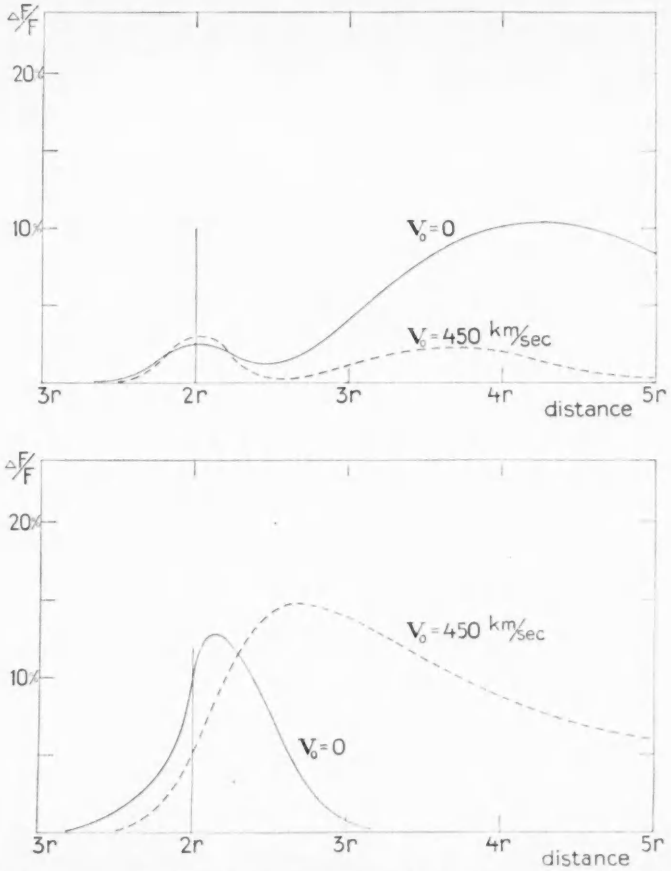

FIG. 5.—Relative increase of attraction between the nebulae (caused by tidal deformations) as a function of the distance between the centers. The distance of closest approach equals the diameter ($=2r$) of the nebulae. The rotations are clockwise (*upper figure*) and counterclockwise (*lower figure*).

problem. It has not yet been possible to decide whether these points remain fixed in space or rotate with the nebula.

On account of the above-mentioned asymmetry in space, the tidal deformations will cause an increase in the gravitational attraction between the two nebulae. In Figure 5 the relative increase is given as a function of the distance between the centers of the nebulae, expressed in terms of the radius. The distance of closest approach equals the diameter of the nebulae. The two curves correspond to initial velocities of 0 (parabolic motion) and 450 km/sec, respectively. The asymmetry of the curves, with respect to the distance of closest approach ($2r$), is very conspicuous. The increase in the attraction

amounts to as much as 10–15 per cent. In the case of clockwise rotations the parabolic motion gives a larger increase than the hyperbolic one. This is quite natural, since the slower motion should correspond to larger disturbances. A peculiarity is found in the two maxima, corresponding to distances of about $2r$ and $4r$, respectively. The maxima are caused by the same bulk of ejected matter and are separated by an interval of time corresponding roughly to one full rotation of the nebulae. In the case of counterclock-

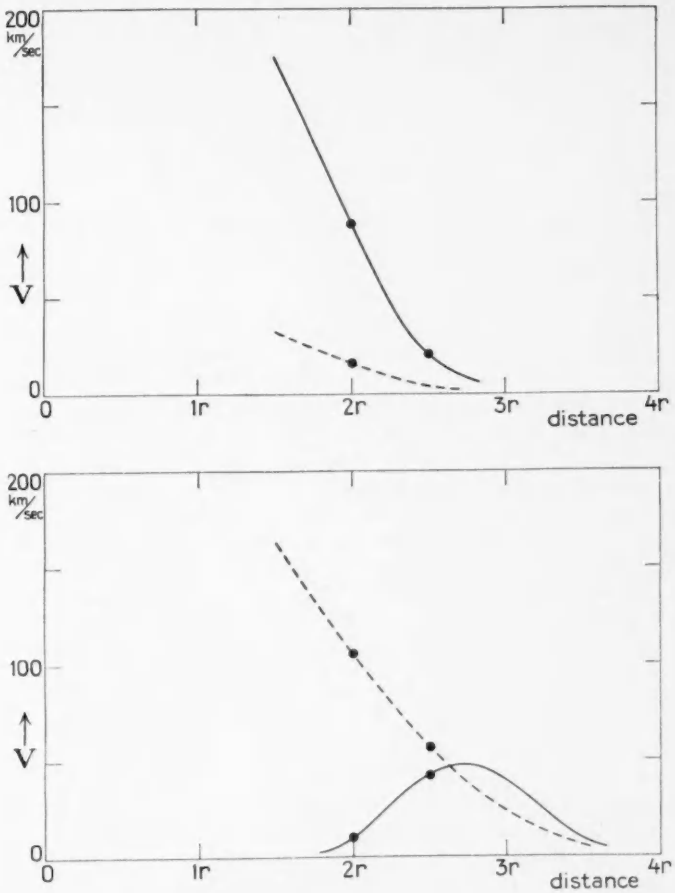

FIG. 6.—Total loss of energy (represented by the velocity V instead of the expression $MV^2/2$) as a function of the distance of closest approach (expressed in terms of the radii of the nebulae). The different curves correspond to those of Figure 5.

wise rotations the parabolic motion also corresponds to larger disturbances than the hyperbolic motion. However, the deformations in this case will be so large that individual mass elements belonging to each nebula are captured by the other, resulting in a decrease in the attraction. The exchange of matter is larger for parabolic motion. This explains the peculiar forms of the two attraction-curves corresponding to counterclockwise rotation.

Having derived the curves giving the increase in attraction, we are able to determine the total loss of energy accompanying a close encounter. In Figure 6 the loss of energy

is given as a function of the distance of closest approach between the nebulae, expressed in terms of the radius of the objects. The ordinate represents the velocity V, instead of the expression $MV^2/2$, the decrease in velocity being a more convenient measure of the loss of energy. The different curves correspond to those of Figure 5, i.e., parabolic motion is represented by full curves and hyperbolic motion (V_∞ = 450 km/sec) by dotted lines. Numerical values are given for distances of $2r$ and $2.5r$. The curves are drawn in such a way as to give the most probable relation between velocity V and distance. The values have been computed by a process of numerical integration. An additional attraction, corresponding to a certain point of time, results in an additional acceleration of the nebula, directed toward the other nebula. By summing up all additional accelerations in x and y, corresponding to the whole interval of time of the encounter, a final velocity (approximately opposite to the space motion of the nebula) is derived that is representative of the total loss of energy. It should be pointed out that the numerical values corresponding to a distance of $2.5r$ are somewhat uncertain. The tidal effects in these cases are rather small, and the deformations are more or less comparable to the errors of measurement and the uncertainties in the construction of the orbits of individual mass elements. However, the principal results of the present investigation depend mainly on the order of size of the computed numerical values. No attempt has been made to find the loss of energy corresponding to encounters at smaller distances than $1.5r$. In such cases the two nebulae will be extensively intermingled, and complications may arise that cannot be properly reproduced by the simple experimental arrangements used in the present case.

In the case of clockwise rotations of the nebulae it appears from Figure 6 that the parabolic motion gives a considerably larger loss of energy than the hyperbolic motion corresponding to an initial velocity of 450 km/sec. It should be remarked that the full curve gives approximately the loss of energy even for nebulae moving in hyperbolas with small eccentricities, since the changes corresponding to values of V_∞ equal to 100–200 km/sec are rather small. The loss of energy increases rapidly when the distance of closest approach becomes smaller. The full curve gives an increase in V from 20 to about 175 km/sec when the distance changes from $2.5r$ to $1.5r$. This means that a capture will take place if the initial velocities of the two nebulae are smaller than these values. The loss of energy given by the dotted line is very small. Since the velocity V does not reach the initial value of 450 km/sec, no capture will take place. In the case of counterclockwise rotations the hyperbolic motion generally gives a larger loss of energy than the parabolic motion. This is explained by the peculiar form of the corresponding attraction-curves given in Figure 5. However, the hyperbolic motion will not result in a capture, since the maximum value of V given by the dotted curve is below 450 km/sec. The curve corresponding to parabolic motion shows a maximum for a distance approximately equal to $3r$. This depends on the exchange of matter between the two nebulae, the exchange being smaller when the distance of closest approach is larger. The largest value of initial velocity that corresponds to a capture equals about 50 km/sec.

The numerical values given in Figure 6 depend to some extent on the mass and diameter of the nebulae. In the case of parabolic motions the velocity V is proportional to the square root of the total mass and inversely proportional to the square root of the absolute diameter. In the case of hyperbolic motions the dependence is somewhat smaller. The numerical values used in the present case are 10^{11} solar masses and 2500 parsecs, respectively. However, only the ratio between the two values needs to be fixed. If the diameter is assumed to be equal to 1000 parsecs, the curves of Figure 6 will correspond to a mass of $4 \cdot 10^{10}$ solar units.

The above results are, of course, subject to a certain degree of uncertainty, depending on errors involved in the measurements and on difficulties in constructing exactly the orbits of individual mass elements. Furthermore, the results depend on the special

assumptions made in the present case about orientation of the nebulae and internal distribution of mass. In spite of these restrictions it seems justified to conclude that the numerical values derived above indicate the proper order of size of the energy loss in a close encounter between extragalactic nebulae and that, in favorable cases, captures may occur.

The laboratory work was performed at the Lund University Observatory. The author wishes to express his sincere thanks to Dr. Knut Lundmark for generous economic support in procuring and constructing the experimental equipment. The author also expresses his gratitude to the Luma Factory of Stockholm for valuable help in designing and manufacturing the special light-bulbs that were used in the present investigation.

JULY 1941

THE PHOTOGRAPHIC DETERMINATION OF STELLAR PARALLAXES WITH THE 60- AND 100-INCH REFLECTORS*

EIGHTEENTH SERIES

ADRIAAN VAN MAANEN

ABSTRACT

Trigonometric parallaxes determined with the 60- and 100-inch reflectors are given for 25 fields, including 27 stars, 23 of which have photographic absolute magnitudes of +10 or fainter; 3 are fainter than +15.

The present paper gives the results for 27 stars in 25 fields, which have recently been measured for parallax. The work has been carried out in the same way as for the previously published series.[1] The results are given in Table 1. Practically all the stars are faint, with considerable proper motion. They were put on the program in the hope of finding more stars of very faint absolute magnitudes. Not less than 23 of the 27 stars have a photographic absolute magnitude fainter than +10; Ross 513B is even +16.2; Wolf 1084, +15.6; and Luyten 789–6, +16.8.

Ross 29 is a close double with $\Delta = 0''.75$, while Ross 513 has a companion at a distance of about 10″, sharing its large proper motion of $1''.2$ annually.

Ross 128 and Luyten 789–6 are within 5 parsecs of the sun. Of stars within that distance, the total number known at present is 50, including 13 companions, while between 5 and 10 parsecs we know at present 136 stars, including 32 companions.

In any kind of routine work it is well occasionally to survey the results obtained and to consider possible changes in the program. With the completion of the eighteenth series of Mount Wilson trigonometric parallaxes, the total number of entries in my card catalogue from Mount Wilson is 501; 383 objects were taken at the Cassegrain focus of the 60-inch reflector, and 118 at the Newtonian focus of the 100-inch reflector. To my surprise I found that there are now as many as 481 entries for the same objects from other observers—411 for 193 stars taken at the 60-inch and 70 for 35 stars at the 100-inch reflector. Algebraic mean differences (Mount Wilson *minus* Other observers) are $+0''.0017$ and $+0''.0044$, respectively, for the two instruments.

The mean deviations without regard to sign are $0''.0194$ and $0''.0396$, respectively. The first value for the 60-inch reflector is identical with that derived a few years ago for the mean difference of all modern observers *inter se*. The large value found for the 100-inch reflector would indicate large probable errors for that instrument. The case, however, is far less serious than it looks at first sight. The reason is that most of the objects observed in common with other observers are brighter stars, for which a sector had to be used, which at the Newtonian focus means that the comparison stars are at considerably greater distances from the center than when no sector is used. At the Newtonian focus a great deal of the uncertainty in the measures comes from the coma, which at the 100-inch reflector begins to be noticeable at about 5′ from the center and which changes with the "seeing" and with the condition of the mirror. For the 23 stars for which a sector was used there are 53 entries by other observers, giving a mean deviation of $0''.0483$, while

* *Contributions from the Mount Wilson Observatory, Carnegie Institution of Washington*, No. 652.

[1] *Mt. W. Contr.*, Nos. 111, 1916; 136, 1917; 158, 1918; 182, 1920; 204, 1921; 237, 1922; 270, 1923; 290, 1925; 321, 1926; 356, 1928; 391, 1929; 435, 1931; 468, 1933; 506, 1935; 553, 1936 (*Ap. J.*, **84**, 409); 590, 1938 (*Ap. J.*, **87**, 424); 630, 1940 (*Ap. J.*, **91**, 503).

for the 12 stars taken without a sector (17 entries by others) this difference is reduced to 0".0127. The large uncertainty when the sector was used is further corroborated by the internal probable errors, which, with and without sector, are 0".018 and 0".007, respectively.

There is no reason why the 100-inch reflector should not yield first-class parallaxes for fainter stars, for which no sector is necessary, viz., for 91 out of the 118 parallaxes published. The stars for which a sector would be necessary have for some time been omitted from the observing program; while in the cases where a sector has been used, this fact has been mentioned in the original publications.

TABLE 1

STELLAR PARALLAXES DETERMINED AT MOUNT WILSON

Object	α 1900	δ 1900	m_{pg}	Spectrum	Relative Parallax	μ_α Rel.	P.E.	No. of Exp.	Instrument
Wolf 56	1h 1m54s	+62° 59′	12.6	K2	+0".023	+1".027	2 1	20	60"
vM-W 36	1 14 35	+15 6	15.7	.....	+ .023	+0.180	5 2	20	100
vM-W 44	2 16 44	+15 16	13.6	.....	+ .031	+0.366	5 3	20	60
Ross 34	3 22 12	+37 3	12.0	K5	+ .035	+1.109	7 7	18	60
vM-W 1	3 39 44	+45 13	13.0	.....	+ .006	+0.138	5 2	20	60
Ross 29 AB	4 5 42	+50 17	14.0	.....	+ .060	−0.394	5 5	18	60
Radcl. 72, 126	4 9 46	+15 8	15.2	.....	+ .023	+0.163	4 2	18	100
Ross 594	4 23 36	+39 39	14.8	M7	+ .096	+0.272	10 3	18	60
Ci. 20, 398	6 40 54	+37 39	11.9	F	+ .039	−0.202	5 6	18	60
Ross 394	7 31 42	+28 31	15.6	.....	+ .038	+0.364	2 1	18	100
Radcl. 52, 212	8 25 55	+29 48	14.5	.....	+ .036	−0.193	6 2	18	100
Ross 84	9 25 54	+20 44	13.5	.....	+ .047	+0.031	6 2	18	60
Star near W UMa	9 35 27	+56 27	14.1	.....	+ .067	−0.700	4 4	20	60
Radcl. 29, 130*	9 40 19	+44 22	13.2	.....	+ .037	−0.011	7 3	18	60
A. G. Hels. 6113	9 48 48	+63 17	10.5	M1	+ .113	−0.294	3 7	20	60
Ross 128	11 42 34	+ 1 23	12.7	.....	+ .290	+0.615	7 2	18	60
Wolf 1426	11 56 12	+23 29	14.1	.....	+ .012	−0.195	10 2	18	100
Radcl. 81, 208	13 11 5	+14 48	14.0	.....	+ .020	−0.006	8 5	18	60
Ross 494	13 54 49	+25 44	12.7	.....	+ .027	−0.530	6 1	18	60
Radcl. 59, 354	15 0 8	+29 52	14.2	.....	+ .043	+0.243	5 3	18	60
Ross 513 A	15 30 55	+18 3	14.0	Mo	+ .078	−1.199	16 3	18	100
Ross 513 B	15 30 55	+18 3	16.5	.....	+ .092	−1.198	7 2	18	100
Wolf 1084	20 40 28	+54 57	16.3	Mye	+ .070	+0.879	11 4	18	60
vM-W 74	21 8 16	+15 24	16.3	.....	+ .048	−0.059	6 3	18	100
Wolf 1329†	22 4 21	− 5 8	11.8	M5	+ .125	+1.115	14 3	18	100
Luyten 789–6	22 33 0	−1° 52	14.3	M6	+0.315	+2.249	7 6	18	100

* In list of stars of large proper motion, *Radcliffe Catalogue of Proper Motions*. † Sector used.

In recent years most of the observing program with both instruments has been made up of faint stars of large motion. Of the stars whose annual proper motion exceeds 0".5, parallaxes were determined at the 60-inch for 68 stars with photographic magnitudes ranging from 10 to 16.3 and at the 100-inch for 58 stars with magnitudes ranging from 12.2 to 18.3. The distribution of the absolute magnitudes for these stars is given in Table 2.

For stars fainter than the tenth magnitude, but with proper motions less than 0".5 annually, 24 and 15 parallaxes were determined at the 60-inch and 100-inch reflectors, respectively; the distribution of the absolute magnitudes of these stars is given in the last two columns of Table 2. The table shows that the 60-inch and the 100-inch reflector each added 67 to the list of stars with absolute photographic magnitudes +10 or fainter.

In the material for the very faintest stars, whose absolute photographic magnitudes are fainter than +15.0, the 100-inch work takes a still more predominant position. Of the 21 stars known at present to belong to that class, 13 have parallaxes determined at the 100-inch and 4 at the 60-inch; of these, 11 and 3, respectively, have parallaxes determined at Mount Wilson only. The 100-inch parallaxes include the very faintest star known at present, Wolf 359, as well as the faintest white dwarf, Wolf 457.

In the finding of near-by stars, both instruments have contributed a fair share: of the stars within 5 parsecs from the sun, 5 were found at the 100-inch (4 at the 100-inch only) and 6 at the 60-inch (2 at the 60-inch only); of the stars between 5 and 10 parsecs from the sun, 12 had parallaxes determined at the 100-inch (6 at the 100-inch only) and 11 at the 60-inch (3 at the 60-inch only).

TABLE 2

ABSOLUTE MAGNITUDES OF PARALLAX STARS

M	$\mu \geqq 0''.5$		$\mu < 0''.5$	
	60″	100″	60″	100″
$<+10.0$	13	3	12	3
$+10.0$ to $+10.9$	9	1	3	0
$+11.0$ to $+11.9$	13	10	4	2
$+12.0$ to $+12.9$	11	9	3	4
$+13.0$ to $+13.9$	9	18	2	0
$+14.0$ to $+14.9$	8	4	0	5
$+15.0$ to $+15.9$	4	6	0	1
$+16.0$ to $+16.9$	1	6	0	0
$+17.0$ to $+17.9$	0	0	0	0
$>+18.0$	0	1	0	0

From these remarks it may be concluded that the parallaxes determined at the Newtonian focus of the 100-inch reflector have yielded some of the most interesting results obtained in recent parallax work. The only restriction in the use of this instrument is that the comparison stars should be close to the central stars, but for stars of very faint apparent magnitude this condition is always easily fulfilled.

CARNEGIE INSTITUTION OF WASHINGTON
MOUNT WILSON OBSERVATORY
July 1941

INVESTIGATIONS ON PROPER MOTION. XXII. FAINT MEMBERS OF THE PLEIADES CLUSTER*

ADRIAAN VAN MAANEN

ABSTRACT

Two pairs of plates with intervals of 15 and 19 years, respectively, taken at the Newtonian focus of the 100-inch reflector, have yielded proper motions which revealed in a region 40′ by 30′ around Alcyone more than two dozen new members of the Pleiades group.

The photographic magnitudes of the new members range from 12.4 to about 17.5. The observations indicate that the maximum of the frequency-curve of apparent magnitude has not been passed. This is not surprising, however, since the absolute photographic magnitude of the faintest stars identified with the group is about +12, while in the immediate neighborhood of the sun I have found the photographic maximum of the luminosity-curve to be about +14.5.

At the twenty-first meeting of the American Astronomical Society in 1917, Trumpler announced that in the Pleiades cluster 84 stars brighter than photographic magnitude 9.5 and possibly 11 fainter stars had been found.

In 1919 the present writer[1] measured a few plates of the region around Atlas and Pleione, which had been taken at the Cassegrain focus of the 60-inch reflector with an interval of only 5 years; 2 new stars were found for which the proper motion coincided so closely with that of the cluster that little doubt remained of their belonging to the group; their photographic magnitudes were 10.2 and 13.7. For 8 other stars the proper motion indicated a possible membership in the group. Later researches have shown that 5 of these 8 stars, 1 as faint as 15.8, also belong to the cluster.

A great step forward was made in 1921 when Trumpler published[2] a list of 174 stars within 1° of Alcyone, including 140 "very probable" members, 21 "probable," and 13 "uncertain" members of the group. The magnitudes of these stars range from 2.8 to 15.2. A second list contains 72 stars more than 1° distant from Alcyone and includes 36 very probable, 17 probable, and 19 uncertain members of the group; the magnitudes range from 6.0 to 13.6.

Finally, in 1929, Hertzsprung in his Darwin lecture[3] included 187 stars down to the 16th magnitude in a region 2 degrees square with Alcyone in the center. The distribution among the different magnitudes, while provisional, indicates a maximum frequency at the 13th magnitude, but Hertzsprung concludes that, when more material on fainter stars becomes available, the maximum frequency may be found to be at a still fainter magnitude.

Since I had taken a few plates of the Pleiades at the Newtonian focus of the 100-inch reflector as early as 1921 and 1922, it seemed worth while to compare these plates with some recent ones. The exposures were secured with an 84-inch diaphragm to improve the images at greater distances from the center; they were taken on Eastman 33 and Eclipse 850 plates with exposures of 30–60 minutes; the field covers 42 by 31 minutes of arc with Alcyone in the center. The provisional magnitude of the faintest stars measured was 17.5 or 17.8.

The plates show about 800 stars. To avoid measuring such a considerable number of stars, the plates were first blinked in the stereocomparator in order to pick out those which seem to have a total motion of more than 0″.5 of arc. Seventy stars showing definite motion were found; to these were added 67 comparison stars, well distributed over the field.

* *Contributions from the Mount Wilson Observatory, Carnegie Institution of Washington*, No. 653.

[1] *Mt. W. Contr.*, No. 167, 1919. [2] *Lick Obs. Bull.*, **10**, 110, 1921. [3] *M.N.*, **89**, 660, 1929.

TABLE 1

PROPER MOTIONS OF STARS MEASURED

No.	m_{pg}	1900		$\bar{\mu}_\alpha$	$\bar{\mu}_\delta$	REMARKS*
		α	δ			
1	15.0	$3^h40^m11^s$	$+23^\circ 50'$	$+0''.010$	$+0''.006$	c.s.
2	15.1	3 40 13	23 46	+ .004	− .080	V
3	16.8	3 40 16	23 39	+ .012	+ .002	c.s.
4	14.65	3 40 15	23 45	− .002	+ .006	c.s.
5	15.54	3 40 16	23 45	+ .030	− .045	III
6	13.78	3 40 17	23 53	− .003	− .003	c.s.
7	14.05	3 40 19	23 40	− .004	+ .002	c.s.
8	8.05	3 40 19	23 53	+ .026	− .056	H III
9	14.86	3 40 24	23 36	+ .005	− .010	c.s.
10	15.43	3 40 22	23 58	− .003	− .002	c.s.
11	4.2	3 40 24	23 38	+ .038	− .046	H IV
12	13.80	3 40 23	23 43	− .004	− .002	c.s.
13	15.95	3 40 24	24 0	− .002	− .001	c.s.
14	16.5	3 40 25	23 40	+ .004	− .038	III
15	16.4	3 40 26	23 49	+ .014	− .018	c.s.
16	>17	3 40 27	23 39	+ .082	− .047	V
17	16.28	3 40 28	23 34	+ .010	+ .014	c.s.
18	13.85	3 40 27	24 3	+ .012	− .038	H II
19	16.7	3 40 28	23 51	+ .026	− .050	II
20	15.20	3 40 29	23 38	.000	.000	c.s.
21	7.21	3 40 30	23 57	+ .016	− .053	H II
22	15.05	3 40 33	23 34	− .002	+ .013	c.s.
23	>17	3 40 33	23 46	+ .054:	− .040:	V
24	>17	3 40 34	23 46	+ .051:	− .040:	V
25	15.55	3 40 35	23 48	+ .022	− .043	I
26	15.18	3 40 41	23 32	− .029:	− .042:	V
27	14.91	3 40 35	23 40	+ .038	− .054	IV
28	14.21	3 40 35	24 1	− .008	+ .001	c.s.
29	12.38	3 40 37	23 50	+ .036	− .041	IV
30	13.79	3 40 39	23 41	− .012	+ .002	c.s.
31	15.66	3 40 40	23 39	+ .016	− .035	II
32	11.57	3 40 36	23 33	− .011:	− .015:	V
33	13.35	3 40 40	24 2	+ .012	− .039	H II
34	15.32	3 40 42	23 53	.000	− .002	c.s.
35	9.63	3 40 43	23 48	+ .020	− .046	H I
36	13.14	3 40 43	23 43	+ .014	− .046	H I
37	>17	3 40 47	23 41	+ .024	− .042	II
38	14.20	3 40 47	23 57	− .010	+ .018	c.s.
39	13.37	3 40 49	24 2	− .005	− .004	c.s.
40	16.01	3 40 52	+23 37	+0.008	−0.038	II

* In the column of remarks the comparison stars are marked c.s.; the members of the group given by Hertzsprung are indicated by an H, while the proper-motion stars measured in this paper are marked I, II, III, IV, and V, depending upon whether they fall in the central circle of Figure 1, in the first, second, or third ring or outside the limits used for possible members of the group.

TABLE 1—*Continued*

No.	m_{pg}	1900		$\bar{\mu}_\alpha$	$\bar{\mu}_\delta$	Remarks*
		α	δ			
41	14.91	$3^h40^m56^s$	$+23°41'$	$0''.000$	$-0''.002$	c.s.
42	>17	3 40 56	23 59	+ .026	− .046	II
43	15.37	3 40 58	23 48	+ .028	− .028	IV
44	>17	3 40 58	23 54	+ .015:	− .042:	I
45	15.86	3 41 1	23 59	+ .010	+ .006	c.s.
46	12.77	3 41 2	23 47	− .002	− .012	c.s.
47	12.81	3 41 4	23 40	− .016	− .001	c.s.
48	14.85	3 41 5	23 34	+ .003	+ .009	c.s.
49	15.56	3 41 5	23 53	− .001	+ .012	c.s.
50	14.87	3 41 6	23 50	− .003	+ .006	c.s.
51	15.61	3 41 7	23 51	+ .018	− .040	I
52	8.51	3 41 8	23 41	+ .018	− .044	H I
53	16.3	3 41 9	24 0	+ .002	− .004	c.s.
54	>17	3 41 11	24 0	+ .032	− .049	III
55	>17	3 41 13	23 45	+ .017	− .043	I
56	9.68	3 41 13	23 58	+ .018	− .040	H I
57	14.69	3 41 14	23 44	− .010	− .006	c.s.
58	12.96	3 41 18	23 53	+ .022	− .004	c.s.
59	14.09	3 41 18	23 48	− .008	.000	c.s.
60	8.80	3 41 20	23 49	+ .019	− .038	H II
61	12.24	3 41 21	23 36	− .002	− .006	c.s.
62	15.27	3 41 21	23 48	+ .032	− .037	III
63	14.91	3 41 22	23 38	− .003	− .022	V
64	15.11	3 41 22	23 44	+ .010	− .046	H II
65	8.21	3 41 23	23 50	+ .022	− .040	H II
66	14.07	3 41 23	23 42	− .004	− .013	c.s.
67	6.3	3 41 24	23 48	+ .020	− .042	H I
68	14.00	3 41 24	23 46	− .008	− .003	c.s.
69	15.08	3 41 26	23 42	+ .008	− .002	c.s.
70	14.82	3 41 28	23 35	+ .002	− .027	IV
71	10.51	3 41 27	23 36	+ .016	− .053	H II
72	7.20	3 41 28	23 36	+ .030	− .048	H III
73	16.9	3 41 27	23 50	.000	− .030	IV
74	16.8	3 41 29	23 44	+ .020	− .046	I
75	15.64	3 41 29	23 44	.000	+ .004	c.s.
76	14.92	3 41 32	23 34	+ .002	− .014	V
77	15.72	3 41 31	24 2	+ .006	− .010	c.s.
78	6.76	3 41 32	23 59	+ .016	− .040	H I
79	16.3	3 41 38	23 34	− .002	− .013	V
80	13.53	3 41 39	23 54	+ .002	+ .006	c.s.
81	>17	3 41 44	23 38	+ .011:	− .032:	III
82	11.05	3 41 43	24 3	+ .008	− .026	H IV
83	15.22	3 41 43	24 0	+ .028	− .035	III
84	12.56	3 41 44	23 50	+ .002	+ .005	c.s.
85	11.94	3 41 44	+23 42	+0.006	+0.005	c.s.

TABLE 1—*Continued*

No.	m_{pg}	1900		$\bar{\mu}_\alpha$	$\bar{\mu}_\delta$	Remarks*
		α	δ			
86	14.50	$3^h41^m45^s$	+23° 40′	+0″.026	−0″.049	H II
87	15.71	3 41 47	23 35	− .016	− .001	c.s.
88	12.48	3 41 46	23 58	− .008	+ .012	c.s.
89	15.64	3 41 48	23 38	− .154	− .020	V
90	16.4	3 41 50	23 44	+ .024	− .045	II
91	14.90	3 41 51	23 56	+ .008	+ .016	c.s.
92	16.6	3 41 53	23 44	− .002	+ .005	c.s.
93	15.51	3 41 54	23 52	+ .008	.000	c.s.
94	15.14	3 41 55	23 36	+ .006	− .014	c.s.
95	10.21	3 41 56	23 38	+ .020	− .046	H I
96	14.56	3 41 57	23 41	+ .020	− .044	H I
97	14.22	3 42 0	24 1	− .002	− .002	c.s.
98	15.29	3 42 2	23 40	+ .008	− .010	c.s.
99	10.56	3 42 3	23 47	− .012	− .018	V
100	16.09	3 42 5	23 45	+ .007	.000	c.s.
101	16.5	3 42 8	23 45	+ .026	− .043	II
102	9.47	3 42 10	23 50	+ .014	− .048	H I
103	13.07	3 42 11	23 33	+ .007	− .009	c.s.
104	13.30	3 42 12	23 56	+ .005	− .012	c.s.
105	13.86	3 42 16	23 41	+ .004	− .002	c.s.
106	8.19	3 42 16	24 1	+ .008	− .038	H II
107	14.65	3 42 20	23 52	+ .008	+ .016	c.s.
108	13.47	3 42 20	23 59	+ .008	+ .001	c.s.
109	14.75	3 42 21	23 47	+ .004	.000	c.s.
110	10.86	3 42 21	23 35	+ .018	− .054	H II
111	15.7	3 42 22	23 35	+ .011	− .048	II
112	14.86	3 42 27	23 54	− .004	+ .006	c.s.
113	10.44	3 42 30	23 44	+ .014	− .046	H I
114	6.96	3 42 33	24 2	+ .009	− .035	H II
115	14.79	3 42 34	23 39	− .004	− .010	c.s.
116	16.08	3 42 34	23 50	− .004	+ .004	c.s.
117	12.57	3 42 34	23 58	+ .010	− .002	c.s.
118	17.0	3 42 34	23 59	+ .022:	− .040:	II
119	15.7	3 42 36	23 34	− .012	+ .012	c.s.
120	13.54	3 42 37	23 36	+ .010	− .008	c.s.
121	9.28	3 42 38	23 52	+ .012	− .054	H II
122	15.57	3 42 40	23 34	− .017:	− .031:	V
123	15.49	3 42 47	23 47	− .008	+ .002	c.s.
124	15.63	3 42 47	23 50	− .002	+ .001	c.s.
125	15.12	3 42 49	24 1	.000	− .008	c.s.
126	15.1	3 42 50	23 42	− .005	+ .002	c.s.
127	>17	3 42 51	23 44	− .008:	− .017:	V
128	15.5	3 42 51	23 54	+ .029	− .040	III
129	15.0	3 42 52	24 2	− .004	− .005	c.s.
130	11.63	3 42 52	+23 58	+0.014	−0.042	H I

TABLE 1—*Continued*

No.	m_{pg}	1900		$\bar{\mu}_\alpha$	$\bar{\mu}_\delta$	Remarks*
		α	δ			
131	14.2	$3^h42^m53^s$	$+23°40'$	$+0''.015$	$-0''.040$	H I
132	15.8	3 42 55	23 53	− .014	− .011	c.s.
133	>17	3 42 55	23 54	+ .007:	− .027:	IV
134	>17	3 43 1	24 1	+ .016	− .052	II
135	7.0	3 43 1	23 33	+ .045	− .064	V
136	16.5	3 43 3	23 59	− .008	.000	c.s.
137	13.9	3 43 5	+23 39	+0.016	+0.018	c.s.

These 137 stars were measured on two pairs of plates, with intervals of 19 and 15 years, respectively, in four positions each—east, west, north, and south—in the direction of increasing reading of the micrometer screw. Quadratic terms were used in the solutions. The results are in Table 1. On one pair of plates 10 stars were not measured because too faint or just outside the field of the other pair. Table 1 gives in the successive columns the current number, the photographic magnitudes, the right ascension and declination for 1900, the mean μ_α and μ_δ, and some remarks. The stars measured on only one pair of plates are marked by a colon after the $\bar{\mu}_\alpha$ and $\bar{\mu}_\delta$.

TABLE 2

INTERNAL PROBABLE ERROR IN $\bar{\mu}_\alpha$ AND $\bar{\mu}_\delta$

(Unit $0''.001$)

Distance from Center	P.E. in $\bar{\mu}_\alpha$	P.E. in $\bar{\mu}_\delta$	n
<5′	1.7	2.0	11
5′–10′	2.4	1.6	25
10′–15′	2.9	3.3	41
15′–20′	3.9	2.6	37
>20′	5.8	3.4	13

The magnitudes are those published by Hertzsprung in *Astronomische Nachrichten*, **199**, 247, 1914; for stars not in Hertzsprung's list the magnitudes were interpolated, only one decimal being given. The stars fainter than 16.9 mag. are indicated by >17. From counts of the numbers of stars we derive for the faintest stars measured 17.5 mag., while a comparison with some plates of a few selected areas indicates that the faintest stars measured are about 17.8 mag.

It is interesting to notice the variation in accuracy of the measures with the distance from the center (see Table 2). Up to 10′ from the center the probable error is about $0''.002$, from 10′ to 20′ a little over $0''.003$, while for distances more than 20′ it becomes $0''.004$[5].

With as large a range in magnitudes as was used in the present paper, it is gratifying to find that there seems to be no systematic error due to magnitudes. This may be seen from Table 3, which gives the mean $\bar{\mu}_\alpha$ and $\bar{\mu}_\delta$ for the comparison stars of different magnitudes.

The absence of a systematic magnitude-error is still more strongly evidenced by the mean motions of the 56 stars of different magnitudes accepted as members of the Pleiades (see Table 4).

If the small numbers of stars involved in each group are kept in mind, it is evident that no appreciable systematic error due to magnitude exists in a range of more than 13 magnitudes.

In order to decide which stars might be physical members of the group, all the motions were plotted as in Figure 1. It was then accepted that the 28 stars in the small region covered by our plates which, according to Hertzsprung, were members of the group give the best value for its mean motion. The result for their relative motion is $\mu_a = +0''.017$, $\mu_\delta = -0''.044$; the probable error of a total motion was found to be

TABLE 3

MEAN PROPER MOTIONS OF COMPARISON STARS ACCORDING TO MAGNITUDE

(Unit 0".001)

Mag.	11.9–12.9	13.0–13.9	14.0–14.9	15.0–15.9	16.0–16.5
$\bar{\mu}_a$	+1.5	+ 2.5	− 2.2	− 1.7	+4.1
$\bar{\mu}_\delta$	−0.4	− 1.2	+ 1.9	− 0.8	0.0
n	8	11	18	21	9

TABLE 4

MEAN PROPER MOTIONS OF GROUP STARS ACCORDING TO MAGNITUDE

(Unit 0".001)

Mag.	4.2–7.9	8.0–10.9	11.0–13.9	14.0–15.9	16.0–17.8
$\bar{\mu}_a$	+21	+17[5]	+16	+22	+17
$\bar{\mu}_\delta$	−44	−47	−39	−41	−41
n	6	13	6	15	16

0".006. With the mean motion as center, circles were drawn with radii of 0".006, 0".012, 0".018, and 0".024. We find that 17 stars fall inside the central circle, and 22, 9, and 8 in the successive concentric rings. The first two groups are "almost certain" members of the cluster; the third group, "probable," and the last, "possible" members of the cluster. This selection as members of the Pleiades cluster is somewhat more liberal than that used by Trumpler, who called stars within a circle of 0".010 "very probable" members and those in the concentric rings between 0".010 and 0".015 and between 0".015 and 0".020, respectively, "probable" and "uncertain" members of the group. Since nearly all the new members are fainter than the 15th magnitude, our larger limits are probably all right, as the chance that such faint stars have proper motions of the order of 0".050 annually is very small, unless they are members of the group. In Figure 1 the stars of different categories are indicated as follows: The comparison stars are represented by small dots; the stars which were measured for proper motion are given by larger circles and, when these stars by Hertzsprung's researches were already known to be members of the cluster, by larger dots; the stars measured on only one pair of plates are marked by crossed circles; star 89 only has a motion so large that it falls outside the

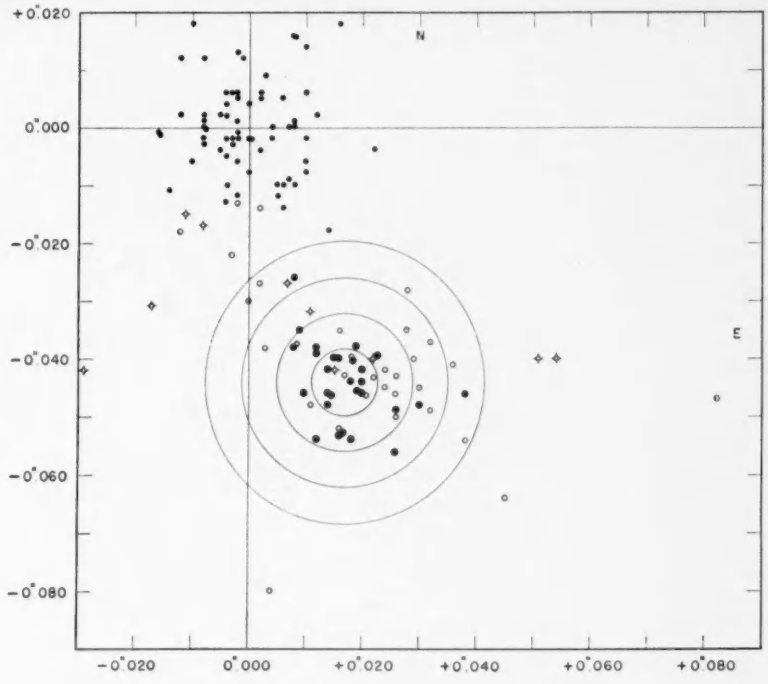

FIG. 1.—Distribution of the proper motions

TABLE 5

DISTRIBUTION OF POSSIBLE CLUSTER STARS ACCORDING TO APPARENT MAGNITUDE

m_{pg}	Within 2×P.E.	Within 3×P.E.	Within 4×P.E.	Hertzsprung	Increase
<6	1	1	2	2	.....
6– 7	2	2	2	2	.....
7– 8	1	2	2	2	.....
8– 9	4	5	5	5	.....
9–10	4	4	4	4	.....
10–11	4	4	4	4	.....
11–12	1	1	2	2	.....
12–13	0	0	1	0	1
13–14	3	3	3	3	.....
14–15	3	3	5	3	2
15–16	5	9	10	1	9
16–17	5	6	7	0	7
>17	6	8	9	0	9
Total	39	48	56	28	28

limits of the figure. The most interesting result is the fact that so many faint stars apparently have the same proper motion as the cluster. This can best be seen from Table 5. The table gives according to apparent magnitude the numbers of stars which we have called "almost certain," "probable," and "possible" members of the cluster; the stars which were already published by Hertzsprung as members of the group; and the increase of these numbers by the present investigation. It is evident from the table that the maximum frequency has not yet been passed; this fact can be seen even better if we plot the total number N_m according to apparent magnitude, for the three groups of almost certain, probable, and possible members, as in Figure 2. In all three cases the curve shows no sign of decreasing slope, which indicates that we have not yet passed the

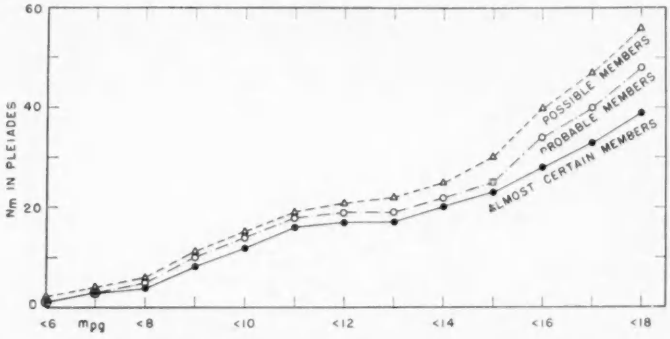

FIG. 2.—Relation of N_m to magnitude for members of various groups

maximum in the frequency-curve. This is not surprising, if we keep in mind the absolute magnitudes of the stars in question. The mean spectroscopic parallax of 27 Pleiades stars is $+0''.0070 \pm 0''.0003$; the mean trigonometric parallax of 30 stars, $+0''.0125 \pm 0''.0023$. Accepting $0''.008$ as the most probable value of the parallax of the cluster, we compute for the faintest members of the group found here an absolute photographic magnitude of about $+12$. As the visual absolute magnitude of the maximum in the luminosity-curve of stars in our immediate neighborhood was found[4] to fall at $+12.7$, which would correspond to a photographic absolute magnitude of $+14.5$, it is not surprising that at $+12$ we have not yet reached the maximum frequency in the cluster, although it is, of course, possible that a cluster may not contain stars as faint as are to be found in other parts of the universe.

CARNEGIE INSTITUTION OF WASHINGTON
MOUNT WILSON OBSERVATORY
July 1941

[4] *Mt. W. Contr.*, No. 562, p. 13; *Ap. J.*, **85**, 38, 1937.

A SPECTROGRAPHIC STUDY OF THE ECLIPSING VARIABLE STAR, WW DRACONIS*

ALFRED H. JOY

ABSTRACT

Velocity-curves and orbital elements.—The radial velocities of the components of the eclipsing variable WW Draconis, ADS 10152 A, were measured from 31 spectrograms. The velocity-curve of the primary star, type G2, is well determined. The secondary spectrum, type Ko, is too faint for reliable measurement. The elements of the spectrographic orbit are: $e = 0.0$ (assumed), $\gamma_1 = -28.5 \pm 0.9$ km/sec, $K_1 = 86.8 \pm 1.1$ km/sec, $K_2 = 147.6$ km/sec, $a_1 \sin i = 5{,}526{,}000$ km, $a_2 \sin i = 9{,}396{,}000$ km, $m_1 \sin^3 i = 3.9\odot$, $m_2 \sin^3 i = 2.3\odot$.

Absolute dimensions and physical properties.—With the aid of Plaut's photometric solution the following values were deduced: $a_1 = 5{,}561{,}000$ km, $a_2 = 9{,}457{,}000$ km, $r_1 = 2.7\odot$, $r_2 = 4.9\odot$, $m_1 = 4.0\odot$, $m_2 = 2.3\odot$, $\rho_1 = 0.20\odot$, $\rho_2 = 0.02\odot$, $M_1 = 3.2$ vis. mag., $M_2 = 3.2$ vis. mag.

Emission lines of calcium.—Emission H and K lines of calcium are displaced in the same direction as the lines of the secondary star, but have a smaller range.

ADS 10152 B.—The mean velocity of the northern star of the visual pair is -33.7 km/sec. Its spectral type is F9; the spectroscopic absolute magnitude, $+2.2$.

WW Draconis ($\alpha = 16^h37^m.7$, $\delta = +60°54'$ [1900]; G5; mag. 9.3–10.0), the southern component of the visual binary ADS 10152, was discovered to be an eclipsing variable by Miss Margaret Harwood[1] from a study of Harvard plates. The correct period was first given by Zverev,[2] who, from comparisons with the North Polar Sequence, estimated the visual range at primary minimum as 0.65 mag. The secondary minimum is shallow and could not be observed satisfactorily.

An extensive photographic study of the light-changes was made by L. Plaut[3] in Leiden. He used 5882 extra-focal photographic exposures calibrated with a coarse grating and measured with a Schilt photometer. The northern component of the visual pair was used as comparison star. Plaut's light-curve shows a photographic range of 1.15 mag. at primary minimum and 0.11 mag. at secondary. The photometric elements deduced from his observations are

$$\text{Minimum} = \text{JD } 2428020.3693 + 4^d.629583E\,.$$

For uniform and darkened disks the results in Table 1 were obtained. The radii are expressed in terms of the radius of the relative orbit. The primary eclipse is nearly total. The brighter component is smaller but has greater surface brightness. There is no certain indication of eccentricity of the orbit or prolateness of the stars.

Thirty-one spectrograms have been obtained at Mount Wilson since 1934 (see Table 2). The phases are derived from Plaut's elements. All plates have a dispersion of about 70 A/mm at $H\gamma$, except four with 35 A/mm and three, taken at minimum, with 120 A/mm.

The spectral type of the more massive primary star is G2 with numerous well-defined lines. The radial velocities are satisfactory, considering the dispersion used.

The lines of the secondary star are extremely weak and uncertain. Only a few of the

* *Contributions from the Mount Wilson Observatory, Carnegie Institution of Washington*, No. 654.

[1] *Harvard Circ.*, No. 194, 1916.

[2] *Nishni-Novgorad, Veränderliche Sterne*, **4**, 235, 1934; *Bull. Astr. Inst. Netherlands*, **9**, 122, 1940.

[3] *Bull. Astr. Inst. Netherlands*, **9**, 121, 1940.

TABLE 1

PHOTOMETRIC RESULTS BY PLAUT

Elements	Uniform	Darkened
Radius of small bright star	0.125	0.148
Radius of large faint star	0.228	0.231
Inclination of orbit	83°.5	82°.2
Ratio of surface brightness	6.73	6.99
Difference in photographic magnitude	0.73 mag.	1.14 mag.
Duration of eclipse	0.109 per.	0.116 per.

TABLE 2

RADIAL VELOCITIES OF WW DRACONIS

Plate	JD 242	Phase	Primary		Secondary		Emission *H* and *K*	
			Vel.	Wt.	Vel.	Wt.	Vel.	Wt.
		days	km/sec		km/sec		km/sec	
C 6472	7643.663	2.920	+ 42.3	0.7	.....	.....	− 93	0.2
6501	7670.642	2.121	− 47.3	1.0	.....	.....	.....	.....
6504	7671.638	3.116	+ 50.7	1.0	.....	.....	.....	.....
6656	7908.866	4.236	+ 3.5	0.3	.....	.....	.....	.....
γ 20741	7913.815	4.555	− 17.2	1.0	.....	.....	.....	.....
C 6689	7963.667	3.482	+ 56.8	1.0	.....	.....	−105	.6
6696	7965.662	0.848	−105.8	1.0	+ 95	0.3	+ 51	.4
6748	7992.672	0.080	− 33.6	1.0	.....	.....	− 23	.2
6752	7993.660	1.068	−109.9	1.0	+133	0.7	.....	.....
γ 20950	8232.905	4.204	+ 24.9	1.0	.....	.....	.....	.....
C 6917	8316.733	0.070	− 39	0.4	.....	.....	.....	.....
γ 21118	8582.010	1.462	−106.8	1.0	+116	0.3	+ 36	.2
C 7009	8613.047	0.091	− 38	0.6	.....	.....	.....	.....
γ 21127	8647.894	2.531	+ 5.1	1.0	.....	.....	.....	.....
21132	8648.847	3.484	+ 59.4	1.0	−155	0.3	.....	.....
C 7059	8700.969	0.051	− 34	0.6	.....	.....	.....	.....
γ 21159	8734.733	1.408	−116.4	0.5	+119	0.5	.....	.....
21162	8735.686	2.360	− 27.1	1.0	.....	.....	.....	.....
21203	8764.710	3.607	+ 57.8	1.0	.....	.....	.....	.....
21208	8765.769	0.037	.....	.....	− 24.3	1.0	.....	.....
21304	8997.984	0.773	−109.7	0.5	.....	.....	.....	.....
21970	9450.927	0.017	.....	.....	− 24.9	1.0	− 33	.6
21973	9451.750	0.840	−103.5	1.0	+139	0.3	+ 51	.6
22094	9504.751	2.916	+ 43.4	1.0	−138	0.3	− 82	.4
22847	9856.699	3.015	+ 41.4	1.0	−141	0.3	− 88	.4
E 108	0119.984*	2.404	− 30.7	1.0	.....	.....	.....	.....
γ 23379	0120.962	3.382	+ 53.9	1.0	−178	0.3	−125	.6
23381	0121.767	4.187	+ 4.9	1.0	.....	.....	− 76	.4
E 142	0147.670	2.322	− 33.3	1.0	.....	.....	.....	.....
γ 23448	0150.911	0.934	−113.1	1.5	+ 89	0.7	+ 64	.4
23452	0151.889	1.921	− 72.8	1.0	.....	.....	+ 18	0.4

* JD 243.

stronger ones can be discerned, and the velocities derived from them should be accepted with caution. Fortunately, the principal eclipse is total or nearly so, and the spectrum of the fainter, less massive star can be clearly seen at the time of minimum light. The spectral type at this phase is K0.

In Figure 1 the individual observations are plotted. The velocity-curves represent the course of the changes in velocity during the period from minimum to minimum. The elements of the spectrographic orbit deduced from the observations outside eclipse with the aid of a least-squares solution are:

$$\begin{aligned} e &= \quad 0.0 \text{ (assumed)} \\ \gamma_1 &= -\ 28.5 \pm 0.9 \text{ km/sec} \\ K_1 &= \quad 86.8 \pm 1.1 \text{ km/sec} \\ K_2 &= \quad 147.6 \text{ km/sec} \\ a_1 \sin i &= 5{,}526{,}000 \text{ km} \\ a_2 \sin i &= 9{,}396{,}000 \text{ km} \\ m_1 \sin^3 i &= 3.9\odot \\ m_2 \sin^3 i &= 2.3\odot \end{aligned}$$

Using $i = 83°.5$, $k = 0.55$, and $r_2 = 0.228$ from Plaut's uniform photometric solution, we derive the following absolute dimensions of the system:

$$\begin{aligned} a_1 &= \text{Semimajor axis of primary orbit} = 5{,}561{,}000 \text{ km} \\ a_2 &= \text{Semimajor axis of secondary orbit} = 9{,}457{,}000 \text{ km} \\ a_2 + a_2 &= \text{Semimajor axis of relative orbit} = 15{,}018{,}000 \text{ km} \\ r_1 &= \text{Radius of primary bright star} = 1{,}880{,}000 \text{ km } (2.7\odot) \\ r_2 &= \text{Radius of secondary faint star} = 3{,}420{,}000 \text{ km } (4.9\odot) \\ m_1 &= \text{Mass of primary star} = 4.0\odot \\ m_2 &= \text{Mass of secondary star} = 2.3\odot \\ \rho_1 &= \text{Density of primary star} = 0.20\odot \\ \rho_2 &= \text{Density of secondary star} = 0.02\odot \\ M_1 &= \text{Absolute visual magnitude of bright star} = +3.2 \\ M_2 &= \text{Absolute visual magnitude of faint star} = +3.2 \end{aligned}$$

The absolute magnitudes are computed from the formula

$$M = \frac{29500}{T} - 5 \log r - 0.08 ,$$

temperatures of 5400° and 4400° being assumed for the spectral types G2 and K0, respectively. The equality of the absolute magnitudes determined in this way is not in agreement with the difference in apparent magnitude indicated by the light-curve. This discrepancy could be avoided by taking a larger value of k (the ratio of the diameters), but this value is closely defined by the photometric solution. The spectroscopic absolute magnitudes determined by the use of subgiant tables are +1.5 and +2.1 for the brighter

and fainter components, respectively. Both methods give considerably lower luminosities than those derived from Eddington's mass-luminosity-curve with the masses obtained from the velocity-curves. It is admitted that the masses are uncertain on account

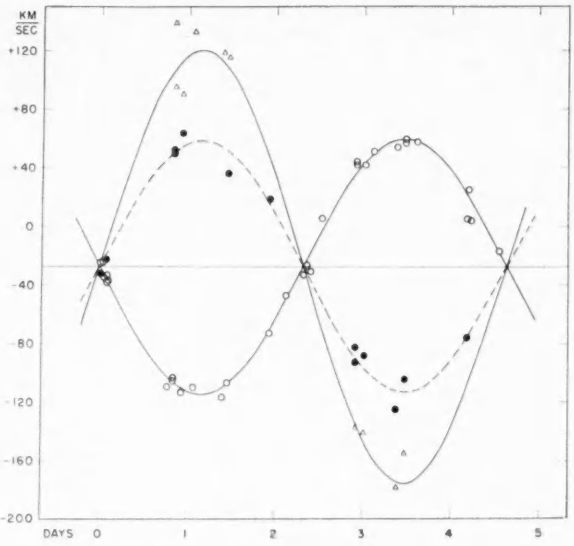

FIG. 1.—Velocity-curves of WW Draconis. The circles, triangles, and dots represent, respectively, the observed radial velocities of the primary, the secondary, and the calcium emission (H and K).

TABLE 3

RADIAL VELOCITIES OF ADS 10152 B

Plate	JD 242	Vel.	Wt.
γ 20742	7913.861	−27.5 km/sec	1.0
C 7101	8763.744	−33.8	1.0
γ 22740	9804.774	−31.4	1.0
22846	9856.660	−41.1	1.0
23382	0121.883*	−30.5	1.0
E 143	0147.890	−43.4	1.0
148	0148.882	−29.8	1.0
γ 23457	0154.882	−29.4	1.0
E 169	0177.677	−36.7	1.0
Mean	.....	−33.7	.....

* JD 243.

of the weakness of the lines of the secondary component. On the other hand, since K_1 is well determined, K_2 would have to be much reduced in order to satisfy the mass-luminosity relationship; and the masses would become nearly alike, which seems improbable without equal luminosities and approximately equal spectral lines. Thus it appears impossible to reconcile the luminosities with the mass-luminosity-curve.

The strongly exposed spectrograms show fairly narrow single emission H and K lines of ionized calcium. As shown in Figure 1, these emission lines are displaced in the same direction as the absorption lines of the secondary component. They can be represented by a velocity-curve with a semiamplitude of 86 km/sec. A possible explanation of this extraordinary behavior is that the secondary star is surrounded with an envelope of calcium gas which is greatly extended in the direction of the primary by tidal attraction. Since the center of the envelope is nearer the center of mass of the system, it describes a smaller orbit and has a lower velocity than the secondary star. This theory is supported to some extent by the fact that the emission lines are weaker at the phase of secondary minimum when the primary star eclipses much of the gaseous material lying between the two bodies.

ADS 10152 B.—Nine spectrograms of the northern star of the visual pair are listed in Table 3. The range in velocity, while somewhat more than would be expected from good plates with a dispersion of 70 A/mm, is hardly enough to make it certain that the star is a spectroscopic binary. The mean velocity of -33.7 km/sec differs somewhat from the γ-velocity of WW Draconis, -28.5 km/sec; but, since with a proper motion of $0''.07$ no change of position angle or distance has occurred in one hundred years, there can be little doubt that the visual binary is a physical system. The angular distance between the two components is $8''.0$. The spectral type of the northern star is F9; the spectroscopic absolute magnitude, $+2.2$.

CARNEGIE INSTITUTION OF WASHINGTON
MOUNT WILSON OBSERVATORY
August 1941

STELLAR RADIOMETRIC EQUIPMENT OF THE HARVARD COLLEGE OBSERVATORY

THEODORE EUGENE STERNE AND RICHARD MAURY EMBERSON

ABSTRACT

Stellar radiometric measurements have been made at the Oak Ridge station of the Harvard College Observatory. The radiometric equipment consists of vacuum thermocouples at the Newtonian focus of the 61-inch Wyeth reflecting telescope; the electrical leads; the moving-magnet galvanometer; the automatic recording mechanism; and certain auxiliary devices. In this paper the equipment is described. A concise account is also presented of the theory of the design of the electrical circuit that is necessary to obtain a high and usable sensitivity; instructions are provided for making the small thermocouples; and the reasons are stated which determined the choice of a galvanometer of the moving-magnet rather than of the moving-coil type.

INTRODUCTION

Thermoelectric measurements of stellar radiation have been made at the Oak Ridge Station of the Harvard College Observatory. Vacuum thermocouples were mounted on the Wyeth telescope, a 61-inch reflector. The observations themselves will be reported upon in another paper by Emberson; here we describe briefly the apparatus that has been employed and some of the problems of design that were involved in the construction of the apparatus.

The electrical parts, essential to the apparatus, consist of the thermocouples, the lead wires, and the galvanometer. Each of these parts will be described, along with its necessary auxiliary apparatus.

THE THERMOCOUPLES

Of the stellar radiation falling upon either of the thermocouple receivers, some is reradiated by both receivers and some is conducted away along the electrical wires. The loss by conducting may be diminished by lengthening the wires or by making them thinner; but the electrical resistance of the circuit is thereby increased, and there comes eventually a stage beyond which any further lengthening or thinning of the wires results in a diminished galvanometer deflection. For a given amount of radiation, concentrated within a given area, the problem is to achieve the largest usable deflection; and obviously there is a best shape of wire. In addition there is a loss of heat by radiation from the wires themselves. This loss can be made as small as possible by diminishing the cross-sectional area of each wire and its length, in the same proportion, so as not to alter the total conductivity. The wires should also be bright, so as further to diminish the radiation from their surfaces; and short, thin wires have the further advantage of rapidly reaching a steady thermal state after the image of a star has been brought to one of the receivers. Both cross-sectional area and length should be as small as possible, and the cross-section should be circular in order to yield the smallest radiating surface for a given cross-sectional area.

If the galvanometer is of the moving-magnet type, the resistance of its windings, for greatest efficiency, is determined by the resistance of the thermocouples. Then it is known that the deflection per unit current varies as the square root of the resistance of the thermocouples or perhaps more nearly—if account is taken of the thickness of insulation on the galvanometer's windings—as the two-fifths power of the resistance of the thermocouples. The one-half-power law was used. One should consider that, except for the variations of the resistance of the windings of the galvanometer, the remaining design of the galvanometer is not varied. If the galvanometer is of the moving-coil type, it must

be critically damped for highest efficiency, and its indications must be amplified in some manner before the same sensitivity can be reached as with a moving magnet. Then, in the limit of small deflections comparable in size to the Brownian motion, the smallest measurable voltage varies very nearly as the one-half power of the thermocouple resistance. In a real sense, then, the deflection of a moving-coil galvanometer for a unit current varies as the one-half power of the resistance of the thermocouples, and thus the problem of the design of the thermocouples is nearly the same with a moving coil as with a moving magnet. It is not quite the same, however, because there are practical difficulties in designing moving-coil galvanometers for very low or for very high external resistances which do not arise with moving magnets.

The theory of the design of thermocouples, nearly appropriate to the present problem, was given by Johansen.[1] We give the theory here in our own notation, in a form slightly better adapted to our particular problem, in which there must be two thermocouples, each with its own receiver, in order to balance the electrical circuit and avoid the ill effects of radiation from the sky. The important point is that the radiation to be measured is concentrated into a limited area. A receiver does not need to be much larger than this area; and, if the receiver is too large, the re-radiation losses will be increased, and there will be a loss of sensitivity. If the receiver is too small, on the other hand, the star's image will wander about, from unsteady seeing and imperfect guiding, sufficiently to produce an irregular and unmeasurable deflection of the galvanometer. Thus, the receiver has a certain best diameter which, at the Newtonian focus of the Wyeth telescope, was found to be about 0.48 mm. Receivers 0.16 mm in diameter were found to be definitely too small; and, while those 0.48 mm in diameter may be a trifle larger than is necessary, any considerable reduction below 0.48 mm would greatly increase the difficulty of guiding and diminish the number of usable nights. For stellar measures the receivers should be thin circular disks whose unused sides may well be bright so as to diminish re-radiation.

Denote the area of a receiver, effective for re-radiation, by A. Attached in linear order to a massive lead (whose temperature we call zero) are a length l_1 of wire of metal 1, then a receiver, of area A, then a length l_2 of metal 2, then another receiver, of area A, and then a length l_1 of metal 1. The last wire is attached to another massive lead at temperature zero. The radii of the wires are r_1, r_2, r_1, respectively; the thermal conductivities of metals 1 and 2 are k_1 and k_2; the electrical resistivities are e_1 and e_2. The wires are bright, and radiation from them is considered to be negligible and is here neglected. The energy radiated in one second from a receiver at a temperature T is AHT, where H is a constant whose value, determinable from Stefan's law, is 1.47×10^{-4} cal/cm^2 sec °C at ordinary temperatures. Thus, if an amount of heat Q is absorbed per second by receiver A from a star image focused upon it, we can easily show that the difference between the temperatures, T_A and T_B, of the two receivers is

$$T_A - T_B = \frac{Q}{xk_1 + 2yk_2 + AH},$$

Where $x = \pi r_1^2/l_1$ and $y = \pi r_2^2/l_2$. The resistance, R, of the thermocouple system, is obviously given by

$$R = \frac{2e_1}{x} + \frac{e_2}{y}.$$

If Q, A, and the natures of metals 1 and 2 are fixed, the deflection of the galvanometer varies as $(T_A - T_B)/R^{1/2}$, and the deflection is greatest when x and y have values such as

[1] *Ann. d. phys.*, **33**, 517, 1910.

to make $R/(T_A - T_B)^2$ a minimum. It is readily found that the best values of x and of y are

$$\left.\begin{aligned} x &= \frac{HA}{k_1 + \sqrt{\frac{e_2 k_1 k_2}{e_1}}} \\ y &= \frac{HA}{2\left(k_2 + \sqrt{\frac{e_1 k_1 k_2}{e_2}}\right)}; \end{aligned}\right\} \tag{1}$$

and, if the dimensions of the wires conform to these conditions, then the deflection is proportional to

$$\frac{(T_A - T_B)E_{1,2}}{R^{1/2}} = \frac{QE_{1,2}}{2\sqrt{2}\,(HA)^{1/2}} \cdot \frac{1}{\sqrt{e_1 k_1} + \sqrt{e_2 k_2}}, \tag{2}$$

where the factor of proportionality depends only on the design of the galvanometer, of which the winding is supposed to have been properly chosen. The symbol $E_{1,2}$ denotes the thermoelectric power of the combination of metals 1 and 2. Not only are the values of x and y given by equation (1) the best values, but they also are values such that considerable departures from them, either way, will result in only small diminutions of the deflection.

From the Wiedemann-Franz law one would expect the denominator of the right-hand member of equation (2) to be insensitive to the choice of metals; and according to the law in question one would therefore employ the metals with the largest $E_{1,2}$. Some alloys, however, yield enormous $E_{1,2}$'s but are nearly perfect insulators, and violate the Wiedemann-Franz law, so that for them the denominator is large enough to offset the advantage of a large value of $E_{1,2}$. It is best to use known values of $E_{1,2}$ and of the e's and k's, in choosing the metals; and it is unwise to rely on the Wiedemann-Franz law. Pettit and Nicholson[2, 3] in their thermocouples, used wires of bismuth and of bismuth-tin alloy. These metals are good, but the $E_{1,2}$ is critically dependent upon the composition of the alloy. It was therefore decided to use pure antimony as metal 1 and pure bismuth as metal 2, in order to avoid uncertainties of composition.

Aside from the presence of the factor $A^{1/2}$ in the denominator of equation (2), which renders it advantageous to keep the receivers as small as is consistent with the difficulties of guiding and with the conditions of seeing, small receivers have other advantages. They cause the optimum resistance of the thermocouples to be high; in ours the actual resistances have been of the order of 100 ohms or more. A high resistance diminishes the ill effects of parasitic electromotive forces, which arise wherever in the electrical circuit there is a contact between two dissimilar metals or between two different specimens of the same metal that contain slightly different amounts of impurities and wherever there are, simultaneously, gradients of temperature and of composition along the electrical leads. A high resistance also allows the use of conveniently thin, flexible, and long lead wires to connect the thermocouples to the galvanometer.

It can be shown that with receivers as small as ours and of a fixed size no gain can result from the employment of more than a single thermojunction to a receiver.

[2] *Ap. J.*, **56**, 295, 1922. [3] *Ibid.*, **68**, 279, 1928.

THE CONSTRUCTION OF THERMOCOUPLES

The method of constructing very small thermocouples is of sufficient interest to merit a rather detailed description. In general it is necessary that the workroom be free of insects and drafts, that the illumination be good, and that the worker be equipped with at least average eyesight and muscular control and a great deal of patience. Surface tension plays an important role in the manipulation of very small objects; sometimes it may be used to advantage; frequently it is only troublesome. The use of a micromanipulator has been suggested. This would not eliminate the surface-tension difficulties, and, as there was never a need for exceedingly fine control of the motions of the various small parts, all the work has been done by hand, aided only by several tools and a binocular microscope. This instrument should have a power of 10–15, a working distance of at least 1 inch, with a field diameter of about 1 cm, and an adjustable support such that the work may be done on a flat table top. The various parts of the thermocouples were assembled on microscope slides. It was convenient to have these on a small piece of glass, about 5×7 inches, backed by a piece of white paper to provide a bright background; with this arrangement, it is possible to shift quickly from one slide to another without changing their relative position.

The fine wires were prepared by the Taylor[4] process. For a typical case the diameters were 7 μ. The presence of oxide or other surface films on the wires makes soldering rather difficult. Such surface coatings may be prevented, to a large extent, by mixing some borax with the powdered metal to be drawn, by using a glass of low melting-point, and by cleaning off the glass only a short time (several days) before the wires are to be used.

After the glass was removed, the wires were washed with water and alcohol and stored on glass slides. As needed, wires of the specified diameters were selected with the aid of a microscope and micrometer eyepiece, cut to the desired lengths, refloated in alcohol, and drawn off the edge of the slide. A special tool was needed to handle the fine wires, receiver disks, or bits of solder. This tool consisted of a small needle stuck into a handle, such as a penholder; the point was hammered and polished so as to form a small spade. If such a spade is touched with the fingers, enough grease will remain so that any small object will cling to the spade rather than to a clean surface. The following procedure was found to be very successful for moving the fine wire segments from one slide to another. The wire-slide was flushed with alcohol so that the liquid stood out to the edge of the glass; the wire was moved over near and perpendicular to the edge; the spade was slipped under the end of the wire and the end brought out a millimeter or so from the edge of the slide; the spade was then contaminated a bit, the free wire-end picked up, and the section of wire slipped off the slide.

One side of each receiver disk was blackened and the other left bright. As the thermocouples were mounted in an evacuated cell, the bright surface did not tarnish. The only requirements of the metal for the disks are that it be fairly ductile, that it solder easily, and that its melting-point be well above that of the solder. Our disks were made of copper. Sections were cut from a piece of bare copper wire, size 36 or smaller; the small sections were pressed between two pieces of polished steel until disks of the desired diameter were formed. With a little practice such sections may be cut to a thickness of only a fraction of the wire diameter; the pressed disks will then be only a few microns thick. The disks should be made as light as possible so that the finished thermocouples will not be so likely to be broken by jars or vibrations and the heat capacity of the system will be small.

Near the center of a carefully cleaned slide, two pressed disks were placed and wetted with flux. A piece of millimeter cross-section paper placed under the slide provides a method of sufficient accuracy for adjusting the separation of the disks to the specified distance. A piece of paper, cut to a point and held in a penholder, was useful for the

[4] G. F. Taylor, *Phys. Rev.*, **23**, 655, 1924.

application of flux. Our flux was zinc dissolved in hydrochloric acid and mixed with ammonium chloride in the ratio of 3:1 to form a eutectic mixture; this has a lower melting- or fluxing-point than the simple and widely used flux of zinc in hydrochloric acid.

The next step was to place a piece of bismuth wire across the two disks. The wire section was removed from the storage slide, as described above, the free end was laid across one of the wetted disks, and the other end was brought down over the second disk and freed by twisting the spade. If the wire projected up in the air above the disk, the spade was washed with alcohol and, when dry, was used to push the free end of the wire down upon the disk.

The antimony wires were then placed in position. One wire was cut 2 or 3 mm longer than the specified length; the second wire was cut perhaps 1 mm too long. These wires were handled in exactly the same manner as the bismuth wire. The job was simpler, however, as only one end of each wire needed to be placed on a disk. As far as possible, the ends of the wires were kept parallel, close together, and centered across the disks.

Finally, a small shaving of solder was laid across each disk. The choice of solder is rather important. Originally, ordinary lead-tin solder was tried. When such a solder melts, it dissolves the ends of the bismuth wire. The difficulty was overcome by using a solder that is saturated with bismuth even when heated quite a few degrees above the softening-point. The exact composition is not important. For practical reasons, the melting-point of the solder should be above that of the flux and below that of pure bismuth. A bismuth-tin solder made of 70 per cent bismuth and 30 per cent tin satisfies these requirements.[5]

Heat for soldering was obtained from a small electrically heated loop of Nichrome wire; a small transformer with voltage taps permitted sufficient control of the current. The slide with the assembled thermocouple was first gently heated; without this preliminary warming, the slide sometimes cracked with intense local heating. The hot Nichrome loop was then placed directly beneath the junction to be soldered. After a few moments the flux and then the solder would melt, and the hot loop was then removed. Frequently the solder melted and drew up into a sphere without wetting either the wires or the disk. Under such circumstances it was found best to replace the sphere with a new shaving of solder. The flux is somewhat hygroscopic. If one breathes on it gently, it will become fluid again after being heated, and it may not be necessary to add more flux. Usually only a few trials were needed for a successful soldering operation; the second junction was then completed. The junctions were washed carefully and were finally left in an atmosphere of alcohol. Surface tension may prove troublesome during the washing process; one must proceed slowly.

Usually the finished thermocouple will stick to the slide at one or two places. It may be held by flux, which is soluble in water; by grease, which is soluble in alcohol; or by a combination of the two. One should try to free the system first while it is in a water atmosphere, as there is almost sure to be some flux holding the system at the receiver disks. The procedure is as follows: Free the antimony wires first; start at the outer ends and work in. Next, free the bismuth wire; start at the center and work out toward the receivers. Finally, loosen the receivers. When trying to free the system, one should try to constrain the motions or forces to a direction more nearly parallel than perpendicular to the wires. A single fiber on the end of a strip of filter paper is a rather effective and yet safe tool for freeing the thermocouple system. It may be necessary to use the stronger spade tool at the more obstinate spots, especially at the receiver disks. Eventually the thermocouple system will be freed; it then should be kept floating in an alcohol atmosphere until transferred to the final support.

The thermocouple cell, mounting, radiation shields, and other accessories will be described in considerable detail in later paragraphs. We need discuss here only the ther-

[5] *International Critical Tables*, 2, 416.

mocouple support. The cell is fitted with a plug, ground to a standard taper. Two No. 23 copper wires are sealed through the plug. These two support wires are cut off so that one will project only a few millimeters, and the other 2 cm or more, into the cell. To the ends of these wires are soldered short lengths of No. 36 copper wire. These small pieces are then bent around, so that the distance between their free ends equals the specified overall length of the thermocouple system, and the ends are tinned. As far as possible, the ends of the support wires also should be adjusted so as to lie in the focal plane of the telescope when the cell is mounted in the tailpiece. With our system of mounting, vibration of the support wires had little tendency to stretch and compress the thermocouples longitudinally, but rather produced a slight tilting motion.

The next step was to transfer the thermocouples to the final support. The support plug was held in a clamp so that the ends of the support wires were approximately horizontal. The slide, on which the thermocouple system was floating in alcohol, was built up on blocks to be at the same level as the support wires.

To move the thermocouples, a special transfer apparatus was needed, which consisted of a small piece of thin glass, about 5×10 mm, mounted on the end of a short metal rod; half the rod was milled off near the end so that one surface of the glass was very close to the axis of the rod. The other end of the rod was held in a small clamp that permitted rotation of the rod about its longitudinal axis; the height of the clamp was such that the axis of the rod was at about the same level as the support wires when the plug was mounted in its clamp.

In the same manner as that described for floating single wires off a slide, the thermocouples were removed from their slide, the only difference being that the longer end wire of the thermocouple was picked up on the transfer apparatus rather than on the spade tool. To accomplish this, a drop of alcohol and a bit of resin were placed on the glass part of the transfer apparatus, and the wet surface was brought up under the projecting free end of antimony wire. When the alcohol evaporated, the resin held the end of the thermocouple system. The system was then removed from the large slide, which was kept well wetted with alcohol. When the thermocouples were in free air, supported only from one end, the weight of the wires and disks caused the system to droop. Under such circumstances there is little danger of breakage if precautions have been taken to keep the mass of the disks and solder as small as possible.

The next step was to solder the free end of the thermocouple system to the shorter support wire. The end of this wire was wetted with flux, and the thermocouples were moved up alongside the support. When necessary, the rod of the transfer apparatus was rotated somewhat so that the surfaces of the receiver disks would be parallel to the focal plane of the telescope. With the needle tool the end of the antimony wire was laid up on top of the support wire, and then the transfer apparatus was moved away from the support, in a direction parallel to the system, until the receiver disks were centered between the end supports. The antimony wires were thus automatically adjusted to the specified length. The connection was soldered, after a shaving of solder was laid over the wires, heat for the operation being applied with the small Nichrome loop. When the first end connection was completed, alcohol was put on the resin-covered surface of the transfer apparatus, so that the other end of the thermocouple system could be freed and the transfer apparatus removed. The second end connection was made in the same manner as the first, and both were then thoroughly washed.

The front surfaces of the receiver disks were blackened by Pfund's[6] method. An alloy of zinc *plus* a small trace of antimony was used. In order to get a good coat it was necessary to place a massive piece of metal very close beneath the light receiver disks. A shield was used to keep the black off the support plug and the wires and parts of the thermocouple wires.

[6] *J. Opt. Soc.*, **23**, 375, 1933.

THE THERMOCOUPLE CELL

The pyrex glass thermocouple cell had the shape and dimensions of a rather thick pocket watch. There were two half-inch openings, at the centers of the front and back, and three appendages. Of these, the top one was ground to receive the thermocouple support plug; one side tube, of relatively large diameter, was provided for an out-gassing agent, and the opposite one was the seal-off tube, by means of which the cell was connected to the vacuum pumps. The reasons for using a small cell were twofold. First, the cell was mounted in the double-slide plateholder of the telescope, which could be done easily only if the dimensions of the cell and mounting were limited to the size of a normal photographic plateholder (4×5 inches). Second, and of greater importance, it is advantageous to maintain the entire thermocouple cell at a uniform temperature; hence a small cell is decidedly to be preferred.

A piece of optical fluorite[7] was cemented to the cell for the front window; a piece of glass served at the back. The fluorite was cemented to the cell in an oven in order that everything could be at a high but uniform temperature and thus decrease the chances of cracking the crystal. A small open flame was used in mounting the glass window and the support plug. Apiezon wax W proved to be satisfactory for all this work.

Because of the presence of the fluorite window, the several wax seals, and the low melting-point of the thermocouple system itself, it was impossible to out-gas the entire thermocouple cell by heating it while it was on the pumps. Activated charcoal proved to be quite satisfactory as an out-gassing agent, even superior to metallic calcium. The charcoal in the side tube was separated from the body of the cell by a plug of glass wool. While the cell was being pumped out, the side arm was heated to about 300° C and kept there until most of the gas had been driven off the charcoal. If it was necessary to open the cell for any reason, the charcoal was not cleaned out but was only reheated when the cell was again pumped out.

The support plug merits a detailed description. There are obvious reasons for having a homogeneous copper circuit from the thermocouples to the galvanometer. All glass-to-metal seals, except possibly copper-glass, are thus eliminated. But it was decided that the actual process of sealing the copper wire into the glass might conceivably alter its physical properties sufficiently to introduce troublesome thermojunctions into the circuit.

Our plug was made hollow; the outer end terminated in two tubes, forming a Y. The inner end was sealed across, just below the ground joint, except for three small holes. One of these holes was left entirely open; and the plug was evacuated through it. The lead, or support, wires, mentioned in previous sections, fitted rather tightly in the other holes. The wires passed through and out of the plug, one in each branch of the Y; they were soldered through small copper caps which, in turn, were waxed in place over the ends of the Y. This manner of sealing the wires into the cell has never caused any trouble.

Originally the seal-off tube was fastened to the pumping system by a glass-to-glass seal, and the cell was sealed in the usual manner. Several attempts to open the cell by breaking off the tip of the seal-off tube all resulted in a broken thermocouple system. It was decided, therefore, to place a small stopcock in the seal-off tube and to wax its end to the vacuum pumps. A grease compounded of Apiezon grease N and wax W, of such proportions that the small stopcock is held rather firmly at normal room temperatures, has been very satisfactory for the stopcock.

The thermocouple cell was mounted in a box of aluminum, with outside dimensions of $3\times3\times1$ inches; the walls were about $\frac{1}{8}$ inch thick. Inside were layers of asbestos, copper, and loose wool packing. A filter-holder was mounted on the front of the box. The holder was a large, thin gear wheel pivoted below the center of the box; six evenly spaced holes

[7] Professor Theodore Lyman very kindly supplied us two fluorite windows.

were drilled through the gear and a short length of ½-inch tubing was soldered over each. Filters could be mounted in these short tubes. A knob, with six deep-cut graduations in the rim, against which an index arm bears, was mounted on the back of the box. A shaft from this knob passed through to a pinion at the front of the box. The pinion and the large filter-holder gear were constantly in mesh; they were of such sizes that the gear ratio was exactly 7:1. As one and one-sixth rotations of the knob would be required to move from any one filter opening to the next, if the filter-holder were turned so that there was a full clear aperture for the thermocouples, one could tell from the graduated knob, without any ambiguity, which filter opening was being used. An eyepiece, in focus on the thermocouples, was mounted at the center of the back of the box.

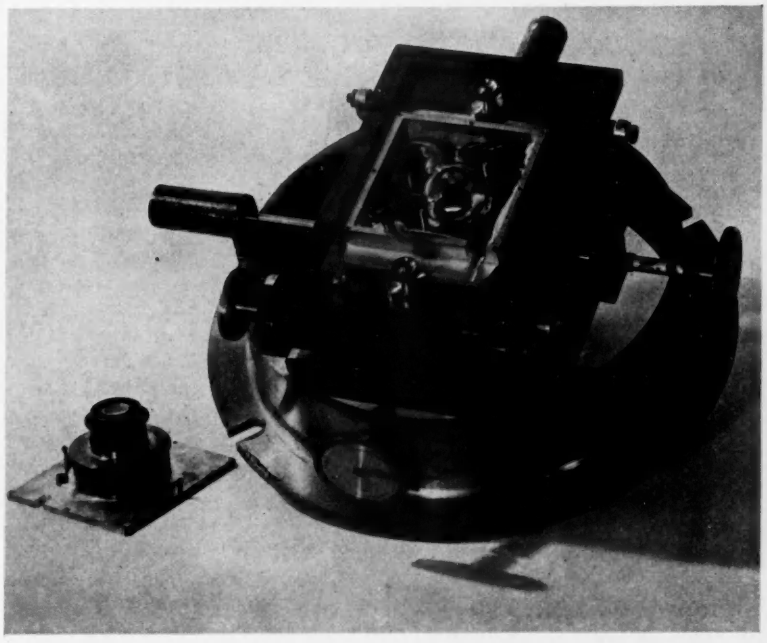

FIG. 1.—Thermocouple cell mounted in cell box in double-slide plateholder. The eyepiece and packing have been removed; the galvanometer cable would terminate in the copper junction box shown in the upper right-hand corner of the cell box.

The thermocouple box was clamped to an adapter plate that fitted on the double-slide plateholder. This adapter itself had a quick motion in the vertical direction with a range of a little more than ½ inch; the fast motion was used to shift a star image from one thermojunction to the other. The fine motions of the double-slide plateholder were used only for guiding out small irregularities.

THE RADIATION SHIELD

It was found that motion of the thermocouple assembly up and down in the telescope, even through the small distance necessary to transfer the star image from one receiver to the other, resulted in a measurable deflection in the absence of any star. This was attributed to the effects of radiation coming from the holder of the Newtonian flat, situated 2 feet in front of the thermocouples. As the couples were moved up and down, they were exposed to slightly different portions of the metal rim of the flat-holder. The effect was

almost completely eliminated by the installation of a radiation shield, containing black diaphragms and constructed wholly of heavy copper, placed in front of the thermocouple cell. The shield was so disposed that all the starlight coming from the flat, but no radiation from the metal rim of the flat, could reach the receiver. However, to insure against any minute residual effects, it was the practice when measuring the faintest images to move them from receiver to receiver, not by a motion of the receivers relative to the telescope (the simplest procedure), but by moving the whole telescope, receivers and all, without any displacement of the receivers relative to the flat.

When the observer looked into the eyepiece, his warm breath, plus direct radiation, slightly warmed the thermocouple box and produced small disturbances. A light-weight shield clipped to the back of the box was effective in removing this trouble.

THE ELECTRICAL LEADS

The leads, which connect the thermocouples to the galvanometer, are an important part of the apparatus. It is necessary to connect the thermocouples to the galvanometer, at a distance from them, in a way that does not introduce parasitic thermal electromotive forces, electromagnetically induced currents, or electrostatically induced currents. The galvanometer can easily detect 10^{-11} ampere or 10^{-9} volt.

To avoid as far as possible the ill effects of unnecessary thermojunctions in the circuit, the entire circuit, with the exception of the galvanometer windings and the thermocouple wires, was made of No. 23 copper wire from a single manufacturer's spool. The only joints were soldered joints in the thermocouple assembly, to enable the assembly to be removed from the lead wires when necessary. From these joints wires (from the same spool) ran into the vacuum through high-vacuum wax. The soldered joints that have been mentioned, from copper to copper, were placed side by side within a cavity inside a little copper block mounted in the aluminum cell box, to equalize temperatures. The other ends of the long lead wires were connected directly to the copper terminals of the galvanometer and were protected with cotton wool. The length of the leads was about 100 meters, and their combined resistance was 12 ohms. The entire electrical circuit, except for the thermocouple metals but including the galvanometer connections and windings, was of copper.

The two wires of the leads, which were insulated with enamel and silk, were twisted together to avoid electromagnetic induction and were insulated, after twisting, by woven fabric and many layers of lacquer. They were then inclosed in electrostatic shielding for the whole of their length. The rigid portions were inclosed in copper tubing, the flexible portions in rubber tubing which, in turn, was inclosed in flexible braided metal shielding. The whole 100 meters of shielding were made into a single conductor by soldering all the joints between the braid and the copper tubing, and the shielding was then grounded at one point, and at that point only. To prevent earth currents from flowing along the shielding and inducing electrostatic charges on the lead wires, the shielding tube of copper was heavily insulated with varnished tape for its entire length, while the flexible, braid-covered portions of the leads were inclosed in an insulating and waterproof covering of heavy but soft rubber tubing, placed outside the braid. Since, without special precautions, the taped portions of the shielding would soon have deteriorated from moisture, the assembly was protected by an outer layer of copper pipe, with tight joints, where it ran underground from the 61-inch building to the galvanometer house. Wherever the taped copper tube was above ground, as inside the 61-inch building and on the telescope, there was no copper pipe; instead, the tape was covered with a heavy coat of paraffin wax. The result was that the insulation on the shielding was thoroughly protected from moisture along its entire length, both under the ground and above it and along both its rigid and its flexible portions. There are three flexible portions: at the declination axis, at the polar axis, and at the upper end of the 61-inch telescope. The leads have func-

tioned perfectly through the several years since their installation, giving no trouble from electrostatic disturbances, from changes of temperature, from changing magnetic fields, or from water. There is considerable water of condensation at Oak Ridge, which would have caused serious trouble if not properly circumvented.

THE GALVANOMETER

We had the choice of using a moving-coil or a moving-magnet galvanometer. The former is generally regarded as being the more "stable," and so it usually is if it is used directly in the ordinary way without amplification and if no attention is paid to its sensitivity. But, used in the ordinary way, the moving-coil galvanometer is very much less sensitive—usually of the order of at least a hundred times—than a good moving-magnet galvanometer of the same period, adjusted to a circuit with the same external resistance. To obtain from the moving coil a usable sensitivity and one that is high enough for measuring stellar radiation, it is necessary to amplify the deflections by using a very long optical path or by using a secondary galvanometer. Pettit and Nicholson used a very long optical path with a moving-coil galvanometer. This procedure was not convenient for us; and amplification by a secondary galvanometer complicates the apparatus considerably and tends to introduce sources of instability. But in any case, once the deflections of a moving coil have been increased by any method sufficiently to compare favorably with the unamplified deflections of a moving magnet, the amplified deflection is hardly (if at all) more stable than the unamplified deflection of a moving magnet. Any slight tremor of the supports of an amplified moving-coil galvanometer results in a motion of the moving system which is amplified to the same degree as an electrical deflection. It was not considered probable that an amplified moving-coil instrument, used at the same sensitivity as an unamplified moving-magnet instrument, would be any more stable than the latter.

The damping adjustments of both moving-coil and moving-magnet galvanometers are easily made, the former by varying the magnetic-field strength, the latter by varying the adjustment of some damping vane close to the moving system; and there is little choice between the instruments with respect to damping. On the other hand, the period and sensitivity of a moving-magnet instrument can be very easily altered, whereas the period of a moving-coil instrument cannot. A moving-coil instrument usually involves in its electrical circuit more than one metal, while a moving-magnet instrument can have its entire circuit made out of copper and is thus less likely to be troubled by thermal electromotive forces arising from thermal inequalities within it. And, as a final mechanical advantage, the quartz suspension fiber of a moving magnet is completely free from even traces of elastic hysteresis.

With regard to ultimate sensitivity, both types of galvanometer are limited by the Brownian motion of the moving system, and their sensitivities as limited by Brownian motion are of comparable orders of magnitude; such advantage as exists is somewhat in favor of the moving coil. However, this statement refers to actual instruments; and the theoretical limiting voltage sensitivity has already been reached in actual moving-coil galvanometers, while there is no obvious theoretical limit to the smallest voltage that can be detected by a moving-magnet galvanometer. For any particular instrument the smallest voltage that can be detected is proportional to the Brownian motion of the moving system. No improvements in design can ever increase the ratio of the electrical deflection of a moving coil per unit of voltage to its Brownian motion for a given period and a given circuit resistance at a given temperature. But for a moving-magnet galvanometer under the same conditions it is conceivable that the ratio may be increased by changes in the design of the coils and of the moving system with new magnetic materials.

It was finally decided to use a moving-magnet galvanometer, and the instrument selected was of an improved Paschen type, made by the Cambridge Instrument Com-

pany. The galvanometer was well shielded magnetically by the makers' shield of sheet mumetal rolled spirally into a cylinder, and it had four coils of 250 ohms each. The coils were originally intended to be used in series with a thermocouple system having a resistance of the order of 1000 ohms; but when it was found that considerably larger receivers were necessary than had originally been anticipated, the coils of the galvanometer were connected in series parallel to give a resistance of 250 ohms. With the coils in series and the undamped period adjusted to 3.75 seconds, a deflection of 1 mm was produced at a distance of 1 meter by a current of approximately 2×10^{-11} ampere. One meter was the normal scale distance.

The Brownian motion[8, 9] of the galvanometer was measured by a series of readings on open circuit and was found to agree closely with the expected amount. The kinetic theory of gases shows that the root-mean-square deviation of the moving system, when the full undamped period is P and the absolute temperature is T, is $(P/2\pi)(KT/I)^{1/2}$ radians where k is Boltzmann's constant and I is the moment of inertia of the moving system. In a typical series the observed period of the galvanometer was 7 seconds, and the decrement was such as to indicate an undamped period of 6.0. The maker's value of I was approximately 6×10^{-6} gm cm^2, and T was approximately 300°. The expected standard deviation was, therefore, 0.00008 radians, or (there being a reflection) 0.16 mm at a scale distance of 1 meter. The observed value was 0.20 mm. A repetition, under the same conditions, yielded the value 0.17 mm. The observed average, 0.18 mm, agrees satisfactorily with the expected value. A deflection of 0.18 mm would have been produced at the same undamped period by 7×10^{-10} volt applied, without external resistance, across the galvanometer terminals with the coils in series parallel. This voltage was, roughly, the limiting voltage sensitivity of the galvanometer under such conditions.

The galvanometer was mounted upon a concrete pier, was covered with thick felt, and was further protected from changes of temperature by an outer wooden box. A thermostatic temperature control, initially installed, was discarded when it caused sinuous changes of the zero point. The galvanometer was sensitive to changes of temperature, and this sensitivity was found to be mechanical rather than electrical, since it was observed to occur on open circuit. A change in temperature changed the position of the control magnets relative to the moving magnets, thereby displacing the zero point. The same effect was noticed from minute changes in level, and drifts of the zero point were kept small by the firm pier and the thermal insulation. The galvanometer was very insensitive to tremors such as those caused by tapping on its case but was rendered useless, when placed on a concrete pier in Cambridge, by neighboring vehicular traffic. At Oak Ridge, traffic caused no observable trouble. Despite the magnetic shielding it was found that the rotation of the dome of the 61-inch telescope building caused troublesome changes of zero point and of sensitivity. The galvanometer was therefore placed in a wooden building, roughly 200 feet from the telescope, and no further magnetic difficulties were experienced.

At frequent intervals the departures of the response of the galvanometer from perfect linearity were electrically measured. Such departures were found to be so small that no significant errors could thereby be introduced into the radiometric magnitudes.

THE RECORDING APPARATUS

One important part of the instrumental equipment remains to be discussed—that for the observation and reduction of the galvanometer deflections. A brief outline of the observing procedure is needed to understand better the requirements of this apparatus.

With two opposed thermojunctions, general radiation from the sky or from the interior of the telescope turret is balanced out. Except for occasional small disturbances,

[8] Ising, *Phil. Mag.*, 1, 827, 1926. [9] Hill, *J. Sc. Instr.*, 4, 72, 1926.

the galvanometer is deflected only when more radiation falls on one thermojunction than on the other, e.g., when a star image is focused on one junction. A double-deflection method is used in which the star image is placed first on one junction and then on the other. As the junctions are opposed, the galvanometer will deflect in opposite directions at the two times. In our work we refer to this double deflection as simply "the deflection."

Although the zero position of the galvanometer is not recorded as such, nevertheless we are interested in the behavior of the zero point, both over a short time interval of a few minutes and over a longer interval of a night. The galvanometer is used at such high sensitivity that Brownian motion of the moving system is discernible. To this small random motion may be added larger drifts which may be neither periodic nor at random. These drifts are caused by magnetic storms, residual temperature changes at either the thermocouple box or the galvanometer, or a very small tilting of the galvanometer pier. In order to obtain a value of the deflection freed of these disturbances as far as possible, the star image is shifted back and forth at regular intervals from one junction to the other, and the corresponding positions of the galvanometer spot are recorded. We decided to use ten such readings. A larger number adds little to the accuracy, especially as the increased time interval needed for the observations may allow third- or higher-order terms of the galvanometer zero-point drift to become appreciable.[10]

When the star image is moved from one thermojunction to the other, 5 or more seconds are required for the thermocouples to come to thermal equilibrium. In order that all readings might be taken under exactly similar conditions, eleven readings were taken, and the first was discarded. At the beginning of the observational work the galvanometer readings were taken visually from a transparent celluloid scale, which was graduated in millimeters and supported from the galvanometer pier. Two observers worked together. One stayed on the observing platform near the Newtonian focus of the telescope. The other worked back and forth between the telescope and the galvanometer house. A telephone line between the observing platform and the galvanometer house provided a means of communication.

At the conclusion of the observation of a star the observer at the galvanometer house would return to the telescope building. The observer at the telescope would record the time of observation, the sky conditions, and the number, designation, and position of the star next to be observed. The observer below would then move the telescope to this new position, while the platform observer moved the turret and platform around. The telescope circles proved to be sufficiently accurate to place the object in the field of the finder. While the observer was returning to the galvanometer house, the platform observer would center the star for observation. With all in readiness, the observers would check the number of the observation; then the platform observer would place the star image on the lower thermojunction and start counting seconds in groups of fifteen, shifting the star image to the other thermojunction at the end of each group. At the count of fifteen the galvanometer observer noted and recorded the reading of the galvanometer spot. This procedure was continued until the galvanometer observer made known the fact that ten readings had been obtained. Then the whole cycle would be repeated for the next star.

This procedure had one distinct advantage. At the end of the night the actual numerical values of the galvanometer readings were recorded, ready for reduction. There were disadvantages, however. The recorded position was the more or less instantaneous value at the end of the 15-second interval and thus did not average out Brownian motion. Of more importance, there was no possibility of checking the galvanometer readings.

The photographic recorder built for this work could perform most of the duties of the

[10] T. E. Sterne, *Harvard Bull.*, No. 908, 1938.

galvanometer observer; it also relieved the telescope observer of the necessity of counting. The second observer had sufficient time to measure and reduce the records of the previous night in the intervals between settings of the telescope.

The recorder was built to use photographic paper up to 20 inches wide. The paper was stored in a box mounted on top of the machine and passed down around a typewriter roller and into a second storage box. Small rollers and guides were provided to keep the paper running straight and tight around the main roller.

A synchronous motor provided power for the recorder. The motor was geared to a shaft on which was mounted a thick bakelite commutator disk about 4 inches in diameter. The disk was geared to the paper roller. By an interchange of some of the gears the speed of rotation of the commutator disk could be varied; independent of these changes, the relative speeds of the disk and paper roller could be changed also.

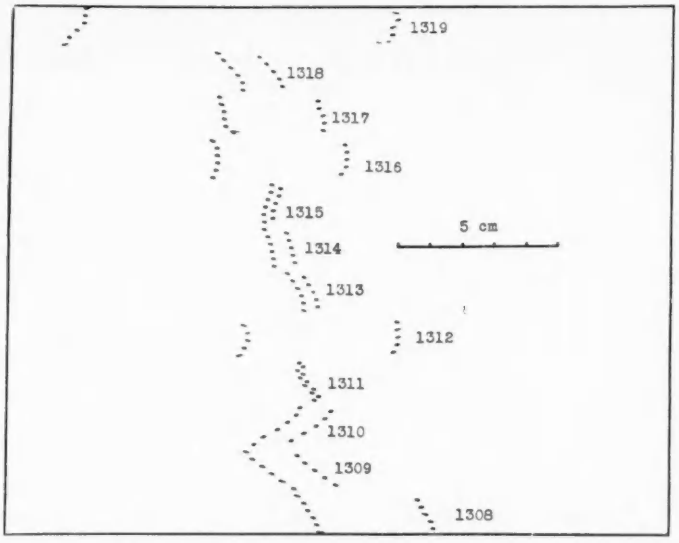

FIG. 2.—A portion of a typical galvanometer record

A long cylindrical lens $2\frac{1}{2}$ inches in focal length and a simple flap-type shutter were mounted in front of the paper roller. On the front of the recorder were mounted a lamp, a slit, a lens, and a prism. These, *plus* the galvanometer mirror with a lens just in front of it and the long cylindrical lens, formed the optical system.[11] The recorder was mounted on a concrete pier which, like the galvanometer pier, was independent of the floor of the galvanometer house.

Current for the recorder was obtained from the 110-volt a.c. mains. The relay control circuits were wired for 10 volts, which were supplied by a small transformer. On the control panel at the top of the telescope were mounted a combination counter and switch, an auxiliary switch for running the recorder steadily, and a signal buzzer and light. A three-wire cable connected the recorder and the control panel.

The operation of the recorder may be described best by an outline of one complete cycle of observation. Let us suppose that the observer at the telescope has a star image centered ready for observation. He moves the image to the lower junction and presses

[11] A. C. Hardy, *J. Opt. Soc. and Rev. Sc. Instr.*, **14**, 511, 1927.

down the handle of the counter on the control panel. This checks up the number of the observation. As long as the handle is held down, the starting circuit of the recorder is closed. This circuit may be completed also by closing the auxiliary switch mounted beneath the counter. Completion of the starting circuit activates the motor relay.

As soon as the commutator disk has rotated through a small angle, two brushes connected in parallel with the motor relay are shorted. Thus the motor will continue to run, even after the starting circuit and motor relay are open, until the commutator disk has completed one revolution. The rim of the disk is divided into twelve equal parts. Thin plates are mounted at eleven of these divisions; the blank division coincides with the "off" position of the motor circuit. Three brushes are mounted to bear against the rim and are shorted when each of the eleven plates passes by. When the first two brushes are shorted, a relay is operated that completes the circuit for the galvanometer light; the plates are so shaped that the galvanometer light is on and off for equal intervals of time. When the first and third brushes are shorted, the signal circuit is completed, and the observer at the telescope is notified that the galvanometer light is about to be turned off; the signal circuit is completed for only a few moments before the galvanometer light goes off. At the end of each signal the observer immediately shifts the star image to the other thermojunction. A small bar, mounted just back of the last—the eleventh—plate, results in a double signal to indicate when eleven observations have been recorded and the cycle is completed. Throughout a cycle the photographic paper moves. If the galvanometer light burned all the time the paper would record not only the steady position of the spot of light, reached after a star image had been on a receiver for about 5 seconds, but also the motion of the spot between successive steady positions. By its intermittent burning the galvanometer light records only the eleven steady positions and thus simplifies measurement of the photographic deflections.

A special device warns the observer of any failures of the galvanometer light. A small resistance was connected in series with the galvanometer light, and the two were connected in parallel with the coils of a relay; the combination was in series with a second resistance. Normally the current in the circuit divided between the relay coils and the light bulb. Obviously, if the bulb were removed, all the current would pass through the relay. The resistances could be so adjusted that the partial current was not large enough, but the total current was sufficient to operate the relay; the relay closed the signal circuit. Thus, if the galvanometer light went out for any reason, except having the circuit opened by the commutator disk, the signal would notify the observer of the fact and would continue to do so until the trouble was remedied.

A small switch and bulb were mounted on the galvanometer pier. After every ten stars, the second observer went to the galvanometer house to make sure that everything was functioning properly; at that time the small bulb was turned on for a few seconds. This made a fine line across the paper parallel to the deflections, and these lines were used to align the paper when the deflections were measured.

Very small deflections, less than 1 mm, were measured on the observatory measuring machine. Most of the deflections, however, could be measured by a method that was quick and accurate and yet wonderfully simple. The paper was set up on a drawing-board with the deflections approximately parallel to the base. Deviation from exact parallelism enters only as the cosine of the angle; it would make absolutely no error if it were the same for all the measures. A 60-cm rule was mounted on a T-square that rested on top of the paper. The rule was checked and found to be uniform over its entire length to better than 10 μ, but the unit of length differs by an appreciable amount from 1 mm. A uniform scale is all that is necessary for our work.

A piece of glass was obtained of such thickness that when it rested on top of the paper the top surface of the glass was even with the edge of the rule. On the lower surface were

etched two cross-lines. At the edge of the top surface a ten-part vernier was etched. With this device there was practically no parallax error, either in setting the cross-line on the spots on the paper or in reading the vernier against the rule. With spots of normal quality, an experienced worker can repeat settings to a tenth of a millimeter with great rapidity.

It is a pleasure to acknowledge grants made to us from the Draper Fund of the National Academy of Sciences, the Milton Fund of Harvard University, and the Rumford and Permanent Science Funds of the American Academy of Arts and Sciences. It is also a pleasure to acknowledge the helpful participation, in the work, of Mr. Richard E. Leary and of Mr. Robert Loevinger and to acknowledge the assistance provided by Dr. Shapley through his encouragement and through the Observatory's resources and facilities.

HARVARD COLLEGE OBSERVATORY
July 1941

RADIOMETRIC MAGNITUDES OF SOME OF THE BRIGHTER STARS

RICHARD M. EMBERSON

ABSTRACT

The radiometric equipment of the Harvard College Observatory has been used to determine the brightness of 82 bright, nonvariable stars, fairly well distributed over the northern hemisphere. Care was taken in the reductions to allow for the effects of atmospheric extinction and of the aging of the silvered surface of the mirror.

The resulting magnitudes agree in scale with the Mount Wilson radiometric magnitudes, but there is a difference in zero point and a systematic spectral effect: the Mount Wilson magnitudes are brighter for early, fainter for late, spectral classes, the difference between Ao and Mo stars being 0.136 mag.

The correlation between color index and photographic heat index is close. Within each spectral class from F to late K (possibly also M) the dwarf stars have smaller heat indices than the giants or supergiants.

A few large residuals occur, but there is no reason to consider that they furnish evidence of true variability.

The radiometric apparatus used at the Harvard College Observatory has been discussed, from both theoretical and practical viewpoints, in another paper in this issue of the *Journal*. The present discussion will deal with some observational material, the reduction of the data, and some conclusions that may be drawn from the results. The stars observed were selected only for position and brightness. They are fairly well distributed over the northern hemisphere. All spectral classes are represented, the early types being more numerous than the late types. As it was hoped to form a network of standard stars to be used in future work, bright stars listed in Prager's catalogue of variable stars were not included.

The material was obtained on twenty-three nights, in the summer and fall of 1938, with the bismuth-antimony thermocouples mounted at the Newtonian focus of the 61-inch Wyeth reflector of the Oak Ridge station. Since October, 1938, the galvanometer deflections have been recorded photographically; prior to that time they were obtained by the visual method. The numerical values of the deflections are obtained at once in the visual method; in the automatic method the photographic paper must be measured to obtain the numerical values. After that point the method of reduction is the same.

The data have been divided into two groups. Group I consists of all the earlier, visually recorded observations. Group II consists of the later, automatically recorded data. For a given star the galvanometer deflection Δ, referred to throughout this paper as simply "the deflection," is the double deflection obtained when the star image is focused first on one and then on the other thermojunction. Of the photographically recorded deflections, those larger than about 1 mm were measured with a device consisting of an accurate millimeter rule and a plate of glass on which cross-lines and a vernier had been etched. Deflections smaller than 1 mm were measured on the "Coast and Geodetic" measuring machine of the Observatory. With average galvanometer sensitivity a star of third radiometric magnitude gave a deflection of 3–4 mm. The precision of a magnitude determination is practically independent of the brightness of the star down to the fourth magnitude; it decreases for fainter stars. A measurement of a sixth-magnitude star, with a deflection of a few tenths of a millimeter, would have a probable error of one- or two-tenths of a magnitude.

The data of group I were reduced by the formula[1]

$$\Delta = \tfrac{1}{6}(2y_1 - 3y_2 + 2y_3 - 3y_4 + 2y_5) ,$$

[1] T. E. Sterne, *Harvard Bull.*, No. 908, p. 15, 1938.

in which the y's are the individual galvanometer deflections. For group II the formula

$$\Delta = \tfrac{1}{8}(y_1 - 4y_2 + 6y_3 - 4y_4 + y_5)$$

was used. There are ten values of y for each observation of a star. They were divided into two sets of five each, and the Δ's were computed. The final Δ was taken as the simple mean of the two values. Subsequently, the formula

$$\Delta = \tfrac{1}{16}(y_1 - 3y_2 + 4y_3 - 4y_4 + 4y_5 - 4y_6 + 4y_7 - 4y_8 + 3y_9 - y_{10})$$

was thought to be preferable in that it not only removed linear and quadratic terms of the galvanometer zero-point drift but also did not give such low weight to the well-determined middle observations of the series of ten. If the formula for $n=4$ in Dr. Sterne's paper is written out for successive groups of observations, the sum of the expressions is exactly the third formula above. As the value of Δ was found to depend on the reduction formula in only a very few cases, it was not considered worth while to repeat the reduction of all the data with this new formula.

A quantity $a = \frac{5}{2} \log \Delta$, called the "versed" magnitude, is computed next. This quantity is on a negative magnitude scale so that the numerical value increases with the brightness of the star; when it is subtracted from a suitable zero-point constant, the magnitude of the star is obtained. If the galvanometer sensitivity changes during the night, a correction must be applied to the versed magnitudes. Ordinarily, only corrections for extinction and aging of the telescope mirrors are needed.

The extinction correction was assumed to vary as the secant of the zenith distance. The value of the extinction coefficient ϵ was determined on most of the nights. A few bright stars were observed several times each, the observations being well separated so that the range of zenith distances would be as large as possible. Reasonable values are usually given by the formula

$$\epsilon = -\frac{\Sigma w a' s'}{\Sigma w s'^2},$$

in which s' and a' are residuals from the mean, for each star, of the secant of the zenith distance and the versed magnitude, respectively. In a few cases the data were not sufficient to determine the extinction coefficient, and a mean value of 0.25 was assumed. All observations were reduced to the zenith at Oak Ridge. In practice, not the secant of the zenith distance but the quantity $s = (\sec z - 1)$ was used in the correction for extinction. A family of curves was plotted on a rather large scale, with s as ordinate, declination as abscissae, and hour angle the parameter from one curve to the next of the family. The value of s, corresponding to any given values of the hour angle and declination, may be read at once from these curves with an accuracy of $\frac{1}{100}$ in the range of values ordinarily encountered. The extinction correction makes the stars brighter at the zenith, i.e., the numerical value of the versed magnitude larger. The data of any one night are not sufficient to show any dependence of the extinction coefficient on spectral class. An analysis of the data of all the nights would yield mean values for the coefficient that might show some dependence on spectral class, but the mean values would not allow for small variation of the extinction from night to night, and such an analysis has not been made.

In Table 1 are listed the dates of the twenty-three nights on which the observations were made. The second column gives the extinction coefficient for each night. Pettit and Nicholson[2] found it necessary to apply a correction for the aging of the telescope mirrors.

[2] *Ap. J.*, **56**, 295, 1922; **68**, 279, 1928; **78**, 320, 1933.

The correction varies with the spectral class of the star. The third column of Table 1 gives the number of days since silvering the mirrors; normally both the primary mirror and the Newtonian flat were silvered at the same time. For the stars in group II that were well observed over the entire period mean versed magnitudes were formed and residuals computed. The stars were then grouped according to spectral class, and the residuals of each group were plotted as a function of the time since silvering. The scatter was too large for a straight line to be drawn in by inspection only; a least-squares solution was made, and the coefficients were adjusted to give zero correction for class Ao. Table 2 gives the values of the coefficients so determined and, for comparison, Pettit and

TABLE 1

JOURNAL OF OBSERVATIONS

1938	ϵ	Days since Silvering	w_k	1938	ϵ	Days since Silvering	w_k
June 8– 9	0.39	120	1	Nov. 9–10	0.25	29	1
13–14	.30	125	1	14–15	.10	34	1
14–15	.30	126	1	20–21	.25	40	1
19–20	.48	131	1	27–28	.07	47	2
20–21	.00	132	1	28–29	.25	48	1
21–22	.22	133	1	Dec. 1– 2	.13	51	3
29–30	.32	141	1	2– 3	.25	52	1
July 6– 7	.11	148	1	7– 8	.25	57	1
10–11	.25	152	1	12–13	.15	62	2
Oct. 25–26	.14	14	2	13–14	.15	63	1
26–27	.40	15	1	15–16	0.19	65	2
31– 1	0.14	20	3				

TABLE 2

AGING COEFFICIENTS FOR SILVERED MIRRORS

Spectral Class	Aging Coefficient $\left(0.01 \frac{\text{Mag.}}{\text{Day}}\right)$		Spectral Class	Aging Coefficient $\left(0.01 \frac{\text{Mag.}}{\text{Day}}\right)$	
	Oak Ridge	Mt. Wilson		Oak Ridge	Mt. Wilson
B	+0.1862	+0.0205	G	−0.1230	−0.0110
A	.0000	.0000	K	− .1896	− .0156
F	−0.0682	−0.0057	M	−0.3357	−0.0194

Nicholson's values. It is obvious that a mirror ages more rapidly at Oak Ridge than at Mount Wilson. Group I does not contain sufficient data to give good values for these coefficients. Therefore, the values obtained from group II have been used in reducing all the material. But these coefficients contain not only the correction for aging of the mirrors but also any seasonal variation, differential with respect to spectral class, of the atmospheric extinction at Oak Ridge. This effect, while small, must certainly exist. Since the observations of group I were obtained at a different time of year from those of group II and especially since the elapsed times and therefore the corrections are rather large for group I, half-weight was given to the material of group I when it was combined with that of group II.

The observations have been weighted in accordance with the atmospheric conditions and the zenith distance. Each night was assigned a weight depending on the quality of

the atmosphere. The weights are contained in the fourth column of Table 1. The criteria, more or less arbitrarily assumed, are as follows:

Best nights.....	No visible clouds, small value of ϵ	$w_k=3$
Good nights.....	No visible clouds but $\epsilon>0.25$	2
Good nights.....	Suspected change in sky during the night, but $\epsilon<0.25$	2
Poor nights.....	No visible or only suspected changes in the sky conditions, but ϵ not determined	1
Poor nights.....	Visible changes, but $\epsilon<0.25$	1
Reject.....	$\epsilon>0.50$, regardless of visible sky conditions	0

The stars observed on any one night were given weights that depend on the value of the zenith distance at the time of observation. The weights assigned were

$$s < 0.25\,, \qquad w_{n(k)} = 1\,,$$

$$0.25 \leqq s < 0.50\,, \qquad w_{n(k)} = \tfrac{1}{2}\,,$$

$$0.50 \leqq s\,, \qquad w_{n(k)} = \tfrac{1}{4}\,.$$

If the extinction coefficient, with an average value of about one-fourth, were in error by 50 per cent, the extinction correction would be in error by only 0.03 mag. for a star of unit weight. A table was formed for each night, listing the stars observed, the versed magnitudes, and the weights. If a star was observed several times during a given night, the sum of the weights of the single observations forms the weight for that star; the weighted mean of the versed magnitudes is the versed magnitude for the night. The final weight for the nth star on the kth night, used to combine observations made on different nights, is the product of the weight of the star and the weight of the night, i.e., in general,

$$w_{nk} = w_k \sum_j w_{jn(k)}\,.$$

To reduce the observations of all the nights to a homogeneous system it is necessary to determine a "night" constant C for each night, which is to be added to the versed magnitudes. This constant corrects for the changes in the galvanometer sensitivity from one night to the next. From four of the best nights—November 27–28, December 1–2, 12–13, 15–16—ten stars were chosen that were observed on at least three of the four nights. A least-squares solution was made to determine the values of the constants that would reduce these nights to the same system (that of the last night). With the preliminary C_k's so determined, a provisional catalogue of mean versed magnitudes was formed containing the stars observed on the four nights. The observing program was arranged so that there was considerable overlapping in the lists of stars from night to night. The list observed on any of the nights therefore included at least a few of the stars in the provisional catalogue. A constant was determined for each of the nights from the formula

$$C_k = \frac{\sum_n w_{nk} m_{nk} - \sum_n w_{nk} \bar{m}_n}{\sum_n w_{nk}}\,,$$

where $\bar{m}_n$ is the catalogue value of the versed magnitude of the nth star, m_{nk} is the versed magnitude of the nth star on the kth night, and w_{nk} is the corresponding weight. In the event that for some star the weight on the kth night was larger than the weight in the provisional catalogue, that star entered into the determination of C_k by the smaller weight only. It is evident that stars not observed on any one of the four catalogue nights could not be used in the determination of the C_k's.

A second catalogue was now formed from the versed magnitudes of all the nights. This catalogue contained more stars than the first and provided more overlapping. The procedure outlined above was repeated, and slightly revised values for some of the C_k's were obtained. A new catalogue of versed magnitudes was formed, etc. Several repetitions of this procedure resulted in values of the C_k's and the mean versed magnitudes that were not changed by another reduction. As mentioned before, the material from group I was given half-weight in the formation of the mean versed magnitudes. Residuals from the mean and the sums of the weights squared were computed for each star. Two stars,

TABLE 3

STARS FOR DETERMINATION OF ZERO POINT

STAR	SPECTRAL CLASS		m_{pv}	m_{pg}	vers. m_r
	HD	D. H.			
γ Gem	A0	A1	1.94	2.02	4.842
β UMa	A0	A1	2.34	2.40	4.210
γ UMa	A0	A1	2.44	2.43	4.307
α Lyr	A0	A1	0.08	0.14	6.696
α Peg	A0	A1	2.50	2.53	4.192
δ Cyg	A0	A0	2.85	2.91	3.792
α Leo	B8	B9	1.33	1.30	5.296
β Tau	B8	B8	1.68	1.52	5.102
ζ Dra	B5	B7	3.20	3.02	3.517

o Andromedae and ϵ Cygni, had a residual that seemed to be abnormally large. If these two observations are rejected, the probable error of a single observation of unit weight is 0.056 mag. Probable errors have not been computed for each star.

The zero-point constant, from which the versed magnitudes are subtracted to obtain the usual magnitudes, was determined from the nine stars listed in Table 3. The second column contains the spectral classification given in the *Henry Draper Catalogue*, the third gives the spectral classification kindly furnished by Dr. Hoffleit, the fourth and fifth columns give the photovisual and photographic magnitudes, and the sixth column gives the versed radiometric magnitudes. The stars are distributed with about zero resultant moment referred to A0; as a first approximation the sums of the magnitudes and the versed magnitudes were formed and the simple mean obtained. This gave for the zero-point constant 6.702 $\pm$ 0.018 for the photovisual system and 6.692 $\pm$ 0.025 for the photographic system. From the residuals, corrections were determined to allow for the fact that the zero-point stars were not all of class A0; for this, Hoffleit's spectral classification was used. The correction was zero for the photovisual system and +0.008 for the photographic, although the significance of the latter is somewhat doubtful. If the correction is applied, however, the mean of the photovisual and the photographic values gives 6.701 $\pm$ 0.022 (p.e.) for the zero-point constant.

The data and results are listed in Table 4, where successive columns give (1) the name of the star; (2) its position; (3) the *Henry Draper* number; (4) the spectral class given by Hoffleit; (5) the spectral class and luminosity classification given by Morgan;[3] (6) m_{pv},

[3] *Ap. J.*, **87**, 460, 1938.

TABLE 4

OBSERVATIONAL DATA AND RESULTS

STAR	α_{1900}	δ_{1900}	HD	SPECTRAL CLASS		m_{pv}	m_{pg}	m_r		CI	HI_{pv}	HI_{pg}	w	n
				D. H.	W. W. M.			Mt.W.	Har					
α And	0^h03^m	+28.5	358	B9	.....	2.11	2.08	+2.15	+2.09	−0.03	+0.02	−0.01	4.5	3
β Cas	0 04	+58.6	432	F3	F2 III	2.34	2.82	+2.25	+2.01	+0.48	+0.33	+0.81	12.75	8
γ Peg	0 08	+14.6	886	B2	.....	3.00	2.67	+2.91	+2.78	−0.33	+0.22	−0.11	3	2
β And	1 04	+35.1	6860	K6	K5 III	2.07	3.94	+0.45	+0.23	+1.87	+1.84	+3.71	17.5	7
ε Cas	1 47	+63.2	11415	B4	.....	3.38	3.23	.....	+3.22	−0.15	+0.16	+0.01	5.5	3
α Ari	2 02	+23.0	12929	K1	K1 III	2.01	3.37	.....	+0.94	+1.36	+1.07	+2.43	6	4
β Tri	2 04	+34.5	13161	A4	.....	2.97	3.24	.....	+2.88	+0.27	+0.09	+0.36	14	8
α Cet	2 57	+ 3.7	18884	Mo	Mo III	2.54	4.47	+0.72	+0.48	+1.93	+2.06	+3.99	7	6
γ Per	2 58	+53.1	18925–6	F8p	.....	2.93	3.75	.....	+2.17	+0.82	+0.76	+1.58	13	3
α Per	3 17	+49.5	20902	F3	F5 I	1.78	2.43	+1.62	+1.36	+0.65	+0.42	+1.07	24	6
δ Per	3 36	+47.5	22928	B4	.....	3.05	2.94	.....	+2.93	−0.11	+0.12	+0.01	5.5	3
η Tau	3 42	+23.8	23630	B5:	.....	2.90	2.92	+2.98	+2.76	+0.02	+0.14	+0.16	6	4
ζ Per	3 48	+31.6	24398	B1	.....	2.83	3.00	.....	+2.60	+0.17	+0.23	+0.40	10	7
ε Per	3 51	+39.7	24760	B2:	.....	2.87	2.67	.....	+2.84	−0.20	+0.03	−0.17	10.5	6
ξ Per	3 52	+35.5	24912	Oe5:	.....	4.04	4.08	.....	+3.78	+0.04	+0.26	+0.30	3	2
α Tau	4 30	+16.3	29139	K5	K5 III	0.77	2.70	−0.60	−0.88	+1.93	+1.65	+3.58	12.75	7
ι Aur	4 50	+33.0	31398	K2	K2 II	2.64	4.46	.....	+1.23	+1.82	+1.41	+3.23	21	9
η Aur	5 00	+41.4	32630	B3	.....	3.23	2.95	.....	+3.06	−0.28	+0.17	−0.11	18	10
α Aur	5 09	+45.9	34029	G2	G2 I	0.14	1.03	−0.38	−0.61	+0.89	+0.75	+1.64	17.5	7
β Ori	5 10	− 8.3	34085	B7(+A1?)	.....	0.31	0.10	.....	+0.11	−0.21	+0.20	−0.01	1.75	4
γ Ori	5 20	+ 6.3	35468	B2	.....	1.68	1.35	+1.66	+1.60	−0.33	+0.08	−0.25	2	2
β Tau	5 20	+28.5	35497	B8	.....	1.68	1.52	+1.74	+1.60	−0.16	+0.08	−0.08	4	3
ε Ori	5 31	− 1.3	37128	Bo	.....	1.71	1.51	+1.69	+1.77	−0.20	−0.06	−0.26	1.5	1
θ Aur	5 53	+37.2	40312	Aop	.....	2.66	2.61	.....	+2.56	−0.05	+0.10	+0.05	13	6
γ Gem	6 32	+16.5	47105	A1	.....	1.94	2.02	.....	+1.86	+0.08	+0.08	+0.16	5.5	3
ε Gem	6 38	+25.2	48329	G8g	G7 I	2.97	4.67	.....	+1.84	+1.70	+1.13	+2.83	8	5
51 Gem	7 08	+16.3	55383	M6	.....	4.85	.....	+2.35	+2.16	.....	+2.69	.....	7.5	5
δ Gem	7 14	+22.2	56986	Fo	.....	3.38	3.89	.....	+3.23	+0.51	+0.15	+0.66	5	3
ι Gem	7 20	+28.0	58207	G8	G9 III	3.59	.....	.....	+2.92	.....	+0.67	.....	5	3
α CMi	7 34	+ 5.5	61421	F5	F4 V	0.40	0.83	+0.22	+0.04	+0.43	+0.30	+0.79	8	7
β Gem	7 39	+28.3	62509	Ko	K0 III	1.13	2.31	+0.53	+0.31	+1.18	+0.82	+2.00	15.5	9
ο UMa	8 22	+61.0	71369	G3	G7 III	3.30	.....	.....	+2.52	.....	+0.78	.....	3.5	2
ι UMa	8 52	+48.4	76644	A5	.....	3.07	3.42	.....	+2.92	+0.35	+0.15	+0.50	3	1
κ UMa	8 57	+47.6	77327	A1	.....	3.60	.....	.....	+3.52	.....	+0.08	.....	3	1
h UMa	9 24	+63.5	81937	F1	.....	3.65	.....	.....	+3.28	.....	+0.37	.....	3.5	2
θ UMa	9 26	+52.1	82328	F5d	F6 III	3.18	3.82	.....	+2.75	+0.64	+0.43	+1.07	3.5	2
ε Leo	9 40	+24.2	84441	Go	G1 II	2.96	.....	+2.64	+2.32	.....	+0.64	.....	8	4
ν UMa	9 44	+59.5	84999	Fo	.....	3.77	.....	.....	+3.52	.....	+0.25	.....	3.5	2
π Leo	9 55	+ 8.5	86663	M2	.....	4.52	.....	+3.02	+2.66	.....	+1.86	.....	3.5	3
α Leo	10 03	+12.4	87901	B9	.....	1.33	1.30	.....	+1.40	−0.03	−0.07	−0.10	9	6
λ UMa	10 11	+43.4	89021	A2	.....	3.44	.....	.....	+3.48	.....	−0.04	.....	3	1
γ Leo	10 14	+20.4	89484–5	Ko	K2 III	2.08	3.29	.....	+0.98	+1.21	+1.10	+2.31	6.5	4
μ UMa	10 16	+42.0	89758	Mo	K5 III	2.92	4.88	.....	+1.23	+1.96	+1.69	+3.65	2	1
β UMa	10 56	+56.9	95418	A1	.....	2.34	2.40	+2.51	+2.49	+0.06	−0.15	−0.09	8.62	8
α UMa	10 58	+62.3	95689	G7	K0 III	1.70	3.09	+1.11	+1.03	+1.39	+0.67	+2.06	7.12	8
ψ UMa	11 04	+45.0	96833	Ko	K1 III	2.92	.....	.....	+2.17	.....	+0.75	.....	0.5	2
δ Leo	11 09	+21.1	97603	A4	.....	2.52	2.69	.....	+2.51	+0.17	+0.01	+0.18	6	3
χ UMa	11 41	+48.3	102224	Ko	K0 III	3.56	.....	.....	+2.74	.....	+0.82	.....	0.5	2
ν Vir	11 41	+ 7.1	102212	Mo	.....	3.72	.....	.....	+2.20	.....	+1.52	.....	1.5	1
β Leo	11 44	+15.1	102647	A3	.....	2.43	2.29	.....	+2.09	−0.14	+0.34	+0.20	3	2
γ UMa	11 49	+54.2	103287	A1	.....	2.44	2.43	.....	+2.39	−0.01	+0.05	+0.04	3.5	5
ε UMa	12 50	+56.5	112185	Ao	.....	1.65	1.84	.....	+1.77	+0.19	−0.12	+0.07	10.25	9
12 CVn	12 51	+38.9	112412–3	B9p	.....	2.64	2.71	.....	+2.94	+0.07	−0.30	−0.23	3.62	4
ζ_1 UMa	13 20	+55.4	116656	A1	.....	2.22	2.20	.....	+2.27	−0.02	−0.05	−0.07	3	4
η UMa	13 44	+49.8	120315	B3	.....	1.90	1.73	.....	+1.80	−0.17	+0.10	−0.07	3	5
β UMi	14 51	+74.6	131873	K4	K4 III	1.96	3.72	.....	+0.73	+1.76	+1.23	+2.99	7	7
β Boo	14 58	+40.8	133208	G5	G7 III	3.45	4.64	.....	+2.71	+1.19	+0.74	+1.93	0.25	1
δ Boo	15 12	+33.7	135722	G7	G9 III	3.42	.....	.....	+2.92	.....	+0.50	.....	0.25	1
γ UMi	15 21	+72.2	137422	A2	.....	3.08	3.21	.....	+2.95	+0.13	+0.13	+0.26	4.25	6
η Dra	16 23	+61.7	148387	G7	.....	2.74	3.78	.....	+2.05	+1.04	+0.69	+1.73	3.5	6
ζ Her	16 38	+31.8	150680	God	G1 V	2.83	3.49	.....	+2.46	+0.66	+0.37	+1.03	0.5	1
η Her	16 40	+39.1	150997	G7	G6 III	3.39	.....	.....	+2.88	.....	+0.51	.....	1	1
ζ Dra	17 08	+65.8	155763	B7	.....	3.20	3.02	.....	+3.18	−0.18	+0.02	−0.16	3	5
π Her	17 12	+36.9	156283	K5	K3 II–III	3.00	4.85	.....	+2.01	+1.85	+0.99	+2.84	0.5	1
β Dra	17 28	+52.4	159181	Fog	F9 I	2.84	3.86	.....	+2.09	+1.02	+0.75	+1.77	5.75	8
γ Dra	17 54	+51.5	164058	K5	K5 III	2.15	4.00	.....	+0.85	+1.85	+1.30	+3.15	7.75	8
α Lyr	18 34	+38.7	172167	A1	.....	0.08	0.14	.....	0.00	+0.06	+0.08	+0.14	9.5	11
γ Lyr	18 55	+32.6	176437	Ao	.....	3.26	3.20	.....	+3.17	−0.06	+0.09	+0.03	1	1
δ Cyg	19 42	+44.9	186882	Ao	.....	2.85	2.91	.....	+2.91	+0.06	−0.06	0.00	7.5	10
δ Sge	19 43	+18.3	187076–7	M1	.....	3.64	5.47	.....	+1.49	+1.83	+2.15	+3.98	1	1
δ Aql	19 46	+ 8.6	187642	A7	.....	0.80	1.11	.....	+0.63	+0.31	+0.17	+0.48	0.5	1
γ Sge	19 54	+19.2	189319	K5	K5 III	3.41	.....	.....	+1.82	.....	+1.59	.....	1	1
γ Cyg	20 19	+39.9	194093	F7g	F8 I	2.30	3.02	.....	+1.83	+0.72	+0.47	+1.19	5	6
α Cyg	20 38	+44.9	197345	A2p	.....	1.24	1.40	+1.24	+1.11	+0.16	+0.13	+0.29	25	17
ε Cyg	20 42	+36.6	197989	Ko	K0 III–IV	2.38	3.66	.....	+1.59	+1.28	+0.79	+2.07	1.5	3
ζ Cyg	21 09	+29.8	202109	G8	G9 II	3.13	.....	.....	+2.53	.....	+0.60	.....	1	1
α Cep	21 16	+62.2	203280	A6	.....	2.57	2.81	.....	+2.35	+0.24	+0.22	+0.46	19.25	11
ε Peg	21 39	+ 9.4	206778	K1	K1 I	2.45	4.11	.....	+1.12	+1.66	+1.33	+2.99	1	1
ο And	22 57	+41.8	217675–6	B6+A1	.....	3.51	3.59	.....	+3.56	+0.08	−0.05	+0.03	11.5	8
β Peg	22 59	+27.5	217906	M3	.....	2.25	4.39	+0.27	+0.11	+2.14	+2.14	+4.28	5.75	3
α Peg	23 00	+14.7	218045	A1	.....	2.56	2.53	+2.67	+2.51	−0.03	+0.05	+0.02	6.5	5
γ Cep	23 35	+77.1	222404	K1	K1 IV	3.30	.....	.....	+2.38	.....	+0.92	.....	9.75	6

the photovisual magnitude;[4] (7) m_{pg}, the photographic magnitude;[5] (8) and (9) m_r, the Mount Wilson and Harvard radiometric magnitudes; (10) $CI = (m_{pg} - m_{pv})$, the color index; (11) HI_{pv}, the heat index as defined by Pettit and Nicholson; (12) HI_{pg}, the corresponding index if photographic magnitudes are used in place of photovisual, i.e., $HI_{pg} = m_{pg} - m_r$; (13) w, the weight; and (14) n, the number of nights observed. The radio-

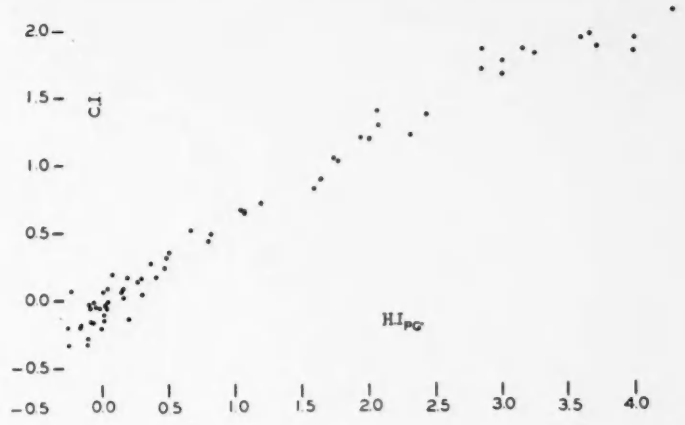

FIG. 1

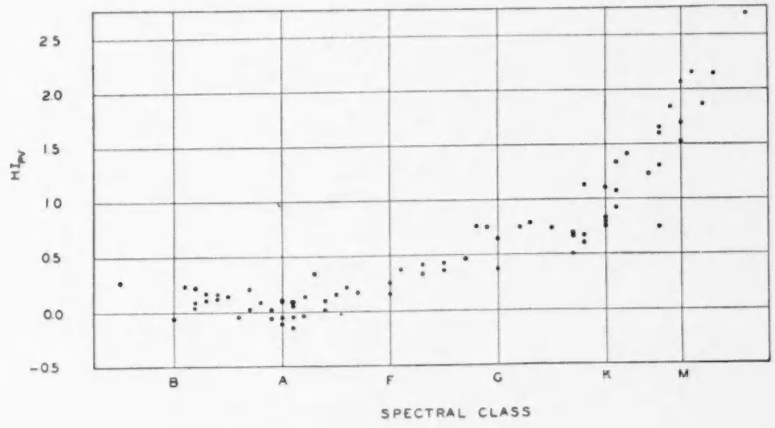

FIG. 2

metric magnitudes are for the following standard conditions: the zenith at Oak Ridge, two reflections from fresh silver, and a fluorite window on the thermopile cell.

The determination of either photographic or photovisual magnitudes for the bright stars presents considerable difficulty. In addition to the usual difficulties of photometry with photographic plates, there are the extinction troubles encountered in the radiometric work that come in when one observes points as widely separated in the sky as the brighter stars. In recent years the bright stars have been neglected. King's magni-

[4] C. Payne-Gaposchkin, *Harvard Obs. Mimeograms*, Ser. III, Nos. 1 and 2.

[5] E. S. King, *Harvard Ann.*, **59**, 157, 1912.

tudes have been used in the present paper because they were considered the best of all those available, especially in regard to the magnitude scale.

A simple mean of the differences between the Mount Wilson and the Harvard radiometric magnitudes indicates a difference in zero point of 0.166 mag., additive to the Harvard magnitudes to reduce them to the Mount Wilson zero point. The magnitude differences plotted against spectral class have a distribution that indicates both a difference in zero point and a systematic spectral effect. If one assumes that a linear relation-

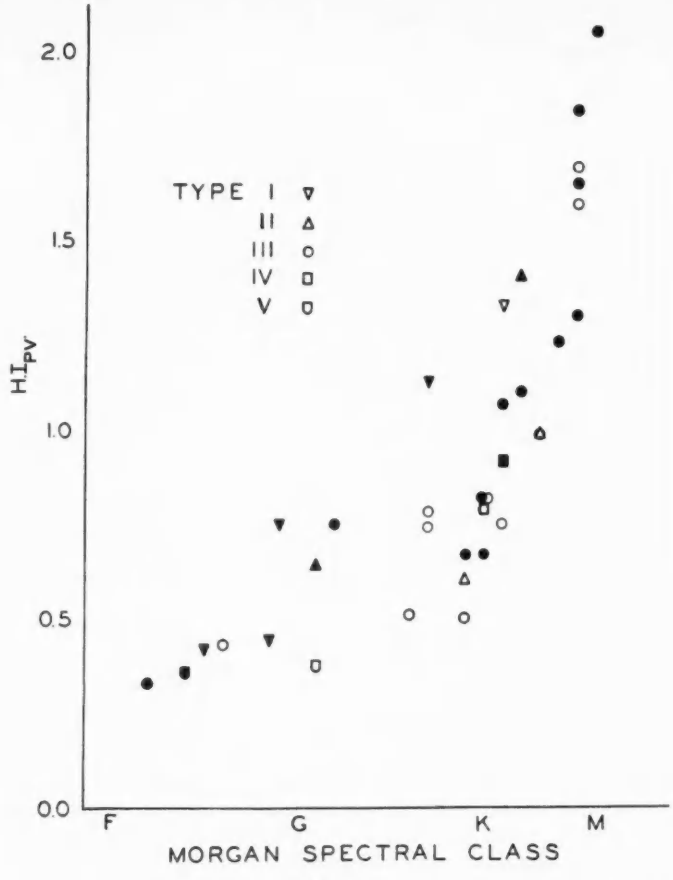

FIG. 3

ship exists, the correction is 0.118 and 0.254 mag. for Ao and Mo stars, respectively. This means that if the Mount Wilson and Harvard magnitudes are made to agree for Ao stars, then the Mount Wilson magnitudes, compared with the Harvard magnitudes, are brighter for early, and fainter for late, spectral classes. There is no significant difference between the Mount Wilson and the Harvard magnitude scales.

Figure 1 shows color index as a function of the photographic heat index. As one would expect, there is very good correlation between the two indices. A plot of color index against the photovisual heat index shows considerably more scatter than appears in Figure 1. Part of this is due to the shrinkage of the scale of abscissae. Part is due, perhaps, to larger errors in the photovisual magnitudes than are present in the photographic

system. The probable error of the photovisual catalogue is 0.06 mag. The bright stars, however, form a very small percentage of the catalogue and as a group have an error that most likely is larger than that of the mean. Since errors in the photovisual magnitudes affect CI and HI_{pv} in opposite directions, their presence is more noticeable than similar errors in the photographic magnitudes.

Figure 2 shows photovisual heat indices plotted against spectral class. In Figure 3 the heat indices are plotted for those stars for which spectral classifications and luminosities by Morgan were available. Points for observations of high weight are solid; points for observations of low weight are open. A curve published by Kuiper[6] gives the relation between the bolometric correction and the spectral type. Since it shows a definite absolute-magnitude effect, one would expect the results shown in Figure 3 of the present paper. From spectral class F through late K or perhaps M, the dwarf stars have smaller heat indices than the giants or supergiants.

Five stars in the list have rather large residuals; if one were to judge by that criterion alone, they might be variables. However, a large range in the residuals is not conclusive proof of variability but rather indicates one of the great difficulties in making photometric comparisons between widely separated stars. The best examples are furnished by α and β Ursae Majoris, two stars with abnormally large ranges in the residuals. By the standards of radiometric work these stars are close together in the sky; almost without fail they were observed in succession. All the observations were made at a time of year when these stars were at a rather unfavorable position, that is, they had large zenith distances. One would expect that these two stars, although not of the same spectral class, would both show the same systematic extinction effect, if any were present. This fact is verified by the residuals. The correlation is perfect; without exception the two residuals are simultaneously large or small, positive or negative, with only a small difference of a few hundredths of a magnitude between their numerical values. With the exception of o Andromedae, the stars listed in Table 4 are not known to be variable. Only a few observations have been made on ϵ Cygni, and these are not sufficient cause for placing any significance on the single large residual.

In conclusion, the author wishes to acknowledge his indebtedness to Dr. Harlow Shapley for placing the facilities of the Observatory at his disposal; to Dr. T. E. Sterne for his advice and encouragement, to Mr. Robert Loevinger, who read the galvanometer and gave suggestions and assistance both with the experimental difficulties and with the method of reduction throughout the early stages of the work, and to Mr. R. M. Scott, who aided with the more recent observations and measured most of the photographic records, for their able and patient assistance; to Mr. Richard Hanau for assistance on several nights; to Dr. Dorrit Hoffleit for redetermining the spectral types of the stars; and in some degree to many other members of the Observatory staff. The work was aided by grants from the Rumford Committee of the American Academy of Arts and Sciences, the Draper Fund of the National Academy of Sciences, the Milton Fund of Harvard University, and the Permanent Science Fund of the American Academy of Arts and Sciences.

HARVARD COLLEGE OBSERVATORY
July 1941

[6] *Ap. J.*, **88**, 452, 1938.

PHYSICAL PROCESSES IN GASEOUS NEBULAE

XVII. FLUORESCENCE IN HIGH-EXCITATION PLANETARIES

DONALD H. MENZEL AND LAWRENCE H. ALLER[1]

ABSTRACT

Some years ago Bowen attributed the appearance of "fractional multiplets" of *O* III in the spectra of high-excitation planetaries to absorption by *O* III atoms in the $^2p^2\ ^3p_2$ level of the λ 303.80 "Lyman alpha" radiation of helium. The subsequent cascading of these atoms from $2p3d\ ^3D_2$ of *O* III back to the ground level via the 2p3p and 2p3s configurations are supposed to produce the observed lines. We have attempted to put this theory on a quantitative basis by setting up the appropriate equations of statistical equilibrium for the excited levels and predicting the relative intensities of the observed ultraviolet lines. A comparison of observed relative intensities with predicted relative intensities yields a consistency check on the theory. The populations of the excited levels are found to be 10^{-14}–10^{-16} atoms cm^{-3}. The intensity of the radiation in the *O* III 303.80 line is from 10^2 to 10^3 times greater than that radiated by the nuclear star, which illustrates why permitted lines of *O* III, other than those originating by cascade from $3d^3P_2$, are not observed. The excess is attributed to the concentration of radiation in these lines, by cyclic processes resulting from ionization of He^+. We have also shown that theoretically the images of the Bowen lines should be about 5 per cent larger than those of the *He* II lines, which is in rough agreement with the observational data. The paper contains tables of the relevant *f*'s and *A*'s *computed* from approximate wave functions based on Slater's rules.

In the spectra of certain planetaries, e.g., NGC 7662 and NGC 7027, a number of strong permitted lines appear in the astronomically accessible ultraviolet. Wright,[2] who obtained the observational data, pointed out that other lines, equally strong in laboratory spectra, are entirely absent from the nebular radiation. Bowen[3] has noted the fact that all the observed lines emanate either directly or indirectly from excitation of a single upper level, $3d\ ^3P_2$. He further noticed that the λ 303.799 line corresponding to the transition $2p^2\ ^3P_2 - 2p3d\ ^3P_2$ almost coincides with the Lyman α line of ionized helium, whose wave length is λ 303.780 A.

Bowen suggested that the excitation of the *O* III level was caused by resonance absorption of the helium radiation. An *O* III atom, thus raised to the $2p3d\ ^3P_2$ level, would either return directly to the ground level or cascade back via the terms of the configurations 2p3p and 2p3s, emitting the observed lines in transit. The λ 304 radiation of *He* II provides a very rich reservoir of energy for the *O* III atoms, upon which transitions other than $2p^2\ ^3P_2 - 2p3d\ ^3P_2$ cannot draw. The circumstance that the ultraviolet *O* III radiations appear only in planetaries where λ 4686 of *He* II is strong strengthens this suggestion. The images of the ultraviolet *O* III lines are never significantly larger than those of *He* II (e.g., λ 3203). An excellent example is NGC 7009. Although the Bowen fluorescent lines are conspicuous in the main body of the planetary, they are quite missing in the ansae. The spectra of the latter are definitely of a low-excitation type in which the *He* II lines do not appear.[4] The occurrence of the green nebular lines, even though they are faint, shows that some *O* III is present in the outer portions of the nebula, in a state where it could absorb the λ 304 radiation if it existed.

Bowen's suggestion provides an excellent qualitative explanation for the observed

[1] Society of Fellows, Harvard University.

[2] *Lick Obs. Bull.*, **17**, 1, 1934. [3] *Ap. J.*, **81**, 1, 1935.

[4] For the observational data see Paper XIV of this series (*Ap. J.*, **93**, 236, 1941). See also Papers XII (*Ap. J.*, **93**, 195, 1941) and XVI (*Ap. J.*, **94**, 30, 1941) for the electron density and *O* III density determinations, respectively.

phenomena. We propose, in the present paper, to investigate the theory of the Bowen fluorescent mechanism from the quantitative viewpoint.

Previous studies[4] have yielded estimates of the densities of atoms of *O* III, electrons, and hydrogen ions in typical planetaries. Rough intensities of the ultraviolet lines of helium, neon, and oxygen are available. We shall proceed by setting up the equations of statistical equilibrium for each of the excited levels. The number of atoms entering any excited level per second must equal the number leaving that same level each second. Since all the excited levels are fed from the $3d\ ^3P_2$ level, we should be able to predict the relative intensities of the ultraviolet lines of *O* III.

Atomic theory yields the Einstein A's or oscillator strengths (f-values) for the transitions involved. The A's or f's for the transition $J - J'$ are as follows:

$$A(J, J') = \frac{1}{2J+1} \frac{64\pi^4\nu^3}{3hc^3} \frac{\epsilon^2 a^2}{4l^2 - 1} S\rho^2 , \tag{1}$$

$$f(J', J) = \frac{1}{2J'+1} \frac{8\pi^2 m\nu}{3h} \frac{a^2}{4l^2 - 1} S\rho^2 ; \tag{2}$$

accordingly,

$$A(J, J') = \frac{2J'+1}{2J+1} \frac{8\pi^2\epsilon^2\nu^2}{mc^3} f(J, J') , \tag{2a}$$

where J' and J are the inner quantum numbers of the lower and upper levels, respectively; $a = 0.528 \times 10^{-8}$ cm, the radius of the first Bohr orbit; S is the numerical "strength" of the line; and l refers to the larger of the initial or final values for the two configurations. The symbols, ϵ, m, c, h, and ν have their usual meanings.

Calculation of the radial quantum integral,

$$\rho = \int_0^\infty R_{nl} R_{n'l'} r^3 dr , \tag{3}$$

involves a knowledge of the radial wave functions R_{nl} and $R_{n'l'}$.[5] The detailed and accurate calculation of these functions is a difficult problem. For our present purposes we shall use approximate hydrogen-like radial wave functions whose parameters are fixed according to a rule given by Slater.[6]

The procedure is as follows. We first introduce effective quantum numbers according to the following scheme:

$$\text{for} \quad n = 1, 2, 3, 4, 5, 6 ,$$

$$\text{let} \quad n^* = 1, 2, 3, 3.7, 4.0, 4.2 .$$

Then we divide the orbits up according to shells: 1s; 2s2p; 3s3p3d; 4s4p, ... ; etc. In place of the nuclear charge Z, we use the effective charge, $Z - \sigma$, where σ, the screening constant, is fixed by the following rules. Each electron in the same shell with the

[5] In the present paper we adopt wave functions normalized to give

$$\int_0^\infty R_{nl}^2 r^2 dr = 1$$

instead of the form used in Paper X.

[6] *Phys. Rev.*, **57**, 36, 1930.

"jumping" electron contributes 0.35 to the total σ. For s and p electrons the contribution is 0.85 for each electron with a total quantum number less by 1, and for other electrons the contribution is 1.00; i.e., the screening is supposed to be complete. For d electrons we adopt the value of 1.00 for all electrons in the inner shell.

These rules lead to the following approximate wave function:

$$R_{nl} = \left[\frac{2(Z-\sigma_{nl})}{n^*}\right]^{n^*+1/2} \frac{1}{[\Gamma(2n^*+1)]^{1/2}}\, r^{n^*-1} e^{[-(Z-\sigma_{nl})/n^*]r} . \tag{4}$$

From equation (3) we easily obtain

$$\left.\begin{aligned}\rho = \frac{\Gamma(n^*+n'^*+2)}{[\Gamma(2n^*+1)\Gamma(2n'^*+1)]^{1/2}} &\left[\frac{2(Z-\sigma_{nl})}{n^*}\right]^{n^*+1/2} \\ &\times \left[\frac{2(Z-\sigma_{n'l'})}{n'^*}\right]^{n'^*+1/2} \frac{1}{\left[\dfrac{Z-\sigma_{nl}}{n^*}+\dfrac{Z-\sigma_{n'l'}}{n'^*}\right]^{n^*+n'^*+2}} .\end{aligned}\right\} \tag{5}$$

For *O* III the relevant values of the significant parameters, calculated for the various configurations of *O* III ($Z = 8$) by Slater's rules, are shown in the accompanying table.

Configuration	n	σ	$Z-\sigma$
$1s^2 2s^2 2p^2$	2	2.75	5.25
2p3s	3	4.55	3.45
2p3p	3	4.55	3.45
2p3d	3	5.00	3.00

For the ground configuration of *O* III, however, a Hartree wave function is available, for which Hebb and Menzel[7] have given an analytic approximation. We may use this function in the calculations of radial quantum integrals connecting the higher configurations with the ground configuration. To calculate ρ for the transition $2p^2 - 2p3d$, we have (cf. n. 4, regarding normalization convention)

$$R_{2p} = r(ae^{-br} + ce^{-dr}) , \tag{6}$$

where

$$a = 10.415 , \quad c = 4.520 ,$$

$$b = 3.604 , \quad d = 2.014 ,$$

and

$$R_{3d} = \left[\frac{2(Z-\sigma)}{3}\right]^{7/2} (6!)^{-(1/2)} r^2 e^{-(z-\sigma_{3d})r/3} = 2^{7/2}(6!)^{-(1/2)} r^2 e^{-r} . \tag{7}$$

From equation (3) we now obtain

$$2p - 3d \qquad \rho_1 = (2^7 6!)^{1/2}\left[\frac{a}{(1+b)^7} + \frac{c}{(1+d)^7}\right] = 0.68 \tag{8a}$$

[7] *Ap. J.*, **92**, 408, 1940.

and similarly

$$2p - 3s \qquad \rho_4 = 18.50(6!)^{1/2}\left[\frac{a}{(1.15+b)^7} + \frac{c}{(1.15+d)^7}\right] = 0.81 . \qquad (8b)$$

The modified Slater type of wave function for the ground configuration, with ρ calculated according to equation (5), gives, instead,

$$\rho_1 = 0.47 , \qquad (8a')$$

$$\rho_4 = 0.58 . \qquad (8b')$$

The agreement is satisfying in view of the approximate nature of the calculations. We shall use equations (8*a*) and (8*b*) in preference to equations (8*a'*) and (8*b'*). From equation (5) we find for the transitions between excited levels

$$3p - 3d \qquad \rho_2 = 3.20 , \qquad (8c)$$

$$3\mathring{p} - 3s \qquad \rho_3 = 3.04 . \qquad (8d)$$

The strengths, S, which depend on the angular factors in the wave functions, have been tabulated in a previous paper.[8]

The error in ρ arising from inaccurate wave functions is difficult to estimate. Modified hydrogenic wave functions calculated from Slater's rules are certainly better than pure hydrogenic functions. The variation method might yield better results, but the labor of applying it for excited configurations in such atoms as *O* III would be considerable. We believe that the integrals calculated from the much simpler Slater's rules will be amply accurate for the present purpose.

To obtain a brief and explicit, although somewhat awkward, notation, we have adopted the designations shown in the accompanying table for the levels involved.

Configuration and Level	Present Notation	Configuration and Level	Present Notation
$1s^2 2s^2\ 2p^2\ {}^3P_1$	a'	$^3D_3$	g
$^3P_2$	a	$^3D_2$	h
$2p3d\ {}^3P_2$	b	$^3D_1$	j
$2p3p\ {}^3P_2$	c	$2p3s\ {}^3P_2$	k
$^3P_1$	d	$^3P_1$	m
$^3P_0$	e	$^3P_0$	n
$^3S_1$	f		

In Table 1 we give the wave lengths, term designations, strengths, f-values, and A's for the transitions involved in the Bowen fluorescent mechanism. We found it convenient to recast equations (1), (2), and (2*a*) as follows:

$$\left.\begin{aligned} f &= 3.04 \times 10^{-6}\,\frac{1}{2J'+1}\,\frac{\rho^2 S}{\lambda(4l^2-1)} , \\ A &= 2.01 \times 10^{-6}\,\frac{1}{2J+1}\,\frac{\rho^2 S}{(4l^2-1)\lambda^3} , \end{aligned}\right\} \qquad (9)$$

[8] *Ap. J.*, **91**, 307, 1940.

and

$$f = 1.509 \frac{2J + 1}{2J' + 1} \lambda^2 A \,, \tag{10}$$

where λ is expressed in centimeters.

Atoms in the $2p^2\ {}^3P_2$ (a) level absorb the λ 304 radiation of *He* II and are raised to the $3d\ {}^3P_2$ (b) level. The levels—c, d, f, g, etc.—are populated exclusively by atoms cascading from the b level.

TABLE 1

TRANSITION PROBABILITIES FOR *O* III

Transition		Wave Length	S	f	A
$1s^22s^22p3d\ {}^3P_2 - 2p3p\ {}^3D_3$		2836.35	7/10	0.0073	8.43×10^6
	${}^3D_2$	2818.80	1/8	.00184	1.53
	${}^3D_1$	2808	1/120	.00020	0.103
	${}^3P_2$	3444.15	75/8	.113	6.31×10^7
	${}^3P_1$	3428.70	25/8	.063	2.13
	${}^3S_1$	3132.87	50/3	.368	1.49×10^8
$1s^22s^22p3d\ {}^3P_1 - 2p3p\ {}^3S_1$		3121.71	10	.222	1.50×10^8
$1s^22s^22p3p\ {}^3D_3 - 2p3s\ {}^3P_2$		3759.83	7	.346	1.16×10^8
${}^3D_2 -$	${}^3P_2$	3791.26	5/4	.062	2.84×10^7
${}^3D_2 -$	${}^3P_1$	3754.65	15/4	.313	8.80
${}^3D_1 -$	${}^3P_2$	3810.99	1/12	.0041	0.312
	${}^3P_1$	3774.01	5/4	.103	4.80
	${}^3P_0$	3757.20	5/3	.416	6.50
${}^3P_2 -$	${}^3P_2$	3047.14	15/4	.230	1.64×10^8
	${}^3P_1$	3023.42	5/4	.129	0.561
${}^3P_1 -$	${}^3P_2$	3059.31	5/4	.0765	9.02×10^7
	${}^3P_1$	3035.92	3/4	.077	5.55
	${}^3P_0$	3024.54	1	.310	7.46
${}^3S_1 -$	${}^3P_2$	3340.78	5/3	.0935	9.25×10^7
	${}^3P_1$	3312.35	1	.0940	5.68
	${}^3P_0$	3299.39	1/3	.0946	1.92
$1s^22s^22p3s\ {}^3P_2 - 2p^2\ {}^3P_2$		374.00	15/2	.266	1.26×10^{10}
	${}^3P_1$	.....	5/2	.148	0.42
${}^3P_1 -$	${}^3P_0$	.....	5/2	.090	0.701
	${}^3P_1$	.....	3/2	.089	0.421
	${}^3P_0$	374.00	2	.035	0.558×10^{10}
${}^3P_0 -$	${}^3P_1$	.....	2	.119	1.68
$1s^22s^22p^2\ {}^3P_2 - 2p3d\ {}^3P_2$		303.80	18.75	.116	8.31×10^9
	${}^3P_1$	303.80	6.25	.039	4.63
${}^3P_1 -$	${}^3P_2$	303.62	6.25	0.0645	2.78×10^9

Our first problem will be to use the computed A's to set up the equations of statistical equilibrium for each of these excited levels in turn. We shall be able to predict the populations of each of the c, d, f levels in terms of that of the b level. Since the intensity of an emission line is proportional to the product of the population of the upper level of the transition of the A- or f-value, we may use the observed intensities of the *O* III fluorescent lines to evaluate N_b. The values of N_b obtained from the various observable permitted lines should agree with one another to within the errors of observation.

The equation of statistical equilibrium for the $2p3d\ {}^3P_2$ level, (b) follows from elementary considerations. We must have

$$F_{ab} = F_{ba} + F_{ba'} + F_{bc} + F_{bd} + F_{bf} + F_{bg} + F_{bh} + F_{bi} \,, \tag{11}$$

where F, in accordance with the earlier notation of this series, is the number of transitions per unit volume per second from one level to another as indicated by the subscripts. The number of downward transitions is $N_b \sum_i A_{bi}$, where A is the Einstein coefficient of spontaneous emission. The summation is to be carried out over all lower levels connecting with level b. We sum the appropriate A's in Table 1 to obtain the right-hand side of equation (11),

$$N_b \Sigma A_{bi} = 1.13 \times 10^{10} N_b . \tag{12}$$

Now F_{ab} is the number of transitions from $2p^2\ {}^3P_2$ to $2p3d\ {}^3P_2$. Practically all the O III atoms are in the ground term. In an earlier paper Hebb and Menzel[6] have shown that collisions are sufficiently active to give a statistical distribution among the three levels of ${}^3P$. Hence we take the fraction

$$\frac{(2J+1)}{\Sigma(2J+1)} = \frac{5}{9}$$

of O III atoms to be in the level $2p^2\ {}^3P_2$, i.e., $N_a = \frac{5}{9} N_P$. Thus the number of transitions from the ground level will be

$$F_{ab} = \tfrac{5}{9} N_P \frac{4\pi}{h\nu_{ab}} \int W_\nu I^0_\nu a_{ab}(\nu) d\nu , \tag{13}$$

where I^0_ν is the frequency distribution of the intensity of the radiation in a black body of an arbitrary temperature T_0 and W_ν is the dilution factor averaged over all angles for the frequency ν. We cannot formulate this function for the general case because of the complications introduced by the structure and large-scale mass motions in the planetary nebula. For a similar reason we are unable to specify $a(\nu)$. We know, however, that

$$\int a(\nu) d\nu = \frac{\pi e^2}{mc} f ,$$

and we shall find it convenient to use a mean dilution factor, W, defined by

$$\int I^0_\nu W_\nu a_{ab}(\nu) d\nu = \frac{\pi e^2}{mc} f_{ab} I^0 \overline{W} , \tag{14}$$

where I^0 is supposed to vary slowly across the line at λ 304, which corresponds to the transition (ab). Then equation (13) becomes

$$F_{ab} = \tfrac{5}{9} N_P \frac{4\pi^2 e^2}{h\nu mc} f_{ab} \bar{I} \overline{W} = 3.27 \times 10^8 \bar{I} \overline{W} N_P , \tag{15}$$

and, by equation (12),

$$\overline{W} \bar{I} = 34.6 \frac{N_b}{N_P} . \tag{16}$$

We obtain the equations of statistical equilibrium for each of the levels, c, d, f, etc., by equating the number entering a level by cascade to the number leaving. Thus,

$$N_b A_{bc} = N_c(A_{ck} + A_{cm}) , \qquad N_c = 0.286 N_b , \tag{17}$$

$$N_b A_{bd} = N_d(A_{dk} + A_{dm} + A_{dn}) , \qquad N_d = 0.097 N_b , \tag{18}$$

$$N_b A_{bf} = N_f(A_{fk} + A_{fm} + A_{fn}) , \qquad N_f = 0.885 N_b , \tag{19}$$

$$N_b A_{bg} = N_g A_{gk} , \qquad N_g = 0.072 N_b , \tag{20}$$

$$N_b A_{bh} = N_h(A_{hk} + A_{hm}) , \qquad N_h = 0.0131 N_b , \tag{21}$$

$$N_b A_{bj} = N_j(A_{jk} + A_{jm} + A_{jn}) , \qquad N_j = 8.9 \times 10^{-4} N_b . \tag{22}$$

From

$$N_c A_{ck} + N_d A_{dk} + N_f A_{fk} + N_g A_{gk} + N_h A_{hk} = N_k(A_{ka} + A_{ka'}) , \tag{23}$$

$$N_c A_{cm} + N_d A_{dm} + N_f A_{fm} + N_h A_{hm} = N_m(A_{ma} + A_{ma'}) , \tag{24}$$

$$N_d A_{dn} + N_f A_{fn} = N_n(A_{na} + A_{na'}) , \tag{25}$$

we obtain, by the use of equations (17), (18), and (19),

$$N_k = 8.3 \times 10^{-3} N_b , \tag{26}$$

$$N_m = 4.34 \times 10^{-3} N_b , \tag{27}$$

$$N_n = 1.4 \times 10^{-3} N_f . \tag{28}$$

The small values of the coefficients in equations (26), (27), and (28) arise from the large values of $A_{k,\,m,\,n-a,\,a'}$. In the derivation of these equations we have assumed that transitions from the ground level to $2p3d\ {}^3P_1$ are relatively infrequent.

Our observational data now afford a consistency check on the theory. From the intensities of the *O* III lines, originating from the b, f, or c levels we have calculated N_b, directly or by use of equation (17) or equation (19), from N_c or N_f. If the theory is correct and our assumed A values are not too much in error, the various values of N_b should agree with one another to within the limits of observational error.

The observed surface brightness, S_λ, of any line expressed in terms of magnitudes per square minute of arc, H_λ, is related to the number of atoms in the upper level, N'', by means of the expression (cf. XI, 9)

$$S_\lambda = \tfrac{1}{3} D N'' A h\nu = 8.40 \times 10^2 (2.512)^{-H_\lambda} \quad \text{or} \quad N'' = \frac{25.2 \times 10^2}{DA h\nu} (2.512)^{-H_\lambda} . \tag{29}$$

To derive N'' from the observed intensity, I_o, we have proceeded as in Paper XI and have adopted for the dimensions of the *O* III fluorescent images of NGC 7009, 7662, and 3242, the values given by Curtis[9] for the inner shells of these planetaries. Table 2 sum-

[9] *Pub. Lick Obs.*, **13**, 55, 1918.

marizes in successive columns the observed lines,[10] the upper levels, H_λ, N'', and N_b computed from equation (17) or equation (19). The straight mean values of the numbers of atoms in the 3d $^3P_2$ level are given in the accompanying table. An approximate

NGC 2022....	1.0×10^{-16}	NGC 7027....	$(1.6\pm0.2)\times10^{-15}$
3242....	3.0×10^{-15}	7662....	$(1.2\pm0.2)\times10^{-14}$
7009....	$(5.9\pm0.2)\times10^{-15}$		

reduction of an unstandardized plate by Stoy yielded the estimate of the value of N_b in NGC 3242. The probable errors quoted are a measure of the internal agreement of the values deduced from the different lines with the aid of the equations of statistical equilibrium.

TABLE 2

POPULATION OF THE 3d $^3P_2$ LEVEL OF *O* III

λ	Upper Level	H_λ				$N''\times10^{15}$				$N_b\times10^{15}$			
		2022	7009	7027	7662	2022	7009	7027	7662	2022	7009	7027	7662
3444.15.....	3d $^3P_2$	11.87	10.38	10.64	10.80	0.39	6.05	2.41	12.8	.....	6.05	2.41	12.7
3312.35.....	3p $^3S_1$	.....	10.67	11.50	10.45	.....	4.87	1.18	7.2	.....	5.5	1.33	8.1
3299.39.....	3p $^3S_1$	.....	.....	13.20	11.96	.....	.....	0.73	5.2	.....	.....	0.83	4.9
3132.87.....	3d $^3P_2$	12.25	9.42	9.98	8.38	0.10	6.11	1.73	17.2	0.10	6.1	1.73	17.2
3121.71.....	3d $^3P_1$	.....	.....	.....	10.96	.....	.....	.....	1.6	.....	.....	.....	1.6
3047.14.....	3p $^3P_2$	.....	.....	.....	9.70	.....	.....	.....	3.9	.....	.....	.....	3.9

Within the errors of observation, theory and observation seem to agree. The lines λ 3312 and λ 3299 appear to be too weak. The fainter lines seem to yield too small a population, as if there is present in the observations a systematic error depending on intensity.

These values of N_b at first sight may seem very small compared with the populations of the metastable $^1D_2$ and ^1S levels of the p^2 configuration. The strongest Bowen fluorescent lines have an intensity approximately one-tenth that of the green nebular lines. The ratio of transition probabilities of the permitted and forbidden lines is of the order of 10^{10}. Hence one readily sees that the effect of a small population in the excited levels is more than offset by a high transition probability.

The λ 304 radiation of *He* II corresponds to the Lyman α radiation of hydrogen. Accordingly, if the optical thickness of the nebula is sufficient, most of the quanta absorbed in the far ultraviolet—i.e., at frequencies greater than that corresponding to the series limit of *He* II—will be degraded into the λ 304 radiation in accordance with the mechanism proposed for hydrogen by Zanstra and by Menzel. Hence this radiation may be expected to be intense, especially in a nebula possessing strong lines of *He* II. The energy available in λ 304 should be far greater than the nuclear star would provide of itself.

From our observational data and equation (16) we may compute the intensity of the radiation in the *O* III 304 radiation in units of ergs/cm²/sec. If we make some reasonable assumption about the size and ultraviolet color temperatures of the central stars of the planetaries, we can estimate the intensity of the λ 304 radiation from the star itself and

[10] Since the intensities of the *O* III 3428 and 3341 lines are somewhat uncertain because of the contiguous *Ne* V lines, we have omitted them from this discussion. The evidence suggests that *Ne* V is very strong in NGC 7027 and perhaps also in NGC 2022, whereas it is much weaker in NGC 7662 and NGC 7009. Slit spectra are necessary to separate the *Ne* V from the *O* III lines.

of the geometrical dilution factor. Then a comparison of the observed and computed dilution will indicate a lower limit to the degree of concentration of energy in the λ 304 radiation produced by the atoms of *He* II.

Accordingly, we have calculated $(I^0\overline{W})$ for the five planetaries for which we have estimates of N_b and N_a. Also we have estimated the sizes of the central stars and the geometrical dilution factor for various assumed ultraviolet color temperatures.

Berman[11] tabulates the apparent photographic magnitudes and distances of these planetaries. In the expression relating distance and absolute and apparent magnitude,

$$m = M + 5 \log \frac{r}{10} + A(r) ,$$

we have taken the correction for space absorption as[12] 0.7 mag. per kiloparsec. The calculated absolute photographic magnitudes for the nuclei of the five planetary nebulae are

TABLE 3

ESTIMATED ABSOLUTE PHOTOGRAPHIC MAGNITUDES OF THE PLANETARY NUCLEI

Nebula	m_s	r	$A(r)$	M
NGC 2022	14.7	4570	3.2	−1.8
3242	11.9	1640	1.2	−0.3
7009	11.9	930	0.6	+1.4
7027	(15.6)	2130	1.5	+2.5
7662	12.7	1200	0.8	+1.5

given in Table 3. The radius of the central star is related to its absolute magnitude by the expression[13]

$$\log R_c = \frac{7340}{T} - 0.14 - 0.2M_p + 0.5 \log (1 - 10^{-1.47\times10^4/T}) . \qquad (30)$$

Let

$$W_g \sim \frac{1}{4}\frac{R^2}{r^2} \qquad (31)$$

denote the geometrical dilution factor; R_c is the radius of the central star in terms of the sun's radius as unity and r the mean radius of the radiating layers of the planetary.

The radii of the central stars and the dilution factors have been calculated for the three assumed values of the color temperature—80,000, 100,000, and 150,000; hence the three computed values for each pair of tabular arguments in Table 4. The successive columns of Table 4 give the designation of the planetary, the computed radii, dilution factors, and $(WI)_c$ for the three assumed temperatures. The column headed $(WI)_{obs}$ is obtained from the use of equation (16), and the final column from the ratio of observed and computed dilution factors. As we expected, the observed dilution factor is larger, by

[11] *Lick Obs. Bull.*, **18**, 73, 1937.

[12] This value, adopted from Trumpler's investigation of galactic star clusters, represents some kind of an average over different galactic longitudes. A correction based on the assumption of uniform space absorption is admittedly rough but adequate for our present purposes.

[13] Russell, Dugan, and Stewart, *Astronomy*, p. 732, Boston: Ginn & Co.

a factor of 10^2 or 10^3, than the dilution factor predicted on the basis of geometrical considerations alone. Evidently the concentration of energy in the λ 304 line of *He* II is considerable. The absence of the other high-level permitted lines of *O* III is easy to understand; they cannot draw on the rich sources of energy available for excitation of the $3d\ ^3P_2$ level.

Photoionization and subsequent recapture of electrons in responsible for the radiations emitted by *He* II. It is this energy, radiated in the strongest *He* II line, that can be absorbed by the *O* III atoms. The observations show that the lines of the Bowen fluorescent mechanism are confined closely to the region in which the *He* II lines occur. We can reconcile this observational result with theory only if the opacity of the *O* III atoms is sufficiently great to use up all the *He* II 304 radiation within a small fraction of the total nebular radius.

TABLE 4

DILUTION OF λ 304 RADIATION IN PLANETARY NEBULAE

NGC	R_c	$W_g \times 10^{15}$	$(WI)_c \times 10^{16}$	$\times 10^{13}$ $(WI)_{obs}$	W_{obs}/W_{comp}
2022	1.20	4.6	1.82	14.	74. $\times 10^2$
	1.05	3.5	4.05	.....	33.
	0.83	2.2	14.	.....	9.6
3242	0.62	9.6	3.8	3.4	8.8
	0.54	7.2	9.3	.....	3.6
	0.43	4.6	29.	.....	1.2
7009	0.28	8.2	3.2	1.6	5.0
	0.24	6.2	8.0	.....	2.0
	0.19	3.9	25.	.....	0.65
7027	0.17	2.2	0.85	0.42	4.9
	0.15	1.6	2.1	.....	2.0
	0.12	1.0	6.6	.....	0.63
7662	0.27	5.3	2.1	3.3	16.
	0.23	4.0	5.2	.....	6.4
	0.19	2.5	16.	.....	2.1

We now investigate this question quantitatively. An *O* III atom that has just absorbed a λ 304 quantum and is raised to the $3d\ ^3P_2$ level may do one of three things: return to the initial level $2p^2\ ^3P_2$, drop to $2p^2\ ^3P_1$, or emit the lines of the Bowen fluorescent mechanism. The first two of these processes produce quanta that are immediately available for starting the cycle again. Only when the atom has started the cascade of the Bowen mechanism is the energy lost as far as concerns further excitation of *O* III.

In the zone of *He* II the major excitation of *O* III arises from the energy in the λ 304 line of that atom. Outside the *He* II zone, i.e., when all the ultraviolet radiation has been degraded in λ 304, a greater percentage of the radiation will lie in λ 303.62 of $2p^2\ ^3P_1 - 2p3d\ ^3P_2$. As we have stated above, this energy also can be used by *O* III to initiate the Bowen cycle. The Einstein *A*'s for the respective downward transitions *b* to *a* and *b* to *a'* have the ratio 3:1. The corresponding products of the populations in the lower levels and the absorption coefficients, $N_a a_\nu(ab)$ and $N_{a'} a_\nu(a'b)$, possess the same ratio. Hence, if the beams in the two wave lengths possess the same intensity, the absorptions and emissions will balance, except for the small fraction removed through the operation of the cyclic process. This loss of energy will in no way disturb the initial equality of the two beams. Should one or the other of the beams be initially of different intensity, absorption and emission of radiation will tend to bring them toward equality. The phenomenon is closely related to that of "interlocking," as discussed by Woolley.

We shall investigate the case when the two beams are equal. Then, according to the

above argument, gains and losses from one beam into the other are exactly offset. Now, of the number of upward transitions caused by both beams, the fraction,

$$\frac{A_{ba} + A_{ba'}}{\Sigma A_{bi}} = 0.978 ,$$

reappears as downward transitions. Because of the much greater Einstein A's associated with the far ultraviolet lines, only 2.2 per cent of the transitions initiate the Bowen cycle. Thus, as far as the disappearance of radiation is concerned, the effective absorption coefficient a_{eff} is only about 0.022 times that of the true absorption coefficient. An element $d\tau_{\text{eff}}$ of effective optical depth is

$$d\tau_{\text{eff}} \sim 0.022 N_a a_\nu(ab) = 0.022 N_{a'} a_\nu(a'b) . \tag{32}$$

We do not know a_ν exactly, but we may adopt a mean value over the effective width of the line according to the formula

$$\bar{a}_\nu = \frac{\pi\epsilon^2}{mc} f \frac{1}{\Delta\nu} , \tag{33}$$

where we set

$$\frac{\Delta\nu}{\nu} = \frac{2v}{c} . \tag{34}$$

The quantity v is defined by the root-mean-square formula

$$v = \sqrt{\frac{2kT}{m_a}} = 0.321 \times 10^4 T^{1/2} . \tag{35}$$

We suppose the atoms to have the same kinetic temperature as the electrons, 10,000°. Therefore $\Delta\nu \sim 2.11 \times 10^{11}$ and

$$d\tau_{\text{eff}} \sim 3.2 \times 10^{-16} N_a dx . \tag{36}$$

Taking $N_a \sim 0.5$ and assuming that within a range of $\tau = 1 = 1.6 \times 10^{-16} x$, whence $x \sim 6 \times 10^{15}$ cm. or 400 astronomical units, we calculate that the intensity will fall to $1/e$ of its original value. The images of the O III lines should be about 5 per cent larger than those of the helium lines in a typical planetary.

To treat the problem more exactly, let us set up the equations of transfer for the $\nu(ab)$ and $\nu(a'b)$ transitions. If $I^0 W_1'$ and $I^0 W_2'$ are the intensities of the $\nu(ab)$ and $\nu(a'b)$ radiations, respectively, we have

$$\cos\theta \frac{d(I^0 W_1')}{dx} = -\bar{a}_1 N_a (I^0 W_1') + \bar{a}_1 N_b \frac{2h\nu^3}{c^2} \frac{\varpi_a}{\varpi_b} , \tag{37a}$$

$$\cos\theta \frac{d(I^0 W_2')}{dx} = -\bar{a}_2 N_{a'} (I^0 W_2') + \bar{a}_2 N_b \frac{2h\nu^3}{c^2} \frac{\varpi_a}{\varpi_b} , \tag{37b}$$

where

$$\bar{a}_1 = \frac{\pi\epsilon^2}{mc} f_{ab} \frac{1}{\Delta\nu}, \qquad \bar{a}_2 = \frac{\pi\epsilon^2}{mc} f_{a'b} \frac{1}{\Delta\nu}. \tag{38}$$

We also write, for the equation of statistical equilibrium,

$$\left.\begin{aligned} &\frac{4\pi}{h\nu_{ab}} \frac{\pi\epsilon^2}{mc} [N_a I^0 W_1' f_{ab} + N_{a'} I^0 W_2' f_{a'b}] \\ &\quad = N_b \frac{8\pi^2\epsilon^2\nu_{ab}^2}{mc^3} \left\{ \left(\frac{\varpi_a}{\varpi_b} f_{ab} + \frac{\varpi_{a'}}{\varpi_b} f_{a'b} \right) + \sum_{i \neq a, a'} \frac{\varpi_i}{\varpi_b} \frac{\nu_i^2}{\nu_{ab}^2} f_{ib} \right\} = N_b \sum_j A_{jb}, \end{aligned}\right\} \tag{39}$$

where the summations are to be carried out over all the lower levels connecting with b. If we add equations (37a) and (37b) and substitute for N_b, we obtain

$$\left.\begin{aligned} \cos\theta \frac{d[I^0(W_1' + W_2')]}{dx} &= -I^0(N_a\bar{a}_1 W_1' + N_a\bar{a}_2 W_2') \\ &\quad + \left(\bar{a}_1 \frac{\varpi_a}{\varpi_b} + \bar{a}_2 \frac{\varpi_{a'}}{\varpi_b} \right) \frac{8\pi^2\epsilon^2\nu_{ab}^2}{mc^3} [N_a W_1' f_{ab} + N_{a'} W_2' f_{a'b}] \frac{I^0}{\Sigma A}. \end{aligned}\right\} \tag{40}$$

Now $N_{a'} = \frac{3}{5} N_a$ and

$$a_2 = \tfrac{5}{9}\bar{a}_1, \qquad \varpi_a = \varpi_b = 5, \qquad \varpi_{a'} = 3. \tag{41}$$

If we further suppose that everywhere

$$W_2'/W_1' = \text{constant} = 1, \tag{42}$$

in accord with the argument presented above for equality of the two beams, equation (40) becomes

$$\left.\begin{aligned} \cos\theta \frac{d(I^0 W_1')}{dx} &= -N_a\bar{a}_1 \tfrac{2}{3} I^0 W_1' \left[1 - \frac{4}{3} \frac{A_{ab}}{\Sigma A} \right] \\ &= -N_a\bar{a}_1 \tfrac{2}{3} I^0 W_1' \left[\frac{\Sigma A - (A_{a'b} + A_{ab})}{\Sigma A} \right] = -0.0215\bar{a}_1 \tfrac{2}{3} N_a I^0 W_1', \end{aligned}\right\} \tag{43}$$

by the use of equation (2a) and the substitution of numerical values. Let

$$d\tau = 0.0215\ \bar{a}_1 \tfrac{2}{3} N_a dx = 0.0215 \frac{\pi\epsilon^2}{mc} f_{ab} \frac{1}{\Delta\nu} \tfrac{2}{3} N_a dx = 2.07 \times 10^{-16} N_a dx. \tag{44}$$

Then equation (43) becomes

$$\cos\theta \frac{d(I^0 w_1')}{d\tau} = -W_1' I^0. \tag{45}$$

Integrating over all solid angles, we obtain the result

$$\frac{\partial F}{\partial\tau} = \int \cos\theta \frac{dI^0 W_1'}{d\tau} d\omega = -J, \tag{46}$$

where

$$J = \int I^0 W_1' d\omega = 4\pi \overline{W}_1 I^0 . \tag{47}$$

Now, according to the Eddington approximation,

$$F = -\frac{1}{3}\frac{\partial J}{\partial \tau} , \tag{48}$$

whence

$$-\frac{1}{3}\frac{d^2J}{d\tau^2} = -J \qquad \text{or} \qquad \frac{d^2J}{d\tau^2} = +3J . \tag{49}$$

Integration gives the following result:

$$\overline{W} = \overline{W}_a e^{-\sqrt{3}\tau} . \tag{50}$$

For the intensity to fall to $1/e$ of its original value, we must have

$$1 \sim 3.6 \times 10^{-16} N_a . \tag{51}$$

If $N_a \sim 0.5$, we find that $x \sim 5.5 \times 10^{15}$ cm or 370 astronomical units. The radii of the planetaries are about 10^{17} cm. Hence the images of the lines of the Bowen fluorescent mechanism should be only about 5 per cent larger than those of the helium images.

Bowen has mentioned the similarity in size between the λ 4686 image and the images of the ultraviolet radiations of *O* III. Measures of the sizes of the nebular images on microphotometer tracings of slitless spectrograms of NGC 7662 yield results which are in accordance with this suggestion; they indicate that the λ 3133 images of *O* III may be slightly larger than the λ 3203 image of ionized helium.

We shall discuss the fluorescent cycle in *N* III after treating the question of abundances.

HARVARD COLLEGE OBSERVATORY
August 2, 1941

THE GRATING INFRARED SOLAR SPECTRUM

V. ATOMIC LINES IN THE FAR INFRARED

ARTHUR ADEL

ABSTRACT

Six intense lines in the grating infrared solar spectrum are tentatively correlated with the transitions $3D - 4P$ of normal sodium and $6P - 5D$ of normal potassium.

In the course of mapping the infrared solar spectrum to 14 μ with a 2400-line echelette grating, the author has observed, besides the lines of the powerful atmospheric bands of molecular origin, numerous intense lines apparently of atomic origin.[1]

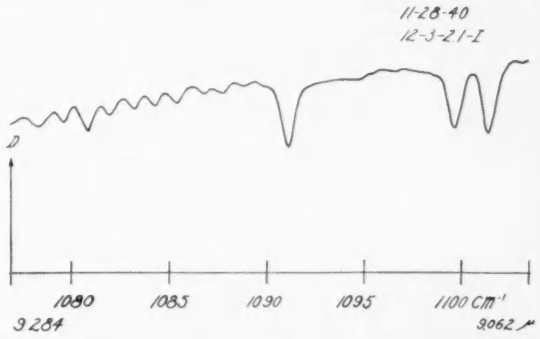

FIG. 1.—Energy plot of the infrared solar spectrum from 9.284 μ to 9.062 μ. Frequency listed at intervals of 5 cm^{-1}. The strong lines at 1091.0, 1099,6, and 1101.3 cm^{-1} are attributed to *Na* I. The pattern of weak lines which occupies the long-wave-length half of the figure is a portion of the rotational structure in the positive branch of the 9.40 μ atmospheric band of CO_2. This structure in the solar spectrum has been discussed (see Arthur Adel, *Ap. J.*, in Press).

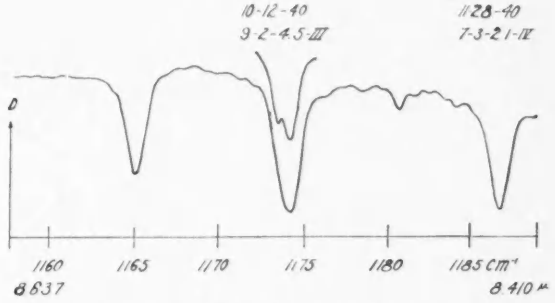

FIG. 2.—Energy plot of the infrared solar spectrum from 8.637 μ to 8.410 μ. Frequency listed at intervals of 5 cm^{-1}. The strong lines at 1173.5, 1174.2, and 1186.8 cm^{-1} are attributed to *K* I. The origin of the intense line at 1165 cm^{-1} is not known.

Such, for example, are the three lines at 1091.04 cm^{-1}, 1099.59 cm^{-1}, and 1101.33 cm^{-1} shown in Figure 1 and the three lines 1173.49 cm^{-1}, 1174.19 cm^{-1}, and 1186.84 cm^{-1} shown in Figure 2.

[1] *Phys. Rev.*, **59**, 915A, 1941.

From tables of energy states one finds for $3D-4P$ of *Na* I 1100.04 cm^{-1} for the unresolved doublet and 1094.55 cm^{-1} for the third line; and for $6P-5D$ of *K* I one finds 1179.29 cm^{-1} for the unresolved doublet and 1187.44 cm^{-1} for the third line.[2] These are probable transitions of elements known to be plentiful in the atmosphere of the sun; and it would appear, therefore, that the solar lines in question may well be due to these transitions as follows:

Na I	*K* I
$3D(3/2) - 4P(1/2) = 1091.04\ cm^{-1}$	$6P(1/2) - 5D(3/2) = 1186.84\ cm^{-1}$
$3D(3/2) - 4P(3/2) = 1101.33$	$6P(3/2) - 5D(3/2) = 1173.49$
$3D(5/2) - 4P(3/2) = 1099.59$	$6P(3/2) - 5D(5/2) = 1174.19$
$\delta P = 10.29\ cm^{-1}$	$\delta P = 13.35\ cm^{-1}$
$\delta D = 1.74$	$\delta D = 0.70$

LOWELL OBSERVATORY
FLAGSTAFF, ARIZONA

[2] Bacher and Goudsmit, *Atomic Energy States*. New York: McGraw-Hill, 1932.

THE GRATING INFRARED SOLAR SPECTRUM

VI. THE MAP FROM 14 μ TO 7 μ

ARTHUR ADEL

ABSTRACT

A high-resolution map of the infrared solar spectrum is presented. It covers the region from 14 μ to 7 μ and exhibits an actual resolving-power of $\sim$1 cm^{-1} throughout. About 400 absorption lines are contained in the map, including the rotation-vibration lines of the great atmospheric bands and numerous intense lines apparently of atomic origin. Tables of wave lengths and frequencies accompany the map.

In a continuation and extension of work begun at the University of Michigan, the author has recently mapped the infrared solar spectrum from 14 to 2 μ in the first order of an echelette grating having 2400 lines per inch.[1] In previous communications concerning isolated portions of this map of the solar spectrum, lines have been identified as follows:

I. ν_2 of *HDO* with center at 7.12 μ
II. ν_1 of *NNO* with center at 7.78 μ
III. "ν_2" of *OCO* with center at 13.9 μ
IV. $\nu_3 - (\nu_1, 2\nu_2)$ of *OCO* with centers at 10.4 μ and 9.4 μ
V. 3D $-$ 4P of *Na* I and 6P $-$ 5D of *K* I near 9.1 μ and 8.5 μ, respectively[2]

The present paper is concerned with a presentation of that portion of the solar-spectrum map which lies between 14 and 7 μ. Very nearly 400 solar and terrestrial lines occupy this spectral interval. In addition to the numerous rotation-vibration lines of the great atmospheric bands, many intense lines of atomic origin are present.

As given in this paper the map from 14 to 7 μ is composed of 36 segments, shown in Figures 1–36. Each segment is a direct trace of an original run or observation.[3] In general, a run covers about 0.2 μ (2000 A). The 36 segments, each of which gives only the envelope of its corresponding original, either join or overlap, so that there are no gaps in the map.[4] Segments which join in wave length do not necessarily match in intensity at the point of joining because of the different degrees of amplification employed in recording the different segments. Each curve is in the form of an energy trace, solar energy versus wave length or frequency, which should facilitate the determination of the equivalent widths of the absorption lines. The relative energies are correctly shown within each continuous section of curve.[5]

[1] *Phys. Rev.*, **59**, 915, 1941.

[2] Paper I, *Ap. J.*, **93**, 506, 1941; paper II, *ibid.*, p. 509; paper III, *ibid.*, **94**, 375, 1941; paper IV, *ibid.*, p. 379; paper V, *ibid.* (in press).

[3] An original recorded observation is reproduced in paper III.

[4] In this connection note that, although Fig. 31 appreciably overlaps Fig. 30, the latter was observed with considerably less resolving-power.

[5] The discontinuities in Figs. 18, 30, and 35 are due to changes in amplification. The relative intensities are correct within each continuous portion of curve.

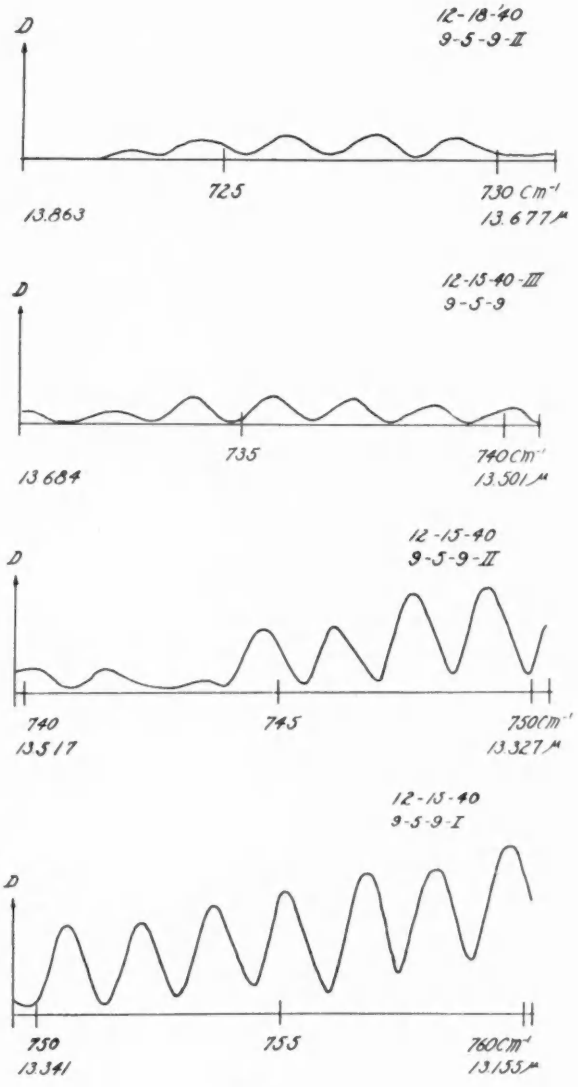
D
12-18-40
9-5-9-II
725
730 Cm⁻¹
13.863
13.677 μ
D
12-13-40-III
9-5-9
735
740 Cm⁻¹
13.684
13.501 μ
D
12-15-40
9-5-9-II
740
745
750 Cm⁻¹
13.517
13.327 μ
12-15-40
9-5-9-I
D
750
755
760 Cm⁻¹
13.341
13.155 μ

FIGS. 1–4

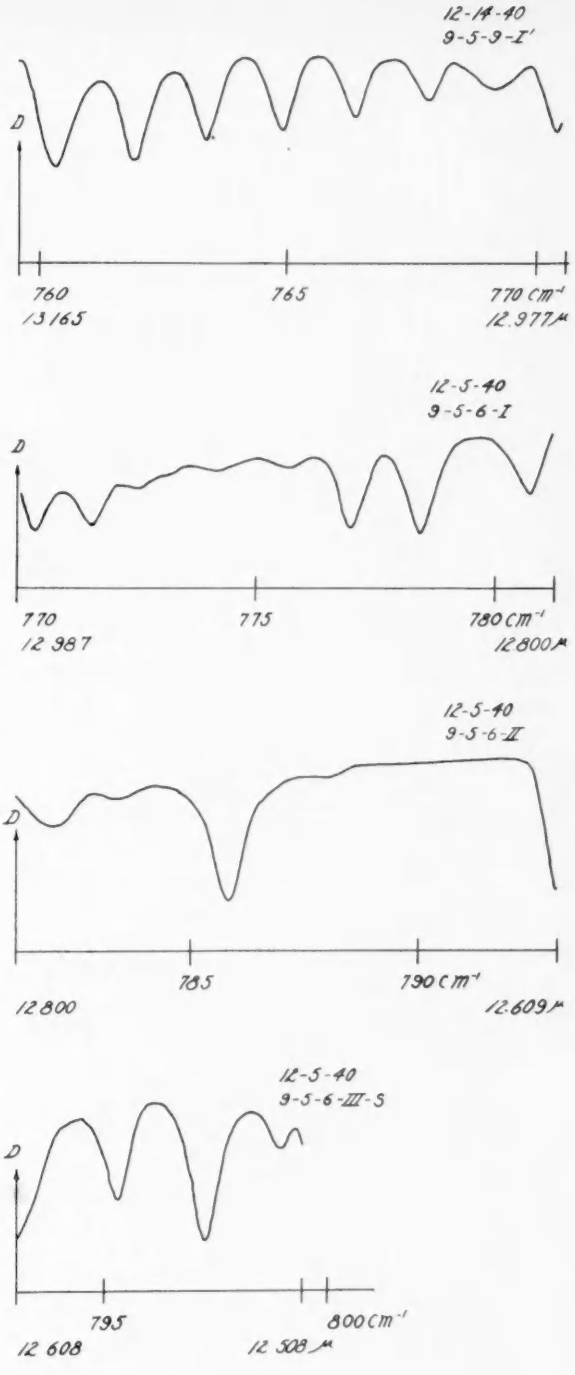
12-14-40
9-5-9-I'
D
760
13165
765
770 cm⁻¹
12.977μ
12-5-40
9-5-6-I
D
770
12 987
775
780 cm⁻¹
12800μ
12-5-40
9-5-6-II
D
785
790 cm⁻¹
12 800
12.609μ
12-5-40
9-5-6-III-S
D
795
800 cm⁻¹
12 608
12 508μ

FIGS. 5–8

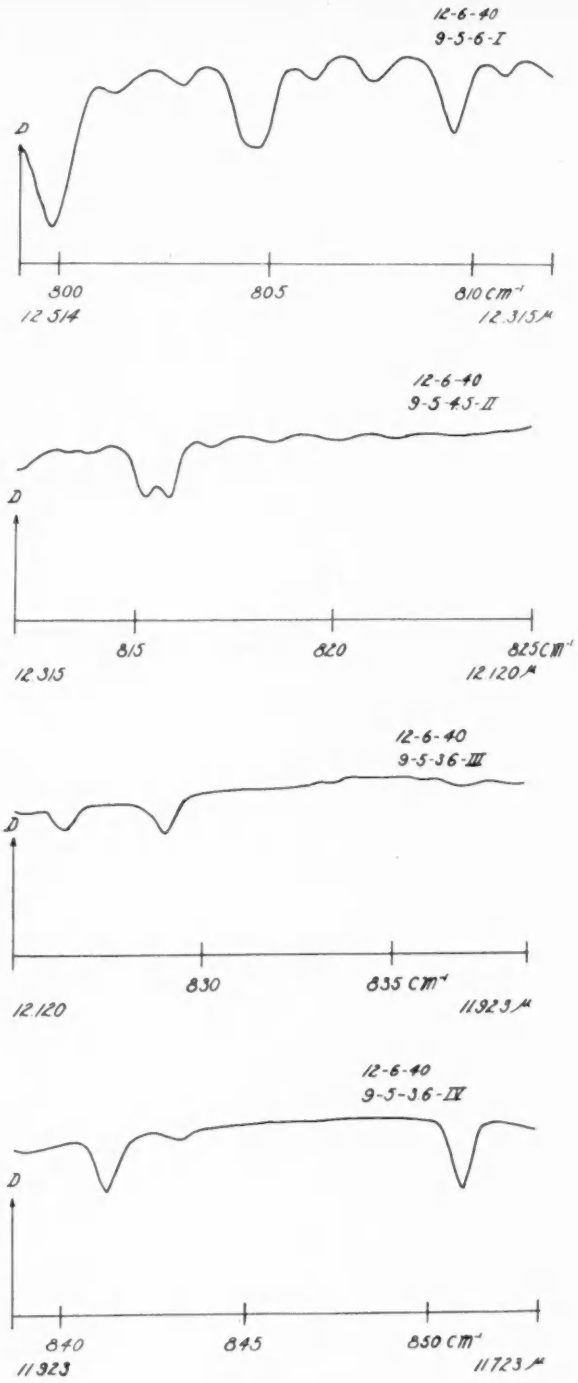
12-6-40
9-5-6-I
D
800
805
810 cm⁻¹
12.514
12.315 μ
12-6-40
9-5-45-II
D
815
820
825 cm⁻¹
12.315
12.120 μ
12-6-40
9-5-36-III
D
830
835 cm⁻¹
12.120
11.923 μ
12-6-40
9-5-36-IV
D
840
845
850 cm⁻¹
11.923
11.723 μ

FIGS. 9–12

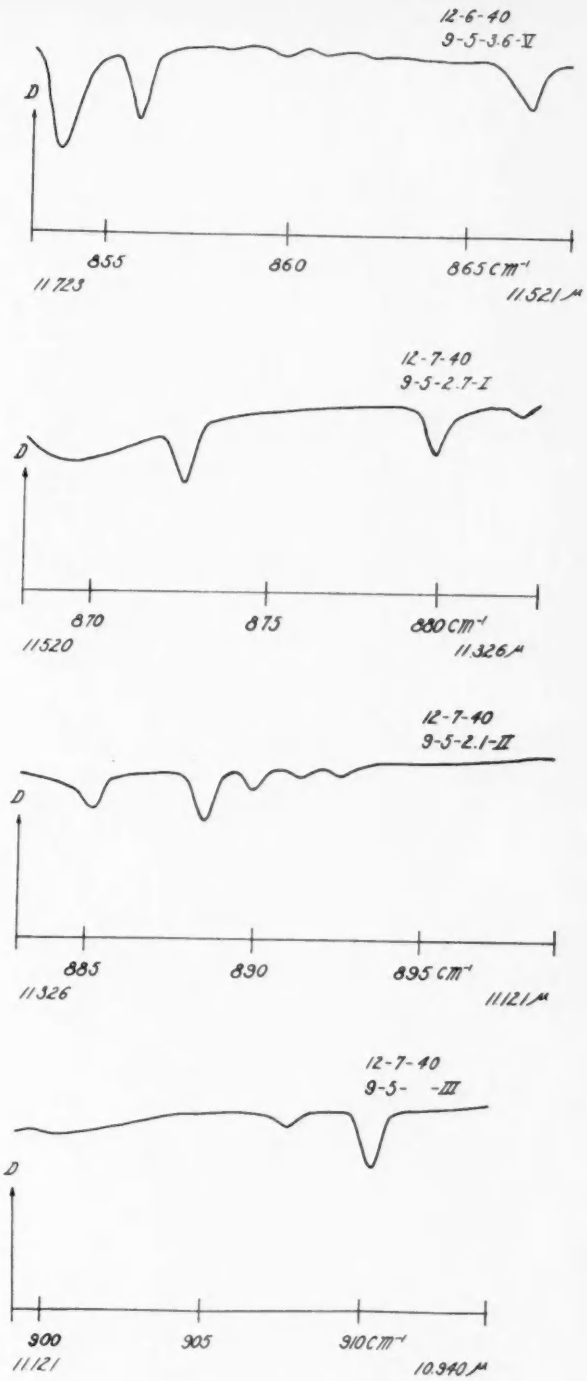
12-6-40
9-5-3.6-V
D
855
860
865 cm⁻¹
11.723
11.521 μ
12-7-40
9-5-2.7-I
D
870
875
880 cm⁻¹
11.520
11.326 μ
12-7-40
9-5-2.1-II
D
885
890
895 cm⁻¹
11.326
11.121 μ
12-7-40
9-5- -III
D
900
905
910 cm⁻¹
11.121
10.940 μ

FIGS. 13–16

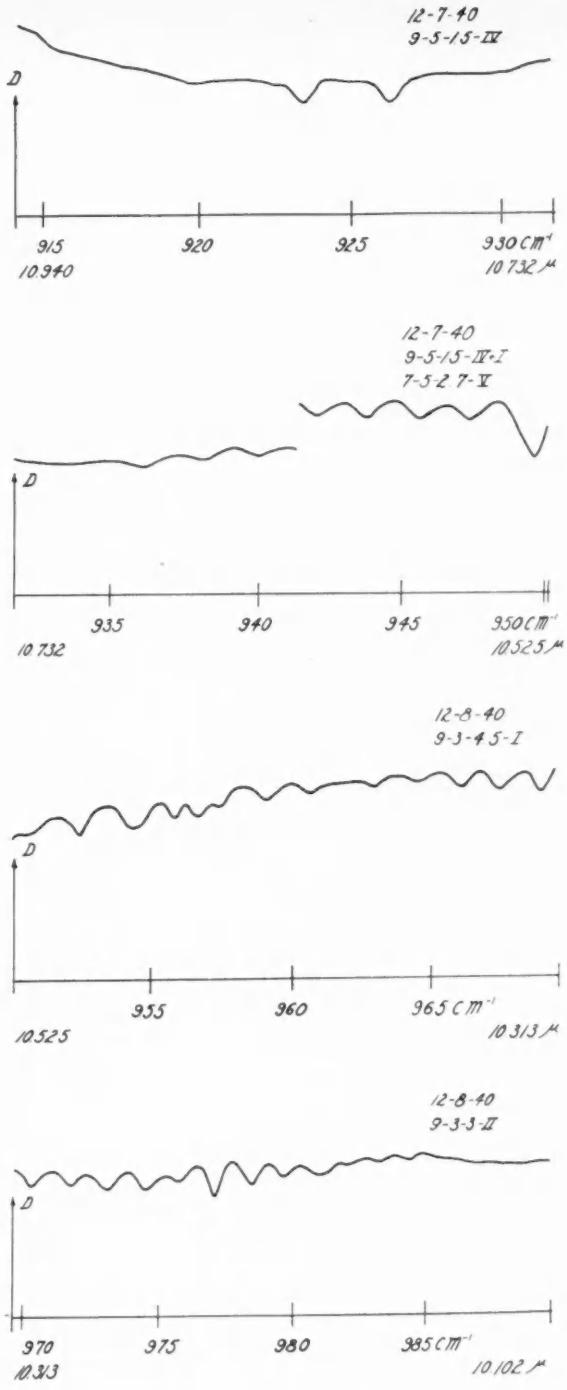
12-7-40
9-5-15-IV
D
915
10940
920
925
930 cm⁻¹
10732 μ
12-7-40
9-5-15-IV+I
7-5-27-V
D
935
10732
940
945
950 cm⁻¹
10525 μ
12-8-40
9-3-45-I
D
955
10525
960
965 cm⁻¹
10313 μ
12-8-40
9-3-3-II
D
970
10313
975
980
985 cm⁻¹
10102 μ

FIGS. 17–20

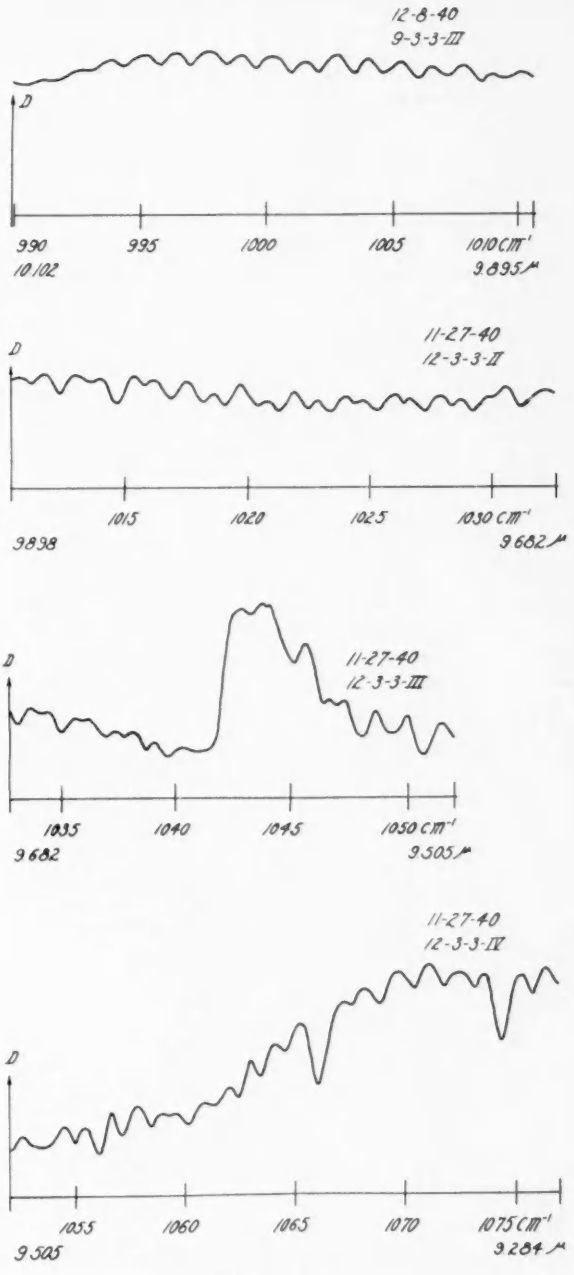
12-8-40
9-3-3-III
D
990
995
1000
1005
1010 cm⁻¹
10.102
9.895 μ
11-27-40
12-3-3-II
D
1015
1020
1025
1030 cm⁻¹
9.838
9.682 μ
11-27-40
12-3-3-III
D
1035
1040
1045
1050 cm⁻¹
9.682
9.505 μ
11-27-40
12-3-3-IV
D
1055
1060
1065
1070
1075 cm⁻¹
9.505
9.284 μ

FIGS. 21–24

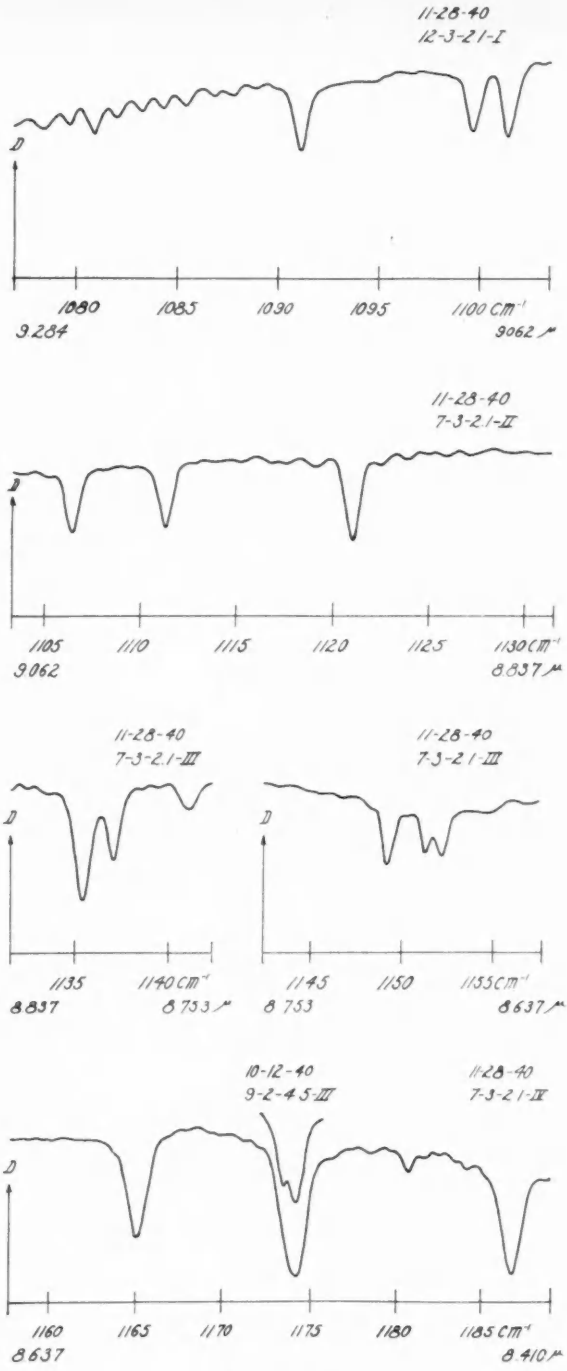
11-28-40
12-3-21-I
D
1080
1085
1090
1095
1100 cm⁻¹
9.284
9.062 μ
11-28-40
7-3-2.1-II
D
1105
1110
1115
1120
1125
1130 cm⁻¹
9.062
8.837 μ
11-28-40
7-3-2.1-III
D
1135
1140 cm⁻¹
8.837
8.753 μ
11-28-40
7-3-21-III
D
1145
1150
1155 cm⁻¹
8.753
8.637 μ
10-12-40
9-2-45-III
11-28-40
7-3-21-II
D
1160
1165
1170
1175
1180
1185 cm⁻¹
8.637
8.410 μ

FIGS. 25–28

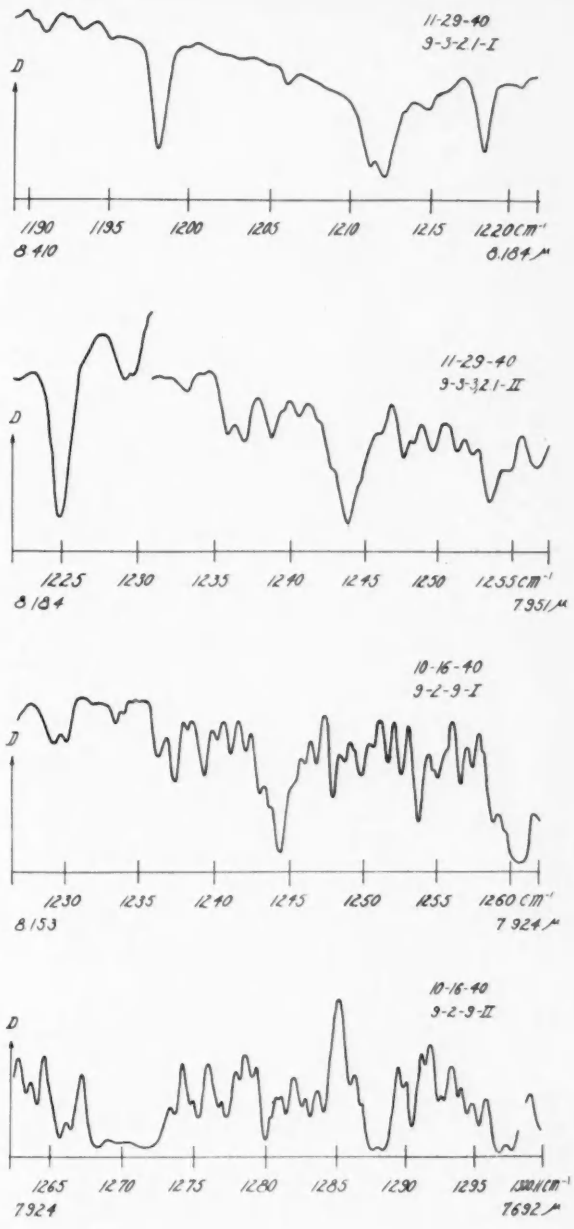
11-29-40
9-3-21-I
D
1190 1195 1200 1205 1210 1215 1220 cm⁻¹
8.410 8.184 μ
11-29-40
9-3-3,21-II
D
1225 1230 1235 1240 1245 1250 1255 cm⁻¹
8.184 7.951 μ
10-16-40
9-2-9-I
D
1230 1235 1240 1245 1250 1255 1260 cm⁻¹
8.153 7.924 μ
10-16-40
9-2-9-II
D
1265 1270 1275 1280 1285 1290 1295 1300.4 cm⁻¹
7.924 7.692 μ

FIGS. 29–32

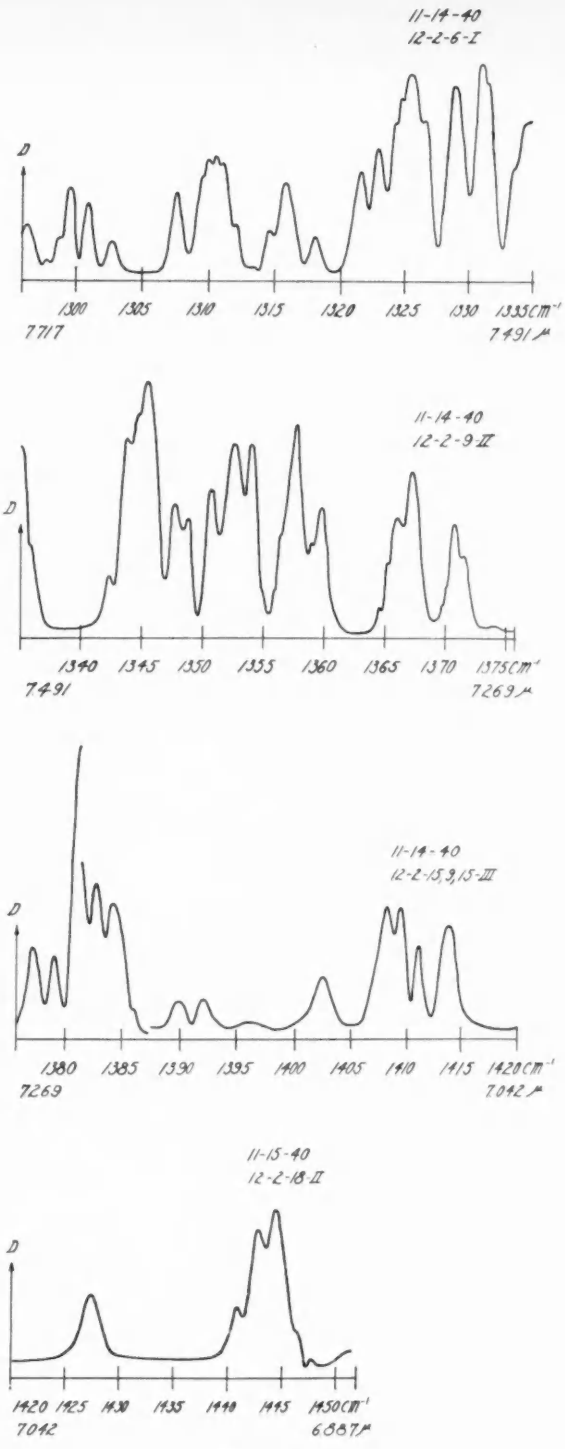
11-14-40
12-2-6-I
D
1300 1305 1310 1315 1320 1325 1330 1335 cm⁻¹
7717
7491 μ
11-14-40
12-2-9-II
D
1340 1345 1350 1355 1360 1365 1370 1375 cm⁻¹
7491
7269 μ
11-14-40
12-2-15,3,15-III
D
1380 1385 1390 1395 1400 1405 1410 1415 1420 cm⁻¹
7269
7042 μ
11-15-40
12-2-18-II
D
1420 1425 1430 1435 1440 1445 1450 cm⁻¹
7042
6887 μ

FIGS. 33–36

TABLE 1

LINES IN THE INFRARED SOLAR SPECTRUM FROM 13.863 μ TO 6.887 μ

Wave Length	Frequency	Wave Length	Frequency	Wave Length	Frequency
Fig. 1		Fig. 2		Fig. 3	
13.863 μ	721.33 cm^{-1}	13.684 μ	730.79 cm^{-1}	13.518 μ	739.77 cm^{-1}
13.814	723.90	13.668	731.65	13.497	740.90
13.784	725.48	13.639	733.19	13.464	742.72
13.755	727.00	13.610	734.77	13.443	743.90
13.725	728.62	13.582	736.29	13.415	745.45
13.695	730.20	13.553	737.84	13.388	746.93
13.677	731.14	13.525	739.34	13.362	748.40
		13.501	740.71	13.336	749.87
				13.327	750.33
Fig. 4		Fig. 5		Fig. 6	
13.341	749.54	13.165	759.59	12.987	769.98
13.336	749.86	13.153	760.30	12.980	770.40
13.309	751.37	13.126	761.87	12.961	771.53
13.282	752.88	13.101	763.28	12.945	772.52
13.256	754.39	13.075	764.84	12.935	773.12
13.229	755.93	13.049	766.32	12.917	774.17
13.204	757.37	13.024	767.80	12.893	775.61
13.177	758.87	13.001	769.19	12.871	776.96
13.156	760.14	12.979	770.46	12.847	778.40
		12.977	770.59	12.809	780.71
				12.800	781.25
Fig. 7		Fig. 8		Fig. 9	
12.800	781.25	12.608	793.13	12.514	799.11
12.787	782.04	12.573	795.35	12.501	799.94
12.764	783.46	12.542	797.29	12.478	801.41
12.725	785.83	12.516	798.96	12.454	802.98
12.610	793.03	12.509	799.45	12.426	804.74
12.609	793.07			12.405	806.13
				12.382	807.62
				12.353	809.54
				12.334	810.10
				12.315	811.99
Fig. 10		Fig. 11		Fig. 12	
12.315	811.99	12.120	825.06	11.924	838.68
12.315	812.04	12.092	827.01	11.917	839.15
12.295	813.32	12.054	829.62	11.888	841.21
12.287	813.89	11.924	838.68	11.860	843.18
12.267	815.23			11.752	850.95
12.258	815.83			11.723	853.00
12.241	816.93				
12.218	818.43				
12.194	820.07				
12.172	821.57				
12.120	825.06				

TABLE 1—*Continued*

Wave Length	Frequency	Wave Length	Frequency	Wave Length	Frequency
Fig. 13		Fig. 14		Fig. 15	
11.723 μ	853.00 cm^{-1}	11.520 μ	868.05 cm^{-1}	11.326 μ	882.95 cm^{-1}
11.712	853.80	11.501	869.50	11.297	885.17
11.684	855.90	11.460	872.60	11.255	888.47
11.650	858.36	11.365	879.87	11.237	889.93
11.629	859.92	11.332	882.43	11.219	891.34
11.614	861.01	11.326	882.95	11.204	892.54
11.596	862.37			11.121	899.20
11.537	866.78				
11.521	867.98				
Fig. 16		Fig. 17		Fig. 18	
11.121	899.20	10.940	914.07	10.732	931.77
11.103	900.63	10.871	919.91	10.682	936.13
11.018	907.63	10.829	923.47	10.659	938.20
10.985	910.33	10.797	926.21	10.638	940.05
10.940	914.07	10.732	931.77	10.616	942.00
				10.597	943.68
				10.576	945.55
				10.556	947.29
				10.531	949.59
				10.525	950.09
Fig. 19		Fig. 20		Fig. 21	
10.525	950.09	10.313	969.67	10.102	989.86
10.519	950.62	10.305	970.30	10.096	990.44
10.499	952.45	10.290	971.82	10.085	991.59
10.478	954.37	10.276	973.16	10.071	992.93
10.463	955.79	10.260	974.62	10.058	994.21
10.453	956.62	10.247	975.89	10.044	995.63
10.445	957.37	10.234	977.16	10.032	996.81
10.427	959.05	10.219	978.56	10.017	998.30
10.411	960.60	10.207	979.76	10.005	999.45
10.385	962.92	10.193	981.08	9.991	1000.87
10.368	964.53	10.182	982.17	9.980	1002.00
10.351	966.09	10.169	983.34	9.966	1003.36
10.336	967.49	10.157	984.50	9.954	1004.59
10.320	968.96	10.102	989.86	9.941	1005.96
10.313	969.67			9.929	1007.12
				9.916	1008.50
				9.905	1009.59
				9.895	1010.65
Fig. 22		Fig. 23		Fig. 24	
9.898	1010.30	9.682	1032.82	9.505	1052.06
9.891	1011.05	9.679	1033.20	9.504	1052.20
9.879	1012.25	9.670	1034.14	9.491	1053.59
9.867	1013.52	9.661	1035.04	9.478	1055.03
9.856	1014.57	9.652	1036.06	9.468	1056.15
9.846	1015.65	9.644	1036.89	9.459	1057.16

TABLE 1—*Continued*

Wave Length	Frequency	Wave Length	Frequency	Wave Length	Frequency
Fig. 22—*Continued*		Fig. 23—*Continued*		Fig. 24—*Continued*	
9.835 μ	1016.82 cm^{-1}	9.637 μ	1037.71 cm^{-1}	9.448 μ	1058.44 cm^{-1}
9.822	1018.09	9.628	1038.62	9.440	1059.27
9.813	1019.05	9.619	1039.62	9.433	1060.13
9.801	1020.36	9.606	1041.02	9.422	1061.40
9.791	1021.30	9.586	1043.14	9.413	1062.39
9.780	1022.50	9.580	1043.87	9.404	1063.37
9.772	1023.34	9.569	1045.06	9.394	1064.51
9.762	1024.39	9.557	1046.34	9.381	1066.00
9.753	1025.30	9.552	1046.86	9.368	1067.52
9.742	1026.47	9.542	1047.99	9.356	1068.81
9.734	1027.31	9.530	1049.34	9.342	1070.45
9.723	1028.46	9.517	1050.70	9.330	1071.80
9.715	1029.33	9.505	1052.06	9.317	1073.26
9.707	1030.20			9.307	1074.49
9.696	1031.40			9.294	1075.94
9.682	1032.82			9.284	1077.13
Fig. 25		Fig. 26		Fig. 27	
9.284	1077.13	9.062	1103.50	8.837	1131.58
9.272	1078.49	9.057	1104.12	8.830	1132.53
9.261	1079.78	9.049	1105.13	8.821	1133.61
9.250	1081.03	9.037	1106.56	8.807	1135.49
9.241	1082.09	9.022	1108.35	8.794	1137.19
9.231	1083.32	9.013	1109.46	8.782	1138.70
9.222	1084.33	8.998	1111.31	8.775	1139.56
9.213	1085.42	8.987	1112.70	8.762	1141.24
9.202	1086.77	8.968	1115.07	8.753	1142.50
9.194	1087.70	8.955	1116.63	8.746	1143.38
9.184	1088.84	8.949	1117.51	8.736	1144.65
9.177	1089.74	8.937	1118.97	8.729	1145.56
9.166	1091.04	8.921	1120.90	8.720	1146.75
9.094	1099.59	8.909	1122.50	8.709	1148.27
9.080	1101.33	8.898	1123.80	8.701	1149.27
9.065	1103.10	8.890	1124.84	8.686	1151.33
9.062	1103.50	8.883	1125.78	8.679	1152.26
		8.873	1127.08	8.658	1154.94
		8.837	1131.58	8.643	1157.05
				8.637	1157.85
Fig. 28		Fig. 29		Fig. 30	
8.637	1157.85	8.410	1189.10	8.184	1221.93
8.592	1163.83	8.402	1190.20	8.182	1222.17
8.584	1165.03	8.396	1191.05	8.164	1224.94
8.571	1166.79	8.387	1192.36	8.152	1226.76
8.562	1167.91	8.380	1193.30	8.136	1229.09
8.553	1169.14	8.368	1195.02	8.132	1229.67
8.548	1169.90	8.348	1197.96	8.109	1233.19
8.538	1171.22	8.334	1199.85	8.101	1234.35
8.533	1171.98	8.292	1206.04	8.091	1235.95

TABLE 1—*Continued*

Wave Length	Frequency	Wave Length	Frequency	Wave Length	Frequency
Fig. 28—*Continued*		Fig. 29—*Continued*		Fig. 30—*Continued*	
8.517 μ	1174.19 cm^{-1}	8.256 μ	1211.23 cm^{-1}	8.084 μ	1236.95 cm^{-1}
8.501	1176.34	8.250	1212.13	8.072	1238.87
8.494	1177.31	8.241	1213.46	8.067	1239.57
8.485	1178.54	8.231	1214.86	8.060	1240.64
8.476	1179.79	8.222	1216.22	8.052	1241.97
8.469	1180.74	8.207	1218.50	8.045	1242.96
8.462	1181.71	8.191	1220.79	8.039	1243.97
8.456	1182.54	8.184	1221.93	8.034	1244.73
8.449	1183.52			8.025	1246.17
8.445	1184.15			8.015	1247.70
8.437	1185.28			8.010	1248.37
8.426	1186.84			8.002	1249.65
8.412	1188.81			7.992	1251.32
8.410	1189.10			7.985	1252.35
				7.977	1253.58
				7.969	1254.84
				7.957	1256.78
				7.951	1257.66
Fig. 31		Fig. 32		Fig. 33	
8.153	1226.61	7.924	1262.03	7.717	1295.89
8.135	1229.33	7.916	1263.24	7.709	1297.24
8.129	1230.17	7.912	1263.96	7.704	1297.96
8.117	1231.92	7.901	1265.60	7.699	1298.79
8.108	1233.41	7.897	1266.33	7.692	1300.11
8.105	1233.85	7.885	1268.28	7.682	1301.78
8.101	1234.45	7.877	1269.53	7.664	1304.89
8.097	1235.01	7.865	1271.52	7.643	1308.32
8.089	1236.20	7.852	1273.62	7.637	1309.45
8.082	1237.30	7.845	1274.68	7.633	1310.12
8.077	1238.12	7.842	1275.12	7.629	1310.75
8.069	1239.28	7.833	1276.69	7.624	1311.71
8.064	1240.07	7.829	1277.23	7.615	1313.19
8.058	1240.99	7.824	1278.13	7.612	1313.76
8.051	1242.07	7.818	1279.04	7.605	1314.93
8.045	1243.05	7.812	1280.05	7.592	1317.24
8.040	1243.72	7.810	1280.42	7.579	1319.49
8.036	1244.38	7.807	1280.96	7.563	1322.18
8.030	1245.40	7.803	1281.50	7.556	1323.51
8.026	1246.01	7.796	1282.64	7.551	1324.34
8.021	1246.78	7.793	1283.18	7.549	1324.73
8.013	1247.96	7.787	1284.20	7.540	1326.25
8.009	1248.66	7.776	1286.03	7.533	1327.52
8.005	1249.27	7.772	1286.75	7.519	1329.98
8.001	1249.85	7.766	1287.63	7.511	1331.33
7.996	1250.65	7.762	1288.35	7.504	1332.60
7.990	1251.61	7.753	1289.81	7.498	1333.70
7.984	1252.55	7.749	1290.57	7.491	1335.01
7.976	1253.74	7.743	1291.46		
7.970	1254.71	7.737	1292.45		
7.968	1255.03	7.735	1292.83		
7.964	1255.62	7.729	1293.89		

TABLE 1—*Continued*

Wave Length	Frequency	Wave Length	Frequency	Wave Length	Frequency
Fig. 31—*Continued*		Fig. 32—*Continued*		Fig. 33—*Continued*	
.958 μ	1256.62 cm^{-1}	7.725 μ	1294.51 cm^{-1}		
7.953	1257.40	7.720	1295.34		
7.948	1258.18	7.711	1296.82		
7.943	1258.90	7.706	1297.69		
7.939	1259.58	7.692	1300.11		
7.932	1260.72				
7.924	1262.03				
Fig. 34		Fig. 35		Fig. 36	
7.491	1335.01	7.269	1375.76	7.042 μ	1419.98 cm^{-1}
7.487	1335.71	7.256	1378.21	6.938	1441.37
7.467	1339.16	7.247	1379.89	6.928	1443.47
7.448	1342.56	7.236	1382.01	6.910	1447.29
7.441	1343.93	7.229	1383.34	6.901	1449.01
7.437	1344.56	7.206	1387.68	6.887	1452.04
7.425	1346.72	7.189	1390.97		
7.418	1348.10	7.173	1394.08		
7.413	1349.03	7.149	1398.80		
7.402	1351.06	7.117	1405.02		
7.390	1353.12	7.099	1408.72		
7.379	1355.16	7.091	1410.31		
7.373	1356.25	7.081	1412.15		
7.362	1358.33	7.052	1417.95		
7.360	1358.75	7.042	1419.98		
7.340	1362.44				
7.329	1364.50				
7.325	1365.11				
7.319	1366.30				
7.305	1368.91				
7.293	1371.19				
7.281	1373.35				
7.272	1375.14				
7.269	1375.76				

The positions of the absorption lines can be readily obtained from the map segments[6] or, more accurately, from the accompanying Table 1 of wave lengths and frequencies.[7] Each figure (1–36) gives the wave lengths of the beginning and end points of the map segment and further provides markers at intervals of 5 cm^{-1}. The columns of Table 1 give the wave-length and frequency limits of the corresponding map segments and provide, in addition, the wave lengths and frequencies of the absorption lines.[8] From a

[6] The map segments are tracings of the original recorded observations. The true abscissa of any point in the curves is therefore ϑ, where $\lambda = 20.540 \sin \vartheta$, $K = 20.540\ \mu$ being the spectrometer constant. However, the scale of the spectrum is so large that, over the small spectral interval of a single segment of map, $d\lambda$ is substantially proportional to $d\vartheta$. Table 1 was computed from the above formula, as were also the end points of Figs. 1–36.

[7] Note that the short-wave-length member of the close doublet obtained by resolving the strong asymetrical line at 1174.19 cm^{-1} is not listed in Table 1. Its position is 1173.49 cm^{-1}.

[8] In the Ann Arbor observations of the grating solar spectrum (Arthur Adel and V. M. Slipher, *Ap. J.*, **84**, 354, 1936) 101 lines were mapped between 11.0 and 7.7 μ. Of these, 25 were classified as SS or S, that is, very strong or strong lines. These lines are listed in Table 2 together with the positions that they occupy in the new map made at Flagstaff.

comparison with laboratory observations of infrared band spectra it is believed that the positions of the lines given in this paper are correct to ~ 1 cm^{-1}.

Plate XX[9] shows the rock-salt prismatic solar spectrum from 14 to 7 μ. The fine details of the grating solar spectrum lie, of course, within the broader features of the prismatic solar spectrum.

TABLE 2

A COMPARISON OF THE ANN ARBOR AND FLAGSTAFF OBSERVATIONS OF STRONG LINES IN THE GRATING INFRARED SOLAR SPECTRUM, 11.0 μ–7.7 μ

Ann Arbor	Flagstaff	Difference (A–F)
909.6 cm^{-1}	910.33 cm^{-1}	−0.7 cm^{-1}
941.5	.....	.....
943.4	.....	.....
949.0	949.59	−0.6
972.0	.....	.....
1067.0	1066.00	1.0
1075.2	1074.49	0.7
1091.9	1091.04	0.9
1100.3	1099.59	0.7
1102.3	1101.33	1.0
1107.6	1106.56	1.0
1112.4	1111.31	1.1
1118.5	.....	.....
1122.2	1120.90	1.3
1137.3	1135.49, 1137.19	.....
1150.3	1149.27	1.0
1153.3	1151.33, 1152.26	.....
1166.3	1165.03	1.3
1175.3	1174.19	1.1
1188.4	1186.84	1.6
1199.6	1197.96	1.6
1213.3	1212.13	1.2
1219.8	1218.50	1.3
1225.8	1224.94	0.9
1255.1	1255.03, 1253.74	.....

Some of the more prominent features of the map which have been identified are briefly enumerated below, as are also the most striking correspondences between the grating and the prismatic solar spectra.

1. Figures 1, 2, 3, 4, and 5 contain the lines of the positive branch of "ν_2" of CO_2 with center at 13.9 μ.[2]

2. The absorption line at 12.6 μ in the prismatic solar spectrum is intense even when there is a minimum of water vapor in the earth's atmosphere.[10] In the grating solar spectrum this line is resolved into the four strong lines of Figures 7 and 8.

3. Like the broad prismatic line at 12.6 μ, the prismatic line at 11.7 μ is resolved into a group of strong lines in the grating solar spectrum—the long-wave-length member of Figure 12 and the short-wave-length ones of Figure 13.

4. The prominent lines 923.47 cm^{-1} and 926.21 cm^{-1} of Figure 17 agree fairly well with the expected positions of 6P – 6S of *Na* I and are perhaps to be identified with the latter.[11]

[9] Arthur Adel and C. O. Lampland, *Ap. J.*, **91**, 1, 1940; and *ibid.*, p. 481.

[10] See Fig. 37.

[11] Bacher and Goudsmit, *Atomic Energy States*, New York: McGraw-Hill, 1932.

PLATE XX

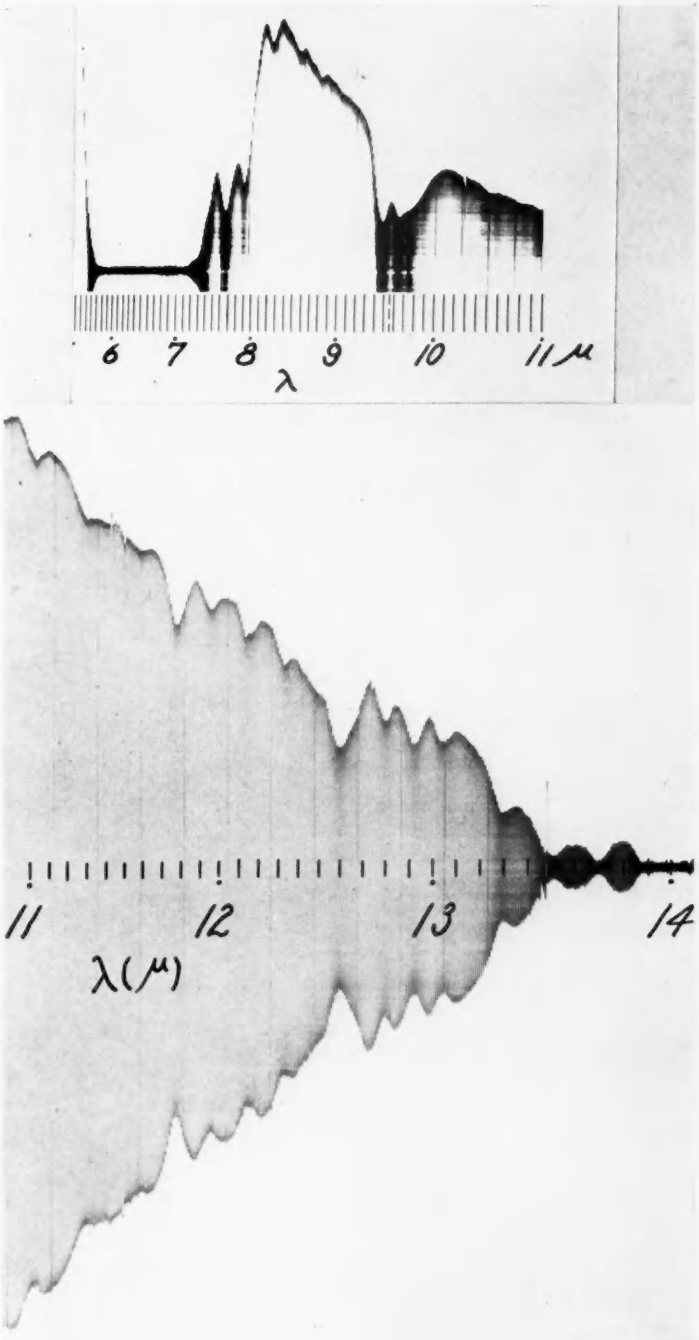

INFRARED SOLAR SPECTRUM

5. Figures 18, 19, and 20 contain the lines of the 10.4 μ band of CO_2.[2]

6. Figure 21 begins after the absorption by the 10.4 μ CO_2 band terminates, and it terminates before the absorption by the 9.4 μ band of CO_2 begins. It is, therefore, presumably part of the long-wave-length branch of the 9.6 μ ozone band, and it is remarkable for the regularity of its structure.[10]

7. The background contour of Figures 22, 23, and 24 is created by the great band of ozone at 9.6 μ.[10] The rotation lines in these figures, however, are a mixture of the band lines of ozone at 9.6 μ and CO_2 at 9.4 μ.[2] The massive "center" of the ozone band is at once apparent in Figure 23.[10]

8. Figure 25 contains the short-wave-length end of the rotational structure of the 9.4 μ CO_2 band.[2] It contains, also, the three lines of the compound doublet $3D - 4P$ of *Na* I.[2]

9. Figure 28 contains the three lines of the compound doublet $6P - 5D$ of *K* I.[2]

10. Figure 29 and the first quarter of Figure 30 provide a good example of the difference in scale between the prismatic and the grating solar spectra. This spectral interval is occupied by but a single line in the prismatic spectrum.[10] This single line is shown greatly expanded in the figures referred to, and impressed upon it are many narrow lines apparently of radically different origin.

11. Figures 30–36 contain the detail imbedded in the long-wave-length slope of the great water band, including the rotation lines of ν_1 of N_2O and ν_2 of HDO.[2]

LOWELL OBSERVATORY
FLAGSTAFF, ARIZONA

THE GALACTIC STRUCTURE IN TAURUS

III. DENSITY GRADIENTS FROM SPECTRAL TYPE DISTRIBUTION
IV. THE DARK NEBULA IN TAURUS

S. W. MCCUSKEY

ABSTRACT

The 2040 spectra of an unpublished portion of the *Henry Draper Extension* centered at $\alpha\ 4^{h}00^{m}$, $\delta+30°$ have been distributed according to intervals of apparent magnitude in five subregions of the Taurus area. Color-excess determinations for 450 early-type stars, obtained from blue-yellow color indices indicate an absorption of 2.0 mag. in photographic light for four of the five subregions. In the fifth subregion, that at highest galactic latitude ($b = -18°$), the absorption amounts to only 1.0 mag. In all cases the absorption seems to be complete at 200 parsecs, no increase being indicated beyond.

Space-density analyses indicate that the stars as a whole thin out rather rapidly with the distance, the density at 400 parsecs being 20 per cent of that at 100 parsecs. On the other hand, the intrinsically bright stars in region I($b = -11°$) are two to four times more numerous at distances of 250–400 parsecs than in the region near the sun. In regions II and III($b = -15°$ and $-18°$) the space density of the giant stars remains sensibly constant or decreases slightly with the distance in the interval 100–400 parsecs.

A detailed comparison of the luminosity function, obtained from the Taurus spectra with the function usually adopted for the analysis of general star counts, indicates again a two- to fourfold excess of stars with $M < +2$ and a deficiency of stars with $+2 < M < +6$. The latter are only 45 per cent as numerous as in the immediate vicinity of the sun.

Four areas of dense nebulosity have absorptions of 2.7, 4.9, 3.5, and 3.0 mag. in photographic light. The nebula apparently sets in at 113 ± 39 (m.e.) parsecs.

The irregularity of the distribution of stars in Taurus and Auriga immediately raises the question as to how much of the effect may be attributed to real variations in the stellar density and how much to variations in the obscuring material. Some light on the question may be gained by a study of the stellar distributions for individual spectral groups and by a study of color indices.

In recent years the Taurus nebula itself has been studied by Pannekoek,[1] Shapley,[2] Schalén,[3] Müller,[4] von Klüber,[5] Shajn,[6] Wernberg,[7] and Malmquist.[8] The results of these investigators indicate a total absorption ranging from 0.5 to 4 mag. for various points in the nebula; the distance at which the nebula sets in has been found to be between 70 and 250 parsecs. There remains, however, some controversy as to its extension in the line of sight. Schalén[3] finds an extent of 340 parsecs, while Malmquist[8] concludes from a new analysis of Schalén's data that the thickness of the nebula is negligible. Malmquist also finds some evidence for a second nebula situated at a distance of between 400 and 500 parsecs and absorbing about 0.75 mag.

Two investigations[9] by the author (hereafter referred to as paper I and paper II) concerning the surface and space distributions of the stars in Taurus have shown the galactic structural details for what were chosen as relatively clear parts of this region. In addition very preliminary distances and absorptions were obtained for eight positions in the nebula; the average absorption amounted to 1.9 mag., the nebula setting in at about

[1] *Proc. kon. Akad. Amsterdam*, **23**, Part 5, 1920.

[2] *Harvard Circ.*, No. 240, 1922.

[3] *Upsala Medd.*, No. 37, 1928, and No. 55, 1932.

[4] *Zs. f. Ap.*, **2**, 254, 1931.

[5] *Zs. f. Ap.*, **6**, 259, 1933, and **13**, 174, 1937.

[6] *Pulkovo Circ.*, No. 11, 1936.

[7] *Festskrift tillagnad Osten Bergstrand*, p. 61, Upsala, 1938.

[8] *Stockholm Ann.*, **13**, No. 4, 1939.

[9] *Ap. J.*, **88**, 209, 1938, and **89**, 568, 1939.

140 parsecs. It is well known, however, that the large dispersion in the luminosity function for the stars in general makes such determinations of nebular extent and distance uncertain. On the other hand, since the m, log $A(m)$ curves for the obscured regions were parallel to those for the unobscured areas for a range of 3 or 4 mag., the values of the relative absorptions should be more exact. There remains, of course, the question of how much absorption exists in the so-called clear areas.

The galactic-density gradients found for the stars in the Taurus region were all negative, i.e., there appeared to be a rapid decrease in density with distance from the sun. Such a conclusion, however, rested to some extent on the selection of a reasonable value for the general interstellar absorption in the clear areas. It was found that this gradient in the Milky Way could be removed only by the assumption of an improbable condensation of obscuring material at distances of from 500 to 1000 parsecs from the sun.

Data on spectral types and colors for a portion of the Taurus region are given in the present paper. The investigation is concerned with three problems: (*a*) the determination of the absorption characteristics by means of stellar colors for a part of the region

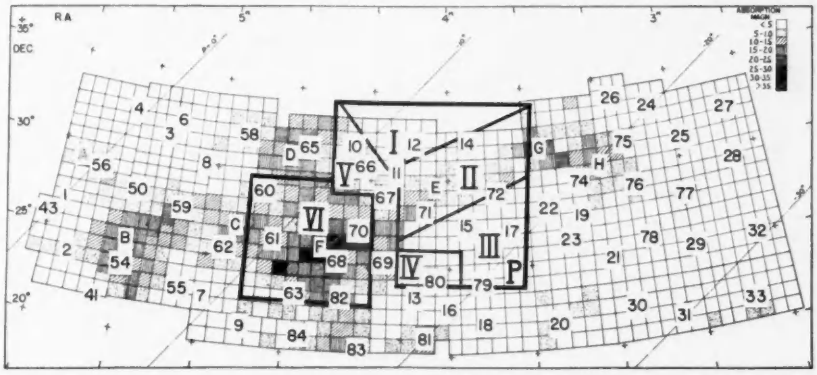

FIG. 1.—The regions covered by an unpublished part of the *Henry Draper Extension* are numbered I-V. That covered only by the *Yale Zone Catalogue* data is VI.

lying between $b = -10°$ and $b = -20°$, close by the main body of the Taurus obscuring material; (*b*) the evaluation of the space-density gradients for stars in selected spectral groups; and (*c*) the absorptions in some of the dense parts of the nebula at $\alpha\ 4^h30^m$, $\delta +26°$. The bulk of the observational material has been taken from the *Henry Draper Extension*.[10]

Spectra.—Through the kindness of Dr. Shapley, Miss Cannon, and Mrs. Mayall, charts giving the classification of stars to the twelfth photographic magnitude in 93 square degrees of the sky centered at $\alpha\ 4^h30^m$, $\delta +30°$ have been made available to me in advance of publication. The total number of stars involved is 2040.

An outline of the region covered by the survey charts, which will eventually form a part of the *Henry Draper Extension*, is indicated on Figure 1. In treating the material statistically, the area around the Pleiades (*P* in Fig. 1) has been omitted.

Magnitudes.—Sequences established for the calibration of the general star counts in the region shown by Figure 1 were used to obtain the photographic magnitudes of the classified stars. An artificial scale of stellar images formed the medium of comparison. It was shown in paper I that the sequence magnitudes are essentially on the international scale.

A comparison of magnitudes determined from pairs of overlapping plates indicated a

[10] Unpublished charts.

probable error of ± 0.12 mag. for a single determination. An adopted magnitude is the mean of at least two determinations, hence the internal probable error is somewhat under ± 0.1 mag. No variation of the probable error with magnitude between $m = 8$ and $m = 12$ was found.

An estimate of the external accuracy of the magnitude system may be gained by comparing the adopted magnitudes m_{RL} with those of the *Henry Draper Catalogue*. For stars whose magnitudes are given to hundredths in the *Catalogue* the average systematic difference $m_{RL} - m_{HDC}$ is $+0.03$ mag. (21 stars); for stars with magnitudes given to tenths, $m_{RL} - m_{HDC}$ is -0.06 mag. (153 stars). Stars with $8 \leqslant m < 9.5$ were used for the comparison.

The spectral distributions.—The area covered by the spectral-type and magnitude data has been divided for analysis into six subregions as indicated on Figure 1, the basis of division being approximately the apparent distribution of absorbing matter for the area. Table 1 gives the frequency distributions according to magnitude for each region and for intervals of spectral class B0–B5, B8–A0, A2–A3, A5–F0, F2–F5, F8–G0, G5–K2, and K5–M8. The area covered by each region is indicated at the bottom of the table. Entries of the table are the counted numbers in each region. For stars brighter than $m = 6$ the counts have been made in the *Henry Draper Catalogue*. The distribution in region VI is based on the magnitudes and spectra published in the *Yale Catalogue*.[11]

Completeness of the spectral data.—A comparison of the numbers of stars in successive intervals of apparent magnitude obtained from Table 1 with corresponding numbers obtained by general star counts is exhibited in Figure 2. Values of $\log A(m)$, the logarithm of the number of stars per square degree in the magnitude range $m - \frac{1}{2}$ to $m + \frac{1}{2}$, are plotted as ordinate against m. The general star counts are for an area of 62 square degrees, coinciding approximately with the area covered by the spectral data.

When due allowance is made for the uncertainties in the general star counts—± 0.1 in $\log A(m)$—the completeness of the spectral data is seen to be satisfactory except at magnitude 12. An inspection of an area of 33 square degrees, about one-third of the whole, indicated that 176 stars with m between 11 and 12.5 had been missed in the spectral classification. In the statistical analyses to follow, the values of $\log A(m)$ for $m = 12$ have been extrapolated from the data for the preceding magnitude intervals.

The color data and their analysis.—An evaluation of the total photographic absorption in five of the six regions has been made through a study of the color indices of faint stars. It has been assumed that the ratio, A_{pg}/E, of photographic absorption to color excess on the international scale is 6—a value reasonably well established by recent work, particularly that of Stebbins, Huffer, and Whitford.[12]

Measurement of blue-yellow color indices has therefore been undertaken for 450 stars of spectral type earlier than *F0* in the regions of Taurus covered by the new *Henry Draper Extension* charts. These data are part of a more extensive survey of colors in adjacent areas of the Milky Way now being carried on by the writer in collaboration with Dr. F. K. Edmondson, of Indiana University. Information will ultimately be at hand for some 2500 stars of early type in the Taurus and Auriga areas.

The yellow magnitudes were measured on Eastman I-G plates taken at the Lowell Observatory with the 13-inch telescope. In this preliminary study the blue magnitudes have been obtained from Cramer Hi-Speed plates taken with the 4-inch RL camera at the Harvard Oak Ridge Station. All measures were made with a graduated scale of stellar images, the probable error of a single observation being ± 0.12 mag. for the blue and ± 0.07 mag. for the yellow plates. The resulting color indices have a probable error of ± 0.09 mag. Measures of 50 late-type stars with spectra ranging from F0 to M indicated that no appreciable zero-point or scale errors were present in the colors. All these data are being re-examined in connection with the furtherance of the color program.

[11] *Trans. Yale Univ. Obs.*, Vols. **9** and **10**.

[12] *Ap. J.*, **91**, 20, 1940.

Table 2 contains a summary of the essential color data together with the adopted normal colors and the absolute magnitudes used in obtaining the average distances of the stars concerned. The fourth to eighth contain the average color indices for each

TABLE 1*

THE DISTRIBUTION OF THE SPECTRAL TYPES

Region \ Spectrum	B0–B5						B8–B9–A0						A2–A3						A5–F0					
	I	II	III	IV	V	VI	I	II	III	IV	V	VI	I	II	III	IV	V	VI	I	II	III	IV	V	VI
m																								
<6	0	2	0	0	0	0	1	0	1	0	0	2	0	1	1	0	0	0	0	1	1	0	0	0
6 – 6.5	1	2	0	0	0	0	0	0	0	0	1	4	0	1	0	0	0	2	0	0	0	0	0	1
6.5– 7	2	0	0	0	0	0	0	0	0	0	0	0	0	0	0	0	0	0	0	0	0	0	0	0
7 – 7.5	0	0	0	0	0	0	0	0	1	0	0	6	0	0	0	0	0	2	0	0	0	0	0	1
7.5– 8	0	0	0	0	0	1	1	2	5	1	1	2	1	0	2	1	0	2	1	0	0	0	1	1
8 – 8.5	0	0	0	0	0	0	5	3	8	2	1	7	1	1	4	2	1	0	0	0	1	0	0	0
8.5– 9	0	1	0	0	0	0	8	8	7	2	1	0	0	1	4	1	1	3	0	0	1	0	1	2
9 – 9.5	0	0	0	0	0	0	6	7	5	2	1	3	1	4	3	2	2	9	0	1	1	0	1	0
9.5–10	0	1	0	0	0	1	6	9	7	0	1	5	7	3	6	3	1	3	3	4	4	1	0	3
10 –10.5	0	0	0	0	0	0	6	9	4	1	2	5	12	8	14	3	0	2	2	5	6	2	2	2
10.5–11	1	0	0	0	0	0	10	6	4	0	3	3	13	6	9	1	3	2	4	3	17	4	1	0
11 –11.5	0	0	0	0	0	...	21	6	4	1	9	...	18	12	11	3	9	...	28	25	21	6	4	..
11.5–12	0	0	0	0	0	...	14	2	8	1	6	...	11	8	1	1	6	...	17	11	15	6	7	..
12 –12.5	0	0	0	0	0	...	3	0	1	0	4	...	1	3	0	0	3	...	6	4	0	0	7	..
>12.5	0	0	0	0	0	...	0	0	0	0	1	...	0	0	0	0	0	...	0	1	1	0	0	..
Total	4	6	0	0	0	2	81	52	55	10	31	37	65	48	55	17	26	25	61	55	68	19	24	10

Region \ Spectrum	F2–F5						F8–G0						G5–K2						K5–M8					
	I	II	III	IV	V	VI	I	II	III	IV	V	VI	I	II	III	IV	V	VI	I	II	III	IV	V	VI
m																								
<6	0	0	0	0	0	2	0	0	0	0	0	0	0	0	0	0	0	0	0	0	0	0	0	0
6 – 6.5	1	0	0	0	0	0	0	0	0	0	0	0	0	0	0	0	0	0	0	0	0	0	0	0
6.5– 7	0	0	0	0	1	1	0	1	0	0	0	1	0	0	0	0	0	1	0	0	0	0	0	0
7 – 7.5	0	0	0	0	0	1	0	0	0	0	0	0	1	0	0	0	0	2	0	0	0	0	0	0
7.5– 8	0	1	0	0	0	3	1	1	1	1	0	1	1	0	1	1	0	0	0	0	0	0	0	0
8 – 8.5	0	1	0	0	1	3	0	1	2	1	0	0	1	2	3	3	0	4	1	0	0	0	0	0
8.5– 9	1	1	1	2	0	4	2	2	6	2	1	7	1	4	7	2	0	3	0	1	0	0	0	0
9 – 9.5	2	1	4	1	0	3	3	4	4	6	3	6	7	6	10	2	1	11	0	0	3	1	0	0
9.5–10	2	2	3	0	2	1	6	5	11	2	1	5	12	5	6	5	3	10	3	1	3	2	1	0
10 –10.5	8	6	11	2	2	2	7	5	16	8	4	6	7	13	26	3	4	5	1	1	9	4	0	6
10.5–11	5	3	12	3	0	1	12	11	23	4	2	3	13	10	25	8	5	8	6	3	13	4	2	3
11 –11.5	10	11	16	6	5	...	30	16	52	14	10	...	60	29	45	13	9	...	18	8	26	7	7	..
11.5–12	24	10	12	1	7	...	40	28	39	9	10	...	33	26	39	13	6	...	18	5	23	4	7	..
12 –12.5	7	2	5	0	3	...	12	2	3	1	6	...	11	2	6	0	9	...	18	1	7	1	5	..
>12.5	2	0	0	0	0	...	0	3	1	0	0	...	1	0	3	0	0	...	5	1	4	1	0	..
Total	62	38	64	15	21	21	113	79	158	48	37	29	148	97	171	50	37	44	70	21	88	24	22	9

* Areas (in square degrees): I, 20.6; II, 24.2; III, 27.8; IV, 11.0; V, 9.4; VI, 55.1.

spectral group at $m = 11.0$. Numbers in parentheses indicate the numbers of stars entering into each average.

Color excesses, E, determined from the data of Table 2 and converted into total photographic absorption by application of the factor $A_{pg} = 6E$, were plotted against the corresponding distances $r = 10^{0.2(16.0-M-6E)}$, the results for all regions being exhibited in Figure 3.

It is apparent from the figure that, when due regard is paid to the scatter in the observations, there is no significant difference in the trend of the absorption for regions I, II, IV, and V. For these areas the absorption amounts to about 2.0 mag. from a distance of 200 parsecs outward from the sun to at least 600 parsecs. The observed effect might well be caused by a relatively thin stratum of material, the general absorption beyond being negligible. Since the galactic latitude of the region is fairly high and in general the absorbing medium is known to be concentrated toward the galactic plane, an effect such as that observed might have been anticipated.

In region III, on the other hand, the absorption appears to be significantly lower. The total absorption at 800 parsecs is about 1.0 mag. In view of the fact, however, that the uncertainty in a given point of Figure 3 may be at least 0.6 mag., the reality of this dif-

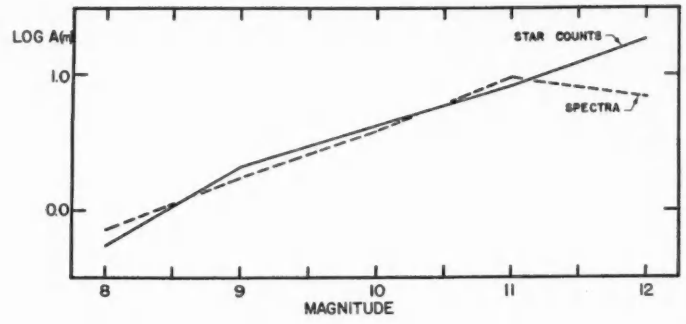

FIG. 2.—Ordinates are values of log $A(m)$; abscissae, apparent photographic magnitudes. The curves indicate the essential completeness of the spectral data to $m_{pg} = 11.0$.

TABLE 2

AVERAGE BLUE-YELLOW COLOR INDICES IN REGIONS I TO V AT $m = 11.0$

SPECTRAL TYPE	NORMAL *CI*	ABSOLUTE MAGNITUDE	REGION				
			I	II	III	IV	V
B8, 9.....	−0.18	−0.5	+0.28(4)	.....	.....	.....	+0.24(1)
A0.....	− .12	+0.5	.23(17)	+0.20(1)	+0.05(5)	+0.30(1)	.46(1)
A2, 3.....	.00	+1.5	.24(9)	.41(9)	.17(6)	.23(2)	.52(6)
A5, 7.....	+0.08	+2.5	+0.37(12)	+0.46(4)	+0.20(14)	+0.30(2)	+0.27(2)

ference is somewhat doubtful. The absorbing stratum would appear to set in at about the same distance as for regions I, II, IV, and V, i.e., at 200 parsecs.

These values may be compared with similar results deduced from the color excesses, E_1, of Stebbins, Huffer, and Whitford.[12] Four of their B stars are located in region I, and 6 in region II. The average color excesses of these groups are +0.11 and +0.14, respectively. If a factor $A_{pg}/E_1 = 9$ is used, the average total absorption becomes 1.2 mag. at a distance of 330 parsecs. There is no apparent difference between the two areas. No comparison data are available for region III.

Counts of galaxies.—The distribution of external galaxies provides one further way in which the total absorption may be estimated. An inspection of a long-exposure photograph taken with the 16-inch Metcalf refractor at Oak Ridge, and kindly placed at my

disposal by Dr. Shapley, reveals 128 extragalactic objects shining through the nebulous material in Taurus. Regions I, II, and III are each partly covered by this plate. To a limiting magnitude of approximately 18 there are, respectively, 2.8, 5.5, and 2.7 nebulae per square degree. Region II contains the very dense nebula B7 which has been omitted in forming the nebular density for this field, since it is practically opaque.

On the assumption of uniform nebular distribution in space, these densities would indicate an average total absorption of 2.0 mag. in excess of that at the galactic poles. The foregoing conclusion, viz., that nearly all the obscuration in this region occurs close by, is strengthened, since the colors have indicated a similar value of A_{pg} from 200 parsecs outward.

A similar estimate of the total absorption may be gained from the nebular data of two of Hubble's[13] survey fields which lie within region II and of two more which lie just out-

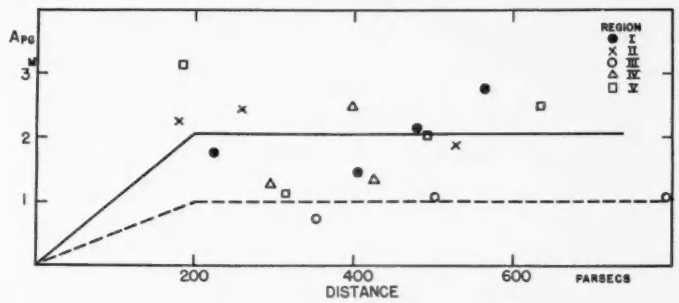

FIG. 3.—The photographic absorption of light as a function of the distance. The number of stars entering into each mean point is indicated in Table 2. A_{pg} is the absorption in magnitudes.

side the boundaries of region I. We find from these data a total absorption of 2.0 mag., in good agreement with that found from the Harvard survey.

The nebular density in region III does not differ greatly from that in the adjoining areas, and hence the lower total absorption found from the colors (1.0 mag. at 800 parsecs) is not confirmed. The possibility, of course, is not excluded that the excess absorption shown by the galaxies takes place beyond the region covered by the color analysis. Star counts to $m = 15$ fail to reveal it, however.

The average color indices of the stars with $m = 10$ and $m = 9$ in region III indicate the same low value of the absorption shown by the fainter stars. For a first analysis, therefore, the absorption values determined from the colors will be used for this region. The variation is shown in the lower curve of Figure 3.

While too much reliance cannot be placed on estimates of absorption deduced from an assumed uniform spatial distribution of external galaxies, still they do serve to show that the values obtained from the colors are of the right order. In computing the space densities of the stars we shall assume that the run of the absorption is that given by the curves of Figure 3. For region VI, the densest part of the Taurus nebula, no color data are available.

Space-density functions.—The spectral counts of faint stars (Table 1) have been supplemented by the bright-star data of the *Henry Draper Catalogue* in order to gain a representative picture of the relative density changes outward from the sun. For this purpose Seydl's[14] compilation of stars with $m = 4$ to $m = 7$ has been used. Curves relating $\log A(m)$ and m for the bright stars in the galactic latitude zone $-10°$ to $-30°$ were found to join smoothly the curves based upon the faint-star data of Table 1. Adopted values of $\log A(m)$ as a function of m derived from these curves are given in Table 3; $A(m)$ is

[13] *Ap. J.*, **79**, 8, 1934. [14] *Pub. Prague*, No. 6, 1929.

the number of stars with apparent magnitudes between $m - \frac{1}{2}$ and $m + \frac{1}{2}$. In order to insure sufficient statistical weight, only regions I, II, and III have been analyzed, the spectral divisions listed in Table 1 having been combined into groups: B8–A_3, A_5–F_5, G_5–K_2, F8–Go, K_5–M. In analyzing the data of the dwarf stars all three regions have been combined.

The numbers of stars in successive distance shells have been derived from these distribution data according to the method of Schalén.[3] It has been assumed that the $A(m)$ stars of apparent magnitudes $m - \frac{1}{2}$ to $m + \frac{1}{2}$ are distributed normally about a mean absolute magnitude $M(m)$ for each spectral group. In each case the dispersion was taken as

TABLE 3

ADOPTED VALUES OF LOG $A(m)+10$

Spectrum / Region	B8–A_3			gF8–Go			gG5–K2			gK5–M		
	I	II	III	I	II	III	I	II	III	I	II	III
$m=$ 5	8.20	8.20	8.20	7.10	7.10	7.10	8.16	8.16	8.16	7.55	7.55	7.55
6	8.81	8.81	8.81	7.74	7.74	7.74	8.57	8.57	8.57	8.00	8.00	8.00
7	9.24	9.24	9.24	8.30	8.35	8.40	8.89	8.89	8.94	8.40	8.40	8.40
8	9.58	9.58	9.58	8.78	8.88	8.98	9.12	9.12	9.30	8.70	8.64	8.68
9	9.88	9.88	9.88	9.20	9.23	9.40	9.53	9.49	9.64	9.00	8.70	9.09
10	0.17	0.00	0.00	9.63	9.45	9.81	9.98	9.84	0.00	9.40	9.00	9.60
11	0.48	0.11	0.11	0.00	9.74	0.17	0.40	0.09	0.33	0.00	9.57	0.11
12	0.77	0.22	0.22	0.32	0.09	0.46	0.82	0.22	0.68	0.58	0.20	0.62

Spectrum / Region	A_5–F_5	dF8–Go	dG5–K2	All Stars		
	I, II, III	I, II, III	I, II, III	I	II	III
$m=$ 5	7.90	6.59	6.80	8.65	8.65	8.65
6	8.30	7.30	7.40	9.19	9.19	9.19
7	8.58	7.95	7.90	9.60	9.60	9.60
8	8.81	8.47	8.29	9.80	9.86	9.98
9	9.29	8.96	8.68	0.21	0.18	0.32
10	9.80	9.42	9.07	0.65	0.47	0.66
11	0.32	9.90	9.69	1.05	0.77	1.00
12	0.84	0.38	0.32	1.47	1.06	1.32

± 1.0 mag. Summation of such distributions for $m_{pg} = 5$ to $m_{pg} = 12$ yielded the space density in succeeding shells of distance, hence the density per cubic parsec. Table 4 gives the mean absolute magnitude per unit volume (M_0) adopted for the computations. Appropriate corrections were applied to convert these into the corresponding values of $M(m)$.

In forming an estimate of the percentages of dwarfs among the G and K stars I have combined the data of Bok[15] and of van Rhijn and Schwassmann[16] in the following manner. From Bok's analysis the ratios of the percentages of dwarfs in high latitudes to those at $\pm 15°$ were found to be 1.37 and 1.44 for the Go–G5 and Ko–K2 stars, respectively. On the approximate assumption that these ratios are independent of the apparent magnitude, I have computed from the tables of van Rhijn and Schwassmann for high lati-

[15] *Harvard Circ.*, No. 400, 1935. [16] *Zs. f. Ap.*, **10**, 161, 1935.

tudes the corresponding percentages for $\pm 15°$ as functions of the apparent magnitude. In this way the following adopted percentages of dwarfs at $\pm 15°$ have been obtained:

F8–G0: $m \leqslant 8.5$, 25%; $8.5 < m \leqslant 10.5$, 30%; $m > 10.5$, 45%;

G5–K2: $m \leqslant 8.5$, 5%; $8.5 < m \leqslant 10.5$, 10%; $m > 10.5$, 25%.

These values may be compared with those found by van de Kamp and Vyssotsky,[17] 53 per cent dwarfs for G0–G7 and 27 per cent for G8–K2, mean magnitude 10.2. Oort[18] finds from a study of the Radcliffe proper motions 45 and 22 per cent dwarfs among the G0–G6 and G7–K2 stars, respectively. These values are for the magnitude range 11.5–13.4 and for galactic latitudes below 30°. Schalén,[3] on the other hand, has found 64 per cent dwarfs among the stars of 8–10 mag. near the galactic plane at $l = 134°$. All the K5–M stars have been assumed to be giants.

TABLE 4

ADOPTED MEAN ABSOLUTE PHOTOGRAPHIC MAGNITUDES

Spectrum	M_0	Spectrum	M_0
B8–A3	+1.0	gK5–M	+2.0
A5–F5	3.0	dF8–G0	5.0
gF8–G0	2.0	dG5–K2	+7.0
gG5–K2	+2.0		

The space densities derived by the Schalén-Lindblad method are subject to some uncertainty at large distances, due to the exclusion of stars beyond the brightness limit of the spectral data. It has thus been necessary to restrict the present analysis to that region of space within which the thirteenth and fourteenth magnitude stars of a given absolute brightness contribute practically nothing to the space density. With due allowance for 2.0-mag. absorption in regions I and II, or 1.0-mag. absorption in region III, this upper limit becomes about 500 parsecs for the data in hand. The small penetrating power of spectral data to magnitude 12 emphasizes the need for fainter spectra in studies of galactic structure.

Table 5, A, summarizes the relative density gradients found for the intrinsically bright stars in these regions. The absolute density, stars per cubic parsec, at 100 parsecs distance has been set equal to unity in each spectral group. Corrections for absorption have been applied according to Figure 3.

Table 5, B, indicates the agreement between relative densities computed from the spectral data as a whole and from the standard luminosity function given by van Rhijn.[19] The Taurus spectral data for the stars from $m = 8$ to $m = 12$ have been combined into an (m, log π) table, from which densities relative to that at 100 parsecs, corrected for absorption, have been derived. These are given in the next-to-the-last column of Table 5, B.

The last column contains the relative density gradient, obtained by applying the (m, log π) tabular method of Bok[20] to the star-count data, the unit density have been adjusted in the same way as for the spectral groups. Van Rhijn's[19] conventional luminosity function for the region near the sun, corrected for changes depending upon height above

[17] *Pub. Leander McCormick Obs.*, **7**, 17, 1937.

[18] *BAN*, No. 290, 1936.

[19] *Groningen Pub.*, No. 47, 1936.

[20] *Harvard Circ.*, No. 371, 1931.

the galactic plane according to recent work by Bok and MacRae,[21] has been used. Although the direct application of this method yields densities in terms of the densities at corresponding heights directly above the sun, it is to be emphasized that the entries in Table 5 are referred to the density values at 100 parsecs in the line of sight. In order to compare these densities with those deduced from the spectral data, only stars between $m = 8$ and $m = 12$ have been included in the analysis. The densities so found would

TABLE 5

SPACE-DENSITY GRADIENTS IN TAURUS

Distance (Parsecs)	A. Individual Spectral Groups					B. All Groups Combined, Including Dwarfs	
	B8–A3	A5–F5	gF8–G0	gG5–K2	gK5–M	Taurus Spectral Data	Standard Luminosity Function
	Region I						
100	1.00	1.00	1.00	1.00	1.00	1.00	1.00
159	0.59	0.62	0.75	0.53	0.51	0.47	0.53
251	1.20	5.18	3.00	2.10	2.70	0.51	0.44
400	0.60	3.97	1.75	1.37	2.54	0.20	0.04
630	0.30	.....	0.75	0.90	2.22	0.05	0.01
	Region II						
100	1.00	1.00	1.00	1.00	1.00	1.00	1.00
159	0.59	0.62	0.88	0.50	0.38	0.46	0.42
251	0.68	5.18	2.00	1.07	0.85	0.38	0.19
400	0.22	3.97	1.00	0.43	0.85	0.11	0.03
630	0.08	.....	0.63	0.07	0.77	0.02	0.00
	Region III						
100	1.00	1.00	1.00	1.00	1.00	1.00	1.00
159	0.59	0.62	1.00	0.61	0.67	0.47	0.63
251	0.48	1.56	1.78	0.76	1.11	0.29	0.26
400	0.17	1.30	1.00	0.42	0.89	0.12	0.04
630	0.06	.....	0.55	0.24	0.78	0.04	0.01

be increased somewhat at distances greater than 300 parsecs if fainter stars were included.

Data for the dwarf stars are too meager for the derivation of reliable gradients. These stars are largely confined to a region within 200 parsecs of the sun.

From Table 5 we may draw the following conclusions, which depend to a considerable extent upon the validity of the absorption in this area and its variation with distance:

a) Disregarding the diminution in density at $r = 159$ parsecs, which is obviously due to uncertainty in the absorption correction, the intrinsically bright stars show a tend-

[21] New York Academy of Sciences, conference on "Fundamental Properties of the Galactic System," 1941.

ency to be clustered between 250 and 500 parsecs in region I ($b = -11°$). In regions II and III, on the other hand ($b = -15°$ and $-18°$, respectively), the space density of these objects either remains sensibly constant or decreases with the distance. The B8–A3 stars, particularly, show a strong tendency to thin out with the distance in regions II and III, an effect due to their galactic concentration. In region III, for instance, $b = -18°$, at 400 parsecs the distance from the galactic plane is 120 parsecs. The B8–A3 stars are only 17 per cent as numerous as in the region near the galactic plane. Bok and MacRae[21] find approximately 35 per cent for stars of $M = +1$ and 45 per cent for $M = +2$. The density appears to decrease somewhat more rapidly in this area.

b) The A5–F5 stars appear to be many times more numerous at distances of the order of 300 parsecs in all three regions. This concentration is evident in the excess of stars between $m = 11.0$ and $m = 12.0$ in Table 1 but may be only apparent and due to a deficiency at 100 parsecs. An indication that this is the case is the scarcity of eighth- and ninth-magnitude stars of these spectral classes.

c) Owing to the inclusion of the dwarf stars for the region near the sun in the densities computed for the stars at large, the relative density gradients as shown by the last two columns are high. There is some indication, as shown by comparing the two columns, that changes in the luminosity function in this direction are present. The column headed "Standard Luminosity Function" was obtained, as mentioned, by using van Rhijn's[19] luminosity function for the region near the sun. The excessive densities of stars with $M < +2$, particularly in region I, at distances between 250 and 400 parsecs indicate that variance is probably present in the luminosity function. This point will be examined further.

It must be emphasized that the figures given for the relative densities at 630 parsecs are only approximate. Inclusion of fainter stars might modify them by as much as 15 per cent.

The general luminosity functions.—Investigations of space density based upon counts of stars of all spectral classes together usually require the assumption of uniformity of the luminosity function, $\phi(M, z)$, over the distances concerned. $\phi(M, z)$ is the number of stars per cubic parsec with absolute magnitude $M - \frac{1}{2}$ to $M + \frac{1}{2}$ at distance z parsecs from the galactic plane at the sun's position. Evidence that this assumption is not valid for the Taurus region has already been indicated in the last two columns of Table 5. For low-latitude regions ($b < 15°$) in Cygnus, F. D. Miller[22] has found deviations from the usually adopted values of $\phi(M, z)$, in the sense that the A and K stars were 30 per cent more numerous and the F and G stars slightly less numerous than predicted by the standard function.

The spectral material at hand has been used to examine this point more in detail for the Taurus region in the following way. Two (m, log π) tables have been constructed, one from the usually adopted luminosity function and the other by summing for each apparent magnitude the contributions of the spectral groups in successive distance shells. The mean absolute magnitudes and dispersions employed have already been described. Only stars with $m_{pg} = 8$ to $m_{pg} = 12$ were included in the analysis. The table compiled from the spectral data obviously yielded the observed values of $A(m)$ for the region concerned. In the table computed from the standard function, $\phi(M, z)$, relative densities for succeeding shells were found by trial, so that the table would represent the observed values of $A(m)$. As an example, these tables for region I are reproduced in Table 6, A and B. The former has been computed from one given by Bok and MacRae[21] based upon van Rhijn's luminosity function; the latter is the compilation of the current spectral data. Both fit equally well the observed values of $A(m)$. The general departure of the luminosity function for this area from the standard is readily apparent from the differences in corresponding cell entries of the two tables.

[22] Unpublished communication.

The numbers in the cells of Table 6, A, represent the product $\phi(M, z) \cdot D(z) \cdot V$, where $\phi(M, z)$ is the usual luminosity function, $D(z)$ the relative density at height z, and V the volume of the cell. Let the cell entries of Table 6, B, be called $\phi_s(M, z) \cdot V$, and let the ratio of corresponding entries in the two tables be $R = \phi_s(M, z)/\phi(M, z) \cdot D(z)$. Then a plot of log R against M for each distance shell will reveal in a clear manner any changes of the luminosity function with distance, as well as the general departure of $\phi_s(M, z)$ from $\phi(M, z)$ for these regions. Curves thus plotted from similar analyses for regions I, II, and III are shown in Figure 4.

From an inspection of the figure we reach the conclusion that no great relative changes in the shape of the luminosity function occur from point to point in this area. There ap-

TABLE 6

m, LOG π ANALYSES FOR REGION I

LOG π	A. FROM STANDARD $\phi(M, z)$ (m)					B. FROM TAURUS SPECTRA (m)				
	8	9	10	11	12	8	9	10	11	12
−1.6	0.021	0.030	0.040	0.05	0.06	0.012	0.024	0.030	0.026	0.010
1.8	.059	.085	0.120	0.16	0.20	.017	.033	0.061	0.123	0.113
2.0	.110	.234	0.339	0.48	0.63	.060	.054	0.096	0.236	0.517
2.2	.235	.317	0.708	1.03	1.46	.179	.143	0.160	0.325	0.961
2.4	.170	.619	0.853	2.05	2.96	.262	.411	0.386	0.496	1.120
2.6	.060	.326	1.242	2.01	5.18	.153	.590	1.019	1.112	1.533
2.8	.010	.091	0.526	2.00	10.02	.037	.340	1.392	2.699	3.259
3.0	.007	.016	0.161	0.95	3.36	0.001	.075	0.787	3.505	7.336
3.2	0.006	0.020	0.049	0.50	2.97	.....	0.004	0.172	1.937	9.064
−3.4	.....	.....	0.073	0.19	1.70	.....	.....	0.015	0.419	4.826
$A(m)$ comp.	0.69	1.75	4.13	9.44	28.57	0.72	1.66	4.12	10.88	28.74
$A(m)$ obs.	0.63	1.62	4.26	11.00	28.20	0.63	1.62	4.26	11.00	28.20

pears to be, however, a dearth of stars of intermediate luminosity coupled with a surplus of absolutely bright stars in all regions. As indicated by Table 5, there is an excess of absolutely bright stars at distances ranging from 250 to 400 parsecs.

The deficiency of stars of intermediate luminosity may be due, in part, to the uniformity of the mean absolute magnitudes assigned to the giants. The value of M_0 assigned to the gG5–K2 group, +2.0, is essentially the same as that used by Schalén,[3] +2.1, and by Bok and MacRae,[21] +2.0. For the gK5–M stars the mean absolute magnitude is more uncertain. However, a variation of ±1.0 mag. in the assumed values of M_0 for any of three groups, gF8–Go, gG5–K2, gK5–M, will not change the picture presented by Figure 4 materially. If, for example, the mean absolute magnitudes for gF8–Go and gK5–M were 1 mag. fainter, the minimum of the curves for region I (Fig. 4) would be raised by 0.09 in log R, while the excesses of stars at $M = -1, 0, +1$ would be decreased by the same amount. The influence of deviations of the order shown by Figure 4 on the general star-count analysis is exhibited in the last two columns of Table 5, B.

The Taurus nebula.—In a region as irregularly streaked by obscuring nebulosity as that centered at α 4^h30^m, δ +26° (region VI), large-scale statistical examinations of space-density distributions to determine the nature of the obscuring cloud are of little value. The most certain approach to the problem is through studies of spectral energy distributions and colors of stars actually imbedded in the nebulosity. However, a first approximation to the absorption characteristics at four points in the Taurus nebula has

been gained by comparing star counts at these points with counts made in the regions I and II, where the absorption has been determined. Mention has already been made of the average distance and absorption found by comparing nebulous areas with zone means of the star-count data (paper II, Table 9).

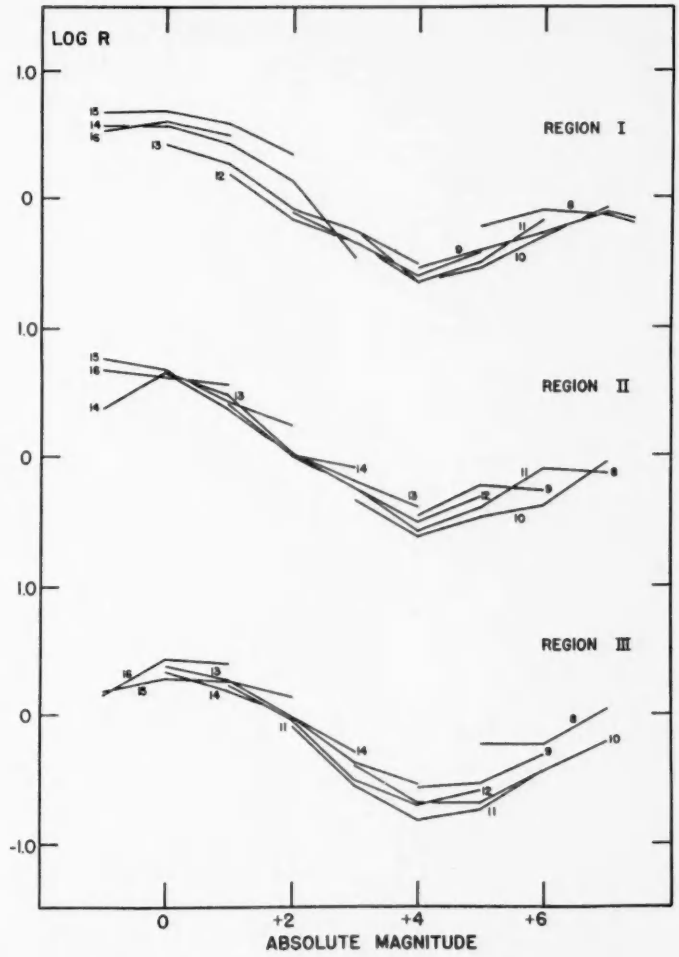

FIG. 4.—Departure of the luminosity function in Taurus from the usually adopted function. Log R is the difference between the logarithmic values of the two functions. Abscissae are photographic absolute magnitudes. The numbers refer to successive distance shells; they are values of 5 log r, where r is the distance in parsecs. A deficiency of solar-type stars and an excess of intrinsically bright stars are shown.

Figure 5 shows the m, log $N(m)$ curves for four small regions at points in the nebula, as well as the curves for the mean star counts of regions I and II and for the zone means at $-12^{\circ}.5$ and -15°. The apparent nearness of the nebula is evident in the parallelism of the curves over a range of 3 or 4 mag. Under such circumstances it is possible to deduce the total absorption from the curves with some degree of certainty. The spread in the general luminosity function precludes a satisfactory evaluation of the distance of the nebula in this way.

The regions chosen for analysis are shown in Figure 1. Region *E* coincides with the lower part of region II (see paper II, Fig. 3), region *F* is below the VI. It is the densest point in the nebula.

The displacements in magnitude between the mean curve for regions I and II and the curves for the obscured areas are assumed to be due principally to the nebula. Add-

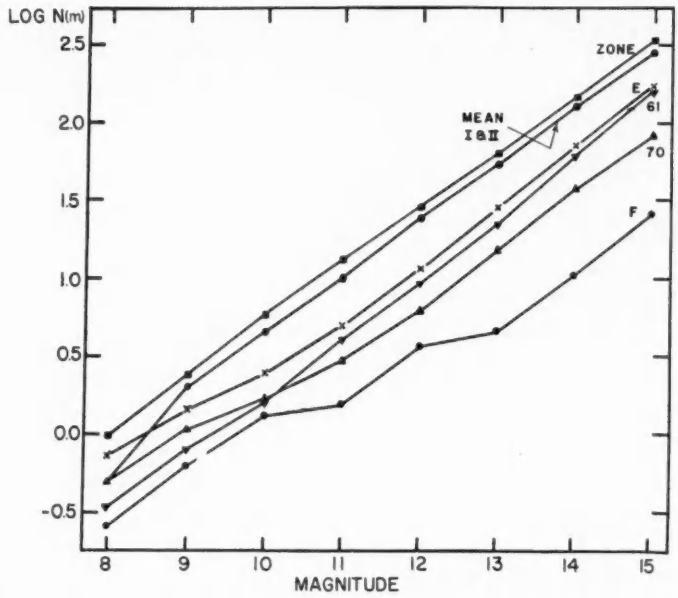

FIG. 5.—Wolf diagrams for the densest nebulosities in Taurus. Ordinates are values of log $N(m)$; abscissae are m_{pg}. The displacements in m_{pg} extending over a range of several magnitudes indicate the amount of the absorption in the nebula.

TABLE 7

ABSORPTION IN THE TAURUS NEBULA

Region	Area (Sq. Deg.)	$N(15)$	l	b	Absorption (Mag.)
E	4.1	170	133°	−15°	2.67
F	3.5	27	141	12	4.90
70	3.1	81	139	13	3.52
61	3.1	159	142	10	2.96
Zone	12.4	332	137	−13	1.72

ing 2.0 mag. to these displacements to allow for the absorption found in regions I and II from color studies, we obtain the total absorptions summarized in Table 7. The number of stars per square degree brighter than magnitude 15 are given in the third column.

It is evident that the absorption in the nebula reaches a very high value at certain points—nearly 5 mag. in the densest part. Furthermore, it appears that the zone means in this latitude are affected by more absorption than was assumed in computing the space densities of stars in paper II. Recomputation of the densities for zone −15° indicates the same run of values as have already been given in the last column of Table 5, B.

Further revision of the densities given in paper II (Table 3) will be deferred until complete color data are available for this region.

An estimate of the distance at which the dense cloud in region VI becomes effective has been obtained from m, log $N(m)$ curves similar to Figure 5 for the separate spectral groups B8–A0, A2–A3, A5–F0, and gG5–K2. The spread in the absolute magnitudes of each group is much smaller than for the stars as a whole, hence a combination of the mean M for the group with the apparent magnitude at which the m, log $N(m)$ curve for region VI definitely departs from those of regions I and II yields a reasonably accurate measure of the distance of the nebula. The mean distance obtained in this way for the nebulous material in region VI is 113 ± 39 (m.e.) parsecs.

We conclude from the present study of colors combined with the star counts and spectra that the densest portions of the Taurus nebula have a very small effective thickness, probably not over 100–150 parsecs, and that the absorption on the average is about 2 mag., with certain dense spots absorbing up to 5 mag. These results are in accord with the previous determinations listed in the beginning of the paper.

WARNER AND SWASEY OBSERVATORY
CASE SCHOOL OF APPLIED SCIENCE
July 1941

ANALYSIS OF THE MILKY WAY IN AURIGA

LOIS KIEFER AND ROBERT H. BAKER

ABSTRACT

This analysis of the Milky Way to the distance of about 2000 parsecs in the direction of Auriga is based upon counts of stars to the fifteenth magnitude and determination of color excesses of stars in certain latitudes of the region. We find obscuration best represented by two clouds: a very patchy cloud at 300 parsecs, which produces most of the visible bright and dark areas of the region, and a more uniform cloud at 800 parsecs. The density gradients are negative in this direction. Comparisons with other data support, in general, the conclusions of this study.

The region of the Milky Way considered in this paper consists of about 800 square degrees, extending roughly from $+30°$ to $+60°$ in declination and from $3^h\ 30^m$ to $7^h\ 30^m$ in right ascension. In galactic co-ordinates, which are referred to the conventional pole at $+28°$ declination and $12^h\ 40^m$ right ascension, the region lies between longitudes 114° and 146° and latitudes $-7°$ and $+32°$. Centered not far from Capella, the region contains practically all of Auriga and a part of Perseus and includes the galactic anticenter near the eastern boundary. The analysis was made chiefly by Miss Kiefer, who is also responsible for the color determinations. The greater part of the counting was done by Mr. Baker.

THE STAR COUNTS

All the plates used were taken at the University of Illinois Observatory with the 4-inch Ross-Fecker camera, 28 inches in focal length. The scale of the plates is 290″ per millimeter, or about 2° to the inch. The plates used for counts are Cramer Hi-Speed Special.

The region is covered with plates taken in pairs on each of thirty-one centers about 5° apart: one with ten minutes' exposure for counting from magnitude 9 to magnitude 13, and one with sixty minutes' exposure for magnitudes 11–15. A nearly circular area of about 4° radius in the middle of the plate, where the star images are best defined, comprises the countable area. No parts of the plate outside this area are used, either for counting or for calibrating the reference scale. The plates overlap to such an extent that the edge of the countable area on one plate comes nearly to the center of the adjacent plate.

The method of counting the stars and of calibrating the scale is the same as that described in a previous paper.[1] The scale is calibrated for each plate, either directly from catalogued magnitudes of stars in one of the six Selected Areas contained in the region or from sequences of stars measured through overlapping plates from one or more of these Areas. Magnitudes on the International Photographic Scale for Areas 10, 11, 23, 24, 25, and 26 are taken from *Bergedorfer Spektral-Durchmusterung* for stars brighter than magnitude 13 and from the *Mount Wilson Catalogue*[2] for fainter stars. The faintest scale image chosen for counting on any plate is about half a magnitude brighter than the very faintest stars on the plate.

A measure of the consistency of the counts is obtained by comparing counts of the same area on each of four pairs of overlapping plates at centers well scattered over the entire region; the plates of each pair overlap from 12 to 20 square degrees. Table 1 shows the resulting probable errors in log $N(m)$, where $N(m)$ is the number of stars

[1] Baker, *Harvard Circ.*, No. 424, 1939.

[2] *Carnegie Institution of Washington Pub.*, No. 402, 1930.

per square degree brighter than apparent magnitude m. These probable errors are considered satisfactorily small.

The consistency of the magnitude system over the region is examined by comparing the Illinois counts in the Selected Areas with those published in the Bergedorf catalogue for the brighter stars and with the Mount Wilson counts of the fainter stars as tabulated by van Rhijn.[3] The first comparisons involve 81 réseau squares, each $0.^{\circ}4$ on a

TABLE 1

PROBABLE ERRORS OF LOG $N(m)$ FROM OVERLAPPING PLATES

	m						
	9.0	10.0	11.0	12.0	13.0	14.0	15.0
In log $N(m)$	±0.02	±0.01	±0.02	±0.02	±0.02	±0.01	±0.01
In magnitude	±0.05	±0.02	±0.06	±0.05	±0.07	±0.02	±0.05

TABLE 2

COMPARISON WITH BERGEDORF AND MOUNT WILSON COUNTS

(Illinois *minus* Bergedorf or Mt. Wilson)

	SELECTED AREA						
	10	11	23	24	25	26	Mean
	Δ log $N(m)$						
Berg.							
$9^{m}0$	−0.09	+0.06	+0.01	−0.06	−0.03	+0.04	−0.01
10.0	− .02	− .04	+ .04	− .07	.00	.00	− .01
11.0	− .05	− .06	− .03	− .05	+ .02	− .02	− .03
12.0	− .11	− .04	− .01	− .01	.00	− .03	− .03
13.0	− .11	− .07	− .03	.00	+ .02	+ .01	− .03
Mt. W.							
13.0	− .07	− .02	.00	− .09	+ .16	+ .09	+ .01
14.0	.00	+ .07	+ .02	+ .02	+ .06	− .11	+ .01
15.0	−0.15	+0.15	−0.12	−0.06	−0.06	−0.06	−0.05

side, of our plates and therefore nearly match the areas, $3.^{\circ}5$ on a side, of Bergedorf; the second comparisons involve only 4 squares to correspond more nearly with the Mount Wilson areas, 15′ on a side. The mean differences, in Table 2, appear to be negligible, though the minus sign predominates. In addition, there seems to be no difference between the counts of the two observers and no noticeable effect for either observer, depending on distance from the center of the plate. We have accordingly employed the log $N(m)$ for all the counts without any correction.

In preparation for the analysis the region is divided into areas arbitrarily lettered, in each of which the surface distribution of the stars seems fairly uniform and different

[3] *Groningen Pub.*, **43**, Table 1, 1929.

in density from that of the surrounding divisions. The region is further divided into zones at 2°.5 intervals of galactic latitude. This arrangement is shown in Figure 1 with the omission of the zones from +17°.5 to +30°, throughout each of which the counts are not far from uniform. The most conspicuous bright area, *G*, contains 110 square degrees and extends through four zones; it surrounds the small area *F* in which the

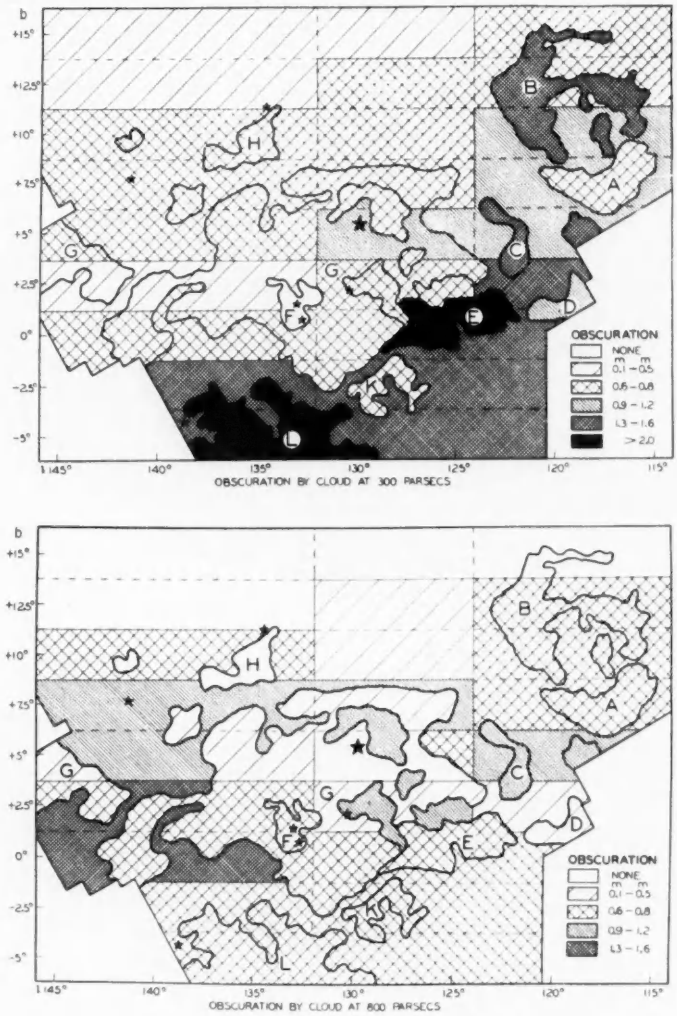

FIG. 1.—Divisions of the Auriga region, showing obscuration at 300 and 800 parsecs

counts run exceptionally high. A succession of four sharply outlined dark areas, *B*, *C*, *E*, and *L*, extends southeastward from the west edge of the region toward the dark clouds of Taurus.

After the bright and dark areas are segregated, the counts in the different zones from latitude +15° to the galactic equator show a significant trend with respect to longitude. In each zone the log $N(m)$ from the separate plates are fairly uniform at longitudes less than 124°, increase from 124° to about 132°, and are again uniform at longitudes

greater than 132°. The increase, which is most conspicuous for the brighter stars, suggests a thinning from west to east of a relatively near-by system of obscuring clouds. Each of these zones is accordingly subdivided for separate analyses into three parts by lines at longitudes 124° and 132°; the latter line is somewhat arbitrarily extended through the $-2\overset{\circ}{.}5$ zone.

Table 3 shows for each division of our region the values of mean log $N(m)$ for magnitudes 9.0–15.0. Before the analysis of the counts is made, these are converted to log $A(m)$ at magnitude intervals from $m = 9.5$ to $m = 14.5$, where $A(m)$ is the number of stars per square degree between $m - \frac{1}{2}$ and $m + \frac{1}{2}$.

THE COLORS

Color excesses of stars from spectral class B8 to class Fo are determined in Selected Areas 10, 25, and 26 and in about 50 square degrees of our areas *G* and *F*, centered in right ascension $5^h\,0^m$, declination $+41\overset{\circ}{.}0$, in order to evaluate the distances of the obscuring clouds and the selective absorption they produce.

Blue magnitudes of the stars were measured on Cramer Hi-Speed Special plates with ten minutes' exposure. The reference scale was similar to that employed in the counting. Red magnitudes were measured on Eastman 103E plates with sixty minutes' exposure behind a ciné-red filter. The star images formed by the Ross-Fecker camera on these excellent plates have so nearly the same appearance as the images on the blue plates that the same reference scale is used for both. Three blue and three red plates were measured in each area. Each blue plate of area *G* and each red plate on all centers was paired with a similar plate of the north polar region taken immediately before or after its mate and similarly exposed and developed.

Photographic-magnitude standards for the Selected Areas are taken from the Bergedorf catalogue, while those for *G* are from the North Polar Sequence.[4] Red-magnitude standards for all areas are taken from the polar-sequence magnitudes determined by C. P. and S. Gaposchkin.[5] Spectra for the Selected Areas are from the Bergedorf catalogue, and those from the area in *G* are from unpublished Harvard Observatory data furnished by Miss Cannon.

Stars from red magnitudes 9 to nearly 13 in spectral classes B8 to Fo are measured in each area. Means of observed blue and red magnitudes are taken for each star. In almost all cases the range in blue or red magnitudes for any star is less than $0^m\overset{\circ}{.}3$. No star is used for which the range is as much as $0^m\overset{\circ}{.}5$. The stars so excluded are, in general, either very bright or very faint near the limit of the plate.

All stars which appear in any one of the divisions previously determined from the counts are grouped together. Within each group the stars are further divided according to spectral class. For stars of each group the observed color index is plotted against red magnitude. The color excess corresponding to a given red magnitude m is determined from the mean observed color index at m by subtracting the normal color index of the spectral class. Values used as normal color indices are as listed by Bok,[6] extended to include spectral classes A8 to Fo. These values and the corresponding mean absolute magnitudes, $\bar{M}$, from the same source are reproduced in Table 4.

The color excess is converted to photographic absorption, K, on the International Scale by multiplying by the factor 3. This factor 3 is chosen to conform with the practice of others who have used plates of this sort, though slightly better agreement of the analysis for different divisions in the same latitude was found by using the factor 2.5. The mean distance in parsecs from the sun, r, for the group of stars giving each value of K is computed by the formula

$$5 \log r = m - \bar{M} + 5 - K .$$

[4] *Trans. I.A.U.*, **1**, 1922. [5] *Harvard Ann.*, **89**, No. 5, 1935. [6] *Ap. J.*, **90**, 249, 1939.

TABLE 3

MEAN LOG $N(m)$ FOR EACH DIVISION

Division	Position of Center		Area (Square Degrees)	m							Total Obscuration (Parsecs)	
	l	b		9.0	10.0	11.0	12.0	13.0	14.0	15.0	300	800
Zone												
+30°0	.....	.....	13	0.35	0.72	1.10	1.48	1.79	2.08	2.35	0m0	0m0
+27.5	.....	.....	20	.37	0.74	1.07	1.44	1.78	2.12	2.40	0.0	0.0
+25.0	.....	.....	19	.35	0.72	1.14	1.51	1.86	2.13	2.46	0.0	0.0
+22.5	.....	.....	20	.32	0.73	1.17	1.52	1.86	2.20	2.51	0.0	0.0
+20.0	.....	.....	50	.45	0.80	1.17	1.53	1.87	2.25	2.49	0.0	0.0
+17.5	.....	.....	65	.26	0.70	1.12	1.51	1.88	2.25	2.52	0.0	0.0
+15.0	119°	.....	22	.24	0.62	1.02	1.45	1.76	2.18	2.42	0.8	0.8
+15.0	135	.....	55	.40	0.77	1.16	1.53	1.91	2.30	2.56	0.4	0.4
+12.5	119	.....	20	.28	0.65	1.09	1.42	1.78	2.15	2.41	0.8	1.3
+12.5	128	.....	20	.44	0.79	1.15	1.49	1.88	2.28	2.57	0.5	0.9
+12.5	139	.....	36	.45	0.84	1.26	1.62	2.00	2.39	2.63	0.4	0.4
+10.0	119	.....	18	.20	0.65	1.10	1.40	1.74	2.11	2.39	1.0	1.5
+10.0	128	.....	19	.35	0.72	1.12	1.49	1.85	2.27	2.55	0.8	1.2
+10.0	139	.....	31	.37	0.78	1.23	1.59	1.98	2.36	2.63	0.5	1.0
+ 7.5	119	.....	14	.17	0.60	1.09	1.50	1.85	2.20	2.51	1.0	1.7
+ 7.5	135	.....	38	.41	0.83	1.23	1.60	1.97	2.34	2.62	0.5	1.5
+ 5.0	121	.....	12	.24	0.70	1.16	1.49	1.78	2.12	2.44	1.0	2.2
+ 5.0	128	.....	4	.22	0.71	1.12	1.51	1.89	2.26	2.56	1.0	1.7
+ 5.0	139	.....	15	.44	0.91	1.36	1.73	2.02	2.33	2.63	0.5	1.5
+ 2.5	121	.....	9	.11	0.55	1.00	1.37	1.77	2.14	2.48	1.7	2.0
+ 2.5	128	.....	8	.34	0.78	1.22	1.57	1.94	2.27	2.54	0.9	2.0
+ 2.5	139	.....	9	.38	0.88	1.34	1.75	2.03	2.35	2.63	0.3	1.7
0.0	121	.....	10	.23	0.73	1.13	1.50	1.85	2.20	2.51	1.5	2.1
0.0	139	.....	19	.39	0.86	1.28	1.64	1.96	2.26	2.57	0.7	2.1
− 2.5	125	.....	25	.48	0.79	1.15	1.52	1.86	2.19	2.48	1.3	2.0
− 2.5	137	.....	13	.12	0.53	1.07	1.44	1.80	2.10	2.44	1.5	2.2
− 5.0	125	.....	30	.41	0.78	1.16	1.51	1.85	2.18	2.45	1.2	2.0
Area												
B	120	+15°0	3	.11	0.43	0.93	1.30	1.65	1.92	2.22	1.3	1.3
B	120	+12.5	12	.08	0.52	0.86	1.24	1.57	1.96	2.21	1.5	2.0
B	118	+10.0	9	.32	0.66	0.99	1.30	1.64	1.98	2.24	1.5	2.0
H	135	+10.0	5	.36	0.86	1.29	1.63	2.00	2.45	2.73	0.5	0.5
A	117	+ 7.5	10	.25	0.78	1.21	1.56	1.91	2.26	2.65	0.7	1.5
C	120	+ 5.0	6	.22	0.58	0.96	1.28	1.59	1.93	2.20	1.8	3.0
G	128	+ 7.5	10	.36	0.82	1.24	1.63	2.04	2.41	2.73	0.7	1.0
G	136	+ 7.5	7	.49	0.93	1.34	1.69	2.06	2.44	2.77	0.5	0.9
G	128	+ 5.0	13	.44	0.83	1.26	1.65	2.03	2.43	2.76	0.9	0.9
G	135	+ 5.0	17	.49	0.92	1.40	1.78	2.13	2.47	2.79	0.5	0.8
G	128	+ 2.5	14	.39	0.84	1.30	1.64	1.99	2.38	2.72	0.9	1.2
G	137	+ 2.5	24	.59	1.04	1.49	1.87	2.20	2.52	2.82	0.3	0.8
G	135	0.0	27	.52	0.98	1.42	1.81	2.14	2.47	2.80	0.7	1.2
F	133	+ 2.5	3	.50	0.92	1.56	1.95	2.33	2.66	2.99	0.0	0.5
D	120	+ 2.5	3	.00	0.72	1.18	1.60	2.00	2.39	2.71	0.9	1.2
E	124	0.0	12	.01	0.44	0.84	1.22	1.58	1.96	2.28	2.2	2.8
K	129	− 2.5	5	.59	0.96	1.28	1.64	1.98	2.30	2.63	0.7	1.5
L	132	− 2.5	4	.24	0.48	0.86	1.16	1.50	1.84	2.16	2.5	3.2
L	132	− 5.0	17	0.11	0.39	0.77	1.14	1.48	1.79	2.10	2.5	3.1

The distance and the effectiveness of the obscuring clouds in each division are determined by plotting the values of K against r and drawing the best-fitting curve. The results in four representative areas are shown in Figure 2. Open dots of the graph represent values of K calculated from means of from only four to eight stars and therefore

TABLE 4

ADOPTED NORMAL COLOR INDICES AND MEAN ABSOLUTE MAGNITUDES FOR SPECTRAL CLASSES

Spectral Class	Normal Color Index	Mean Absolute Magnitude, $\bar{M}$
B8–B9	$-0^{m}.2$	−0.5
A0	− .1	+0.5
A2	.0	+1.5
A3–A7	+ .2	+2.5
A8–F0	+0.3	+3.0

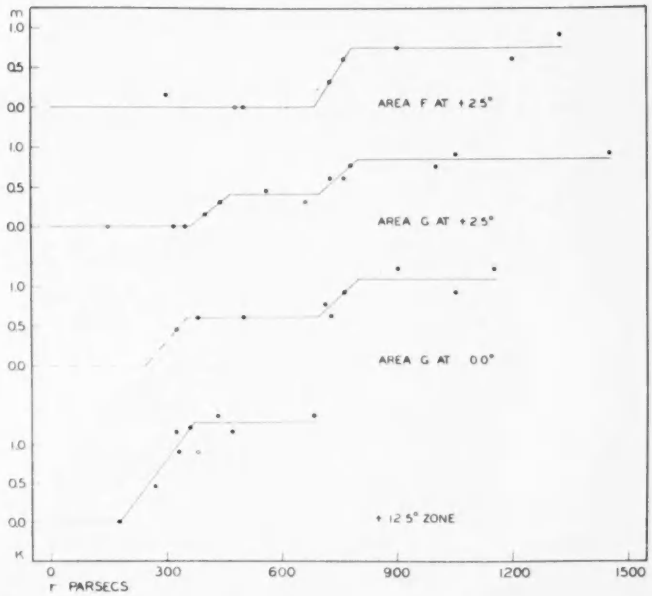

FIG. 2.—Photographic absorption in four divisions of Auriga, determined from color excesses

bear less weight than the solid dots, which represent well-determined absorptions. The data from which points of the graph are determined are listed in Table 5.

The graphs suggest that the absorption is caused by two clouds, one at a mean distance of 300 parsecs, the other at a distance of 800 parsecs. This is supported by the consistency with which obscuration appears at about these distances, with no further obscuration beyond 800 parsecs to the limit of the measurements. The data of the first

three graphs of Figure 2 might also be represented by use of continuous absorption coefficients: $0^m.7$ per kiloparsec, starting at 300 parsecs, for area *F*; $1^m.3$ per kiloparsec, starting at 300 parsecs, for area *G* at $+2°.5$; and $1^m.0$ per kiloparsec for area *G* at 0°. The results of the analyses of the counts made under the two interpretations do not essentially differ. We prefer the two-cloud interpretation because it seems to represent the color determinations more closely, because it gives a somewhat better fit in the analysis of the counts, particularly those of the brighter stars, and because it gives a physical picture.

TABLE 5

ABSORPTION DETERMINED FROM COLORS

Spectral Class	No. of Stars	Mean Red Mag.	Color Excess (Mag.)	Distance (Parsecs)
Area *F* at $+2°.5$				
B8–B9	20	10.5	0.20	1200
	18	11.0	.31	1320
A0–A2	15	10.6	.10	725
	11	11.0	.19	760
	18	11.5	.25	900
A2	6	9.4	.00	480
A3–A7	13	10.0	.05	300
	10	11.0	0.00	500
Area *G* at $+2°.5$				
B8–B9	6	8.9	0.10	660
	8	9.7	.25	780
	19	10.5	.30	1050
	19	11.2	.30	1450
A0	8	9.0	.10	440
	28	10.5	.19	760
	19	11.2	.25	1000
A2	14	9.0	.00	320
	22	10.7	.15	560
	25	11.4	.20	725
A3–A7	25	10.2	.00	350
	33	11.0	.05	400
A8–Fo	4	8.9	0.00	150
Area *G* at 0°.0				
B8–B9	12	9.4	0.18	725
	15	10.5	.29	1050
	26	11.0	.40	1150
A0	14	10.8	.30	760
	13	11.5	.40	900
A2	5	9.5	.15	325
	15	10.6	.20	500
	26	11.5	.25	710
A3–A7	23	11.0	0.20	380
$+12°.5$ Zone				
B8–A0	5	8.8	0.30	380
	11	10.5	.45	680
A2	11	10.0	.31	330
	10	11.0	.45	430
A3–A7	8	10.0	.15	270
	9	11.2	.38	325
	14	12.0	.38	470
A3–Fo	8	9.0	.00	180
A8–Fo	8	12.0	0.40	360

There appears to be no obscuration in the $+17°.5$ to $+30°$ zones. Colors in Selected Area 26 show no obscuration in the $+17°.5$ and $+20°$ zones. Hubble's[7] counts of extragalactic nebulae in fields of or adjacent to our region suggest no obscuration in latitudes higher than $+20°$. The mean of two fields in each zone gives $\log N = 1.96$ at $+30°$, 1.60 at $+25°$, and 1.75 at $+20°$, where *N* is the number of nebulae per field. The mean for the three zones is $\log N = 1.77$, well within the range from 1.60 to 2.22, which Hubble adopts as representing normal distribution of nebulae in the galactic polar caps, where the obscuration must be very little, if any.

Color excesses of some stars and open clusters in certain parts of our region have

[7] *Mt. W. Contr.*, No. 485, 1934.

been measured by other observers. The factors chosen to convert their color excesses to absorption on a scale comparable to our own were determined by the inverse wavelength relation.

The photoelectric survey of the color excesses of class B stars made by Stebbins, Huffer, and Whitford[8] includes a few stars of this region. Their values, multiplied by a factor 7, are compared in Table 6 with our absorption determined from colors in the same divisions. No comparison was attempted in divisions which contained only one star at a suitable distance.

Zug[9] and Cuffey[10] have studied color excesses in a few of the open clusters contained in this region. M37 and M38 appear in Zug's data. Using his distances and converting his color excesses by multiplying by a factor 2.5, we find an absorption of $0^m.4$ at 840 parsecs compared with $0^m.5$ at 300 parsecs and a total of $0^m.8$ at 800 parsecs determined

TABLE 6

COMPARISON WITH STEBBINS, HUFFER, AND WHITFORD

Division	No. of Stars	Distance (Parsecs)	Absorption	
			SHW	Kiefer−SHW
0° zone >132°	5	650	$1^m.0$	$-0^m.3$
+ 2.5 zone >132°	4	1000	1.5	+ .2
F	3	1000	0.3	+ .2
G at +2°.5	6	1000	0.8	.0
+12°.5 zone >132°	2	650	0.2	+0.2

from our colors. Cuffey finds between $1^m.0$ and $2^m.0$ at 900 parsecs for NGC 1893, while we find in the same zone $1^m.2$ at 800 parsecs. He has no obscuration to 600 parsecs for NGC 1857, as compared with $0^m.3$ at 300 parsecs from our colors.

We find in the +7°.5 zone a total absorption of $1^m.5$, which agrees with the results of unpublished measurements in Selected Area 25 kindly supplied by Dr. B. G. Karpov. Thus the agreement of our colors with those of other observers seems generally satisfactory.

ANALYSIS OF THE COUNTS

The analysis is accomplished with the aid of (m, log π) tables whose construction and use have been described by Bok.[11] It is necessary to find for each zone values of log $A(m)$ representing the counts which would be obtained if the zone were unobscured. Zones from +17°.5 to +30° are apparently unobscured, so the required $A(m)$ are taken directly from the counts. Although no unobscured areas appear in the lower latitudes, the amount and distances of the obscuration in most of the zones are determined from color excesses, and the counts may be corrected to give unobscured values. This is accomplished by introducing in the (m, log π) table of a zone the obscuration determined from colors in a division of that zone and finding a set of factors which produce values of $A(m)$ closely approximating the observed $A(m)$ of the division. This set of factors, representing the density gradient with distance from the sun, is used in computing values of unobscured $A(m)$.

The unobscured log $A(m)$ were plotted in order of latitude at each magnitude interval

[8] *Mt. W. Contr.*, No. 621, 1940.

[9] *Lick Obs. Bull.*, No. 454, 1933.

[10] *Harvard Ann.*, **105**, No. 21, 1937.

[11] *The Distribution of the Stars in Space*, p. 26, University of Chicago Press, 1937.

from $m = 9.5$ to $m = 14.5$. The resulting graphs are smooth curves with maxima at 0°, which slope uniformly to +17°.5 and then decrease more gradually to +30°. Unobscured log $A(m)$ for +10° and +15° zones were computed from density factors interpolated from those for adjacent zones. Adopted values of unobscured log $A(m)$ for each zone appear in Table 7.

The analysis of the counts in the obscured divisions is made by introducing in the (m, log π) table the amounts of obscuration necessary to make the log $A(m)$, computed from the density gradient of the zone, fit the log $A(m)$ observed for each division. In general, the difference between computed and observed log $A(m)$ is not so great as 0.05. The exact amounts of obscuration determined for each division are given in the last two columns of Table 3.

A picture of the two absorbing clouds is given by the shaded maps of Figure 1. Most of the obscuration is caused by the cloud at 300 parsecs, which extends over the entire

TABLE 7

VALUES OF UNOBSCURED LOG $A(m)$

Zone	m					
	9.5	10.5	11.5	12.5	13.5	14.5
0°.0	1.12	1.52	1.91	2.25	2.54	2.77
2.5	1.02	1.47	1.85	2.21	2.50	2.74
5.0	0.93	1.43	1.80	2.13	2.42	2.68
7.5	0.94	1.39	1.78	2.10	2.41	2.68
10.0	0.84	1.27	1.67	2.01	2.32	2.60
12.5	0.75	1.15	1.53	1.91	2.22	2.46
15.0	0.71	1.09	1.45	1.81	2.05	2.28
17.5	0.56	0.95	1.32	1.66	1.97	2.20
20.0	0.57	0.93	1.32	1.63	1.93	2.15
22.5	0.54	0.91	1.30	1.62	1.91	2.14
25.0	0.50	0.88	1.23	1.56	1.83	2.06
27.5	0.48	0.83	1.20	1.52	1.79	2.04
30.0	0.45	0.83	1.21	1.53	1.75	1.99

region from −5° to +15° with the exception of area F. This near-by cloud, which causes obscuration varying from $0^m.0$ to $2^m.5$, creates the conspicuous patterns of bright and dark areas shown on the map. Its densest parts form the dark areas B, C, E, and L, and it also outlines the bright areas A, D, F, K and the lower portion of G. The 800-parsec cloud extends from −5° to +12°.5, outlining area H and the upper portion of G. The maximum obscuration of $1^m.4$ occurs near the equator in the eastern part of the region.

A number of investigations related to ours have been made in or near our region. Schalén,[12] in his discussion of Auriga, considers parts of areas F, G, and the −2°.5 zone. He combines F and G, since he attributes the difference in brightness to a preponderance of absolutely bright B and A stars in area F. In the −2°.5 zone, Schalén finds a dark cloud beginning at 70 parsecs and extending to 400–500 parsecs with a total obscuration of $1^m.9$. We find $1^m.5$ at 300 parsecs and a total obscuration of $2^m.2$ at 800 parsecs.

Hartwig[13] uses area F as a comparison field for obscured regions in Taurus. He finds $1^m.4$ obscuration at a distance of 100–200 parsecs, with a total obscuration of $2^m.1$ at 350 parsecs in a region adjacent to our area L where we find an obscuration of $2^m.5$ at 300 parsecs. McCuskey's[14] data in Taurus extend to the border of the Auriga region.

[12] *Upsala Medd.*, **55**, 1931.

[13] *Zs. f. Ap.*, **17**, 191, 1939.

[14] *Ap. J.*, **88**, 209, 1938; **89**, 568, 1939.

He finds in the 0°, −2°.5, and −5° zones heavy obscuration caused by a dark cloud at a distance less than 200 parsecs. The dark cloud *L* is caused by about $2^m.0$ obscuration in McCuskey's analysis and by $2^m.5$ at 300 parsecs in this paper. Our obscurations caused by the near-by cloud run about $0^m.5$ higher than Hartwig's and McCuskey's, which is precisely the amount of obscuration we determined in area *F*, used by them as an un-

TABLE 8

DENSITY GRADIENTS

Zone	*r* in Parsecs							
	125	200	300	500	800	1250	2000	3000
0°.0	1.00	1.00	0.90	0.90	0.60	0.30	0.15	0.05
2.5	1.00	1.00	.90	.90	.60	.30	.15	.05
5.0	1.00	1.00	.90	.90	.60	.30	.10	.05
7.5	1.00	1.00	.90	.80	.60	.35	.10	.05
10.0	1.00	1.00	.80	.60	.50	.25	.10	.05
12.5	1.00	0.80	.75	.50	.30	.25	.10	0.02
15.0	1.00	0.80	.75	.50	.25	.15	.05	.....
17.5	1.00	0.75	.50	.30	.20	.10	.07	.....
20.0	1.00	0.75	.50	.30	.20	.10	.05	.....
22.5	1.00	0.70	.50	.30	.20	.09	.05	.....
25.0	1.00	0.60	.40	.30	.20	.09	.02	.....
27.5	1.00	0.60	.40	.25	.15	.10	.02	.....
30.0	1.00	0.60	0.40	0.25	0.15	0.09	0.01	.....

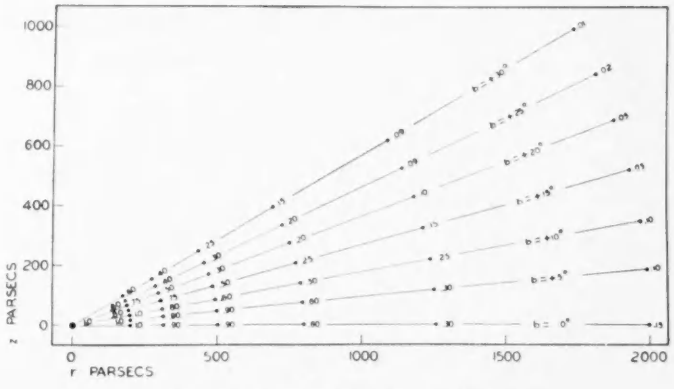

FIG. 3.—Values of density gradients

obscured comparison area. The further obscuration caused by our 800-parsec cloud is balanced by the $0^m.5$-per-kiloparsec continuous absorption coefficient used by McCuskey.

Hubble's[7] counts of extragalactic nebulae indicate an obscuration of $0^m.7$ in the +15° zone as compared with $0^m.4$ from our analysis. Area *B* at +15° has $1^m.4$ from Hubble's counts and $1^m.3$ from our analysis. Hubble finds, in the +10° zone, $1^m.3$ obscuration at longitudes greater than 132° and $1^m.5$ at longitudes less than 132°; we determine $1^m.0$ and $1^m.5$, respectively for the same regions. For area *B* at +10° and for all zones closer to the galactic equator Hubble's counts indicate more than $3^m.0$ absorption. We determine from $2^m.1$ to $3^m.1$ obscuration for these zones within the distance of 2000 parsecs from the sun. Additional obscuration may very well be found beyond this distance.

DENSITY GRADIENTS

The adopted density gradients are listed for all zones in Table 8 and are shown in Figure 3 in relation to distance perpendicular to the galactic plane, z, as well as distance from the sun, r. Density was assumed uniform within 200 parsecs of the sun and outside this range is expressed in terms of unit density near the sun. Star densities were considered symmetrical about the galactic equator; those gradients adopted for positive latitudes are also used for the corresponding negative latitudes.

The negative gradients imply that the sun is situated in a region of high density with respect to the direction of Auriga. In the lower latitudes the density is reduced to about one-half at 800 parsecs and to less than one-third at 1200 parsecs from the sun. The negative character of the gradient is not affected when the obscuration is represented by a continuous absorption coefficient. Density factors computed under this hypothesis vary only slightly from the corresponding adopted factors.

Oort[15] has determined density gradients in this region and finds near the galactic equator in the direction of the anticenter a small but well-defined decrease in density factors to 500 parsecs of the sun, then a rise to 1.6 from 870 to 1500 parsecs. An absorption of $2^{m}.5$ at a distance less than 800 parsecs would be needed in addition to what we have introduced in the 0° to +5° zones in Auriga to bring the $A(m)$ computed from his densities into agreement with the Illinois counts. Such an absorption would not be consistent with our color excesses, which cover this entire range of distances. Accordingly, we conclude that in the direction of Auriga the star density decreases with increasing distance from the sun.

UNIVERSITY OF ILLINOIS OBSERVATORY
August 1941

[15] *B.A.N.*, 308, 1938.

ANALYSIS OF A TRANSVERSE SECTION OF THE MILKY WAY IN AQUILA

ROBERT H. BAKER

ABSTRACT

The analysis of this narrow section, 60° long, across the Milky Way around longitude 13° is based on star counts to magnitude 15, color excesses of stars determined at three centers, and published counts of extragalactic nebulae. The obscuration is ascribed to two clouds: one cloud at 500 parsecs, which covers the entire section and is not far from uniform, aside from darker spots at two places; the second cloud at 2000 parsecs, whose density increases fairly symmetrically from latitude 15° to the galactic equator. The density functions near the galactic plane decrease at first with distance from the sun and then increase to values at 2000–3000 parsecs, which are comparable with that near the sun. Some of the results of the analysis are considered provisional.

This is the first of some studies of the Milky Way in the vicinity of the Great Rift, which are in progress at the University of Illinois Observatory. It was the intention to collaborate in the preparation of the papers with Freeman D. Miller, who was ready to make star counts in the lower latitudes of the region of Aquila. Dr. Miller's service in the United States Navy interrupts the original arrangement. At his suggestion I have proceeded independently with the first paper.

The section under discussion is a narrow strip across the Milky Way at declination $+15°$, except that it turns to the south near its eastern end in order to hold more nearly to the same longitude. The section lies between galactic latitudes $+30°$ and $-30°$, and its mean galactic longitude is about 13°. Beginning near α Herculis, it extends eastward along the northern borders of Ophiuchus and Aquila and then down through Delphinus.

THE STAR COUNTS

All the plates were taken at the University of Illinois Observatory with the 4-inch Ross-Fecker camera, 28 inches in focal length. The scale of the plates is 290″ per millimeter, or about 2° to the inch. The plates used for the counts are Cramer Hi-Speed Special. They are taken in pairs on each of eighteen centers about 5° apart: one with ten minutes' exposure for counting from magnitude 9 to magnitude 13, the other with sixty minutes' exposure for magnitudes 11–15.

The method of counting is the same as that described in a previous paper.[1] Magnitude standards for calibrating the reference scale are available on the plates containing Selected Areas 85, 86, 87, 88, and 112 and are carried by overlapping plates to the remainder of the section. Standards for the fainter stars are taken from the *Mount Wilson Catalogue*;[2] those for the brighter stars are brought from the North Polar Sequence[3] by means of pairs of plates similarly exposed and developed, one centered on the pole and the other on the Area. No corrections are made to the counts for distance from the center of the plate or for any other reason.

In preparation for the analysis of the counts, the section is divided into areas arbitrarily lettered, in each of which the surface distribution of the stars seems fairly uniform and different from that in the neighboring areas. The section is further divided by parallels of galactic latitude into zones 2°.5 wide, especially in the higher latitudes where there are no conspicuous cloud patterns. The arrangement of the divisions is shown in

[1] Baker, *Harvard Circ.*, No. 424, 1939.

[2] *Carnegie Institution of Washington Pub.*, No. 402, 1930.

[3] *Trans. I.A.U.*, **1**, 71, 1922.

Figure 1. The values of the mean log $N(m)$ representing the counts in the different divisions appear in Table 1, where $N(m)$ is the number of stars per square degree brighter than apparent photographic magnitude m. Before the analysis of the counts is made, these are converted to log $A(m)$ at magnitude intervals from $m = 9.5$ to $m = 14.5$, where $A(m)$ is the number of stars per square degree between $m - \frac{1}{2}$ and $m + \frac{1}{2}$.

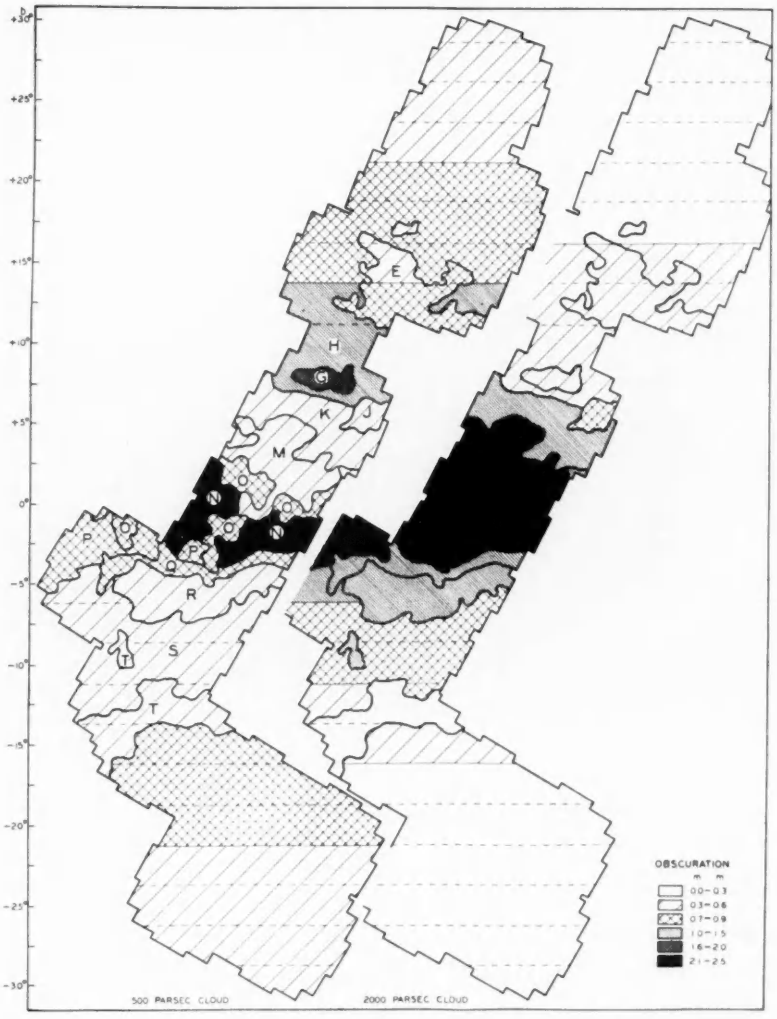

FIG. 1.—Amounts of obscuration in the two clouds

THE COLORS

In order to assist the counts in establishing the distances of obscuring clouds in this region and the amounts of obscuration they produce, color excesses of stars from spectral class B8 to class A7 have been determined in three places, each about 3° in radius, centered at the following right ascensions and declinations: $19^h\ 0^m$, $+15°.6$; $19^h\ 53^m$, $+14°.8$; $19^h\ 51^m$, $20°.1$. The colors at the first center were measured by Miss Vivian

Martin. The spectral classes of the stars measured at the first center are taken from the *Henry Draper Catalogue* and its *Extension*;[4] the classes at the other centers are from an unpublished extension by Miss Cannon kindly furnished by Harvard Observatory.

Blue magnitudes were measured on Cramer Hi-Speed Special plates with five minutes' exposure, and red magnitudes on Eastman 103E plates with sixty minutes' exposure

TABLE 1

MEAN LOG $N(m)$ FOR THE DIFFERENT DIVISIONS

Area Zone	Longitude of Center*	Area in Square Degrees	Limiting Magnitude							Obscuration by Cloud at Parsecs	
			9.0	10.0	11.0	12.0	13.0	14.0	15.0	500	2000
+30	3°	7	0.21	0.61	0.99	1.44	1.80	2.15	2.42	$0^m.4$	.....
+27.5	3	18	.14	0.61	0.97	1.40	1.78	2.14	2.40	0.4	.....
+25	4	21	.29	0.64	1.04	1.45	1.84	2.18	2.43	0.5	.....
+22.5	5	22	.15	0.58	1.05	1.48	1.86	2.22	2.49	0.6	.....
+20	5	28	.29	0.66	1.10	1.54	1.92	2.32	2.57	0.7	.....
+17.5	6	36	.12	0.50	1.08	1.55	1.93	2.33	2.65	0.8	.....
E +17.5	7	2	.30	0.68	1.12	1.60	1.96	2.38	2.76	0.6	.....
+15	6	26	.20	0.59	1.14	1.57	1.93	2.32	2.66	0.8	$0^m.5$
E +15	9	10	.28	0.70	1.25	1.66	2.03	2.44	2.76	0.6	0.4
+12.5	8	19	.17	0.59	1.14	1.52	1.96	2.36	2.68	1.0	0.5
E +12.5	7	15	.32	0.67	1.16	1.57	2.01	2.40	2.78	0.9	0.4
G + 7.5	12	4	.40	0.64	1.07	1.39	1.78	2.33	2.59	1.8	0.6
H + 7.5	13	22	.39	0.77	1.28	1.68	2.02	2.57	2.87	1.0	0.6
J + 5	11	4	.60	1.12	1.53	1.92	2.32	2.84	3.14	0.5	0.9
K + 5	15	29	.48	0.96	1.46	1.85	2.25	2.72	3.01	0.5	1.3
M + 2.5	16	26	.46	0.92	1.38	1.77	2.13	2.51	2.82	0.6	2.2
O + 2.5	20	23	.50	0.92	1.36	1.72	2.02	2.36	2.64	0.9	2.5
N 0	20	8	.40	0.89	1.26	1.60	1.88	2.18	2.50	2.3	2.5
N − 2.5	16	15	.50	0.84	1.16	1.54	1.85	2.15	2.46	2.3	2.5
P − 2.5	25	17	.60	1.03	1.48	1.86	2.16	2.50	2.87	0.8	2.2
Q − 5	22	12	.65	1.01	1.44	1.83	2.19	2.58	2.99	0.8	1.0
R − 5	22	24	.67	1.08	1.48	1.91	2.28	2.75	3.18	0.4	1.0
S − 5	28	7	.53	0.98	1.52	1.90	2.23	2.66	3.07	0.6	1.0
S − 7.5	24	25	.58	0.99	1.42	1.86	2.22	2.66	3.05	0.5	0.8
S −10	22	22	.62	1.06	1.40	1.80	2.20	2.66	3.06	0.4	0.7
T −10	24	2	.58	1.00	1.36	1.79	2.16	2.58	2.98	0.4	1.0
S −12.5	24	8	.40	0.91	1.30	1.73	2.14	2.64	3.03	0.4	0.4
T −12.5	24	15	.46	0.84	1.24	1.67	2.08	2.56	2.95	0.6	0.2
−15	20	18	.46	0.85	1.22	1.59	1.98	2.38	2.68	0.8	0.5
T −15	24	7	.44	0.86	1.26	1.66	2.06	2.52	2.90	0.5	.....
−17.5	18	39	.39	0.81	1.21	1.58	1.96	2.35	2.66	0.8	.....
−20	16	34	.36	0.79	1.18	1.58	1.95	2.32	2.61	0.7	.....
−22.5	16	36	.27	0.78	1.19	1.60	1.95	2.28	2.59	0.6	.....
−25	16	36	.26	0.74	1.16	1.56	1.87	2.23	2.53	0.5	.....
−27.5	18	28	.30	0.74	1.11	1.53	1.86	2.19	2.50	0.4	.....
−30	15	9	0.19	0.68	1.12	1.52	1.80	2.22	2.43	0.4	.....

* All galactic co-ordinates in this paper are referred to the conventional pole at right ascension 12^h40^m and declination +28°.

behind a ciné-red filter. Three blue plates and three red plates were employed at each center. The plates at the first center contain the Harvard Region C 10, in which blue and red magnitude standards are available.[5] The plates at the other centers are paired with similarly exposed and developed plates centered either on the Region C 10 or on

[4] *Harvard Ann.*, **100**, No. 2, 1925.

[5] C. P. Gaposchkin, *Harvard Ann.*, **89**, No. 8, 1937.

the pole where blue standards are taken from the North Polar Sequence and red magnitudes from data by C. P. and S. Gaposchkin.[6]

As the result of a preliminary study of the colors thus determined, the stars are divided into four groups within each of which the selective absorption seems nearly the same. Each group is further divided into four groups, in which the stars are of spectral classes B8–B9, A0, A2, and A3–A7, respectively. The normal color indices of the subgroups in this order are adopted as −0.2, −0.1, 0.0, and +0.2 mag., and the corresponding mean red absolute magnitudes are taken to be −0.5, +0.5, +1.5, and +2.5.

The observed color indices (blue *minus* red magnitudes) of the stars in each subgroup were plotted against their red magnitudes. Means were then taken at half-magnitude intervals wherever the plotted points seemed numerous enough to give significant results. The color excess (observed *minus* normal color index) so determined at each red magnitude appears in Table 2, together with the mean distance of the stars for which the index was determined. The distance, d, is derived by the formula

$$5 \log d = m - M + 5 - K ,$$

where K, the photographic absorption in magnitudes, is three times the color excess.

The values of the photographic absorptions derived from the color excesses of Table 2 are plotted in Figure 2 against the corresponding distances from the sun. While some, and perhaps all, of the arrays of points might well be represented by constant coefficients of absorption, I prefer the interpretation given by the curves in the figure because it seems to produce better fits in the analysis of the star counts and also because it attempts a physical picture. This construction of the evidence shows an absorbing cloud at the distance of about 500 parsecs from the sun and suggests no additional absorption up to the distance of 1500 parsecs.

As can be seen by reference to Table 1, the values of K which are determined from the colors of the stars in various divisions of the region are employed in the analysis as the amounts of obscuration of these divisions by the cloud at 500 parsecs. Colors in an additional area, K, suggest absorption of 0.5 mag., which is accordingly introduced in the analysis of this area, though the available mean excesses are not numerous enough here to define a curve well.

ANALYSIS OF THE STAR COUNTS

The analysis is made with the convenient $(m, \log \pi)$ tables whose construction and use have been described by Bok.[7] Since nothing is known about the variation of the $\log A(m)$ with longitude, it is arbitrarily decided to take means of these values in the corresponding north and south zones from latitudes 15°—30°, exclusive of the areas they contain; thus the analysis is kept within a smaller range of longitude. In addition I assume provisionally that the gradients of the $\log A(m)$ with respect to galactic longitude would be symmetrical relative to the equator if there were no obscuring material present.

If all the obscuration in the section of the Milky Way we are considering and within the range of the star counts were caused by the cloud at 500 parsecs, it would be a simple matter to calculate the values of the unobscured $\log A(m)$ in the different latitudes from the corresponding values derived from the counts. The amounts of the absorption, which I ascribe to this cloud, are known from the color excesses in all zones from the equator to latitude 10°. The total amounts in the higher latitudes, where absorbing material is scarcely to be expected beyond the range of the counts, can be determined from published counts of extragalactic nebulae.

[6] *Harvard Ann.*, **89**, No. 5, 1935.

[7] *The Distribution of the Stars in Space*, University of Chicago, 1937.

A trial analysis with a single cloud at 500 parsecs failed to give satisfactory fits in the lower latitudes between the computed and the observed log $A(m)$. A second trial with the use of constant coefficients of absorption seemed likewise unsatisfactory. It remained to try a second cloud. This cloud must be more remote than 1500 parsecs, as the color determinations indicate. It can hardly be as far away as 3000 parsecs, for the distant cloud

TABLE 2

COLOR EXCESSES

Spectral Class	No. of Stars	Mean Red Mag.	Color Excess	Distance	Spectral Class	No. of Stars	Mean Red Mag.	Color Excess	Distance
Areas O at 0°, P at −2°.5, Q at −5°					Area M at 0° to +5°				
			mag.	parsecs				mag.	parsecs
B8–B9	17	10.5	+0.27	1100	B8–B9	7	9.5	+0.19	760
	16	11.0	+ .34	1260	A0	8	9.0	+ .18	400
A0	12	10.5	+ .20	760		13	9.5	+ .09	550
	22	11.0	+ .34	800		14	10.0	+ .11	690
A2	17	10.5	+ .16	500		9	10.5	+ .16	800
	21	11.0	+ .30	520		16	11.0	+ .21	950
	19	11.5	+ .26	690	A2	8	10.0	+ .18	400
A3–A7	6	9.5	.00	250		33	10.5	+ .22	450
	19	10.5	− .03	400		26	11.0	+ .23	580
	17	11.0	+0.05	460		15	11.5	+ .24	720
					A3–A7	5	9.0	.00	200
						11	10.0	.00	320
						26	10.5	+ .06	360
						18	11.0	+0.11	440
Area S at −5° to −10°					Area R at −5°				
B8–B9	12	10.0	+0.10	1100	B8–B9	18	10.5	+0.17	1250
	15	10.5	+ .20	1200	A0	18	10.5	+ .11	870
	10	11.0	+ .25	1450		33	11.0	+ .16	1000
A0	21	10.5	+ .10	870		15	11.5	+ .17	1300
	17	11.0	+ .25	910	A2	13	10.5	+ .06	580
	20	11.5	+ .15	1300		21	11.0	+ .10	700
A2	15	10.5	+ .10	550		24	11.5	+ .17	800
	18	11.5	+ .22	720	A3–A7	10	10.0	− .04	320
A3–A7	15	9.5	− .02	250		19	10.5	+ .03	400
	28	10.5	+ .01	400		16	11.0	+0.01	500
	23	11.0	+ .04	480					
	18	11.5	+0.02	600					

appears in the analysis as high as the zone of 15° latitude, whose upper border is nearly 1000 parsecs from the plane of the galactic equator at that distance from the sun. The distant cloud is accordingly introduced before the 2000-parsec shell in the analysis and in combination with the nearer cloud permits the observed log $A(m)$ to be closely fitted.

Hubble's[8] counts of extragalactic nebulae provide the amounts of the total absorption in areas $J+5°$, $S-10°$, and $E+15°$, and in the mean 20°, 25°, and 30° zones, from which the unobscured log $A(m)$ are derived. Similar values for the remaining zones are

[8] *Mt. W. Contr.*, No. 485, 1934.

found by interpolation for latitudes greater than 5° and by arbitrarily extending the gradients of log $A(m)$ to the equator. The adopted total absorptions differ from those derived from Hubble's counts by not more than 0.3 mag., where his log $N = 1.90$ is taken to represent no obscuration. The values of his log N in the basic divisions enumerated above are 0.90, 1.07, 1.34, 1.45, 1.60, and 1.64. The contribution of the nearer cloud to the total absorption is known from the colors in the first three divisions and is supposed equal to the total in the remaining three.

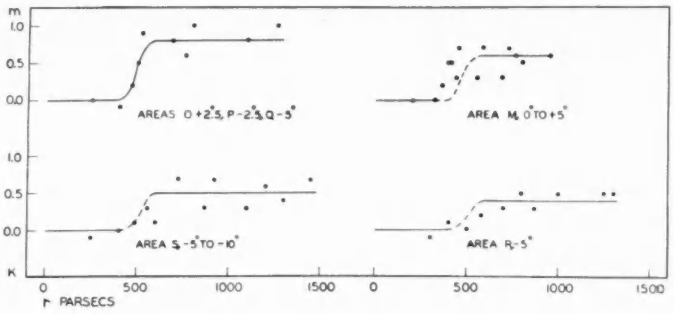

FIG. 2.—Photographic absorptions derived from color excesses

TABLE 3

ADOPTED VALUES OF UNOBSCURED LOG $A(m)$

ZONE	MAG.					
	9.5	10.5	11.5	12.5	13.5	14.5
0°.0	1.52	2.00	2.46	2.94	3.42	3.84
2.5	1.16	1.64	2.20	2.76	3.26	3.70
5.0	1.00	1.51	2.03	2.58	3.08	3.54
7.5	0.91	1.42	1.91	2.43	2.94	3.39
10.0	0.85	1.32	1.81	2.32	2.80	3.23
12.5	0.80	1.26	1.72	2.21	2.67	3.06
15.0	0.76	1.21	1.66	2.11	2.52	2.85
17.5	0.71	1.16	1.60	2.02	2.39	2.70
20.0	0.68	1.12	1.54	1.96	2.26	2.52
22.5	0.64	1.07	1.47	1.87	2.16	2.40
25.0	0.61	1.03	1.40	1.80	2.07	2.32
27.5	0.58	1.00	1.35	1.75	2.02	2.26
30.0	0.55	0.98	1.30	1.70	1.99	2.21

The adopted values of the unobscured log $A(m)$ for the different zones are given in Table 3. Possible sources of uncertainty in these values for the lower latitudes are the small number of areas in which nebulae have been observed, the supposition that all the absorption indicated by the counts of nebulae is produced in the two clouds of the analysis, and the necessity of arbitrarily extending the gradients of the unobscured log $A(m)$ from latitude 5° to the equator. In addition the remote cloud lies beyond the range of distances within which the conclusions from star counts to magnitude 15 are believed to be the most reliable. The degree of the uncertainty in the present results cannot be determined until spectra and colors are extended to greater distances.

The final analysis of the different divisions of this section of the Milky Way employs the color determinations, as far as they go, to establish the amounts of obscuration by the 500-parsec cloud and for the remainder apportions the obscuration between the two clouds from the run of the counts alone. It should be mentioned that a somewhat better fit of the log $A(m)$ in the areas M and O was effected by allowing some of the remote cloud to project into the adjoining nearer shell of the $(m, \log \pi)$ table. The amounts of obscuration by the two clouds are shown in the last two columns of Table 1.

TABLE 4

DENSITY FUNCTIONS FROM ADOPTED UNOBSCURED LOG $A(m)$

ZONE	DISTANCE IN PARSECS									
	125	200	300	500	800	1250	2000	3000	5000	8000
0°.0	1.00	1.00	0.90	0.70	0.60	0.70	1.00	1.00	0.50	0.20
2.5	1.00	1.00	.90	.70	.60	.70	1.00	1.00	.50	.20
5.0	1.00	0.90	.90	.70	.60	.70	0.80	0.80	.40	.20
7.5	1.00	0.90	.80	.70	.60	.60	0.60	0.60	.30	.10
10.0	1.00	0.90	.80	.60	.50	.50	0.50	0.40	.20	0.05
12.5	1.00	0.80	.70	.60	.50	.50	0.30	0.25	.15	.....
15.0	1.00	0.80	.70	.60	.50	.40	0.25	0.10	0.05	.....
17.5	1.00	0.80	.70	.50	.40	.40	0.15	0.07	.....	.....
20.0	1.00	0.80	.60	.50	.40	.35	0.10	.....	.....	.....
22.5	1.00	0.80	.60	.50	.30	.25	0.09	.....	.....	.....
25.0	1.00	0.80	.60	.50	.30	.15	0.07	.....	.....	.....
27.5	1.00	0.70	.50	.40	.20	.14	0.07	.....	.....	.....
30.0	1.00	0.70	0.50	0.40	0.20	0.12	0.07	.....	.....	.....

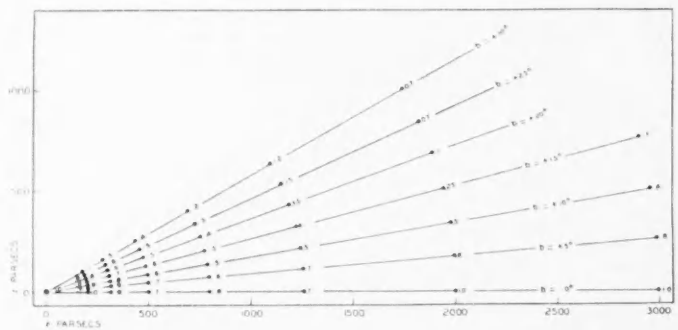

FIG. 3.—Density functions at the different latitudes

The densities of the different parts of the two clouds are represented by the shadings in Figure 1. The nearer cloud appears throughout the section and is remarkably uniform (obscuration 0.4–0.8 mag.), aside from heavier spots near the equator and around latitude $+10°$. The distant cloud lies between latitudes $+15°$ and $-15°$, and its density increases fairly symmetrically to the equator. The darkest part of the Milky Way in this section is the area N, where the combined absorption by the two clouds approaches 5 mag.

THE GRADIENTS OF STAR DENSITY

The relative numbers of stars per cubic parsec, taking as unity the number in the sun's neighborhood, are given in Table 4 for the different latitudes and at the various distances from the sun. These density functions near the galactic plane decrease at first with distance from the sun and then increase, until at 2000–3000 parsecs they become equal to the value near the sun. This conclusion may well be regarded as provisional, subject to confirmation by further studies of the region. Concerning the Scutum cloud, which lies considerably farther south, Schalén[9] remarks that, while in all other regions from Cygnus to Auriga he found negative density gradients, here, in Scutum, there is definite indication of condensations of stars at distances of some 2000–3000 parsecs.

The density functions are also displayed in Figure 3, where one may notice roughly as well how the gradients run at different levels above the plane of the galactic equator. Bok and MacRae's[10] analysis of my counts in the higher latitudes of this section brings out this feature more clearly. They find a marked increase in the star density at different levels with increasing distance from the sun over the density at the same level near the sun.

The study of another transverse section of this part of the Milky Way, based on counts and colors, is in progress at the University of Illinois. This second section runs across at about declination $-15°$, through southern Ophiuchus and northern Sagittarius.

UNIVERSITY OF ILLINOIS OBSERVATORY
August 1941

[9] *Upsala Medd.*, No. 61, 1934.

[10] Unpublished.

THE CLASSIFICATION OF THE RED CARBON STARS

PHILIP C. KEENAN AND W. W. MORGAN

ABSTRACT

The subdivisions of spectral classes R and N do not appear to represent a consistent progression in temperature. In order to set up a more definite temperature sequence, a new classification is suggested on the basis of four criteria: (1) atomic line ratios which are sensitive to temperature changes; (2) intensity gradient of the continuous spectrum in the yellow and red regions; (3) strength of the D-lines of sodium; and (4) intensity gradient within the λ 5635-band group of the molecule C_2.

In the new classification the double maximum shown by the C_2 bands in the R-N system disappears and is replaced by a single broad maximum.

The "lithium" star, WZ Cassiopeiae, whose spectral type in the R-N system is N1p is reclassified at the low-temperature end of the carbon sequence; it appears to be the coolest carbon star known, and the great strength of *Li* may possibly be explained.

A group of five carbon stars has been found which is characterized by extreme weakness of the atomic lines in the photographic region. The bands of *CH* occur with great strength in their spectra; in addition, all five stars have very high radial velocities.

The intensities of the carbon bands vary greatly among stars of the same subclass; this is probably to be considered as evidence of different abundances of carbon in the atmospheres of different stars.

INTRODUCTION

The stars with spectra characterized by strong bands of C_2 and *CN* were grouped into classes R and N by Miss Cannon in the *Henry Draper Catalogue*.[1] Later the subdivisions which had been developed at Harvard were revised and extended by Shane.[2]

The R-N classification was designed to provide a good working summary of the appearance of these stars on spectrograms of low dispersion. It is based chiefly upon the strength of the band absorption and the redness of the spectra as judged from a comparison of the visual and photographic regions. The two criteria are not independent, for the extension of the bands is often so great that no part of the continuum can be assumed to be entirely free of their effect. Evidence that the color depends upon the choice of spectral region is provided in the observations of Wildt,[3] who found that the color differences, infrared *minus* ultraviolet, for a number of R and N stars were not in the same order as their assigned spectral types. These inconsistencies appeared to be too large to be due to errors and led Wildt to state that they ". . . . strengthen the doubts as to whether the physical changes along the sequence R-N can really be explained by the steady variation of a single parameter, namely, the surface temperature." Such doubts had been raised by Shane, largely on the basis of his study of the behavior of the λ 4737 Swan band of C_2. When plotted against spectral type the intensity of this band showed a double maximum,[4] which cannot be reconciled with a continuous decrease of temperature, if one employs the ordinary dissociation theory.

Since there is strong reason to accept the idea, originally put forward by Rufus,[5] that the R and N stars are distinguished from the ordinary stars by having a greater abundance of carbon in their atmospheres, it would not be surprising if the carbon abundance varied within the group also. Consequently, in any classification based in part upon

[1] For definition of the types see *Harvard Ann.*, **91**, 10, 1918. Class N had been proposed and the redder stars assigned to it by Pickering in 1891.

[2] *Lick Obs. Bull.*, **13**, No. 396, 123, 1928.

[3] *Ap. J.*, **84**, 303, 1936; *Mt. W. Contr.*, No. 551.

[4] *Op. cit.*, Fig. 2.

[5] *Pub. Univ. Michigan Obs.*, **2**, 103, 1916.

absolute band intensities there is danger of confusion of the two parameters—temperature and carbon abundance—and this probably occurs to some extent in the R-N system. In contrast, all other types in the *Henry Draper Catalogue*, with the possible exception of type S, are subdivided to run monotonically with respect to temperature. It is highly desirable that a similar arrangement of the carbon stars should be made, for not until this is done can the application of dissociation theory to their atmospheres be more than qualitative.

We attack the problem by first attempting to arrange the stars in a sequence based upon every clue which appears to give an indication of relative temperature. Afterward the strength of the carbon bands in stars of a given temperature class can be used to estimate carbon abundance.

The primary criteria for the temperature sequence are: (1) relative intensities of atomic lines in the blue region of the spectrum; (2) color as estimated from portions of the continuous spectrum in places where the distortion by band absorption is judged to be least; (3) strength of the D-lines of *Na;* and (4) relative intensity of molecular bands within a given system. In actual use each of the criteria has been estimated separately for as many stars as possible.

DISCUSSION OF THE CRITERIA OF CLASSIFICATION

1. *Atomic-line ratios.*—Certain of the atomic lines used in classifying the ordinary stars of types G, K, and M lie between the bands in the carbon stars, permitting estimates to be made of equivalent spectral types of the latter. It is essential to work only with intensity differences of adjacent lines, for absolute intensities are obviously affected by the increased opacity in the strongly banded stars. The lines which have proved most useful on the Yerkes one-prism spectrograms (scale: 120 A/mm at $H\gamma$) are the following:

$$Fe\ 4045 - Mn\ 4032\text{–}4\ ,$$

$$Fe\ 4250,\ 4260 - Cr\ 4254\ .$$

In a few stars *Ca* 4226, *Fe* 4325, and $H\gamma$ can also be taken into account, but the change in *Cr* 4254 with respect to the two adjacent iron lines is the best indicator of temperature.

There are not many carbon stars with spectra sufficiently bright to be observed in the blue region at Yerkes, but they are particularly important in establishing the zero point for the new classification. They are distinguished in Table 1 as the stars with equivalent spectral types (in parentheses) in the sixth column.

2. *Color.*—In the easily observed orange part of the spectrum there are short stretches near λλ 5190, 5670, and 6150 where it appears possible to estimate the intensity of the continuum without serious interference from the band absorption. Because of the short base-line the differences are not very sensitive to color changes, but the temperature range from the earliest to the latest carbon stars is so great that the increased reddening of the latter is conspicuous and should be taken into account in the classification. For this reason estimates of color on an arbitrary scale are included in Table 1 as the eighth column. The scale values range from −4 for the bluest of the stars to nearly +2 for the reddest.

3. *Intensity of Na 5890, 96.*—Among all the atomic lines observable with low dispersion only the resonance D-lines of sodium reach such great strength in the later carbon stars that their absolute intensity is a valuable criterion. The extreme range of variation of the pair, unresolved on our spectrograms, can be seen in Plate XXI. It may be noticed also that their usefulness is limited to the later stars of the sequence illustrated, for in the earlier ones a broad region of absorption extending from λ 5750 to λ 6050 nearly blots out the D-lines (compare HD 137613 and HD 52432 in Plate XXI). This absorp-

PLATE XXI

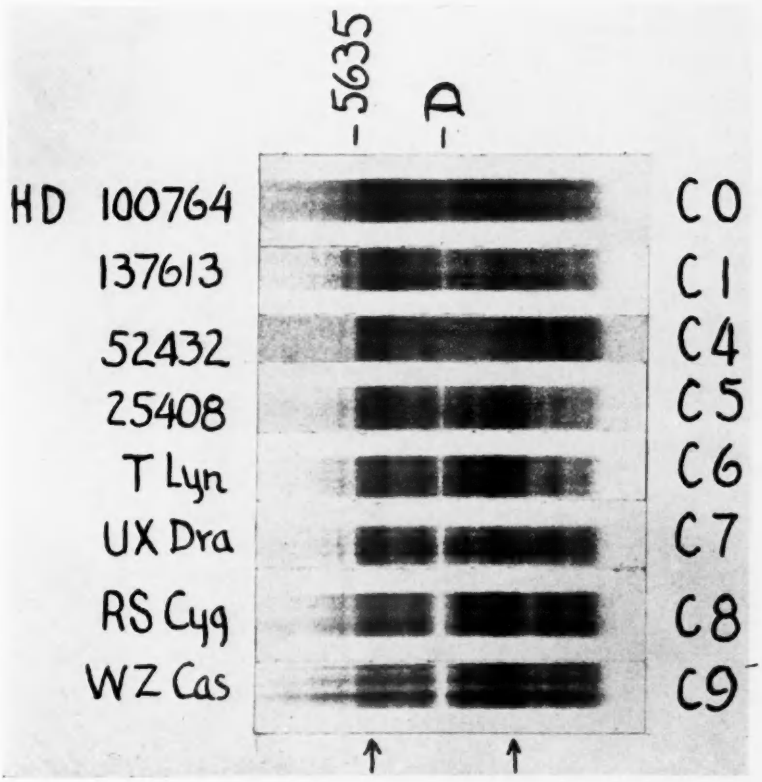

SPECTRAL SEQUENCE OF THE CARBON STARS, REGION 5600–6500 A

Progressive changes in color (at the wave lengths indicated by the arrows), intensity of the D-lines, and bands of the 5635 group, can be followed.

PLATE XXII

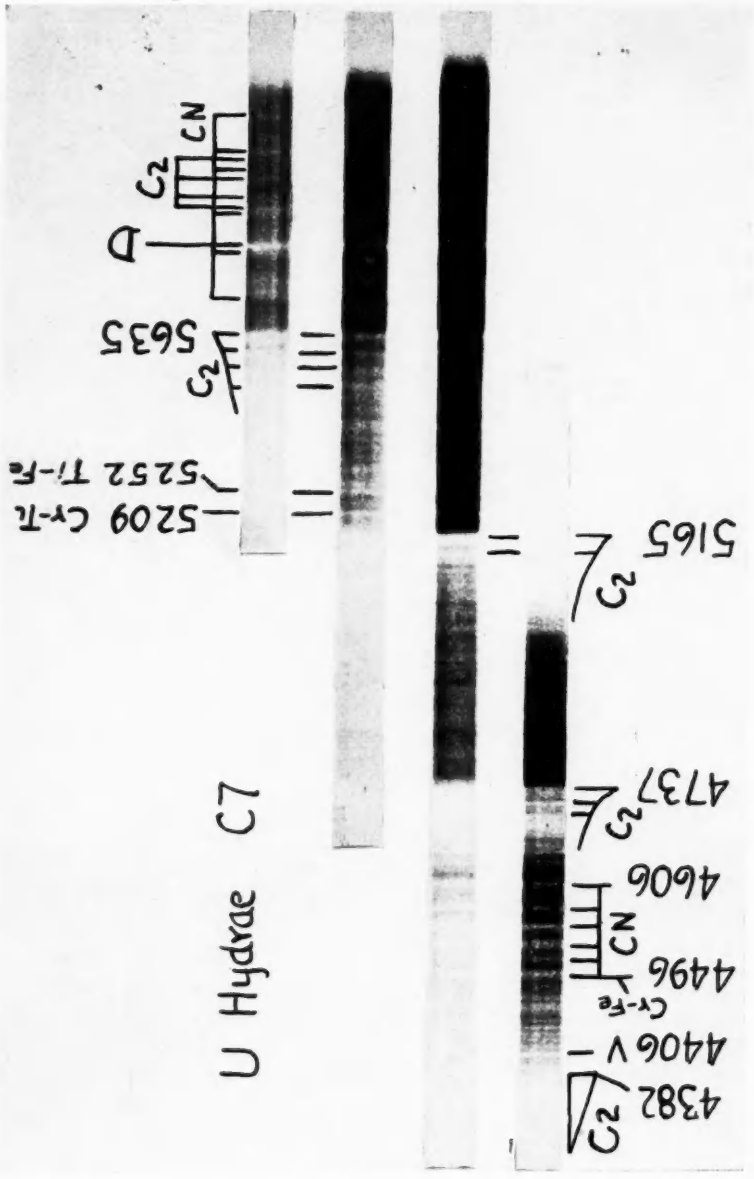

SPECTRUM OF THE GREEN AND RED REGIONS OF THE TYPICAL CARBON STAR U HYDRAE AS OBSERVED WITH ONE-PRISM SPECTROGRAPH ON THE 40-INCH REFRACTOR

Scale of original negatives: 250 A/mm at λ 6100. The upper three spectra were taken on an Eastman Super Panchro Press Plate; the lower one, on a Cramer Hi Speed Special.

tion is due at least in part to the widening of the red-band systems of C_2 and CN in the hotter stars, but there may be some additional contributor. In using the D-lines for classification it is necessary to make allowance for the strength of the carbon bands.

4. *Band-intensity gradients.*—The relative intensities of the different vibrational bands in a sequence vary regularly with temperature in a manner which can be calculated in the case of symmetrical molecules. Computations for several bands of C_2 and CN have been made by Wurm,[6] who applied the method to estimate roughly the temperatures of the carbon stars; but for our purpose it is necessary to consider only the sequence of changes as the temperature is varied. From Wurm's Table 1 it is seen that the ratio of the bands λ 5635/λ 5585 increases from 5/4 at 3000° to 3/1 at 1500°. These bands are well situated for observation on our spectra, and in the thirteenth column of Table 1 their estimated ratio is given. It shows roughly the same range as the theoretical values given above; and, although the estimates are difficult because of overlapping and because of the strong continuum to the right of λ 5635, the ratio is evidently helpful in ordering the spectra according to temperature.

In practice additional bands of this and other C_2 groups are taken into account. On the other hand, such bands as the green sequence of CN are unsuitable for this purpose because of the effects of blends with strong atomic lines.

The temperature variation in the width of the red bands, which was mentioned in the preceding section, is also of some help in classification. In Plate XXI the progressive change in the appearance of the red region is apparent. In connection with the illustration it should be noted that the intensity estimates on the bands in the λ 5635 group are always made on spectra more strongly exposed than those shown.

THE SYSTEM OF CLASSIFICATION

For each of the representative stars listed in Table 1 some or all of the criteria described have been evaluated. The stars could then be arranged in order of decreasing temperature. The next step is the assignment of classes. Since the basis of arrangement is fundamentally different from that of the R-N system, it is preferable to avoid confusion by adopting a new notation. It is most logical to use the letter C for all these stars, inasmuch as the defining characteristic of the group is the predominance of carbon. In assigning subdivisions, the equivalent types established by criterion 1 provide a definite starting-point and have been distributed as follows:

Equivalent Types	Carbon Sequence Type	Approx. Effective Photospheric Temp.	Equivalent Types	Carbon Sequence Type	Approx. Effective Photospheric Temp.
G4–G6	C0	4500	K3–K4	C4	3650
G7–G8	C1	4300	K5–M0	C5	3450
G9–K0	C2	4100	M1–M2	C6	.....
K1–K2	C3	3900	M3–M4	C7	.....

It may be seen from the table that the branching of the carbon stars from the F-G-K sequence occurs between spectral types G4 and G6.

The stars observed in both the red and the blue regions allow a determination of the changes in the other criteria for each interval of one subdivision in type, whence the scale is extended to C9 for stars too red to be observed in the blue part of the spectrum. For this purpose criteria 2, 3, and 4 have been found to be of about equal usefulness.

The strength of the Swan bands of C_2 is the other parameter of classification and is described by the subscript following the type number. The scheme shown below gives

[6] *Zs. f. Ap.*, **5**, 260, 1932.

TABLE 1

CATALOG OF C STARS

Star	α_{1900}	δ_{1900}	m_v	Former Type	Equiv. Type	C Type	Mean Color	I_D	I_{C_2}	I_{CN} (Red)	I_{CH}	$\frac{5635}{5585}$	Notes
HD 1994	0^h19^m	$+53°44'$	9.7–	R5	(K4)	$C4_5$	.....	.....	9	.....	4	.....	.....
HD 5223	0 49	+23 32	8.8–	R3	.....	$C2p_2$	−2.7	1	3	2	6	0+	1
Z Psc	1 11	+25 14	7.4– 8.1	No	.....	$C7_3$	−0.2	5	5	5	.....	2+	.....
V Ari	2 10	+11 47	8.3– 9.0	R8	.....	$C5p_5$	−2.2	2+	9	5	8	1	1
HD 16115	2 30	− 9 53	8.3–	R3	(G9)	$C2_3$	.....	.....	5	.....	8	.....	2
HD 19557	3 04	+57 31	8.1–	R5	(K3)	$C4_5$	−2.2	0+	10	6	5:	0+	.....
HD 25408	3 57	+61 32	7.9–	R8	(K5)	$C5_3$	−2.5	3+	6	5	6:	1	.....
ST Cam	4 41	+67 59	7.0– 8.3	N5	.....	$C6_4$	−1.5	4	8	8	.....	2	.....
R Lep	4 55	−14 57	6.1– 9.7	N6e	.....	$C7_4+$	+1:	6	8	6	.....	3:	.....
W Ori	5 00	+ 1 02	5.9– 7.7	N5	.....	$C5_5$	−1.5	3	6	8	.....	2	.....
BD+16°1194	6 29	+16 09	9.1–	N	.....	$C8_5$	0	6	5	7	.....	3	3
UU Aur	6 30	+38 31	6.2– 6.7	N3	.....	$C5_3$	−1.5	4+	6	7	.....	2	.....
RV Mon	6 53	+ 6 18	7.0– 8.2	N6	.....	$C5_4$	−1.5	3	8	8	.....	1+	.....
HD 52432	6 56	− 3 06	7.5–	R5	(K4)	$C4_4$	−2.7	1	8	5	6	1	.....
RY Mon	7 02	− 7 24	7.7– 9.1	N5	.....	$C6_5$	0	4	9	8	.....	1	.....
RU Cam	7 11	+69 52	7.9	Ko	(G4)	Co_1-	.....	.....	.....	.....	3:	.....	Max.
			9.0	Ro	(K3)	$C3_4$	−2.5	1	2	0:	2:	.....	Min.
HD 59643	7 26	+24 44	8.2–	R9	.....	$C6_2$	−1.5	4	4	5	.....	4	.....
HD 60826	7 31	+ 2 18	8.7– 9.1	Na	.....	$C5_5$	−1.7	2+	9	8	.....	2:	.....
T Lyn	8 16	+33 50	8.0–12.0	Noe	.....	$C6_3$	−1	4	5	7	.....	3	.....
X Cnc	8 50	+17 37	6.1– 6.6	N3	.....	$C5_4$	−2	4	7	8	.....	2	.....
HD 76396	8 51	+51 49	8.8–	R5	.....	$C1p_2$	−3	1−	3	1	10	0	1
HD 79319	9 08	+14 37	8.9–	R4	.....	$C4_4$	−3	2	8	5	.....	1	.....
Y Hya	9 46	−22 32	6.5– 8.0	N3	.....	$C5_4$	−1	2+	7	6	.....	1	.....
U Hya	10 33	−12 52	4.5– 6.3	N2	(M4)	$C7_3$	−1.5	4+	6	8	4:	3	.....
HD 92839	10 38	+67 56	6.3–	No	(M2)	$C6_3$	−2	3+	5	7	4	3	.....
V Hya	10 47	−20 43	6.7–12.0	N6	.....	$C7_5$	−2:	5	9+	9	.....	2:	.....
HD 100764	11 31	−14 02	8.7–	Ro	.....	Co_2	−3.5	1+	3	1	.....	0	.....
SS Vir	12 20	+ 1 20	7.2– 9.0	Np	.....	$C6_3$	0	4	6	8	.....	2	.....
Y CVn	12 40	+45 58	4.8– 6.0	N3	.....	$C5_4$	−2	2	7	5	2:	2	.....
RY Dra	12 52	+66 32	6.1– 7.1	N4p	.....	$C4_4$	−2	1	7	4	.....	1	4
HD 112869	12 55	+38 20	9.2– 9.6	R6p	.....	Cp_5	−2.7	2	9	5	8	1+	1
HD 113801	13 01	−19 31	8.7–	K5R	(G7)	$C1_1$	.....	.....	1−	.....	7	.....	.....
HD 137613	15 22	−24 49	7.4–	R3	(G7)	$C1_2$	−3	2+	4	3	1	0	5
V CrB	15 46	+39 52	7.2–12.0	N2	.....	$C6_3$	−0.7	5	6	6	.....	2+	Max.
RR Her	16 02	+50 46	7.8– 9.5	K5–Noe	.....	$C7_2$	−1	6	4	5	.....	3	Min.
V Oph	16 21	−12 12	7.0–10.5	Nb	.....	$C7_4$	−0.2	5	7:	8	.....	3	.....
HD 156074	17 10	+42 15	7.7–	R1	(G8)	$C1_2$	−2.7	1+	3	2	4	0	.....
TW Oph	17 24	−19 24	8.0– 8.7	Nb	.....	$C6_5$	−1	3	9	9	.....	1+	.....
SZ Sgr	17 39	−18 38	8.5– 9.8	Nb	.....	$C7_3$	−0.2	4+	6	8	.....	3	.....
T Lyr	18 29	+36 54	7.8– 9.6	N3	.....	$C6_3$	−0.5	2+	10	6	.....	1	.....
HD 173291	18 39	+36 51	8.1–	N4	.....	$C6_4$	−1.5	4+	8	8	.....	2	.....
S Sct	18 45	− 8 01	6.4– 7.3	N3	.....	$C5_4$	−1.5	4	8	9	.....	1	.....
V Aql	18 59	− 5 50	6.5– 8.0	N6	.....	$C6_4$	−0.7	4	8	8	.....	1	.....
HD 182040	19 18	−10 53	7.0–	Ro	(G7)	$C1_2$	−2.5	2	3	1:	1	0	.....
UX Dra	19 25	+76 23	6.1– 7.1	No	(M_3)	$C7_3$	−1.2	5	6	7	3	3	.....
RS Cyg	20 10	+38 26	7.5– 8.7	Nope	.....	$C8_2$	0.2	7	3	8	.....	5	.....
U Cyg	20 16	+47 35	6.1–11.8	Npe	.....	$C7_2$	−0.5	5	3	6	.....	5	Max.
						$C9_2$	+2:	10:	8:	6	.....	.....	$m_v=9$
S Cep	21 36	+78 10	7.9–13.1	N6e	.....	$C7_4$	+1.5	5	7	8	.....	2:	Max.
HD 206570	21 38	+35 03	6.4–	N1	.....	$C6_3$	−0.5	4	6	8	.....	2	.....
RV Cyg	21 39	+37 34	7.1– 9.3	N5	.....	$C6_4$	−1	3	8	7	.....	1+	.....
RX Peg	21 52	+22 24	7.7– 8.6	N3	.....	$C5_5$	−2.2	3	10	8	.....	2:	.....
HD 209621	22 00	+20 34	8.8–	R3	.....	$C3p_2$	.....	1−	2	3:	9	.....	1
HD 215484	22 40	+61 12	9.0–	Nb	.....	$C6_4$	−0.5	4+	8	7	.....	2	.....
19 Psc	23 41	+ 2 56	5.3–	No	(M1)	$C6_2$	0	5	4	5	1	4	.....
HD 223392	23 44	+ 5 50	8.8–	R3	(K1)	$C3_2$	.....	.....	3	.....	4	.....	.....
WZ Cas	23 56	+59 48	6.9– 8.5	N1p	.....	$C9_1$	0	8:	2	4	.....	6	6

NOTES

1. Star belongs to peculiar group with *CH* strong and atomic lines weak.
2. Atomic lines somewhat weakened.
3. *Dearborn Obs. Ann.*, **4**, Part 16, 1940.
4. Sanford's green bands very strong.
5. $M_v = -0.6$ from interstellar *Na* (Sanford, *Ap. J.*, **51**, 238, 1939).
6. *Li* 6708 found to be very strong by McKellar.

the relation of the subscripts to the intensities of Table 1, tenth column, which are on essentially the same scale as that used by Shane for the λ 4737 band:

Intensity	Subscript
0–2	1
3–4	2
5–6	3
7–8	4
9–10	5

The use of subscripts makes the notation different from that in any of the HD classes; but, since the parameter described—abundance—is not represented in the other classes, the distinction seems appropriate. In using the system it must be remembered that near

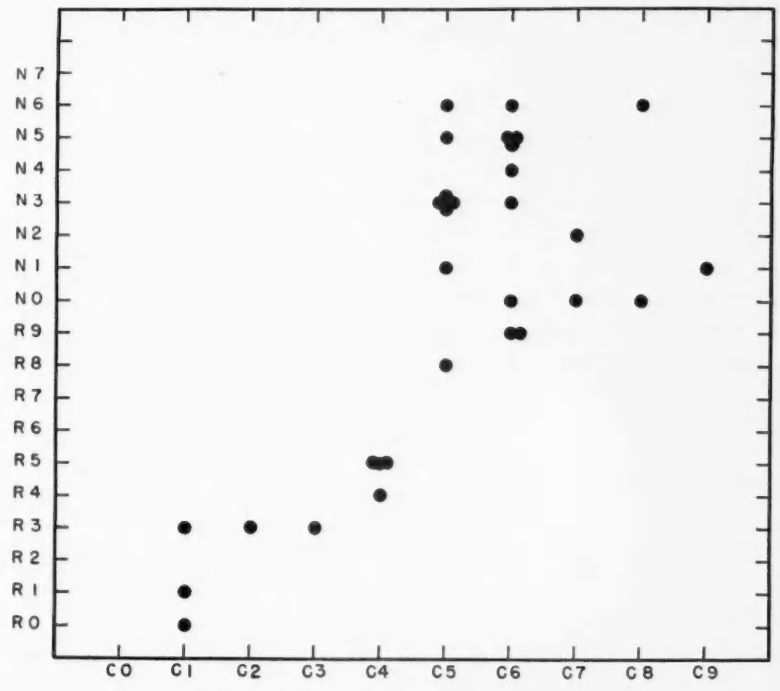

FIG. 1.—Comparison of R-N types with revised types for the carbon sequence

the beginning of the sequence the bands are never very strong and only the lower intensities are represented. This follows from the fact that band intensity depends upon temperature as well as upon abundance. However, since the classification has a definite empirical basis it should eventually prove possible to calibrate the scale to determine the abundance corresponding to a given intensity within each spectral type.

A comparison of C-types with the R-N system[7] is given in Figure 1. Through type R the agreement is good, but the old subdivisions of type N appear to have very little correlation with the reclassification. That the scatter is much greater than the uncertainty in assigning stars to the revised sequence is evident if the data in Table 1 are examined

[7] The types, which are due for the most part to Shane, are taken from Sanford's catalogue, *Ap. J.*, **82**, 202, 1935.

for the extreme cases. For example, all three red criteria agree in indicating that WZ Cas is at a lower temperature than V Aql, although the former types were N1p and N6, respectively.

The uncertainty in classifying stars on the C-system from the Yerkes plates is about ± 1 subdivision. It is not feasible to estimate the error more closely from an analysis of the correlation of the criteria, for the weighting given to each varies rapidly with the type indicated. Thus I_D passes through a minimum at C3–C4 because the overlying band absorption in these classes averages much greater than in the earlier ones and the D-lines are consequently of little value at this point, though they become the most sensitive parameter for the redder stars.

VARIATION OF ABSORPTION FEATURES WITH TYPE

In Plates XXII and XXIII the more important absorption lines and bands seen on medium-dispersion spectra of the typical carbon stars are identified. The behavior of those not already discussed is summarized below:

C_2.—The Swan bands listed in Table 2 dominate the visual spectrum except in the stars at the extreme ends of the sequence. Since the band groups vary consistently in intensity, estimates of the λ 5635 group, expressed on the same scale as Shane's intensities for λ 4737, provide the values of I_{C_2} given in the tenth column of Table 1 and plotted against type in Figure 2. The diagram reveals two important points. First, there is a large range in band strength within each of the types that include any stars having strong bands. This can be interpreted as a variation in carbon abundance at constant temperature. Second, the curve obtained by plotting the mean band intensities for each spectral type shows a broad maximum centered at types C5–C6.

CN.—It was shown by Shane[2] that the λ 4215 group of bands passes through a maximum, becoming very weak in the redder carbon stars. On the other hand, it was known from the early observations of Rufus[5] and of Hale, Ellerman, and Parkhurst[8] that the group at λ 4606 remains strong throughout the subdivisions of type N, and Sanford[7] found the red bands to behave similarly. This behavior of band groups all originating from the same lower level appeared so anomalous that Wurm[6] doubted the correctness of the data. However, Figure 3 shows that the effect is clearly present when the λ 4215 band and the red bands are compared. The region of the green bands has been observed here for only a few stars, but the data indicate that if they have a maximum it must occur later than that of the λ 4215 band. On the other hand, the observations by Wildt suggest that the ultraviolet *CN* bands reach maximum intensity early in the carbon sequence, although here again the material is necessarily scanty.

It is likely that this weakening of the bands on the violet side of λ 4500 is due, at least in part, to the same continuous absorption which it was necessary to postulate in order to explain the abnormally steep intensity gradients in that part of the spectrum of many of the stars of types C4–C6, but it is not certain that the whole of the effect can be accounted for in this way.[9]

CH.—Among the normal carbon stars the narrow band at λ 4300 varies considerably in strength but never becomes much more intense than in the ordinary G-type giants. In the latter the pronounced maximum of the band occurs near types G4–G5, while the carbon sequence shows strong bands in some stars (HD 25408, HD 52432) with equivalent types as late as K4–K5 (C4–C5).

There exists also a noteworthy group of peculiar carbon stars characterized by unusually great *CH* intensity and almost complete absence of atomic lines in the blue region

[8] *Pub. Yerkes Obs.*, **2**, 253, 1903.

[9] The presence of absorption has been discussed by Wildt (cited in n. 3) and by Merrill, *Spectra of Long-Period Variable Stars*, p. 29, 1940.

PLATE XXIII

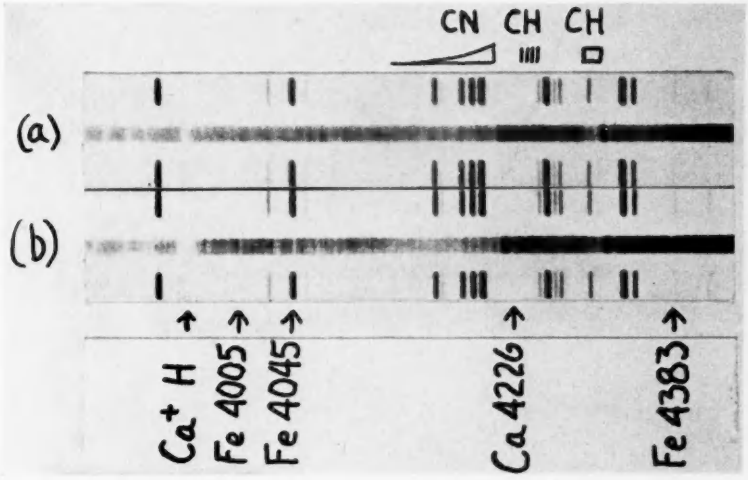

a) HD 5223, Cp_2; *b*) HD 223392, C_{3_2}: COMPARISON OF A PECULIAR *CH* STAR (*above*) WITH A TYPICAL CARBON STAR (*below*)

Arrows point to some of the strongest atomic lines which are almost obliterated in the upper spectrum.

of the spectrum. These stars are easily recognized, for even so strong a line as *Ca* 4226 (see Pl. XXIII) is practically invisible on spectrograms of moderate scale. The five stars which have been assigned to this group are marked Cp in Table 1 and are collected in Table 3. The radial velocities in the sixth column are taken from Sanford's table.[7]

TABLE 2

PRINCIPAL ABSORPTION BANDS IN THE SPECTRA OF THE CARBON STARS

Band Head	Designation	Description
		C_2—Swan bands
	$B^3\pi$–$A^3\pi$	
λ 4383	2–0	Weak. Bands overlapping
4737	1–0	Strong. Bands overlapping
5165	0–0	Strong. Bands overlapping
5636	0–1	Strong. Bands overlapping
6191	0–2	Weak. Bands better separated
		CN
	$B^2\Sigma$–$X^2\Sigma$	
λ 3360	2–0	Very weak. Observed by Wildt.* Probably maximum intensity near C_3–C_4
3590	1–0	Strong. Observed by Wildt.* Probably maximum intensity near C_3–C_4
3883	0–0	Very strong. Observed by Wildt.* Probably maximum intensity near C_3–C_4
4216	0–1	Strong. Maximum at C_3
4606	0–2	Rather weak. No maximum earlier than C6
	$A^2\pi$–$X^2\Sigma$	
6196	3–0	Rather weak. Possibly broad maximum near C6
6333	4–1	Rather weak. Possibly broad maximum near C6
6481	5–2	Rather weak. Possibly broad maximum near C6
		CH
λ 4300	$A^2\Delta$–$X^2\pi$	G-band. Very strong in peculiar stars
3900	$B^2\Sigma$–$X^2\pi$	Probably strong in peculiar stars
		NH
	$B^3\pi$–$A^3\Sigma$	
λ 3360	0–0	Observed by Wildt.* Narrow, symmetrical
3370	1–1	Observed by Wildt.* Narrow, symmetrical
		Green bands found by Merrill, Sanford, and Shane
λ 4540		Moderately wide and strong. Degraded to red
4572		Narrow
4642		Wide. Degraded to red. C_2?
4866		Strong. Moderate width. Degraded to red
4905		Narrow
4932		Weak
4976		Strong and wide. Degraded to red. C_2?
5035		Weak

* *Ap. J.*, **93**, 502, 1941.

The star HD 16115 shows some similarity to the group and may be an intermediate case.

To find the relation of these stars to the members of the normal carbon sequence it will be necessary to use spectra of higher dispersion; but so interesting are their peculiarities

that we list provisionally here those which have been established in addition to the two definitive characteristics:

1. The average radial velocity is much greater than for normal carbon stars. Table 3 includes the three highest radial velocities in Sanford's catalogue.

2. The spectral type is probably in the range C2–C4. There may be some selection here, for only a few of the redder stars have been observed in the blue region.

3. The color is possibly bluer than the average for the same types. HD 76396 and HD 112869 have been observed in the far ultraviolet by Wildt,[10] who notes the unusual strength of the ultraviolet continuum of the former.

4. *CH* is increased in strength relatively to C_2 and *CN*. The intensities of bands of the latter two molecules show great scatter in Table 3. In contrast *CH* is so prominent that in Plate XXIII almost all the absorption features in HD 5223 between λ 4216 and λ 4290 have been identified as bands of the λ 4300 group, which in normal stars are

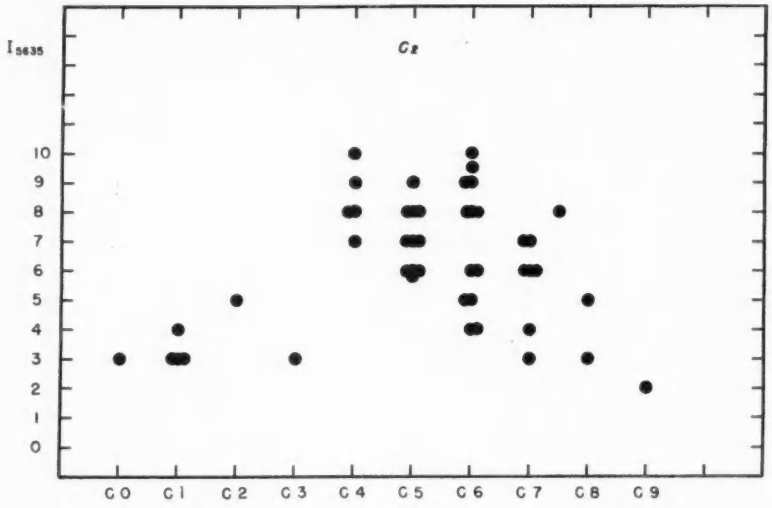

FIG. 2.—Variation of the intensity of the absorption bands of C_2 with spectral type

too faint to be detected without high dispersion. The λ 3900-band group also appears to be strengthened.

Unidentified green bands.—In 1926 Merrill[11] and Sanford[12] called attention to the presence in a number of carbon stars of five well-marked bands, of which the strongest were at λ 4976 and λ 4868. Their behavior was investigated by Shane,[2] who added three more to complete the list given in Table 2. These bands are not well situated for study on our plates, but from the data given by Shane their intensity is evidently correlated with the visual redness of the stars, i.e., with the depression of the blue end of the spectrum. For this reason Shane used them as supplementary criteria in assigning stars to the later subdivisions of class N.

In the C-system the stars in which these bands are strong (W Ori, R Lep, V Aql, RY Dra) are scattered over the range C4–C7. Their correlation with the continuous absorption in the blue region suggests the possibility of a common molecular origin.

A tentative identification of two of these bands, λ 4976 and λ 4642, was made by Wurm,[13] who interpreted them as convergences of higher bands in the great C_2 groups with their heads at λ 4737 and λ 5165. However, the remaining bands remain unaccount-

[10] *Ap. J.*, **93**, 502, 1941.

[11] *Pub. A.S.P.*, **38**, 175, 1926.

[12] *Pub. A.S.P.*, **38**, 177, 1926.

[13] *Zs. f. Ap.*, **13**, 179, 1937.

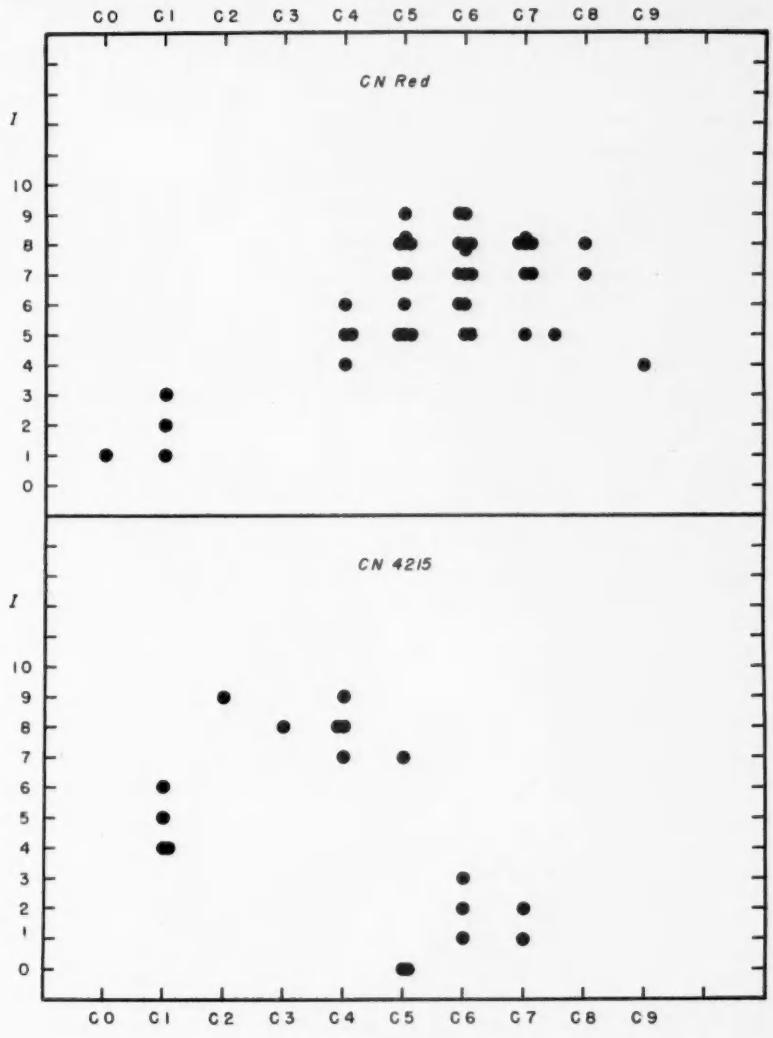

FIG. 3.—Variation with spectral type of the red and blue bands of *CN*

TABLE 3

STARS WITH *CH* STRONG AND ATOMIC LINES WEAK

Star	Former Class	I_{CH}	$I_{CN_{4215}}$	I_{C_2}	V_r
HD 5223	R3	6	3	2	−234 km/sec
V Ari	R8	8:	2	9	183
HD 76396	R5	10	1−	3	52
HD 112869	R6p	8	5	9	128
HD 209621	R3	9	8	2	−383

ed for; and the appearance of the whole set in such stars as RY Dra, where they are deeper than the main λ 4737 band head and practically obliterate the green *CN* group, leaves the question of their identification in doubt.

Absorption marking at λ 6269.—In stars near type C4 the most conspicuous absorption feature to the red of the D-lines on our plates is a band about 25 A wide centered at λ 6269.[14] The band can be seen in the spectrum of HD 52432 in Plate XXI and is especially strong in Y CVn and RY Dra. Whether it is a molecular band or a group of closely packed atomic lines is not certain, but in any case the rapidity with which it falls off in intensity on both sides of the maximum makes it of supplementary value in classification.

Li 6708.—The resonance doublet of neutral lithium at λ 6708 was observed as a strong unresolved line in WZ Cas by McKellar.[15] Since several other late carbon stars showed no well-marked line at this position, he suggested that an abnormal abundance of lithium is present in the atmosphere of WZ Cas. From the standpoint of the present classification this conclusion does not appear quite definite, for WZ Cas is the only star classified as C9, the subdivision corresponding to the lowest temperature. Resonance lines might be expected to be stronger in this star than in any of the others observed, but it must be admitted that the absence of λ 6708 in RS Cyg, which is only slightly earlier in type, remains puzzling.

Sr II 4077.—This line is of particular interest because it shows so strong a positive absolute-magnitude effect that the ratio λ 4077/λ 4045 is used as a criterion of luminosity in normal stars. The value of the ratio appears to be at least as high in several of the carbon stars as in the two giants chosen for comparison. For all the carbon stars showing good atomic lines in this part of the spectrum (types Co–C6) the indicated absolute magnitudes are slightly brighter than those of the ordinary giants. As a group they can be assigned to luminosity class II–III, with $\bar{M}_v \approx -1$. This spectroscopic evidence is in satisfactory agreement with the values of $\bar{M}_v$, −0.50 for the R-stars and −1.84 for the N-stars, derived by R. E. Wilson[16] from proper motions and radial velocities. It may be noted also that Sanford[17] used the intensities of the interstellar *Na* lines to find $M_v = -0.6$ for HD 137613, C1, and $M_v = -2.2$ for the N star HD 189711, not yet classified here.

CONCLUSION

By the use of four criteria the spectra of the carbon stars have been arranged in a sequence in which the independent variable is essentially temperature. Such disturbing factors as the variation in band absorption resulting from changing carbon abundance limit the accuracy of classification, and there is unquestionably room for further improvement. However, the system Co . . . . C9 should be closer to a temperature sequence than the subdivisions of the old types R and N. The greatest discrepancies between the two systems occur for stars which are marked by a general depression of the blue end of the spectrum and the appearance of bands in the green which have not yet been completely identified. These discrepancies provide further evidence of the existence of heavy molecular absorption in such stars, affecting chiefly all wave lengths shorter than λ 5000.

YERKES OBSERVATORY
June 1941

NOTE ADDED IN PROOF.—Since the preparation of this paper a note has been published by Sanford in *Pub. A.S.P.*, **53**, 255, 1941, calling attention to the unidentified band near λ 6269. He finds that it is correlated in intensity with the band head of $C^{12}C^{13}$ at λ 6168.

[14] For the measurement of wave lengths in this part of the spectrum Dr. Struve and Dr. Swings kindly made available several spectrograms of dispersion 150 A/mm at λ 6100 taken with the Cassegrain spectrograph of the McDonald reflector.

[15] *Pub. A.S.P.*, **52**, 407, 1940; *Observatory*, **64**, 4, 1941.

[16] *Ap. J.*, **90**, 352 and 486, 1939.

[17] *Pub. A.S.P.*, **51**, 237, 1939.

A STATISTICAL THEORY OF STELLAR ENCOUNTERS

S. CHANDRASEKHAR

ABSTRACT

In this paper the principles of a statistical theory of stellar encounters are developed. The fundamental idea of this new method is to describe the fluctuating part of the gravitational field acting on a star in terms of two functions: a function $W(F)$, which gives the probability of occurrence of a field strength F, and a function $T(F)$ which gives the average time during which the field strength F acts. With regard to $W(F)$ it is shown that a probability-distribution function derived by Holtsmark to describe the interionic fields in a discharge tube can be adapted to suit the gravitational case. In a certain approximation this probability of a given field is directly related to the probability of finding the nearest neighbor to a given star at some prescribed distance. In this latter approximation the mean life of the state F can be obtained by using a formula due to Smoluchowski in the theory of Brownian motion. In terms of these functions $W(F)$ and $T(F)$ the probable accelerations which a star will undergo can be determined according to the principles of the theory of random walk.

As an application of the methods of this statistical theory, the problem of the time of relaxation, t_R, of a stellar system has been reconsidered. It is found that

$$t_R = \frac{1}{6}\left(\frac{3}{2\pi}\right)^{3/2} \frac{(\overline{v^2})^{3/2}}{G^2M^2N\left[\log_e\left(\frac{D\overline{v^2}}{3GM}\right) - 0.355\right]},$$

where G is the constant of gravitation, N the number of stars per unit volume, $\overline{v^2}$ their mean square speed, M the mass of a star, and, finally, $D = (4\pi/3N)^{-1/3}$. This formula for the time of relaxation is shown to be in agreement with that derived by the alternative method in which the individual encounters are analyzed in terms of the two-body problem.

1. *Introduction.*—In estimating the influence of a fluctuating stellar distribution on the motions of stars it has invariably been supposed that such effects can be considered as the cumulative result of a large number of separate events, each of which can be idealized as distinct two-body encounters.[1] But a closer examination of the problem along these lines reveals an essential inconsistency in the assumptions made. For, on evaluating any of the desired quantities (e.g., $\Sigma|\Delta \bar{E}|^2$ or $\Sigma \sin^2 2\Psi$ [cf. I and II]), it appears that the most important of the effects arise from encounters with impact parameters of the same order as the average distance between the stars. In other words, the physical situations most relevant to the problem are precisely those for which the two-body idealization of stellar encounters fails as a satisfactory mode of description. While this results in a divergence of the appropriate integrals as the impact parameter D tends to infinity and has in consequence to be cut off arbitrarily at some value of D, the really serious drawback of the method consists, however, in the essential inadequacy of the model to take account of the inherent *physical* aspects of the problem. A consideration of this and other related difficulties suggests that we abandon the two-body approximation of stellar encounters altogether and devise a more satisfactory *statistical method*. It is the object of this paper to outline the principles of such a statistical theory and to show its practical feasibility by reconsidering the problem of the time of relaxation of a stellar system along these new lines.

[1] For the most recent version of the theory based on these ideas see S. Chandrasekhar, *Ap. J.*, **93**, 285, 1941; R. E. Williamson and S. Chandrasekhar, *Ap. J.*, **93**, 305, 1941; and S. Chandrasekhar, *Ap. J.*, **93**, 323, 1941. These papers will be referred to as I, II, and III, respectively. References to earlier literature will be found in these papers.

2. *The general principles of the statistical method.*—Quite generally the force $\boldsymbol{F}$ acting on a star, per unit mass, is given by

$$\boldsymbol{F} = -G\Sigma \frac{M_n}{|\boldsymbol{r}_n|^3} \boldsymbol{r}_n , \tag{1}$$

where M_n denotes the mass of a typical field star and $\boldsymbol{r}_n$ its position vector relative to the star under consideration. Further, the summation in equation (1) is taken over all the neighboring stars. The actual value of $\boldsymbol{F}$ at any particular instant will depend on the instantaneous positions of all the other stars and is in consequence subject to *fluctuations*. It would therefore be practically impossible to specify the exact dependence of $\boldsymbol{F}$ on the position and/or the time for individual cases. But, on the other hand, we can ask the probability of occurrence of any particular field strength. In evaluating this probability, we can (consistent with the physical situations we have in view) suppose that fluctuations subject only to the restriction of a constant average density occur.

Let

$$W(X, Y, Z)dXdYdZ \tag{2}$$

be the probability that $\boldsymbol{F}$ occurs in the range

$$(X, Y, Z) \leqslant \boldsymbol{F} \leqslant (X + dX, Y + dY, Z + dZ) . \tag{3}$$

From the symmetry of the problem we should expect that

$$W(F) = 4\pi F^2 W(\boldsymbol{F}) , \tag{4}$$

where F stands for $|\boldsymbol{F}|$. The meaning of $W(F)$ is simply that it gives the fraction of a long-enough interval of time during which a force of intensity F acts. A knowledge of $W(F)$ is therefore essential to our problem. It does not, however, provide all the necessary information. For, in order that we may be able to follow the motion of any particular star statistically, we need to know in addition the average length of time during which a given field strength acts *once it has become operative*. In other words we also require a knowledge of the *mean life* of the statistical state defined by F.

Now the notions of the mean life and the *spontaneous decay* of a given state of fluctuation has been introduced by Smoluchowski in his general investigations on Brownian motion and fluctuation phenomena.[2] According to these ideas of Smoluchowski, the probability $\phi(t)dt$ that a state represented by a well-defined statistical fluctuation continues to exist for a time t and makes a transition to a state of different fluctuation during t and $t + dt$ is expressible in the form

$$\phi(t)dt = e^{-t/T} \frac{dt}{T} , \tag{5}$$

where T is a constant characteristic of the state. Accordingly, we may define T as the mean life of the state under consideration. In our case we need to specify the mean life

$$T(F) \tag{6}$$

[2] Marian von Smoluchowski, *Wien. Ber.*, **123**, IIa, 2381, 1915; *ibid.*, **124**, IIa, 339, 1915; see also his papers in *Phys. Zs.*, **16**, 321, 1915, and **17**, 557, 585, 1916. For a general account of Smoluchowski's ideas see R. Furth, *Schwankungserscheinungen in der Physik* (*Sammlung Vieweg*), Heft 48, Braunschweig, 1920.

of a state in which a force of intensity F acts on a particular star (per unit mass). General considerations would suggest that for the average field strengths $\overline{F}$ we should expect

$$T(\overline{F}) \sim \frac{\overline{D}}{\overline{|v|}}\,, \tag{7}$$

where $\overline{D}$ stands for the average distance between the stars and $\overline{|v|}$ their average speeds.

Now, when a state defined by $\boldsymbol{F}$ becomes realized in consequence of fluctuations, the star will be accelerated at the rate F, and, since the mean life of this state is $T(F)$, the average acceleration to be expected during such a state is

$$\Delta \boldsymbol{v} = T(F)\boldsymbol{F}\,. \tag{8}$$

When this state of fluctuation gives place to another, the star will begin to be accelerated at a different rate and in a direction uncorrelated with that in the earlier state. Hence the net acceleration suffered by the star is formally given by

$$\Sigma \Delta \boldsymbol{v} = \Sigma T(F)\boldsymbol{F}\,, \tag{9}$$

where, as we have already indicated, the frequency of occurrence of the different values of $\boldsymbol{F}$ will be governed by $W(\boldsymbol{F})$.

On the basis of equation (9) we cannot, of course, predict the actual acceleration suffered by a star in any specified length of time. On the other hand, according to the principles of the theory of *random walk*[3] we should be able to predict the probability of a star's having been accelerated by a specified amount in a given length of time. This is the principle of our method.

After this general statement of the fundamental ideas we proceed to a more detailed consideration of the various factors which are involved.

3. *The probability of a given field strength. The Holtsmark distribution.*—According to our remarks in § 2, our first problem is to determine the probability of occurrence of a given field strength at some definite point due to a random distribution of centers of inverse square field of forces. This problem is clearly equivalent to finding the probability of a given *electric* field strength acting at a point in a gas composed of simple ions. This latter problem has been considered by J. Holtsmark;[4] and, re-writing his probability function to be appropriate for the gravitational case, we have

$$W(F) = \frac{2F}{\pi}\int_0^\infty e^{-\frac{\pi}{15}\sqrt{2\pi}\,\pi(GM)^{3/2}N\rho^{3/2}}\,\rho \sin F\rho d\rho\,, \tag{10}$$

where N stands for the number of stars per unit volume. We can re-write the foregoing formula for $W(F)$ more conveniently if we introduce a normal field strength, defined by

$$Q_H = \left(\tfrac{8}{15}\sqrt{2}\right)^{2/3}\pi GMN^{2/3} = 2.603GMN^{2/3}\,, \tag{11}$$

[3] Lord Rayleigh, *Collected Papers*, **1**, 491, Cambridge, England, 1899; **2**, 370, 1903; M. von Smoluchowski, *Bull. Acad. Cracovie*, p. 203, 1906; J. H. Jeans, *An Introduction to the Kinetic Theory of Gases*, p. 219, Cambridge, England, 1940; E. H. Kennard, *Kinetic Theory of Gases*, chap. vii, New York: McGraw-Hill, 1938.

[4] *Ann. d. Phys.*, **58**, 577, 1919. See also the papers by the same author in *Phys. Zs.*, **20**, 162, 1919, and **25**, 73, 1924.

and express F in terms of this unit. According to equations (10) and (11), we have

$$W(F) = \frac{2}{\pi F}\int_0^\infty e^{-(Q_H/F)^{3/2}x^{3/2}} x \sin x dx \,, \tag{12}$$

or, if

$$F = \beta Q_H \,, \tag{13}$$

$$W(\beta)d\beta = \frac{2d\beta}{\pi\beta}\int_0^\infty e^{-(x/\beta)^{3/2}} x \sin x dx \,. \tag{14}$$

The function $W(\beta)$ has been evaluated numerically by Holtsmark and more recently by Verweij.[5]

We may note that, according to equation (12),

$$W(F) \to \frac{3}{2}\frac{Q_H^{3/2}}{F^{5/2}} \,, \qquad F \to \infty \,. \tag{15}$$

This corresponds to a relatively slow decrease of the probability for high field strengths. Indeed, the probability distribution (12) gives an infinite value for the mean square field, $\overline{F^2}$. For certain physical problems this is unsatisfactory, and Gans[6] and Holtsmark[7] have modified the law (12), in the electrical case, to take into account the finite sizes of the ions. For the astronomical applications we have in view, the finite sizes of the stars cannot clearly be of any relevance. However, a modification of a different nature must be introduced before we can use the Holtsmark distribution (12). We shall return to this question in § 5.

4. *The probable field strengths produced by the nearest neighbor.*—In a general way it is clear that the main contribution to the field acting on a star must be due to its nearest neighbor. Indeed, as we shall presently see, the probable field strengths produced by the nearest neighbor provides a sufficiently good first approximation to the probability distribution according to equation (12).

To show this, consider first the probability $w(r)dr$ of finding the nearest neighbor to a given star between r and $r + dr$. It is readily seen that if the distribution of the stars is perfectly random (subject only to the restriction of a constant average density N) then $w(r)$ must satisfy the equation[8]

$$\left[1 - \int_0^r w(r)dr\right] 4\pi r^2 N = w(r) \,. \tag{16}$$

From equation (16) we derive

$$\frac{d}{dr}\left[\frac{w(r)}{4\pi r^2 N}\right] = -4\pi r^2 N \frac{w(r)}{4\pi r^2 N} \,. \tag{17}$$

[5] S. Verweij, *Pub. Ap. Inst. Amsterdam*, No. 5, Table 3, 1936.

[6] *Ann. d. Phys.*, **66**, 396, 1921. [7] *Phys. Zs.*, **25**, 73, 1924.

[8] P. Hertz, *Math. Ann.*, **67**, 387, 1909; R. Gans, *Phys. Zs.*, **23**, 109, 1922; C. V. Raman, *Phil. Mag.*, **47**, 671, 1924.

Hence

$$w(r) = e^{-4\pi r^3 N/3}\, 4\pi r^2 N\,, \tag{18}$$

since, according to equation (16),

$$w(r) \to 4\pi r^2 N\,, \qquad r \to 0\,. \tag{19}$$

If we now suppose that the field acting on a star is entirely due to the nearest neighbor, then

$$F = \frac{GM}{r^2}\,, \tag{20}$$

and the law of distribution of the nearest neighbors (eq. [18]) becomes equivalent to

$$W(F)dF = e^{-4\pi (GM)^{3/2} N/3F^{3/2}} 2\pi N (GM)^{3/2} \frac{dF}{F^{5/2}}\,. \tag{21}$$

If we now introduce the normal field

$$Q = (\tfrac{4}{3}\pi)^{2/3} GMN^{2/3} = 2.599 GMN^{2/3}\,, \tag{22}$$

equation (21) becomes

$$W(F)dF = \tfrac{3}{2} Q^{3/2} e^{-Q^{3/2}/F^{3/2}} \frac{dF}{F^{5/2}}\,. \tag{23}$$

According to equation (23),

$$W(F)dF \to \tfrac{3}{2} Q^{3/2} \frac{dF}{F^{5/2}}\,, \qquad F \to \infty\,. \tag{24}$$

Comparing equations (11) and (15) with equations (22) and (24), respectively, we conclude that for all practical purposes we may regard them as identical. Moreover, a more detailed comparison of the distributions (12) and (23) shows that even as regards the general dependence on F the two agree sufficiently well. There is an appreciable disagreement between the two distributions only for very small values of F/Q; but, as we shall see later, the weak fields have no significant consequences for the statistical theory. Finally, we may remark that the agreement in the asymptotic behaviors of the two distributions for large values of F implies that the highest field strengths are produced by the nearest neighbor.

5. *The modification of the distribution function for high field strengths.*—As we have already remarked in § 3, the Holtsmark distribution (12) predicts too high probabilities for high field strengths. The same remark applies also to the distribution (23). In our present case the high probabilities result from the assumption of the randomness of the stellar distribution for all elements of volume. But it is clear that this assumption cannot be valid for the regions in the immediate neighborhoods of the individual stars. For a star with a linear velocity[9] v cannot come closer to another star than a certain critical distance $r(v)$ such that

$$\tfrac{1}{2} M v^2 = \frac{GM^2}{r(v)} \tag{25}$$

[9] At an average distance from the other stars.

or

$$r(v) = \frac{2GM}{v^2} . \tag{26}$$

For otherwise the star should strictly be regarded as the component of a binary system, and this is inconsistent with our original premises. This restriction naturally implies a departure from true randomness for these stars as $r \to r(v)$. However, it appears that under the conditions of our problem these departures become significant only as $r \to 0$. In any case it is apparent that the relatively high probabilities predicted by equation (12) or equation (23) for high field strengths will be reduced if proper account is taken of the increasing lack of randomness in stellar distribution as we approach the centers of attraction. A rigorous treatment of this effect will require a reconsideration of the whole problem in *phase space*[10] and is beyond the scope of the present investigation. However, an elementary treatment of the effect can be given, and this appears to be adequate for our purposes.

We shall first consider the problem along the lines of § 4. If $w(r)$ represents, as before, the probability of finding the nearest neighbor to a given star between r and $r + dr$, then the circumstance that stars with linear velocities v cannot come closer to the center than the limit given by (26) will modify equation (16) to

$$\left[1 - \int_0^r w(r)dr\right] 4\pi r^2 \chi(r) N = w(r) , \tag{27}$$

where the function $\chi(r)$ has been introduced to take account of the lack of randomness at close distances. Quite generally we should expect that

$$\chi(r) \to 0 , \quad r \to 0 ; \qquad \chi(r) \to 1 , \quad r \to \infty . \tag{28}$$

The formal solution of equation (27) can be readily written down. We have

$$w(r) = e^{-4\pi N \int_0^r r^2 \chi(r) dr} 4\pi r^2 \chi(r) N , \tag{29}$$

or, differently, as

$$w(r) = e^{-4\pi N r^3 \bar{\chi}(r)/3} 4\pi r^2 \chi(r) N , \tag{30}$$

where we have written

$$\bar{\chi}(r) = \frac{3}{r^3} \int_0^r r^2 \chi(r) dr . \tag{31}$$

According to equation (28),

$$\bar{\chi}(r) \to 0 , \qquad r \to 0 ; \qquad \bar{\chi}(r) \to 1 , \quad r \to \infty . \tag{32}$$

To make the law of distribution of the nearest neighbors according to equation (30) more definite, we need an explicit expression for $\chi(r)$. As we have already indicated, the exact specification of $\chi(r)$ will require a detailed consideration of the problem in phase

[10] In contrast to Holtsmark's treatment, in which the probability distribution of the centers of attraction in *configuration space* is assumed to be independent of the velocities of the particles.

space. But it appears that in a first approximation we may suppose that *the distribution of stars of any prescribed velocity* v *about a given star is perfectly random for all distances greater than the critical distance* $\mathrm{r(v)} = 2\mathrm{GM}/\mathrm{v}^2$. Similarly, we may suppose that *no stars with velocity* v *occur within the sphere of radius* r(v).[11] On these assumptions we can readily write down an explicit expression for $\chi(r)$. We have

$$\chi(r) = \int_{|\boldsymbol{v}|=\sqrt{2GM/r}}^{|\boldsymbol{v}|=\infty}\int\int\int f(\boldsymbol{v})dv_x dv_y dv_z , \tag{33}$$

where $f(\boldsymbol{v})$ denotes the frequency function of the velocities among the stars. If, for the sake of definiteness, we suppose that $f(\boldsymbol{v})$ is Maxwellian,

$$f(\boldsymbol{v}) = \frac{j^3}{\pi^{3/2}} e^{-j^2|\boldsymbol{v}|^2} , \tag{34}$$

then

$$\chi(r) = \frac{4j^3}{\pi^{1/2}}\int_{\sqrt{2GM/r}}^{\infty} e^{-j^2v^2}v^2 dv . \tag{35}$$

The foregoing formula for $\chi(r)$ can be expressed more conveniently in the form

$$\chi(r) = \frac{4}{\pi^{1/2}}\int_{a/\sqrt{r}}^{\infty} e^{-y^2}y^2 dy , \tag{36}$$

where we have written

$$y = jv ; \qquad a = \sqrt{2GM}\, j . \tag{37}$$

An alternative form for $\chi(r)$ may be noted:

$$\chi(r) = 1 - \frac{2}{\pi^{1/2}}\left[\int_0^{a/\sqrt{r}} e^{-y^2}dy - \frac{a}{\sqrt{r}} e^{-a^2/r}\right] . \tag{38}$$

Again, according to equation (31), we have

$$\bar{\chi}(r) = \frac{12}{\pi^{1/2}r^3}\int_0^r r^2\left(\int_{a/r^{1/2}}^{\infty} e^{-y^2}y^2 dy\right)dr \tag{39}$$

or, after an integration by parts,

$$\bar{\chi}(r) = \chi(r) - \frac{2a^3}{\pi^{1/2}r^3}\int_0^r r^{1/2}e^{-a^2/r}dr . \tag{40}$$

After some further reductions we find that

$$\bar{\chi}(r) = \chi(r) - \frac{4a^6}{3\pi^{1/2}r^3}\left[e^{-a^2/r}\left(\frac{r^{3/2}}{a^3} - 2\frac{r^{1/2}}{a}\right) + 4\int_{a/r^{1/2}}^{\infty} e^{-y^2}dy\right] . \tag{41}$$

[11] This latter assumption is, however, *necessary* (see the remark immediately following equation [26]).

The functions χ and $\bar{\chi}$ are tabulated in Table 1 for different values of the argument $a/r^{1/2}$. An examination of this table shows that to a first approximation we may write

$$\chi(r) = 1\,, \quad a \leqslant r^{1/2}\,; \qquad \chi(r) = 0\,, \quad a > r^{1/2}\,. \tag{42}$$

In this approximation equation (30) becomes

$$\left.\begin{aligned} w(r) &= e^{-4\pi N(r^3 - r_0^3)/3} 4\pi r^2 N \qquad (r \geqslant r_0)\,, \\ &= 0 \qquad\qquad\qquad\qquad (r < r_0)\,, \end{aligned}\right\} \tag{43}$$

where

$$r_0 = 2GMj^2\,. \tag{44}$$

Returning to equation (30), we see that this law of distribution of the nearest neighbors implies a probability of occurrence of a field strength F (assuming that the field arises principally from the first neighbor) given by

$$W(F) = \tfrac{3}{2} Q^{3/2} e^{-Q^{3/2}\bar{\chi}(\sqrt{GM/F})/F^{3/2}} \frac{\chi(\sqrt{GM/F})}{F^{5/2}}\,, \tag{45}$$

where Q, χ, and $\bar{\chi}$ are defined as in equations (22), (38), and (41). The modification which we have thus effected in the distribution function (23) removes the principal objection to

TABLE 1

$\chi(r)$ AND $\bar{\chi}(r)$

$a/r^{1/2}$	χ	$\bar{\chi}$	$a/r^{1/2}$	χ	$\bar{\chi}$
0	1.000	1.000	1.2	0.410	0.275
0.2	0.994	0.989	1.4	.270	.161
0.4	0.956	0.922	1.6	.163	.086
0.6	0.868	0.787	1.8	.090	.043
0.8	0.734	0.610	2.0	.046	.019
1.0	0.572	0.430	3.0	0.000	0.000

it, namely, the prediction of a nonconvergent value for $\overline{F^2}$, for our present distribution function (45) yields a finite value for the mean square field.

In the approximation (42), equation (45) simplifies to

$$\left.\begin{aligned} W(F) &= \tfrac{3}{2} Q^{3/2} e^{-Q^{3/2}(F^{-3/2} - F_{\max}^{-3/2})} \frac{1}{F^{5/2}} \qquad (F \leqslant F_{\max})\,, \\ &= 0 \qquad\qquad\qquad\qquad\qquad\qquad (F > F_{\max})\,, \end{aligned}\right\} \tag{46}$$

where, according to equation (44),

$$F_{\max} = \frac{1}{4GMj^4}\,. \tag{47}$$

We shall now consider very briefly how the lack of randomness in the immediate neighborhoods of the centers of attraction can be incorporated into the Holtsmark distribution (12). It appears that it is not an altogether simple matter to modify the Holtsmark distribution rigorously even on the basis of the very simplified assumptions which led to the explicit expressions (38) and (41) for $\chi(r)$ and $\overline{\chi}(r)$. But, remembering that the highest fields are produced by the nearest neighbor and, further, that the lack of randomness becomes significant only as $r \to 0$, it appears that we may incorporate the main features by considering an approximation corresponding to equation (42), i.e., by supposing that no star has a first neighbor closer than $r_0 = 2GMj^2$ and that the distribution is random but for this restriction. In this last approximation the problem becomes formally the same as when the ions, in the electrical case, have finite dimensions. With suitable changes we can therefore use the results of Gans and Holtsmark,[12] who have modified the distribution function (12), in the electrical case, for the finite sizes of the ions. We have[13]

$$W(F) = \frac{2F}{\pi} e^{4\pi r_0^3 N/3} \int_0^\infty e^{-(Q_H\rho)^{3/2}} K(\rho)\rho \sin F\rho d\rho , \tag{48}$$

where $K(\rho)$ is a certain correction factor which is defined in Holtsmark's paper.[14]

6. *The mean life of the state* F.—Our next problem is to determine the mean life of a statistical state defined by F. The totality of statistical complexions which go to make up the state in question are not explicitly defined, and Smoluchowski's ideas cannot be applied without further deep generalizations of them. However, in the approximation in which the fluctuating fields are assumed to arise from the nearest neighbor, the statistical complexion is specified explicitly, and a formula due to Smoluchowski can be directly used.

Now, according to Smoluchowski, the mean life of a state in which n particles are found in an element of volume σ is given by[15]

$$T = \frac{\sqrt{6\pi}}{\sqrt{\overline{v^2}}\,(n+\nu)} \frac{\sigma}{S_\sigma} , \tag{49}$$

where $\overline{v^2}$ denotes the mean square speed of the particles, S_σ the surface area of the element σ, and ν the number of particles which the element σ would contain at the constant average density:

$$\nu = N\sigma . \tag{50}$$

For the particular case we have in view

$$\sigma = \tfrac{4}{3}\pi r^3 ; \qquad S_\sigma = 4\pi r^2 ; \qquad n = 1 ; \qquad \nu = \tfrac{4}{3}\pi r^3 N , \tag{51}$$

[12] See the references given in nn. 6 and 7.

[13] J. Holtsmark, *Phys. Zs.*, **25**, 73, 1924; see particularly eqs. (104) and (145).

[14] See eq. (124) in the paper referred to in n. 13. Holtsmark has not evaluated this correction factor explicitly for the case of an inverse square field. But an evaluation of this factor along the lines of Holtsmark's analysis for the dipole field is possible.

[15] Smoluchowski, *Phys. Zs.*, **17**, 557, 1916; and see §§ 5, 6, and 7 in this paper and particularly eq. (30). See also Furth, *op. cit.*, pp. 34, 35, and 43.

since we need the mean life of a state in which a particular star continues to exist as the sole occupant of a sphere of radius r. Accordingly,

$$T(r) = \sqrt{\frac{2\pi}{3\overline{v^2}}}\,\frac{r}{\frac{4}{3}\pi r^3 N + 1}\,. \tag{52}$$

In the approximation of § 4

$$r = \sqrt{\frac{GM}{F}}\,, \tag{53}$$

and equation (52) implies for the state F the mean life

$$T(F) = \sqrt{\frac{2\pi GM}{3\overline{v^2}}}\,\frac{F}{Q^{3/2} + F^{3/2}}\,, \tag{54}$$

where Q is defined as in equation (22).

Formula (54) for $T(F)$ is clearly only an approximate one. But since, according to the Holtsmark distribution, the highest fields are produced by the nearest neighbor, the true expression for $T(F)$ must tend to equation (54) for high field strengths. Consequently, we may expect equation (54) to give as good an approximation to the true values of $T(F)$ as the $W(F)$ according to equation (23) or equation (30) provides an approximation to the Holtsmark distribution. This is probably quite sufficient for most purposes.

7. *The acceleration of a star in the fluctuating gravitational field.*—We shall begin our discussion of this problem by considering the following simplified case: Imagine a star's undergoing a series of accelerations during a large number of intervals of constant duration T, in such a way that during each interval it is accelerated at the same rate F but in directions which are uncorrelated from interval to interval. Under these circumstances the star experiences an increase of velocity of amount TF in each of the intervals; but these increments take place along uncorrelated directions in a random manner. We now ask the probability that at the end of s such intervals the star has undergone a net increase of velocity of mFT in some specified direction. According to the principles of the theory of random walk we have[16]

$$P_m = \sqrt{\frac{3}{2\pi s}}\,e^{-3m^2/2s}\,, \tag{55}$$

when s is sufficiently large. Since the net increase in velocity Δv and the time t during which this increase has taken place are related to m and s by

$$\Delta v = mFT\,; \qquad t = sT\,, \tag{56}$$

we have

$$P(\Delta v) = \sqrt{\frac{3T}{2\pi t}}\,e^{-3|\Delta v|^2/(2F^2Tt)}\,. \tag{57}$$

[16] See the references given in n. 3, particularly Kennard, *op. cit.*, pp. 269–72.

Hence, the probability that there occurs an increase in velocity in the range $[\Delta v, \Delta v + d(\Delta v)]$ during a time t in some prescribed direction is given by

$$P(\Delta v)d(\Delta v) = \sqrt{\frac{3}{2\pi F^2 T t}}\, e^{-3|\Delta v|^2/(2F^2Tt)} d(\Delta v) . \tag{58}$$

Accordingly,

$$\overline{\Delta v^2} = F^2 T t . \tag{59}$$

We shall now generalize the foregoing problem to the case when F does not have a unique value but occurs according to a definite frequency function $W(F)$ and when the average duration of an acceleration at the rate F is given by a function $T(F)$. In view of the addition theorem for the Gaussian error functions, equation (58) becomes modified under these more general circumstances to

$$P(\Delta v) = \sqrt{\frac{3}{2\pi \overline{F^2 T} t}}\, e^{-3|\Delta v|^2/(2\overline{F^2T}t)} , \tag{60}$$

where

$$\overline{F^2 T} = \int_0^\infty W(F) F^2 T(F) dF . \tag{61}$$

Hence, instead of equation (59) we now have

$$\overline{\Delta v^2} = \overline{F^2 T} t . \tag{62}$$

8. *The evaluation of* $\overline{\Delta v^2}$.—According to equations (45), (54), and (61) we have

$$\overline{F^2 T} = \frac{3}{2}\sqrt{\frac{2\pi GM}{3\overline{v^2}}}\, Q^{3/2} \int_0^\infty \frac{F^{1/2}}{Q^{3/2} + F^{3/2}}\, e^{-Q^{3/2}\bar{\chi}(\sqrt{GM/F})/F^{3/2}} \chi(\sqrt{GM/F}) dF . \tag{63}$$

When we introduce a new variable x defined by

$$\frac{Q^{3/2}}{F^{3/2}} = x , \tag{64}$$

equation (63) becomes

$$\overline{F^2 T} = 2\left(\frac{2\pi}{3}\right)^{3/2} \frac{G^2 M^2 N}{\sqrt{\overline{v^2}}} \int_0^\infty e^{-x\bar{\chi}(\sqrt{GM/Q}\, x^{1/3})} \left(\frac{1}{x} - \frac{1}{x+1}\right) \chi(\sqrt{GM/Q}\, x^{1/3}) dx . \tag{65}$$

Substituting for Q from equation (22) in the argument for the functions χ and $\bar{\chi}$ in the foregoing equation, we obtain

$$\sqrt{\frac{GM}{Q}}\, x^{1/3} = \left(\frac{x}{\frac{4}{3}\pi N}\right)^{1/3} = D x^{1/3} , \tag{66}$$

where we have written

$$D = \frac{1}{(\frac{4}{3}\pi N)^{1/3}} . \tag{67}$$

Now, according to equations (38) and (41), the functions χ and $\bar{\chi}$ depend on r only through the combination $a/r^{1/2}$. From equations (37) and (66) we now find that

$$\frac{a}{r^{1/2}} = \sqrt{\frac{2GMj^2}{D}}\, x^{-1/6} . \tag{68}$$

Since

$$\frac{D}{2GM} = 2.33 \times 10^4 \frac{(D/\text{parsec})}{(M/\odot)(10 \text{ km/sec})^2} , \tag{69}$$

it follows that under most stellar conditions $2GMj^2/D \sim 10^{-4}$. Hence, only for values of $x < 10^{-11}$ do the functions χ and $\bar{\chi}$ deviate appreciably from unity (see Table 1). We can therefore replace χ by unity whenever it does not occur multiplied by a factor which diverges at $x = 0$. Similarly, we can replace $\bar{\chi}$ also by unity; but this we can always do since $\bar{\chi}$ occurs in the exponent multiplied with x. Thus, to a high degree of accuracy, the integral on the right-hand side of equation (63) is the same as

$$\int_0^\infty \frac{e^{-x}}{x} \chi(Dx^{1/3})dx - \int_0^\infty \frac{e^{-x}}{x+1}\, dx = J \quad \text{(say)} . \tag{70}$$

Substituting for χ according to (36) in the foregoing equation we obtain

$$J = \frac{4}{\pi^{1/2}} \int_0^\infty \frac{e^{-x}}{x} \left[\int_{\sqrt{2GMj^2/D}\, x^{-1/6}}^\infty e^{-y^2} y^2 dy \right] dx - \int_1^\infty \frac{e^{-(x-1)}}{x}\, dx . \tag{71}$$

Writing

$$-E(-x) = \int_x^\infty \frac{e^{-x}}{x}\, dx , \tag{72}$$

we have

$$J = \frac{4}{\pi^{1/2}} \int_0^\infty \frac{d}{dx} (E(-x)) \int_{\sqrt{2GMj^2/D}\, x^{-1/6}}^\infty e^{-y^2} y^2 dy dx + cE(-1) . \tag{73}$$

Integrating by parts the integral on the right-hand side of equation (73), we find

$$J = -\frac{4}{\pi^{1/2}} \int_0^\infty E\left(-\left[\frac{2GMj^2}{D} \right]^3 z^{-6} \right) e^{-z^2} z^2 dz - 0.5963 . \tag{74}$$

The argument for the exponential integral occurring under the integral sign in equation (74) is seen to be extremely small for the values of x which are at all relevant to the value of the integral. Hence we can use the asymptotic expansion for $E(-x)$ valid for $x \to 0$. We have

$$E(-x) = \log x + 0.5772 + O(x) , \tag{75}$$

where the constant on the right-hand side is the Euler-Mascheroni constant. Using the foregoing expansion for $E(-x)$ in equation (74), we readily find that

$$J = 3 \log \left(\frac{D}{2GMj^2}\right) - 0.5772 + \frac{6}{\pi^{1/2}} \int_0^\infty e^{-x} x^{1/2} \log x dx - 0.5963 . \tag{76}$$

On the other hand, we have

$$\left.\begin{aligned} \int_0^\infty e^{-x} x^{1/2} \log x dx &= \Gamma(\tfrac{3}{2}) \left[\frac{d \log \Gamma(x)}{dx}\right]_{x=3/2}, \\ &= \frac{\pi^{1/2}}{2} \times 0.03649 . \end{aligned}\right\} \tag{77}$$

Hence,

$$J = 3 \log \left(\frac{D}{2GMj^2}\right) - 1.0640 . \tag{78}$$

Finally, substituting for $\overline{F^2T}$ according to equations (65) and (78) in equation (62) we obtain

$$\overline{\Delta v^2} = 6\left(\frac{2\pi}{3}\right)^{3/2} \frac{GM^2N}{\sqrt{\overline{v^2}}} \left[\log \left(\frac{D\overline{v^2}}{3GM}\right) - 0.355\right] t . \tag{79}$$

We may note that if we had used the approximation (46) for $W(F)$ (instead of the more accurate formula [45]) we should have obtained

$$\overline{F^2T} = 2\left(\frac{2\pi}{3}\right)^{3/2} \frac{G^2M^2N}{\sqrt{\overline{v^2}}} \int_{(2GMj^2/D)^3}^\infty \frac{e^{-x}}{x(x+1)} dx \tag{80}$$

instead of equation (65). On evaluating the integral on the right-hand side of (80), we find

$$\int_{(2GMj^2/D)^3}^\infty \frac{e^{-x}}{x(x+1)} dx = 3 \log \left(\frac{D}{2GMj^2}\right) - 1.1735 , \tag{81}$$

which should be compared with equation (78). We thus see that approximations based on the assumption (43) (or their equivalents) are likely to provide sufficient accuracy for most purposes. In particular, the modification of the Holtsmark distribution suggested on page 519 to take account of the lack of randomness in stellar distribution in the immediate neighborhoods of stars can be justified on these grounds.

9. *The time of relaxation of a stellar system.*—An immediate application of the fundamental formula (79) is to the problem of the *time of relaxation* of a stellar system. According to the general ideas outlined in I, § 1, we can definite this as the time required for $\overline{\Delta v^2}$ to become of the same order as $\overline{v^2}$. Thus, if t_R denotes this time, we have

$$t_R = \frac{1}{6}\left(\frac{3}{2\pi}\right)^{3/2} \frac{(\overline{v^2})^{3/2}}{G^2M^2N\left[\log \left(\frac{D\overline{v^2}}{3GM}\right) - 0.355\right]} . \tag{82}$$

We can now compare this formula with that obtained on the basis of the two-body idealization of stellar encounters. We have[17]

$$t_E = \frac{1}{16}\left(\frac{3}{\pi}\right)^{1/2}\frac{(\overline{v^2})^{3/2}}{G^2M^2N\log\left(\frac{\overline{D}\overline{v^2}}{3GM}\right)}, \tag{83}$$

where $\overline{D}$ is the average distance between the stars.[18] We notice that the two equations (82) and (83) are of identical forms; further it is found that the numerical factors in the two formulae differ only by a factor 1.11. This agreement, while confirming the general correctness of our statistical method, exhibits also its immense superiority over the earlier treatments of the same problem both in the appropriateness of the physical ideas and in the simplicity of the mathematical treatment.

10. *Concluding remarks.*—The perfectly natural way in which the solution to the problem of the time of relaxation appears on the present theory suggests the extension of these methods to solve other problems of stellar dynamics. Thus the evolution of wide binaries in a fluctuating gravitational field is a problem to which the principles of the statistical theory are particularly well adapted. For, while on the classical methods the treatment of this problem would require the analysis of individual encounters considered strictly as three-body problems, on the statistical theory all such detailed considerations would be eliminated. Again, the application of the fundamental theorem of statistical dynamics due to Planck and Fokker[19] to problems of stellar dynamics is another field to which the method of the present paper can be used. We shall consider these problems in later papers.

In conclusion I wish to record my indebtedness to Messrs. G. Randers and R. E. Williamson for valuable discussions.

YERKES OBSERVATORY
July 24, 1941

NOTE ADDED IN PROOF.—Since the foregoing paper was written it has been found possible to solve rigorously the question of the half-life treated approximately in section 6. While this exact treatment leads to substantially the same results, it enables a more complete visualization of the phenomenon in question. It is hoped to publish these newer results in the near future.

[17] See. S. Chandrasekhar, *The Principles of Stellar Dynamics*, chap. ii, University of Chicago Press. (In Press.)

[18] According to eq. (18), the average distance $\overline{D}$ between the stars is given by

$$\overline{D} = \int_0^\infty e^{-4\pi r^3N/3}4\pi r^3Ndr \tag{84}$$

or, after some elementary reductions,

$$\overline{D} = \frac{1}{(\frac{4}{3}\pi N)^{1/3}}\int_0^\infty e^{-x}x^{1/3}dx\,. \tag{85}$$

Hence, comparing eqs. (67) and (83), we have

$$\overline{D} = \Gamma(\tfrac{4}{3})D = 0.89300D\,, \tag{86}$$

a result due to Hertz (see the reference in n. 8).

[19] M. Planck, *Sitzungsber. der preuss. Akad.*, p. 324, Berlin, 1917; A. Fokker, *Ann. d. Phys.*, **45**, 812, 1914.

STELLAR MODELS WITH ISOTHERMAL CORES

LOUIS R. HENRICH AND S. CHANDRASEKHAR

ABSTRACT

This paper is devoted to the study of stellar models with isothermal cores. Two types of such configurations have been studied: (1) models with isothermal cores and polytropic envelopes ($n = 3$) and (2) models with isothermal cores and radiative point-source envelopes with a law of opacity $\kappa = \kappa_0 \rho T^{-3.5}$. The most important characteristic of these models is the existence of an upper limit to the fraction ν of the total mass which can be contained in the core. For models of type 2, $\nu_{\max} \sim 35\%$. Also it appears that, as ν increases, the radius of the star first decreases to a minimum value and then increases. Further, the luminosity of the star is found to increase by about a factor 3 from the stage when it has no isothermal core to the stage when the core contains the maximum possible mass.

1. *Introduction.*—The possible physical importance of stellar models with isothermal cores was first indicated by Gamow[1] who suggested that these models may have their counterparts in nature if resonance penetration of charged particles into nuclei should become the main source of energy. For under such circumstances the energy may be thought of as being generated in a spherical shell, in which case the regions interior to the shell would be isothermal. Again, if, following Gamow and Teller,[2] we suppose that the proton disintegration of the light-nuclei (*D*, *Li*, *Be*, and *B*) provides the energy source for the giants, it is conceivable that the available element at a particular time, lithium say, becomes exhausted in the central regions; also the physical conditions may be such that, before the temperature rises sufficiently for the disintegration of the next element, beryllium, to become effective, a situation may arise when the disintegration of lithium in the outer parts becomes the primary source of energy. Under these circumstances, also, the stellar configurations will have isothermal cores. A situation similar to what we have described may prevail quite generally with the exhaustion of hydrogen in the central regions of stars, during the course of their normal evolution. A study of the physical characteristics of stellar models with isothermal cores becomes, therefore, a matter of some interest. A first attempt in this direction has already been made by Critchfield and Gamow.[3] But the essential peculiarities of the model arising from the isothermal nature of the core has been overlooked by these authors.[4] In this paper we therefore propose to study these models under varying conditions to elucidate their physical characteristics.

2. *The equations of the isothermal core.*—We shall consider first the equilibrium of the isothermal core. In the core we can write

$$P = K_2 \rho + D\,, \tag{1}$$

where

$$K_2 = \frac{k}{\mu H} T_c\,; \qquad D = \tfrac{1}{3} a T_c^4\,, \tag{2}$$

[1] *Ap. J.*, **87**, 206, 1938; *Phys. Rev.*, **53**, 595, 1938.

[2] *Phys. Rev.*, **53**, 608, 1938. [3] *Ap. J.*, **89**, 244, 1939.

[4] Thus Critchfield and Gamow assume series expansions for $M(r)$, P, etc., which are valid in the immediate neighborhood of the center, no matter what the equation of state is (cf. eqs. [7] and [8] in the paper referred to in n. 3). Further, it appears that the parts of the isothermal function which are necessary to describe the core cannot be satisfactorily expressed by any kind of series expansion (see §§ 3, 4, and 5 in the present paper).

where K_2 and D are constants. The reduction to the isothermal equation is made by the substitutions[5]

$$\rho = \lambda_2 e^{-\psi}\,; \qquad P = K_2\lambda_2 e^{-\psi} + D\,, \tag{3}$$

and

$$r = \left(\frac{K_2}{4\pi G\lambda_2}\right)^{1/2}\xi\,. \tag{4}$$

Further, we have the mass relation

$$M(\xi) = 4\pi\left(\frac{K_2}{4\pi G}\right)^{3/2}\lambda_2^{-1/2}\xi^2\frac{d\psi}{d\xi}\,. \tag{5}$$

3. *Stellar models with isothermal cores and polytropic* ($n = 3$) *envelopes.*—As a first example of stellar models with isothermal cores we shall consider the case where the structure of the envelope is governed by the isothermal equation of index $n = 3$. Physically, this assumption implies that in the envelope we have the standard model approximation "$\kappa\eta$ = constant." Under these circumstances we can write

$$P = \left[\left(\frac{k}{\mu H}\right)^4\frac{3}{a}\,\frac{1-\beta}{\beta^4}\right]^{1/3}\rho^{4/3} = K_1\rho^{4/3}\,, \tag{6}$$

where K_1 is a constant. The reduction to the polytropic equation is made by the substitutions

$$\left.\begin{aligned}\rho &= \lambda_1\theta^3\,; \qquad P = K_1\lambda_1^{4/3}\theta^4\,;\\ r &= \left(\frac{K_1}{\pi G}\right)^{1/2}\lambda_1^{-1/3}\eta\,.\end{aligned}\right\} \tag{7}$$

Also, we have the relation

$$M(\eta) = -4\pi\left(\frac{K_1}{\pi G}\right)^{3/2}\eta^2\frac{d\theta}{d\eta}\,. \tag{8}$$

The mass M of the whole configuration is given by

$$M = 4\pi\left(\frac{K_1}{\pi G}\right)^{3/2}\omega_3\,, \tag{9}$$

where

$$\omega_3 = -\left(\eta^2\frac{d\theta}{d\eta}\right)_1\,, \tag{10}$$

the subscript 1 indicating that the quantity in parenthesis is evaluated at the point where θ has its zero. It may be noted that ω_3 is a homology-invariant constant.[6]

Now, at the interface where the isothermal core joins the polytropic envelope the values of P, ρ, r, and $M(r)$, given by the two sets of formulae (3), (4) and (5), and (7)

[5] See S. Chandrasekhar, *An Introduction to the Study of Stellar Structure*, p. 155, Chicago, 1939.

[6] See *ibid.*, p. 149.

and (8) should be identical. The resulting four equations of fit can be reduced to two equations involving only the homology-invariant combinations

$$u_\infty = \frac{\xi e^{-\psi}}{\psi'} ; \qquad v_\infty = \xi \frac{d\psi}{d\xi} ; \tag{11}$$

and

$$u_3 = -\frac{\eta\theta^3}{\theta'} ; \qquad v_3 = -\frac{\eta\theta'}{\theta} . \tag{12}$$

We find[7]

$$\left.\begin{aligned} u_\infty(\xi_i) &= u_3(\eta_i) , \\ \tfrac{1}{4}\beta v_\infty(\xi_i) &= v_3(\eta_i) , \end{aligned}\right\} \tag{13}$$

where the subscript i denotes that the respective quantities are evaluated at the interface. According to equations (13) every intersection of a (u_3, v_3)-curve with the $(u_\infty, \frac{1}{4}\beta v_\infty)$-curve derived from the complete isothermal function gives a solution of the equations of fit and corresponds to a definite configuration of the type we are looking for. An examination of the general arrangement of the (u, v)-curves for $n = 3$ and $n = \infty$ readily shows that solutions for equations (13) exist only for (u_3, v_3)-curves derived from M-solutions;[8] however, it may be noted that not all M-solutions provide solutions to equations (13).

According to the views expressed in § 1, in considering stellar models with isothermal cores we are primarily interested in the changes which occur in the parameters describing a star, as the isothermal core at some fixed temperature "grows" at the expense of the envelope. We shall now obtain the relations necessary for this purpose.

Suppose that a (u_3, v_3)-curve labeled by a certain value for the homology-invariant constant ω_3 intersects the $(u_\infty, \frac{1}{4}\beta v_\infty)$-curve derived from an E-solution of the isothermal equation at a point where $\xi = \xi_i$ and $\eta = \eta_i$. At this point the equations of fit (13) are therefore satisfied. The fraction q of the radius R occupied by the core is clearly given by

$$q = \frac{\eta_i}{\eta_1} , \tag{14}$$

where $\eta = \eta_1$ defines the boundary of the particular solution $\theta(\eta, \omega_3)$. The fraction ν of the mass M contained in the core is also readily found. We have

$$\nu = \frac{M(\eta_i)}{M(\eta_1)} = -\frac{(\eta^2\theta')_i}{\omega_3} , \tag{15}$$

where the subscript i indicates that the quantity in parenthesis is evaluated at the interface. Using the definitions of u_3 and v_3 we can re-write equation (15) more conveniently as

$$\nu = \frac{(u_3 v_3^3)_i^{1/2}}{\omega_3} . \tag{16}$$

[7] See *ibid.*, pp. 170–76.

[8] For the classification of the solutions of the Lane-Emden equation see *ibid.*, chap. iv.

The ratio of the central to the mean density is given by[9]

$$\frac{\rho_c}{\bar{\rho}} = \frac{\lambda_2}{\left(\frac{M}{\frac{4}{3}\pi R^3}\right)} = -\frac{\lambda_2}{3\lambda_1\left(\frac{1}{\eta}\frac{d\theta}{d\eta}\right)_1}; \tag{17}$$

or, using the formula

$$\lambda_2 e^{-\psi_i} = \lambda_1 \theta_i^3 , \tag{18}$$

which expresses the equality of the density at the interface, we have

$$\frac{\rho_c}{\bar{\rho}} = -\frac{\theta_i^3 e^{\psi_i}}{3\left(\frac{1}{\eta}\frac{d\theta}{d\eta}\right)_1} = -\frac{\theta_i^3 \eta_i^3 e^{\psi_i}}{3\left(\eta^2\frac{d\theta}{d\eta}\right)_1\left(\frac{\eta_i}{\eta_1}\right)^3} . \tag{19}$$

Hence,

$$\frac{\rho_c}{\bar{\rho}} = \frac{(u_3 v_3)_i^{3/2} e^{\psi_i}}{3\omega_3 q^3} . \tag{20}$$

Finally, to determine the $R(q)$ relation for a given mass and T_c, we start from the relation

$$K_2 = \beta K_1 \lambda_1^{1/3} \theta_i , \tag{21}$$

expressing the equality of p_{gas}/ρ on the two sides of the interface, and eliminate λ_1 from the equation (cf. eq. [7])

$$R = \left(\frac{K_1}{\pi G}\right)^{1/2} \lambda_1^{-1/3} \eta_1 . \tag{22}$$

We obtain

$$R = \pi G \beta \left(\frac{K_1}{\pi G}\right)^{3/2} \frac{1}{K_2}\left(\frac{\eta_1}{\eta_i}\right)\eta_i \theta_i , \tag{23}$$

or, using equations (2), (9), and (12), we have

$$R = Q(q)\beta \frac{\mu H}{k}\frac{GM}{T_c} , \tag{24}$$

where we have written

$$Q(q) = \frac{(u_3 v_3)_i^{1/2}}{4\omega_3 q} . \tag{25}$$

Equation (24) is an important relation which determines the dependence of R on q for a configuration of a given mass and fixed central temperature.

Restricting ourselves to the most important case of negligible radiation pressure and putting $\beta = 1$, four solutions of the equations of fit (13) were obtained, using the two

[9] In writing these equations we have assumed that the particular solution of the isothermal equation used is the one for which $\psi = 0$ at $\xi = 0$, i.e., the solution commonly denoted by $\Psi(\xi)$ (see *ibid.*, p. 156).

M-solutions ($\omega_3 = 1.90$ and 1.50) integrated by Fairclough.[10] The results of the fitting are summarized in Table 1. Further, in Figure 1 we have illustrated the $(M(\text{core})/M, q)$ and the (R, q) relations. We shall return to the physical meanings to be attached to these relationships in § 5.

4. *Stellar models with isothermal cores and point-source envelopes with the law of opacity* $\kappa = \kappa_0 \rho T^{-3.5}$.—The standard model approximation for the envelopes which we have considered in § 3, while giving an insight into the general behavior of these models, is not in strict conformity with the physical circumstances under which we might expect isothermal cores. For, consistent with the views expressed in § 1, we should rather suppose that the energy is generated in a thin spherical shell (of thickness Δr_i, say) at the

TABLE 1

STELLAR MODELS WITH ISOTHERMAL CORES AND $n=3$ ENVELOPES

ω_3	q	ν	$\rho_c/\bar{\rho}$	$Q(q)$
2.018.....	0	0	54.2	0.854
1.90.....	0.151	0.180	101	0.767
1.50.....	.148	.349	708	0.954
1.50.....	.094	.209	6.7×10^5	1.207
1.50.....	.104	.235	2.9×10^6	1.158
1.42(?)*.....	0.100	0.250	∞	1.250

*The figures in this row are not reliable. They give very rough estimates of the points about which the respective curves spiral.

interface between the isothermal core and the outer envelope. Under these circumstances the luminosity of the star will be given by

$$L = 4\pi r_i^2 \rho_i \Delta r_i \epsilon_0 , \tag{26}$$

where ϵ_0 denotes the rate of generation of energy per gram of the material. Accordingly, the regions of the star outside $r = r_i$ will be governed by the same equations as those for the point-source model. The equations of equilibrium for these regions are, therefore,

$$\frac{d}{dr}\left(\frac{k}{\mu H}\rho T + \tfrac{1}{3}aT^4\right) = -\frac{GM(r)}{r^2}\rho \tag{27}$$

and

$$\frac{d}{dr}\left(\tfrac{1}{3}aT^4\right) = -\frac{\kappa_0 L}{4\pi c r^2}\frac{\rho^2}{T^{3.5}} , \tag{28}$$[11]

where we have assumed for the coefficient of opacity the law

$$\kappa = \kappa_0 \frac{\rho}{T^{3.5}} . \tag{29}$$

[10] *M.N.*, **93**, 40, 1932.

[11] It is conceivable that circumstances may arise which require the replacement of equation (28), valid under conditions of radiative equilibrium, by another equation, valid under conditions of convective equilibrium. However, in the models we shall be primarily concerned with, this is not of much significance. Actually, apart from one possible exception, in the models considered the conditions for the validity of radiative equilibrium are not violated.

In equation (29), κ_0 (which is a constant throughout the configuration) may depend on the chemical composition (in particular on the hydrogen and helium abundances).

We shall now consider the method of fitting an isothermal core to a solution of equations (27) and (28): At the interface the quantities ρ, P, $M(r)$, and r as known along a solution of equations (27) and (28) must join continuously with the respective quantities

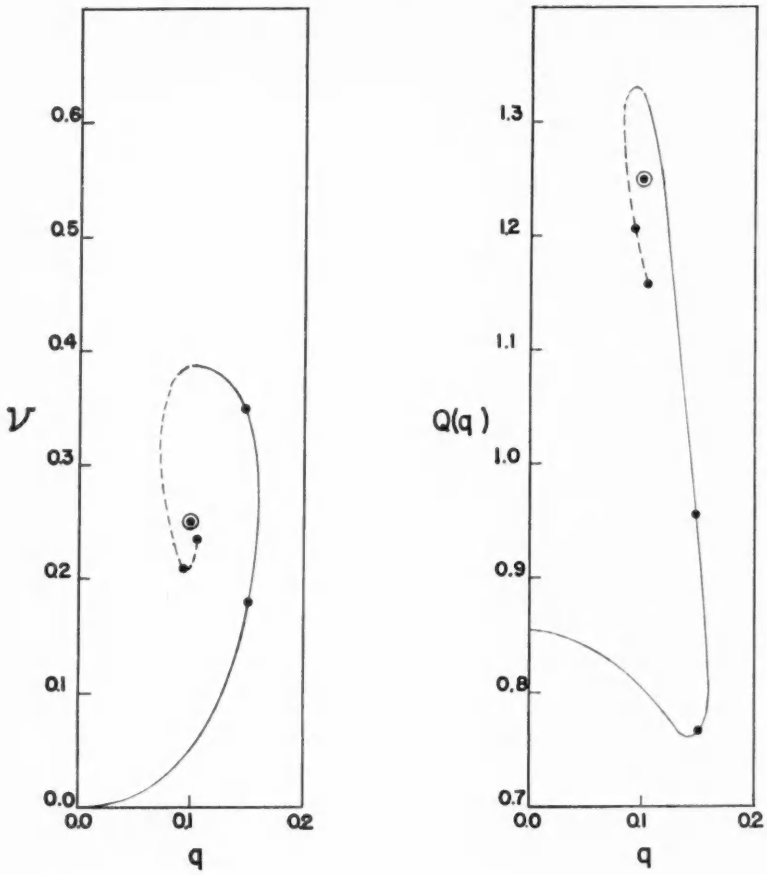

FIG. 1

determined by equations (3), (4), and (5) in terms of an appropriate E-solution of the isothermal equation.

According to equations (3), (4), and (5),

$$u_\infty = \frac{\xi e^{-\psi}}{\psi'} = 4\pi \frac{r^3\rho(r)}{M(r)}, \tag{30}$$

and

$$v_\infty = \xi\psi' = \frac{G}{\beta(r)} \frac{\rho M(r)}{rP(r)} = \frac{\mu H}{k} \frac{GM(r)}{rT(r)}. \tag{31}$$

Hence, an isothermal core can be fitted to a solution of equations (27) and (28) whenever the curve

$$\left[4\pi \frac{r^3\rho(r)}{M(r)}\,;\qquad \frac{\mu H}{k}\frac{GM(r)}{rT(r)}\right] \tag{32}$$

derived from such a solution intersects the (u_∞, v_∞)-curve associated with an E-solution of the isothermal equation. At such an intersection

$$\left.\begin{aligned} u_\infty(\xi_i) &= 4\pi\left(\frac{r^3\rho}{M(r)}\right)_{r=r_i},\\ v_\infty(\xi_i) &= \frac{\mu H}{k}\,G\left(\frac{M(r)}{rT}\right)_{r=r_i},\end{aligned}\right\} \tag{33}$$

and the values of r/R and $M(r)/M$ at this point will determine, at once, the ratios q and ν of the radius and the mass of the core to the radius and the mass of the star, respectively. Further, according to the second of equations (33),

$$T_c = Q(q)\,\frac{\mu H}{k}\frac{GM}{R}\,;\qquad Q = \frac{\nu}{v_\infty(\xi_i)q}\,. \tag{34}$$

The ratio of the mean to the central density is also readily found. We have (cf. eq. [17])

$$\frac{\rho_c}{\bar\rho} = \frac{\lambda_2}{\dfrac{M}{\frac{4}{3}\pi R^3}}\,. \tag{35}$$

On the other hand, according to equations (4) and (5), we have identically

$$\lambda_2 = \frac{M(r_i)}{4\pi r_i^3}\,\frac{\xi_i}{\psi_i'}\,. \tag{36}$$

Hence, combining equations (35) and (36),

$$\frac{\rho_c}{\bar\rho} = \frac{\nu\xi_i}{3q^3\psi_i'} = \frac{\nu u_\infty(\xi_i)}{3q^3}\,e^{\psi_i}\,. \tag{37}$$

Now, there exist five integrations of equations (27) and (28) which can be used for our present purposes. Three of these integrations (due to Miss I. Nielsen[12]) are for the solar values of L, M, and R, with $\mu = 1$ and for values of $\log \kappa_0 = 24.792$, 24.892, and 24.992. Further, in these integrations of Miss Nielsen the radiation pressure as a factor in the equation of hydrostatic equilibrium has been ignored. The two other integrations (which were found to give solutions for the equations of fit) are due to Strömgren.[13] These integrations also refer to the solar values of L, M, and R, but with $\mu = 2.2$ and $\log \kappa_0 = 27.4$ and 27.8. Further, in these integrations the effect of the term $aT^4/3$ in equation (27) has also been taken into account.

[12] Under the supervision of B. Strömgren.

[13] *Zs. f. Ap.*, **2**, 345, 1931.

The results of fitting isothermal cores to the five integrations of equations (27) and (28) referred to, are summarized in Table 2.

It is known that the point-source model with negligible radiation pressure and with a law of opacity of the form $\kappa = \kappa_0 \rho^n T^m$ is a homology-invariant configuration.[14] It follows, therefore, that among the models with negligible radiation pressure, which consist of isothermal cores and point-source envelopes, those with a constant q form a homologous family. Hence, the physical relations derived from the three integrations I of Table 2 are invariant to homologous transformations. In particular the relations

$$R(q) = Q(q) \frac{\mu H}{k} \frac{GM}{T_c} ; \qquad \nu(q) = \frac{M(\text{core})}{M} , \tag{38}$$

will be valid for all stars. In practice, however, the foregoing relations will give sufficient accuracy only for stars of mass less than, say, $5\odot$. This is confirmed, for example,

TABLE 2

STELLAR MODELS WITH ISOTHERMAL CORES AND POINT-SOURCE ENVELOPES

	Integration of Equations (27) and (28)	q	ν	$Q(q)$	$\rho_c/\bar{\rho}$	$\frac{L_0(q)}{[Q(q)]^{3/2}} \times 10^{-24}$	$\Delta r_i/R$ in an Arbitrary Scale	$1-\beta_i$	Remarks
	$\log \kappa_0 = 24.735$; $\mu = 1$	0	0	0.900	37.0	5.73	.....	.....	Cowling model
I	$\log \kappa_0 = 24.792$; $\mu = 1$	0.139	0.103	0.791	54	6.97	1.00	0.0043	Inger Nielsen's integrations for the point-source envelope. Radiation pressure neglected in equation (27)
	$\log \kappa_0 = 24.892$; $\mu = 1$	.158	.176	0.778	80	8.85	0.98	0040	
	$\log \kappa_0 = 24.992$; $\mu = 1$	.166	.231	0.788	115	11.1	1.11	0042	
II	$\log \kappa_0 = 27.4$; $\mu = 2.2$	.158	.239	0.776	160	7.71	0.77	078	Stromgren's integrations for the point-source envelope. Radiation pressure accurately taken into account. The results of fitting valid for configurations having a mass $4.84\,\mu^{-2}\odot$
	$\log \kappa_0 = 27.8$; $\mu = 2.2$	.119	.319	1.07	175	16.5	1.51	103	
	$\log \kappa_0 = 27.8$; $\mu = 2.2$	0.081	0.224	1.33	635	14.8	1.70	0.115	

by the results of the last three rows of Table 2: These have been derived for the solar mass with $\mu = 2.2$, taking full account of the radiation pressure in the equation of hydrostatic equilibrium. It is, however, clear that we shall obtain the same results for a star of mass $M = (2.2)^2\odot = 4.84\odot$ and $\mu = 1$. From the column "$1 - \beta_i$" in Table 2 we notice that the radiation pressure, while it is appreciable in these models II, is still not of primary importance. This is reflected, for instance, in the fact that $Q(q)$ and $\nu(q)$ for these models fall roughly on the same curve as those for the three other cases in which the radiation pressure in equation (27) has been treated as negligible (see Fig. 2 where the models I are indicated by dots and models II by crosses).

5. *The physical characteristics of stellar models with isothermal cores.*—An examination of the results of §§ 3 and 4 (particularly Tables 1 and 2 and Figs. 1 and 2) brings out the following essential features of these models:

a) At a fixed central temperature, the radius R of the star first decreases as q increases from $q = 0$. For a value of $q \sim 0.15$–0.16 the radius passes through a minimum. Further, there exists also a maximum possible value for q ($q_{\max} \sim 0.16$–0.17). As q decreases after passing through $q_{\max}$, R increases very rapidly, reaches a maximum, and begins spiraling about a determinate point.

b) Again, at a fixed central temperature, the fraction of the total mass, ν, contained in the core increases slowly at first and soon very rapidly as q approaches $q_{\max}$. How-

[14] See Chandrasekhar, *op. cit.*, pp. 234–39.

ever, this increase of ν does not continue indefinitely; ν soon attains a maximum value ν_{max}. There exists, therefore, an upper limit to the mass which can be contained in the isothermal core. For the models with point-source envelopes and inappreciable radiation pressure, $\nu_{max} \sim 0.32$ and occurs for $q \sim 0.12$. The curve $\nu(q)$ also shows the spiraling characteristic.[15]

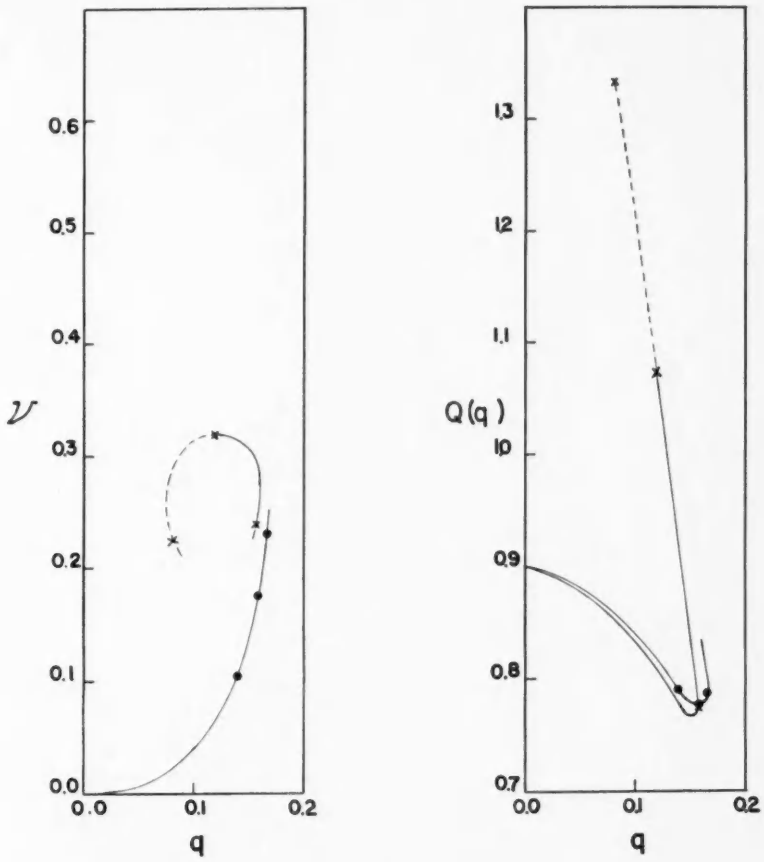

FIG. 2

A result of some importance in the present connection is the variation of the luminosity as q varies at constant central temperature. We shall discuss this variation of the luminosity on the basis of the models considered in § 4.

We may first recall that for a homologous family of stellar configurations derived on the basis of the law of opacity (29) there exists a luminosity formula of the form

$$L = \text{constant} \frac{M^{5.5}}{\kappa_0 R^{0.5}} \mu^{7.5}, \tag{39}$$

[15] This phenomenon of spiraling need not cause any particular surprise. It arises essentially from the oscillatory behavior of the solutions of the isothermal equation as $\xi \to \infty$ (see *ibid.*, pp. 163–66). Situations similar to these described in the text have also been encountered in other connections (see, e.g., S. Chandrasekhar, *Ap. J.*, **87**, 535, 1938; and *M.N.*, **99**, 673, 1939).

where the constant is a characteristic of the family. Consequently, for stellar models with isothermal cores and negligible radiation pressure, we must have a formula of the form

$$L = L_0(q)\,\frac{1}{\kappa_0}\,\frac{M^{5.5}}{R^{0.5}}\,\mu^{7.5}\,, \tag{40}$$

where, as the notation implies, L_0 depends on q only. Remembering that in obtaining the models I of Table 2 we have used integrations of the point-source envelope computed for the solar values of L, M, and R with $\mu = 1$, it follows that

$$L_0(q) = (\kappa_0)_{\text{integration}}\,, \tag{41}$$

if we suppose that in equation (40) L, M, and R are expressed in solar units. Similarly, for the solutions II (see Table 2)

$$L_0(q) = \frac{(\kappa_0)_{\text{integration}}}{(2.2)^{7.5}}\,. \tag{42}$$

Consider now the variation in L as q varies at constant T_c, μ, M, and κ_0. During such a change, R will alter according to (cf. eq. [38])

$$R(q) = Q(q)\,\frac{\mu H}{k}\,\frac{GM}{T_c}\,. \tag{43}$$

Eliminating R between equations (40) and (43),

$$L = \frac{L_0(q)}{[Q(q)]^{1/2}}\left(\frac{k}{GH}\right)^{1/2}\frac{1}{\kappa_0}\,M^5 T_c^{0.5}\mu^7\,. \tag{44}$$

Hence, the variation in the luminosity is governed by the factor

$$\frac{L_0(q)}{[Q(q)]^{1/2}}\,. \tag{45}$$

If we now consider the more general case in which the radiation pressure in equation (27) is taken into account, it is clear that we can still construct a homologous sequence of configurations. But a homologous family is now determined by two parameters: q and $M\mu^2/\odot$. However, as long as we are interested only in the changes in the luminosity occurring in a star of given M and μ, we can always write down a relation of the form (44). Moreover, any such relation will be valid for a sequence of configurations of constant $M\mu^2$.

The factor (45) governing the variation of L for constant M, T_c, κ_0, and μ is tabulated in Table 2. According to the values given in this table, the luminosity increases by a factor of about 3 from the stage where there is no isothermal core to the stage where the core contains the maximum possible mass.

The variation in the luminosity predicted by equation (44) implies a corresponding variation in the thickness of the energy-generating shell, for, according to equations (26) and (44),

$$4\pi r_i^2 \rho_i \Delta r_i \epsilon_0 = \frac{L_0(q)}{[Q(q)]^{1/2}} \frac{1}{\kappa_0} \left(\frac{k}{HG}\right)^{1/2} M^5 T_c^{0.5} \mu^7 . \tag{46}$$

The foregoing equation can be simplified by using equation (30). We find

$$\frac{\Delta r_i \epsilon_0}{r_i} = \frac{L_0(q)}{[Q(q)]^{1/2} u_\infty(\xi_i) \nu} \frac{1}{\kappa_0} \left(\frac{k}{HG}\right)^{1/2} M^4 T_c^{0.5} \mu^7 , \tag{47}$$

or

$$\frac{\Delta r_i}{R} \propto \frac{q L_0(q)}{[Q(q)]^{1/2} u_\infty(\xi_i) \nu} . \tag{48}$$

The quantity on the right-hand side (apart from a constant factor) is tabulated in Table 2. We notice that the variation in the thickness of the shell is not very marked.

6. *General remarks.*—We shall now consider briefly the bearing of the results summarized in § 5 on the physical problems outlined in § 1 and in particular the implication for the Gamow-Teller theory of the energy production in giants. Suppose that to begin with a star has a central temperature $T_c(\sim 10^{6\circ})$ at which the disintegration of lithium can provide for an adequate source of energy. Under these circumstances the star will approximate to the Cowling model which has a convective core occupying 17 per cent of the radius and containing 15 per cent of the mass of the star. Suppose now that the lithium in the central regions is exhausted and that the process of the diffusion of elements does not take place rapidly enough for the restoration of adequate amounts of lithium to the center. We shall then have a shell-source model. In the early stages ($\nu < 0.15$) the star will consist of an isothermal core, a convective fringe, and a point-source radiative envelope. However, very soon (i.e., when $\nu > 0.15$) the star will consist only of an isothermal core and a radiative envelope. It is now clear that energy production from the disintegration of lithium can continue only as long as the mass in the isothermal core increases. But we have seen that ν cannot increase beyond a certain maximum value $\nu_{\max}(\sim 35$ per cent). When this happens the liberation of energy from the process considered will cease. The star must then readjust itself to a contractive model ($\epsilon \propto T$) and evolve according to the Helmholtz-Kelvin time scale. This will continue till the central temperature increases sufficiently for the liberation of nuclear energy from the disintegration of the next element, beryllium, to become effective. The whole cycle of changes will now be repeated.

In considering the course of changes we have described in the foregoing paragraph, it is of interest to trace the track of evolution in the Hertzsprung-Russell diagram. To illustrate this we have plotted

$$\log \frac{L_0(q)}{[Q(q)]^{1/2}} \tag{49}$$

against

$$\log \frac{L_0(q)}{[Q(q)]^{1/2}} - 2 \log Q(q) \tag{50}$$

in Figure 3. According to our earlier remarks, an evolution of the kind we are considering must cease when the luminosity has reached about its maximum value (cf. Table 2). We may note at this point that at no stage during such an evolution does the isothermal core occupy a large fraction of the radius; indeed, it is always less than about 17 per cent.

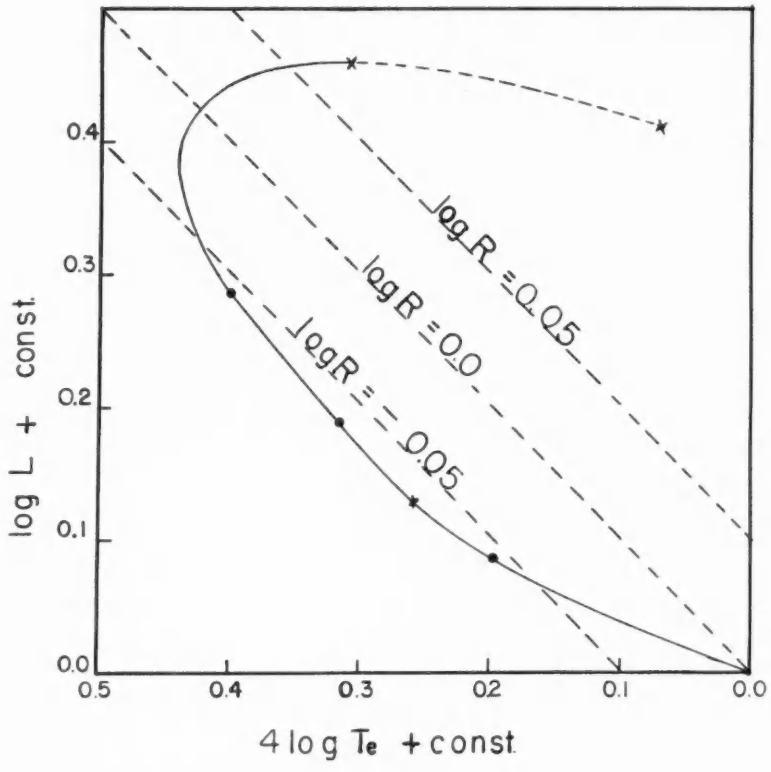

FIG. 3

Consequently, we cannot expect any significant changes in the stability of a star along such a course.

Finally, we may remark that with suitable modifications we may similarly follow the eventual course of evolution of a star as the hydrogen in the central regions becomes exhausted.

YERKES OBSERVATORY
July 30, 1941

ON THE VIBRATIONAL STABILITY OF GASEOUS STARS

P. LEDOUX[1]

ABSTRACT

The dependence of the vibrational stability of stars upon their masses has been investigated, and it has been established that for laws of generation of energy of the type of Bethe's law, the ordinary law of opacity and a ratio of the specific heats of matter γ equal to $\frac{5}{3}$, some instability would first appear for masses larger than $100M_{\odot}$.

Changes in the law of opacity as well as in the ratio of the specific heats are more likely to occur in the outer layers of the stars, and their effects on the stability, especially for the giants, can be important.

If the region where they occur is appropriately chosen, these changes could render the star unstable for one of the higher modes (first or second), although it remains stable for the preceding ones. Some attention was also paid to the stability of "shell-source" and "ball-source" models with the conclusion that they would not exhibit any special instability.

1. The condition for the stability of stars for small radial pulsations was established for the case of radiative equilibrium by S. Rosseland,[2] and T. G. Cowling[3] obtained it for the case where a part of the star is in convective equilibrium. In Cowling's investigation the radiation pressure was treated as negligible (small mass) and the present author,[4] in a paper which will be quoted as I, extended it to the case where the radiation pressure is appreciable.

If we define A_k by

$$A_k = \int_0^M \frac{\delta\rho_k}{\rho}\left[(\Gamma_3 - 1)\delta_k\left\{\epsilon_1 + \epsilon_2 - \epsilon_3 - \frac{d}{dm}\left[4\pi r^2(F_1 + F_3)\right]\right\} - \tfrac{2}{3}\delta_k\left[4\pi r^2 \bar{C}_r \frac{dP}{dm} + \epsilon_2 + \frac{d}{dm}\left[4\pi r^2 F_2\right]\right]\right] dm\,, \tag{1}$$

the condition of stability of the star for its kth mode of vibration is that A_k be negative. In this expression, which is obtained by the ordinary method of perturbations, we have to introduce for the amplitudes δr, $\delta\rho$, δT, etc., their values corresponding to an adiabatic pulsation. The meaning of the different symbols is as follows: $(\Gamma_3 - 1)$, defined[5] by $\delta T/T = (\Gamma_3 - 1)\delta\rho/\rho$ for an adiabatic modification, is equal to $(\Gamma_1 - \beta)/(4 - 3\beta)$, where β is the ratio of the gas pressure p_G to the total pressure $P = p_G + p_R$ and Γ_1, defined by $\delta P/P = \Gamma_1\delta\rho/\rho$, has the well-known value

$$\Gamma_1 = \beta + \frac{(4 - 3\beta)^2(\gamma - 1)}{\beta + 12(\gamma - 1)(1 - \beta)}\,;$$

γ is the ratio of the specific heats for the matter; ϵ_1 is the rate of generation of energy of subatomic origin per unit mass per second; F_1 is the flux of radiation; $\bar{C}_r$ is the mean radial component of the velocity of turbulence at the point considered and has the value

[1] Fellow of the Belgian American Educational Foundation at the Yerkes Observatory.

[2] *Oslo Pub.*, No. 1, 1931.

[3] *M.N.*, **96**, 42, 1936.

[4] *Astrophysica Norvegica*, **3**, 193, 1940.

[5] S. Chandrasekhar, *Introduction to the Study of Stellar Structure*, p. 56, 1939.

given by equation (2) in I; ϵ_2 is the rate of transformation of the turbulent kinetic energy into thermal energy per unit mass per second, due to the viscosity, and its order of magnitude is given by $\epsilon_2 = \text{constant} \times q^3/l$, if q is a mean velocity of turbulence and l the mean free path of the elements in turbulent motion; $\epsilon_3 = P \operatorname{div} \overline{C}_r/\rho$ is the rate of conversion of thermal energy into turbulent kinetic energy per unit mass per second; $F_2 = \overline{\frac{1}{2}\rho C^2 C_r}$ is the mean radial component of the vector representing convection of turbulent energy; and $F_3 = \overline{\rho E C_r}$ is the mean radial component of the vector representing convection of thermal energy and has the value given by equation (3) in I.

However, this condition of stability is valid only if the deviations from an adiabatic pulsation remain small in the whole star. But it is well known[6] that in a relatively small region near the surface ($T < 6T_e$) this is not the case. However, as S. Rosseland[7] has shown, in that region the amplitudes of the oscillations will adjust themselves in such a way that there will be no variation with r of the excess leakage of heat in that region, and it is therefore clear physically that this region cannot affect the stability of the star. Thus, if M_a denotes the mass of the part of the star where the method of perturbations is strictly applicable (i.e., the mass interior to the surface where $T \simeq 6T_e$), then we are likely to obtain results not very far from the truth if, in our condition of stability, we extend the integration from o to M_a instead of from o to M. In this paper we intend to apply this condition of stability to different cases.

2. To investigate the stability of the star for its fundamental mode of vibration we have to evaluate A_0. For laws of generation of energy of the form now admitted there will be a convective core at the center of the star. We can further suppose that the whole generation of energy takes place in the convective core. Now, A_0 will consist of two parts, a part A_C due to the convection in the core and a part A_R due to the generation of energy and the radiative flux. Following the procedure of T. G. Cowling and using the definition of ϵ_2, ϵ_3, F_2, F_3 and the values of $\overline{C}_r$ and $\overline{\rho E C}_r$ given in I, as well as the relation

$$\frac{\delta\beta}{\beta} = (\Gamma_3 - \Gamma_1)\frac{\delta\rho}{\rho},$$

which is valid for an adiabatic change, we can express A_C in the following form:

$$\left.\begin{aligned} A_C = \int_0^{m_C} \frac{\delta r}{r}\cdot\frac{\delta\rho}{\rho}\cdot(\tfrac{5}{3} - \Gamma_3)\frac{Aq^3}{l}\left\{1 - \frac{\sigma r^3}{Gm} + 12\cdot\frac{\Gamma_3 - \Gamma_1}{4 - 3\beta}\right\} dm \\ + \int_0^{m_C} \frac{\delta\rho}{\rho}\cdot\frac{d\Gamma_3}{dm}\{\delta(4\pi r^2 F_3) + \delta(4\pi P r^2 \overline{C}_r)\}\, dm\,, \end{aligned}\right\} \quad (2)$$

where m_C is the mass of the convective core.

If the radiation pressure is negligible, $\Gamma_3 = \Gamma_1 = \gamma = \text{constant}$, and this expression reduces to

$$A_C = -(\gamma - \tfrac{5}{3})\int_0^{m_C} \frac{\delta r}{r}\cdot\frac{\delta\rho}{\rho}\cdot\frac{Aq^3}{l}\left\{1 - \frac{\sigma r^3}{Gm}\right\} dm\,, \quad (2')$$

which is the formula given by Cowling. In the core it is certainly a fair approximation to put $\gamma = \frac{5}{3}$, and we can also consider that $\delta r/r$ and $\delta\rho/\rho$ are practically constant in

[6] Cf. Eddington, *Internal Constitution of the Stars*, p. 198, 1926; J. J. M. Reesink, *M.N.*, **87**, 414, 1927; and S. Rosseland, *op. cit.*, p. 47, n. 2.

[7] *Op. cit.*, sec. 7, n. 2.

it. Then if we evaluate explicitly $d\Gamma_3/dm$, $(\Gamma_3 - \Gamma_1)$, $\delta(4\pi r^2 F_3)$, $\delta(4\pi P r^2 \overline{C}_r)$, using the expression for $\overline{C}_r$ and $F_3 = \overline{\rho E C}_r$ given in I, and further suppose (following Cowling) that $\epsilon_2 = Aq^3/l$ is of the same order as ϵ_1 we find

$$\left.\begin{aligned} A_C = {} & L\left(\frac{\delta r}{r}\right)_C \left(\frac{\delta \rho}{\rho}\right)_C \\ & \times \overline{\frac{8(1-\beta)}{24-21\beta}\left[1 - \frac{\sigma^2 r^3}{Gm} + \frac{12\beta(4.5\beta^4 + 10.5\beta^3 - 432\beta^2 + 576\beta - 256)}{(8-7\beta)^2(4-3\beta)(32-3\beta^2-24\beta)}\right]}, \end{aligned}\right\} \quad (3)$$

where the bar indicates a mean value of the quantity under it, in the convective core. The rest of A_0 is

$$A_R = \int_0^{m_C} \frac{\delta\rho}{\rho}(\Gamma_3 - 1)\delta\epsilon_1 dm - \int_0^{M_a} \frac{\delta\rho}{\rho}(\Gamma_3 - 1)\frac{d}{dm}\delta(4\pi r^2 F_1)dm\,. \quad (4)$$

If the rate of generation of energy is of the form

$$\epsilon_1 = \epsilon_1^0 \rho T^\nu\,, \quad (5)$$

the first term on the right-hand side of equation (4) can be written as

$$(A_R)_\epsilon = L\left(\frac{\delta\rho}{\rho}\right)_C^2 \left\{ \overline{\frac{8-6\beta}{24-21\beta}} + \nu\overline{\left(\frac{8-6\beta}{24-21\beta}\right)^2} \right\}_C . \quad (6)$$

The second term of A_R, due to the flux of radiation, is

$$(A_R)_{F_1} = -\left[\frac{\delta\rho}{\rho}(\Gamma_3 - 1)\delta(4\pi r^2 F_1)\right]_0^{M_a} + \int_0^{M_a} \delta(4\pi r^2 F_1)\frac{d}{dm}\left[(\Gamma_3 - 1)\frac{\delta\rho}{\rho}\right]dm\,. \quad (7)$$

If the law of opacity is given by

$$\kappa = \kappa_0 \rho^n T^{-(3+s)}\,, \quad (8)$$

we have

$$\left.\begin{aligned} \frac{\delta(4\pi r^2 F_1)}{4\pi r^2 F_1} = {} & 4\frac{\delta r}{r}\left[1 - \frac{\Gamma_3 - 1}{\Gamma_1}\left(\frac{\sigma^2 r^3}{Gm} + 4\right)F\right] \\ & - \frac{\delta\rho}{\rho}[n - (3+s)(\Gamma_3 - 1)] + 4\frac{\delta\rho}{\rho}(1 - F) \\ & \times\left\{\frac{\beta^2[57(\gamma-1) - 7] - \beta[120(\gamma-1) - \gamma] + 64(\gamma-1)}{[\beta + 12(1-\beta)(\gamma-1)][16(\gamma-1) - 12\beta(\gamma-1) - \beta^2(3\gamma-4)]}\right\}, \end{aligned}\right\} \quad (9)$$

where

$$F = \frac{1}{4}\cdot\frac{d(\log P)}{d(\log T)} \qquad \text{and} \qquad \sigma = \frac{2\pi}{\tau}$$

if τ is the period of oscillation. In the region in convective equilibrium

$$F_C = \frac{1}{4} \cdot \frac{\Gamma_1}{\Gamma_3 - 1} . \tag{10}$$

In the region in radiative equilibrium, since there is no generation of energy, $4\pi r^2 F_1 = L$, and we have

$$F_R = \frac{4\pi c G m(r)\, T^{3+s}\,(1-\beta)}{\kappa_0 \rho^n L} . \tag{11}$$

Thus $(A_R)_{F_1}$ can be divided into two parts, one for the region in convective equilibrium and one for the radiative envelope. It is obvious a priori (and numerical evaluations confirm it) that the first one must always remain very small so that we can neglect it. Then, if we assume that γ is also equal to $\frac{5}{3}$ in the radiative envelope, we can write

$$(A_R)_{F_1} = -L\left(\frac{\delta\rho}{\rho} \cdot \frac{8-6\beta}{24-21\beta} \cdot V\right)_{m_C}^{M_a} + L\int_{m_C}^{M_a} V \frac{d}{dm}\left(\frac{\delta\rho}{\rho} \cdot \frac{8-6\beta}{24-21\beta}\right) dm , \tag{12}$$

where V is the second member of equation (9) in which $\gamma = \frac{5}{3}$,

$$\left.\begin{aligned} V = 4\frac{\delta r}{r}\left\{1 - \frac{8-6\beta}{32-24\beta-3\beta^2}\left(\frac{\sigma^2 r^3}{Gm}+4\right)F_R\right\} + 4\frac{\delta\rho}{\rho}(1-F_R) \\ \times \frac{2[93\beta^2-216\beta+128]}{(24-21\beta)(32-24\beta-3\beta^2)} - \frac{\delta\rho}{\rho}\left[n-(3+s)\left(\frac{8-6\beta}{24-21\beta}\right)\right] . \end{aligned}\right\} \tag{13}$$

In this manner we can write

$$A_0 = (A_R)_\epsilon + A_C + (A_R)_{F_1} , \tag{14}$$

the different terms being given by equations (6), (3), and (12). The exponents of T and of ρ in ϵ appear explicitly in $(A_R)_\epsilon$, and those in κ appear in $(A_R)_{F_1}$. The problem is to verify whether, for likely values of these exponents, stars of different masses are stable.

3. If we suppose that n and s in the law of opacity are fixed and are equal, respectively, to 1 and 0.5, for a given star we can determine the critical ν_c beyond which this star becomes unstable by the equation

$$A_0 = 0 . \tag{15}$$

Cowling[8] solved equation (15) by an approximate method for a star of small mass ($p_R \ll p_G$), taking $\gamma = \frac{5}{3}$, and found $\nu_c = 3900$. But he reduced this value very much (to ~ 450) by supposing that the sources of energy are perhaps not all concentrated in the convective core. In view of our present knowledge of the source of stellar energy this reduction in ν_c does not seem to be justified, and we should consider the first number as more characteristic of the problem. Performing the integration in A_0 by numerical methods and supposing that M_a corresponds to a radius of $0.982R$, we obtain $\nu_c = 3600$. That this ν_c is smaller than the lower limit of Cowling is due to the

[8] *Op. cit.*, p. 60, n. 3.

fact that his process for evaluating ν_c corresponds to an integration extended up to the surface of the star. If we had extended our integration to M (instead of only to M_a) we should have obtained $\nu_c = 4050$.

In I, we have integrated the equation of pulsation for a star built on a model calculated by J. Wasiutynski in which p_R is not neglected. At the center of this model $\beta_c = 0.8$ and corresponds to a mass equal to $10.263 M_\odot$, if the mean molecular weight $\bar{\mu}$ is taken to be unity. As a result of this integration we found

$$\frac{\sigma^2 r^3}{Gm} = 0.1334 \frac{x^3}{\omega},$$

if $\omega = m/m_0$ and $x = r/r_0$,

$$m_0 = \tfrac{8}{5} \cdot \pi \rho_c r_0^3, \qquad r_0^2 = \frac{5}{8} \cdot \frac{RT_c}{\pi G \bar{\mu} \rho_c}.$$

Further, the values derived for $\delta r/r$, $\delta\rho/\rho$ are tabulated in Table 1. Here we have supposed that the adiabatic approximation is valid for all $r \leqslant 0.980R$.

TABLE 1

$\frac{r}{r_0}$	$\frac{\delta r}{r}$	$-\frac{\delta\rho}{\rho}$	$\frac{r}{r_0}$	$\frac{\delta r}{r}$	$-\frac{\delta\rho}{\rho}$
0.0	1.0	3.0	4.126	1.548	6.61
0.4	1.0	3.0	4.682	1.775	8.14
0.8	1.004	3.011	5.286	2.14	10.12
1.2	1.011	3.128	5.927	2.68	13.68
1.6	1.040	3.281	6.583	3.43	19.51
1.959	1.066	3.398	7.208	4.49	28.61
2.274	1.099	3.57	7.945	6.26	45.0
2.699	1.157	3.96	8.045	6.60	48.0
3.143	1.252	4.58	8.211	7.20	56.5
3.615	1.382	5.39			

In this case the mean value of the quantity under the bar in equation (3) is equal to -1.3 and A_C is equal to $3.9L$. The mean values occurring in equation (6) are equal to 0.46 and 0.211, respectively. For this model the quantity F_R in the radiative envelope is given by

$$F_R = 8.716\omega \cdot \tau^{0.5} \frac{(1-\beta)^2}{\beta}$$

(τ corresponds here to the temperature) and is nearly equal to 1 in all this region, so that the expression for V reduces to

$$V = 4\frac{\delta r}{r}\left\{1 - \frac{8-6\beta}{32-24\beta-3\beta^2}\left[\frac{\sigma^2 r^3}{Gm}+4\right]\right\} - \frac{\delta\rho}{\rho}\left[1 - 3.5 \cdot \frac{8-6\beta}{24-21\beta}\right]. \quad (13')$$

A numerical integration for $(A_R)_{F_1}$ then gives

$$(A_R)_{F_1} = -1150 + 450 = -700.$$

Finally, combining these results, we obtain

$$A_0 = L\{4.14 + 1.899\nu + 3.9 - 700\} .$$

The critical ν_c obtained in solving $A_0 = 0$ is

$$\nu_c = 370 .$$

4. The example considered in section 3 indicates that ν_c decreases very rapidly when the mass increases. For a given ν it would be interesting to determine the critical mass M_c for which the instability sets in. Unfortunately, up to the present we know the correct distribution of density for laws of generation of energy of the type considered only for the two models studied. On the other hand, if we use the standard model, its greater central condensation will lead to higher values of $\delta r/r$ near the surface; further, the fact that β remains constant (instead of tending toward 0 in the outer layers [$r = 1$, $s = 0.5$]) will also tend to increase the stability of the star; we shall therefore be led to values of ν_c and M_c which are a little too large. For this model,[9] we have approximate solutions for $\delta r/r$, for different values of $\alpha = (3 - 4/\Gamma_1)$ and $\gamma = \frac{5}{3}$; these correspond to stars of different masses. Since these models have no convective cores, A_0 is given by

$$A_0 = \int_0^{M_a} \frac{\delta\rho}{\rho}(\Gamma_3 - 1)\delta\left\{\epsilon_1 - \frac{d}{dm}(4\pi r^2 F_1)\right\} dm = (A_R)_{\epsilon_1} + (A_R)_{F_1} .$$

Since β is constant and ϵ is appreciable (ν large) only in a small region in the neighborhood of the center where $\delta\rho/\rho$ is nearly constant, we can write

$$(A_R)_{\epsilon_1} = \left(\frac{\delta\rho}{\rho}\right)_c^2 (\Gamma_3 - 1)\{1 + \nu(\Gamma_3 - 1)\}L . \tag{16}$$

In this case F_R is exactly equal to 1, and V is still given by equation (13′). Furthermore, the region where $4\pi r^2 F_1$ is less than L is very small and near the center. Hence, $(A_R)_{F_1}$ can be written in a fair approximation as

$$(A_R)_{F_1} = -(\Gamma_3 - 1)L\int_0^{M_a}\frac{\delta\rho}{\rho} \cdot \frac{d}{dm}\left\{\left[1 - \frac{\Gamma_3 - 1}{\Gamma_1}\left(\frac{\sigma^2 r^3}{Gm} + 4\right)\right]4\frac{\delta r}{r} - \frac{\delta\rho}{\rho}[n - (3 + s)(\Gamma_3 - 1)]\right\} dm .$$

If we write

$$\sigma^2 = \frac{4\pi G}{3} \cdot \frac{(3\Gamma_1 - 4)}{2.01813} \cdot \bar{\rho}\Sigma^2 ,$$

[9] P. Ledoux and C. L. Pekeris, *Ap.J.*, **94**, 124, 1941.

we can express $(A_R)_{F_1}$ in the following form:

$$\frac{(A_R)_{F_1}}{(\Gamma_3-1)L} = -\left\{\frac{\delta\rho}{\rho}\left[4-\frac{\Gamma_3-1}{\Gamma_1}\left(\frac{4a\Gamma_1\Sigma^2}{2.01813}\cdot\frac{\bar{\rho}(R)}{\bar{\rho}(r)}+16\right)\right]\frac{\delta r}{r}\right.$$
$$-\frac{n-(3+s)(\Gamma_3-1)}{2}\left(\frac{\delta\rho}{\rho}\right)^2\Bigg\}_0^{M_a}+\left(1-4\cdot\frac{\Gamma_3-1}{\Gamma_1}\right)4\int_0^{M_a}\frac{\delta r}{r}$$
$$\left.\cdot\frac{d}{dm}\left(\frac{\delta\rho}{\rho}\right)dm-\frac{\Gamma_3-1}{\Gamma_1}\cdot\frac{\Gamma_1 4a\Sigma^2}{2.01813}\int_0^{M_a}\frac{\bar{\rho}(R)}{\bar{\rho}(r)}\cdot\frac{\delta r}{r}\cdot\frac{d}{dm}\left(\frac{\delta\rho}{\rho}\right)dm\right\}. \quad (17)$$

Although the levels where the temperature is equal to $6T_e$ are not at homologous points in stars of different masses, we shall stop the integration at $r_a = 0.985R$ for all the stars. If we suppose that $n = 1$, $s = 0.5$ ($\kappa = \kappa_0\rho T^{-3.5}$), the numerical evaluation of A_0 gives the critical ν_c contained in the fourth column of Table 2.

TABLE 2

			κ	$\kappa_0\rho T^{-3.5}$	$\kappa_0\rho^{0.5}T^{-2.75}$	$\kappa_0\rho T^{-3.75}$	For $T<400{,}000°$ $\kappa=\kappa_0\rho$		For $T<400{,}000°$ $\kappa=\kappa_0$	
$\left(\frac{M}{M_\odot}\right)\bar{\mu}^2$	β	a	ν_c	ν_c' Dwarfs	ν_c' Giants	ν_c' Giants	ν_c'' Dwarfs	ν_c'' Giants	ν_c''' Dwarfs	ν_c''' Giants
1.0	1.0	0.6	4415	4415	4582	3916	2601	4133	3379	
4.63	0.9468	.5	2168	2219	2257	1676	1171	1864	1677	
9.14	0.8592	.4	808	855	848	653	375	744	635	
18.63	0.7167	.3	248	276	264	192	96	230	199	
47.9	0.5120	.2	60	70	66	44	12	57	50	
220.6	0.2044	0.1	10	15	11	5	− 4.8	9.2	7	

Their dependence upon the mass is illustrated by Figure 1 (solid curve). The dashed curve is extrapolated from the two ν_c's obtained with Cowling's model. From this figure, given a ν, we can always determine the critical mass M_c beyond which instability sets in. For instance, for $\nu = 16$ and $\bar{\mu} = 1$, we obtain $M_c = 128M_\odot$. Probably if we had used a correct model (with a convective core), we should have obtained something like $100M_\odot$.

5. From the work of B. Strömgren[10] and more recently of P. M. Morse[11] it appears that we can roughly take the influence of the guillotine factor into account by replacing $\kappa = \kappa_0\rho T^{-3.5}$ by $\kappa = \kappa_0\rho^{0.5}T^{-2.75}$ for the stars of the main sequence and by $\kappa = \kappa_0\rho T^{-3.75}$ in the case of the giants.[12] In general, the change $\Delta(A_R)_{F_1}$ corresponding to the changes Δn and Δs in the exponents of ρ and T in κ is given by

$$\frac{\Delta(A_R)_{F_1}}{(\Gamma_3-1)L} = [\Delta n-(\Gamma_3-1)\Delta s]\frac{1}{2}\left[\left(\frac{\delta\rho}{\rho}\right)^2\right]_0^{M_a}. \quad (18)$$

[10] *Zs. f. Ap.*, **4**, 118, 1932; **7**, 222, 1933. [11] *Ap. J.*, **92**, 27, 1940.

[12] These laws are obtained in keeping one of the variables ρ (or T) constant and trying to represent the variation of κ in that case as a function of the other T (or ρ). As Dr. Chandrasekhar has pointed out to me, this procedure is likely to lead to errors, and we should rather have to investigate the changes in κ for the simultaneous variations of ρ and T, which take place in the particular star studied. But here we want mainly to get some idea as to the importance of the changes in the stability which correspond to given changes in κ.

Using this, we obtain for the cases considered, values of ν_c' tabulated in the fifth and sixth columns of Table 2. We notice that the stability remains practically unaffected.

However, the calculations by Morse are concerned only with the case of temperatures higher than 4×10^5 degrees, and for smaller values important changes in κ are not impossible. To gain some idea as to the effects of these changes on the stability, we have considered the two following cases: $\kappa \propto \rho$ and $\kappa =$ constant for $T < 400{,}000°$. The corresponding changes in $(A_R)_{F_1}$ are still given by equation (18), where the lower limit 0 has to be replaced by the radius at which the temperature of 4×10^5 degrees is reached. For the stars of the main sequence this happens somewhere at $r = 6.5R/6.9$, if we take a central temperature of the order of 2×10^7 degrees, while for the giants $T < 4 \times 10^5$ for $r \geqslant 5.5R/6.9$. The ν_c'' and ν_c''' obtained in this way are given in the last columns of Table 2. Their values show that the modifications in κ considered, especially the case $\kappa = \kappa_0\rho$, reduce appreciably the stability of the star—particularly in the case of the giants. This is due to the fact that the region where the changes take place extends more deeply in the giants than in the dwarfs. However, for likely laws of generation of energy, the critical mass, even for the giants, still remains high (for $\nu = 18$, $[M/M_\odot]\bar{\mu}^2 \sim 40$).

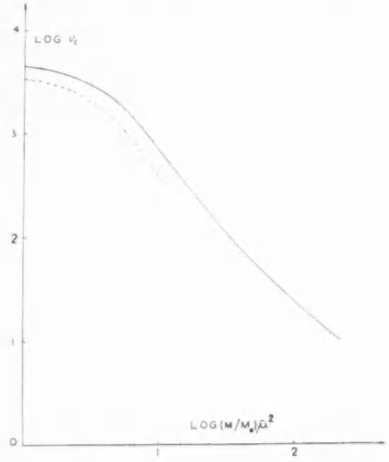

FIG. 1

6. Thus far we have neglected the energy of ionization and excitation. If we take this into account, the adiabatic exponents Γ_1 and Γ_3 are simply replaced by new ones, Γ_1' and Γ_3'. From computations of Γ_1' made by Fowler and Guggenheim[13] for different elements and temperatures greater than 10^6 degrees and from the fact that we now adopt a very high abundance of hydrogen we can conclude that in the main part of the stars ($T > 10^6$ degrees) Γ' is practically the same as Γ. For discussing the stability of the radiative equilibrium in the region with temperatures below 10^6 degrees, Biermann[14] has developed an approximate method of evaluating Γ_1' for the lower temperatures in the case of a mixture of elements. One of his mixtures is given in Table 3.

For this mixture and for a star of small mass ($p_R \ll P$), Biermann found that in the range of temperatures from 6×10^4 degrees to 4×10^5 degrees the mean value of Γ_1' is 1.43. For temperatures between 4×10^5 degrees and 10^6 degrees, the differences in $(\Gamma_1' - \Gamma_1)$ are already much smaller, and we shall neglect them here. As the mass of the star increases, the upper limit of the interesting range of temperatures decreases, for, p_R becoming more important, a given temperature corresponds to a smaller density and this favors higher ionization. We have determined these limits and the mean values of Γ_1' for the same mixture as Biermann, for different masses. Our results are contained in columns 2 and 3 of Table 4.

For the case of one element z in the r and $(r+1)$ states of ionization, with a difference of energy χ_r^z between them, the expression for Γ_3' is

$$\Gamma_3' = 1 + \frac{\left[\left(\frac{\partial N}{\partial T}\right)_\rho \cdot \frac{T}{(N + M_z)} + \frac{4}{\beta} - 3\right]}{\frac{3}{2} + 12\,\frac{(1-\beta)}{\beta} + \left[\frac{3}{2} + \frac{\chi_r^z}{kT}\right]\frac{T}{N + M_z} \cdot \left(\frac{\partial N}{\partial T}\right)_\rho},$$

[13] *M.N.*, **85**, 961, 1925. [14] *A.N.*, **259**, 221, 1936.

where M_z and N are the numbers of atoms and free electrons. Applying the method of Biermann, it is easy to derive a practical form for Γ_3' in the case of a mixture of elements. The interesting range of temperatures is about the same for Γ_3' as for Γ_1', and the fourth column of Table 4 contains the values of $(\Gamma_3' - 1)$. Although the radius corresponding to the upper limit of the range of temperatures varies a little with the mass, especially in the dwarfs (for the giants the diminution of the central temperature, when M increases, compensates this effect), we have adopted as before constant values for this radius equal to $6.5R/6.9$ for the dwarfs and $5.5R/6.9$ for the giants. Introducing the values of Γ_1' and Γ_3' in the part of the condition of stability corresponding to the region considered, we find the values of ν_c contained in the fifth and sixth columns of Table 4.

We see that changes in the Γ as in κ, when confined to a region of the star whose limits depend upon physical conditions, affect the stability of the giants more than that of the dwarfs. If we combine the first change in κ ($\Delta n = 0$, $\Delta s = -3.5$) and the preced-

TABLE 3

Element	*H*	*O*	*Mg*	*Fe*
No. of atoms	127	8	3	1
Weight	128	128	73	56

TABLE 4

$\left(\frac{M}{M_\odot}\right)\bar{\mu}^2$	Upper Limit of Temperature	Γ_1'	$\Gamma_3'-1$	ν_c Dwarfs	ν_c Giants	ν_c' Dwarfs	ν_c' Giants
1.0	400,000	1.43	0.39	3377	1089	3368	469
9.14	280,000	1.415	.363	667	280	486	29
47.9	240,000	1.373	.341	54	31	26	− 10
220.6	225,000	1.355	0.336	9	5	0	− 9

ing changes in Γ we obtain the ν_c' in the two last columns of Table 4. In this case a giant of a mass equal to $10M_\odot$ would already be on the verge of instability for a ν equal to 18. The small values of Γ' adopted in the outer part of the star will also lower the increase of the amplitude with r in that region. This secondary effect will still increase the instability of the star. If the values of the Γ' become small enough, turbulence will appear in that region also, but it is not likely that this would increase the stability of the star, in any case not very much.[15] However, the values of Γ_1', etc., depend very much upon the abundances adopted for the elements. If we took an abundance in *H* appreciably greater or allowed for the presence of *He* in appreciable quantity (already nearly completely ionized for $T = 10^5$ degrees), the region where Γ_1' is different from Γ_1 would be reduced considerably, and in general the stability of the star would increase.

7. Apart from their interest with regard to the stability of ordinary stars, these considerations are still important in their bearing upon the Cepheid phenomenon. In so far as the interior of the star is concerned, the main object of the theory of small pulsations is to provide theoretical periods in agreement with the observed ones and to explain how the star can become unstable in some of its modes of vibration so that the amplitudes of those modes can increase until they reach some limit corresponding to the

[15] Cf. T. G. Cowling, *M.N.*, **98**, 528, 1938.

finite pulsations observed in the Cepheids. The comparison of the observed periods with theoretical ones for likely models indicates that it must be the fundamental mode which is responsible for the pulsation of most of the Cepheids. However, M. Schwarzschild[16] has recently suggested that the first overtone is probably responsible for the pulsation in the Cepheids of type c. For the two first modes the general qualitative run of the amplitudes inside the star would be as schematized in Figure 2.

If the generation of energy is concentrated in the neighborhood of the center of the star and if the opacity decreases with compression in the whole star (this is the case for $n = 1$, $s = 0.5$ and for all likely values of Γ_3), it is obvious from Figure 2 that the star is much more stable for the first mode of pulsation than for the fundamental one. But, as we have seen, in that case even the fundamental mode would be stable (except for very large masses). If we consider the changes in κ and in Γ in the outer regions of

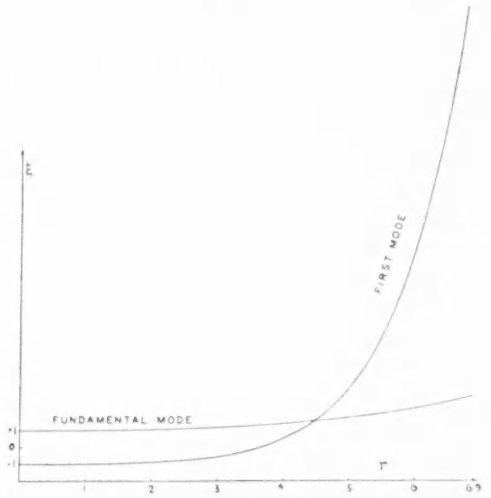

FIG. 2

the star by which we have tried to reduce the stability of the star for the fundamental mode, it appears immediately from the run of the amplitudes that, by choosing appropriately the layer where these changes take place, they could affect the stability of the first mode of pulsation more than that of the fundamental mode. In particular, if the boundaries of this layer are determined by critical temperatures, then, as we go to Cepheids of smaller masses (shorter periods), it is very probable that this layer will recede toward the surface, the effect on the first mode becoming more important. This is in agreement with the suggestion of M. Schwarzschild since it concerns the Cepheids of type c. After the computations of the amplitudes for different modes announced by M. Schwarzschild have been published, an exact discussion will be possible. However, a reliable numerical integration by Miss Kluyver[17] is available for the second mode of pulsation of the standard model in the case $\alpha = 0.4$, and it can be used to illustrate the situation. If we suppose that the region where the adiabatic approximation is valid has the same extension for this mode as for the fundamental one (in reality, it must be a little smaller, but not very much) and that $n = 1$, $s = 0.5$ in the law of opacity, we find a value of ν_c of the order of 10^6 if we do not take into account the possible changes of the Γ in the outer re-

[16] *Harvard Circ.*, No. 437, 1940, and *Pub. A.A.S.*, **10**, No. 3, 1941.

[17] *B.A.N.*, No. 276, p. 313, 1936.

gion ($6 \times 10^4 < T < 4 \times 10^5$) and a ν_c of the order $2.6 \cdot 10^5$ if one considers such changes, adopting the same mixture of elements as previously. Thus, in these cases the star is much more stable for the second mode than for the fundamental one. But, if one determines the Δs in the same outer regions (Δn being equal to 0 and ν being equal to 18) necessary to bring the star on the verge of instability for each mode, in the same two cases (Γ and Γ') one finds for the fundamental mode $(\Delta s_f)_\Gamma = -6.38$, $(\Delta s_f)_{\Gamma'} = -3.66$ and for the second $(\Delta s_2)_\Gamma = -5.73$ and $(\Delta s_2)_{\Gamma'} = -2.77$. In both cases this shows that for the regions chosen an appropriate change in κ (Δs intermediate between the two corresponding limits Δs_f and Δs_2) can make the star unstable for the second mode of vibration, although it remains stable for the fundamental mode. For a still higher mode the point where the amplitude becomes greater than that for the preceding mode will approach the surface, and it will probably occur mostly in the outer region which has very little effect on the stability of the star; and, whatever may be the changes in κ, the star will remain much more stable for this mode than for the lower mode.[18]

The problem is also interesting from the point of view of the generation of energy. First of all, it is well known that the ordinary nuclear reactions, which are so successful in the case of the dwarfs, fail to explain the energy production in the giants. Since the outer regions of the star cannot be the seat of generation of energy, considerations of the kind we are now concerned with cannot contribute to the solution of the question of the relative instability of different modes. Here we shall consider only the fundamental mode of pulsation. Since we cannot expect much higher ν than, say, 20, the only thing to do to decrease the stability of a star on account of the generation of energy is to suppose that it is displaced from the center toward regions where the amplitude of the pulsation is larger. "Shell-source" models satisfying this condition were considered by Gamow (resonance effect), by Gamow and Teller (light elements which would be rapidly consumed near the center), and by Öpik (hydrogen of the primitive core consumed in the course of evolution). This last hypothesis does not seem to be able to remove the difficulties as to the amount of energy generated by the giants.[19]

For our problem the important point is that the extension of the isothermal core will reach a maximum which it cannot outgrow. And, even when its extension is a maximum, the surface of the core is still too deep in the star for the generation of energy starting at the interface to affect very greatly the stability of the star, since the amplitudes are still too small in these central regions. In the case of Gamow another possibility is the "ball-source" model, in which ϵ is a constant in the central part of the star whose surface has a temperature T equal to the temperature of resonance T_R. For such a model the distribution of density will probably not be very different from that of the standard model. In such a case the mass capable of generating energy will increase during a contraction and decrease during an expansion. For small oscillations the term $(A_R)_\epsilon$ will be

$$(A_R)_\epsilon = -L\,\frac{3\rho_R T_R}{\bar{\rho}_R r_R}\cdot\left(\frac{dr}{dT}\right)_R\cdot\left(\frac{\delta T}{T}\right)_R^2 = -L\,\frac{3\rho_R T_R}{\bar{\rho}_R r_R}\cdot\left(\frac{dr}{dT}\right)_R\cdot(\Gamma_3-1)^2\left(\frac{\delta\rho}{\rho}\right)_R^2. \quad (19)$$

Assuming the distribution of density of the standard model and $a = 0.4$, we have calculated the quantity $(A_R)_\epsilon/(\Gamma_3 - 1)L$ by means of equation (19) at different depths (i.e., different T_R) and have compared it with $(\delta\rho/\rho)_c^2[1 + \nu_c(\Gamma_3 - 1)]$ for the corresponding case (cf. Table 2, col. 4, l. 4). Whatever we choose for T_R, the first quantity

[18] If by the consideration of a special process like the one introduced recently by Eddington this outer region can actually be of great importance, it will then be difficult to escape the conclusion that higher modes rather than the fundamental or the first ones must appear. The present investigation was completed before Eddington's paper (*M.N.*, **101**, 182, 1941) reached the author.

[19] Cf., e.g., J. Wasiutynski, *M.N.*, **100**, 362, 1940.

is always smaller than the latter, so the star is always stable. In fact, as we proceed from the center $(\delta T/T)_R$ increases, but the temperature gradient also increases, and the displacement of the upper boundary of the energy-producing mass for the same δT is smaller than in deeper regions in the star. On the other hand, the density is also smaller there, so that the variation of this mass becomes smaller, and this compensates the increase of $(\delta T/T)_R$. Thus, such a model will not introduce any particular instability.

Finally, any reduction in the central condensation of the model used will also favor the instability since $\delta r/r$, $\delta\rho/\rho$, $\delta T/T$ will not reach such high values near the surface of the star. For instance, if the whole star is in convective equilibrium, T. G. Cowling[20] has shown for a star of small mass that vibrational instability could set in much more easily. However, in this case, for larger masses the central condensation would increase and would approach that of the standard model,[21] and this would work against the influence of the decrease of Γ with increasing mass so that, in this case, the condition of stability would be much less sensitive to the mass.

YERKES OBSERVATORY
August 1941

ERRATA

The two wave lengths λ 3330 and λ 3339 in the upper strip of Plate VIII (Vol. **94**) should read λ 3339 and λ 3355.

O. S.

In Table 4, page 325, of Volume **94**, the *NH* lines λλ 3364.7, 3369.1, and 3372.0 should not be attributed to the (1, 1) transition. The identifications should read as follows:

Comet	Laboratory	Notation
3364.7(2)	3364.0	$P_2(2)$
3369.1(3)	3369.1	$P_1(2)$ (0, 0)
3372.0(1)	3372.1	$P_1(3)$

The blending effect of the (1, 1) transition is probably unimportant. References to the (1, 1) band of *NH* should be dropped from the text.

P. SWINGS

October 1941

[20] *M.N.*, **98**, 528, 1938.

[21] L. Henrich, *Ap. J.*, **93**, 483, 1941.

NOTES

HYDROGEN EMISSION IN 25 CYGNI

The naked-eye star 25 Cygni (HD 189687, α $19^h56^m.2$, $\delta + 36°46'$, magnitude 5.15, spectrum B3) was observed on September 17 and 18, 1941, in the course of comparing spectrophotometrically absorption B and Be stars. Both plates show $H\alpha$ as an emission line, while $H\beta$ appears as an absorption line. A slit spectrum taken on October 15, 1941, shows double emission at $H\beta$, which is somewhat fainter than the neighboring continuum and is approximately 8 A wide. A bright line at $H\gamma$ is not evident on this plate. The star is not included in the lists of known objects of class Be, although Mohler[1] reported that it had abnormally weak $H\alpha$ absorption. Since $H\alpha$ emission can easily be seen on spectra taken with a wide slit, it seems safe to conclude that hydrogen emission has developed or that it has increased in intensity since the Cook Observatory spectra were taken. The equivalent widths of $H\alpha$, $H\beta$, and $H\gamma$, measured on the spectrophotometric plates, are listed in the accompanying table. The value given for $H\alpha$ is the excess of radiation

Star	Spectral Class	$H\alpha$	$H\beta$	$H\gamma$
25 Cygni	B3eβ	2.5 A (emission)	5.1 A	5.5 A
81 π^2 Cygni	B3	4.7	5.1	4.6

above the continuum. For comparison the equivalent widths of the same lines of 81π^2 Cygni, an absorption-line star of class B3, are also given.

W. Albert Hiltner

The Observatory
University of Michigan
October 16, 1941

BRUCE PROPER-MOTION SURVEY

Parts A, B, and C of the "General Catalogue of the Bruce Proper-Motion Survey," giving the positions, photographic magnitudes, and proper motions for 28,535 stars south of declination $-50°$, are now being distributed to subscribers. A limited number of copies is still available at the original price of $5.00 a set, but no more will be mimeographed if there is no further demand for them at this time. Those interested in procuring a set should communicate with the University of Minnesota Press, Minneapolis.

W. J. Luyten

[1] *Ap. J.*, **92**, 315, 1940.

PHOTOMETRIC OBSERVATIONS OF μ SAGITTARII

The light from the eclipsing variable μ Sagittarii, α 18^h10^m, δ $-21°.1$, spectrum cB8, was observed at Amherst on nine different nights during May, June, and August, 1941. These observations were made with a photoelectric photometer attached to the 18-inch refractor of the Amherst College Observatory. The combination of cell and filter (Schott RG9) gives an effective wave length of 8000 A. The star 15 Sagittarii of spectral type Bo was used as the comparison star.

The third column of Table 1 shows the number of comparisons, and the final column shows the weights which I have arbitrarily assigned to the mean difference in magnitude.

TABLE 1

OBSERVATIONS OF μ SAGITTARII

Julian Day	ΔM $15-\mu$	N	Weight	Julian Day	ΔM $15-\mu$	N	Weight
2430000+				2430000+			
117.837	+0.648	3	3	135.810	+0.497	3	1
126.840	.688	3	2	156.720	.648	3	2
130.808	.617	5	2	165.697	.610	3	2
133.824	.548	3	3	215.574	+0.645	6	6
134.800	+0.514	6	6				

This was done on the basis of the amount of difficulty encountered because of the proximity of the moon or of the uncertainty in the transparency. A neutral filter which absorbed 1.18 mag. was used in addition to RG9 when the variable was observed.

A brief account of spectral and photometric changes found in this star has been published by Elvey and Morgan.[1] Elvey's photoelectric observations show an eclipse lasting around twenty days and having a maximum depth of about 0.14 mag. It is of interest to see if the depth observed in the infrared is similar to that which Elvey found in the blue.

Minimum light was predicted to occur about JD 2430135. The sky was very clear at Amherst on this night, and six comparisons were made. The observed mean difference in magnitude was 0.514 ± 0.011 mag. The mean difference in magnitude outside eclipse is 0.641. These observations therefore suggest an eclipse of 0.13 mag. with an estimated probable error of 0.02 mag. When this value is compared with that found by Elvey, it appears that no appreciable change in color has been observed during eclipse.

JOHN S. HALL

AMHERST COLLEGE OBSERVATORY
August 1941

[1] *Ap. J.*, **88**, 110, 1938.

THE TEMPERATURE VARIATION OF δ CEPHEI

The photoelectric color of the star δ Cephei was observed at the Steward Observatory at intervals from September to December, 1939. In all, thirty-one color determinations were made, which are well distributed over the light-period of the star. These have been collected into six normal points in Table 1. The photometer was employed in exactly the same manner as in a previous investigation.[1]

TABLE 1

OBSERVATIONS OF δ CEPHEI

Normal Point	No. of Obs.	Phase*	Color	T_e(°K)	Prob. Error
1	7	0.781	+0.014	6030	35
2	3	1.686	+ .109	5550	65
3	4	2.598	+ .154	5350	85
4	8	3.243	+ .263	4950	110
5	6	4.226	+ .122	5510	20
6	3	5.241	−0.123	6820	100

* Days from maximum light.

Kuiper[2] has recently calibrated the effective temperature scale in terms of the photoelectric colors of Becker.[3] The standard stars common to both lists permit the determination of the effective temperatures of δ Cephei from the Tucson observations. They are recorded in the fifth column of Table 1, with the corresponding probable errors in the sixth column.

F. E. ROACH

STEWARD OBSERVATORY
UNIVERSITY OF ARIZONA
September 1941

[1] *Ap. J.*, **89**, 669, 1939.

[2] *Ap. J.*, **88**, 429, 1938.

[3] Cf. *Veröff. Berlin-Babelsberg*, **10**, Heft 3, 1933.

REVIEWS

Introduction to Physical Optics. By JOHN K. ROBERTSON. ("University Physical Series.") 3d ed. New York: Van Nostrand Co., Inc., 1941. Pp. 512+viii. $4.00.

In a subject as extensive as optics the modern textbook-writer is faced with the problem of not what to include in, but what to omit from, his pages. Professor Robertson has met this difficulty by including as many topics as possible and omitting extensive mathematical derivations. Debate over the propriety of this method can, of course, be endless, but there is no doubt that Professor Robertson has used descriptive methods very well. This third edition is strengthened by the inclusion of quite a lot of geometrical optics, including a brief discussion of the microscope. Other changes include several more pages dealing with the velocity of light, some amplification of the work on spectral series in chapter vii, discussions of spectra of heavy hydrogen and hyperfine structure in chapter xviii, and more about band spectra in chapter xix. In all, this edition runs to about ninety pages more than the 1930 edition. Many figures have been redrawn and improved, and the number of plates has been increased to seven.

This reviewer finds chapter vii, entitled "Some Facts concerning the Spectrum," to be rather a jarring interruption to the continuity of the book, coming, as it does, between a chapter on elementary dispersion and one on interference, and feels that what it contains might have been more appropriately associated with later chapters on spectroscopy. On the other hand, he is uneasily conscious that what seems out of place to a pedagogue might be a fine mental fillip for the beginning student. Perhaps Professor Robertson has chosen his order well. One is bound to recognize a certain value in a repetitive type of presentation in which first the elementary ideas are expounded, to be followed later by more rigorous and modern treatment.

An admirable feature of the book is the large number of problems at the end of each chapter, with answers at the end of the book. There is also a supplementary list of problems and their answers. The absence of nearly all mathematical treatment, especially in the classical optics, makes the text quite suitable for intermediate physics courses presented to students in arts or for nonscience students taking optics as a required course. On the other hand, for those students who expect to be candidates for a Bachelor's degree in the physical sciences it seems that there should be considerably more mathematical analysis.

GEORGE S. MONK

Ryerson Physical Laboratory
University of Chicago

Biography of the Earth: Its Past, Present and Future. By GEORGE GAMOW. New York: Viking Press, 1941. Pp. xiv+242; 27 plates; 58 figures. $3.00.

Professor Gamow has made a bold attempt to combine the results of astronomy, geology, and paleontology and to describe the evolutionary history of the earth from its origin (about two billion years ago) to the return and breaking-up of the moon (some fifteen billion years after the final cooling of the sun). The result is a remarkably brilliant synthesis in the form of a fascinating, popular book which is full of stimulating ideas. The author favors the tidal theory for the origin of the earth and stresses its similarity with the original planetesimal hypothesis. Incidentally, he incorrectly states that these two theories "were formulated almost simultaneously"—unless an interval of

time of about fifteen years can be considered as infinitesimal when compared with a time scale of some twenty-seven billion years![1] The origin of the moon is attributed to the breakup of the liquid earth, and the region of the Pacific Ocean is rather convincingly described as the "scar" which remained after the moon became detached from the earth. This and many other problems discussed by Dr. Gamow are still controversial in character, but there can be no doubt that he has, in every instance, given good reasons for preferring one theory to another. The more important scientific data are generally correct. But the astronomers will be disappointed in some of the details. Gamow still recognizes only nine satellites of Jupiter (p. 27), and he somehow concludes that the rotation of Pluto about its axis "is in a direction opposite to that of all the other planets" (p. 24). There are also several errors—some of them confusing—which must have crept in through carelessness in editing. For example, on page 225, the word "precision" must be "precession." But these minor blemishes do not seriously detract from the value of this most unusual and inspiring book.

O. S.

Geomagnetism. By SYDNEY CHAPMAN and JULIUS BARTELS. Oxford: Clarendon Press; New York: Oxford University Press, 114 Fifth Ave., 1940. 2 vols. Pp. xxxviii+1049. $18.

One of the most remarkable features of this really stupendous work—which the authors seem to take entirely as a matter of course—is the manner of its production. It represents a collaboration since 1929 between two men whose countries were continually at cross purposes during this time. The first author is professor of mathematics at the Imperial College of Science and Technology, London; the second is professor of geophysics at the University of Berlin. Thus at least one constructive effort has come out of Anglo-German relations during the last decade.

They have dealt with the rather heterogeneous subject matter of geomagnetism in three parts. Part I, which constitutes the first volume, describes the observed phenomena of geomagnetism. It opens with a discussion of the general principles of electromagnetism, the methods and instruments used in magnetic measurements, and the technique of magnetic prospecting. Next a chapter on motions of the moon and different forms of activity in the solar atmosphere prepares the reader for an account of certain effects they are believed to produce on the earth's magnetic field. These range from slight daily variations in field strength to the more spectacular reactions such as auroras, magnetic storms, radio fadeouts, and the tendency to twenty-seven-day recurrence in magnetic disturbances. The final chapter describes physical and electrical conditions in the upper atmosphere.

Part II is a detailed discussion of the analysis and synthesis of the data in Part I. Many of the usual statistical methods cannot be directly applied to magnetic data and for this reason the authors give in addition to the ordinary processes of harmonic analysis a description of methods that are particularly useful in the statistical study of geomagnetism. These methods are seldom included in textbooks on the subject and should make this section of especial value to students.

Part III is devoted to the theories that have been advanced to explain the phenomena described in Part I and analyzed in Part II. Few sciences can boast of such peculiarly tantalizing problems as those that confront the geophysicist. For example, on first approaching the subject of sunspot activity and magnetic storms one generally feels rather optimistic toward eventually discovering some facts regarding the exact nature of this apparently obvious relationship. But closer investigation only deepens the mystery as flagrant violations of one favored hypothesis after another arise. The cause of magnetic storms, together with the origin of the earth's magnetic field and its secular variation, have persistently defied every assault upon them since Gilbert first began their scientific study in 1600.

The authors remark in the Preface that Part III is the one with which they feel the least satisfied and which they hope will be the first to need revision. But whether the main advance will come from developments in atomic physics, solar physics, or radio physics, they are not prepared to say.

Undoubtedly one of the most important sections, which alone requires 188 pages, is the

[1] See F. R. Moulton, *Science*, **68**, 549, 1928.

elaborate Bibliography, indexes of authors and subjects, and ten tables. Perhaps "lavish" is the best word to describe this treasury of source material that has been provided for research workers. All references are given in great detail with occasional comments by the authors. They have also had the good taste (or the necessary funds) to use full names or obvious contractions instead of the highly abbreviated terms which often make such lists unintelligible to anyone except a librarian.

In addition to the excellent diagrams which occur on nearly every page there are thirty-eight plates of exceptional interest and clarity.

The reviewer is appalled at contemplation of the physical labor that must have been expended in accumulating and checking such a mass of technical matter. And it should be remembered that both men are not mere compilers of information for other people's convenience but foremost among the active leaders in this field.

Geomagnetism by Chapman and Bartels will without question be the standard authority of reference for many years to come.

R. S. RICHARDSON

Mount Wilson Observatory
Pasadena, California

Erdgeschichte und Kosmogonie. By KURT HIMPEL. ("Probleme der kosmischen Physik," ed. CHRISTIAN JENSEN, Band XIX.) Leipzig: Akademische Verlagsgesellschaft, 1940. Pp. 141. Rm. 9.60.

In a book with a title as the one under review one might have expected to find a presentation of those general facts which are relevant to a discussion of terrestrial history and stellar evolution. But the reader will look in vain for such an account; apparently that was not the intention of the author. Far more, the book represents an attempt at a new theory of cosmogony and the development of a wholly personal point of view. The reviewer is not competent to judge the geological and paleoclimatological parts of the book, but the astronomical sections are definitely misleading and are written in the language of an earlier decade.

Thus, an astronomer of the modern school will be surprised that the author regards "the conclusion that the sun was a giant star at the time of the formation of the earth and that since that time the sun has been reduced to its present size by the loss of mass" as well established. The author also believes that he has found in the periodic recurrence of the nova phenomenon the key to all facts of cosmogony and terrestrial history (including the ice ages). The nova phenomenon is also to provide the mechanism for the loss of mass of the sun already presupposed.

The reviewer may be allowed to state quite frankly that in his view the value of this new cosmogony is very doubtful.

S. C.

Atlas typischer Nebelkammerbilder mit Einführung in die Wilsonsche Methode. By W. GENTNER, H. MAIER-LEIBNITZ, and W. BOTHE. Berlin: Julius Springer, 1940. Pp. 125; figs. 92, 20×28 cm. Rm. 21.60.

The first forty pages of this book are devoted to a description of the history, development, and technique of the Wilson Cloud Chamber. The remaining eighty pages contain 131 photographs with detailed descriptions. These photographs illustrate remarkably well the application of the technique of the Wilson Chamber to a variety of physical problems: the study of X-rays, natural and artificial radioactivity, nuclear physics, and cosmic rays. Some of these pictures are published here for the first time and most of the others, although previously published, have been reproduced from the original photographs. It is probable that the illustrations in this atlas represent a selection from well over a million photographs.

The atlas represents a very valuable collection of the best pictures of many workers in this field in England, the United States, France, and Germany. To astronomers and astrophysicists (familiar with atlases of a different kind) the present atlas will provide examples of the art of modern physics.

S. C.

Between Physics and Philosophy. By PHILIPP FRANK. Cambridge: Harvard University Press, 1941. Pp. 238. $2.75.

This is the kind of a book many scientists have been waiting for. Here is a philosophical discussion of science, by a scientist, in the spirit of science. This is writing that does for today what the writings of Poincaré did for an earlier generation; the exposition has the same lucidity, penetration, and simplicity of which Poincaré was a master. It will appeal especially to those who are dissatisfied with the type of speculation Eddington so lavishly deals out and to those who wish to see concretely the impact of the new logic upon the critique of science without having to know the technicalities of this logic. The book is easy reading and yet masterful in the depth of its analysis. A rare combination, and a needed one.

Philipp Frank is a physicist, the successor of Einstein at Prague, and now a visiting lecturer at Harvard University. His standpoint is that of logical empiricism. Greatly influenced by Mach, he holds the position that all statements of science refer in the last analysis to what can be observed; greatly influenced by the views represented by Carnap, he believes that it is important to distinguish such statements from proposals to construct the language of science in a certain way. He thus uses the linguistic conscientiousness fostered by modern logicians to disentangle the factual aspect of science from considerations of the linguistic structure in terms of which statements of fact are made. With great nicety he distinguishes these two aspects in discussions of such topics as causality, length, and quantum mechanics.

In terms of this analysis Frank tries to show that when confusion is avoided, physics (and science in general) needs no supplementation by a superscientific metaphysics, and he gives no support to the spiritualistic or materialistic "world-views" which at each stage of science have turned to it for support. Science in the course of its own development develops its own "philosophy"; as science becomes self-critical, it is, in that sense and in no other, philosophical.

The volume is composed of ten articles, most of which appeared in German during the last ten years. An introduction gives the historical background of logical empiricism. The titles of the ten papers are as follows: "The Law of Causality and Experience," "The Importance of Ernst Mach's Philosophy of Science for Our Times," "Physical Theories of the Twentieth Century and School Philosophy," "Is There a Trend Today toward Idealism in Physics?" "The Positivistic and the Metaphysical Conception of Physics," "Logical Empiricism and the Philosophy of Soviet Russia," "Philosophical Misinterpretations of the Quantum Theory," "What 'Length' Means to the Physicist," "Determinism and Indeterminism in Modern Physics," "Ernst Mach and the Unity of Science."

The main inadequacies of the volume grow out of its article form. Nowhere does Frank really settle down to an analysis of such terms as "experience" or "observation"—terms basic to his account. And, although in places he makes amply clear that to talk about scientific statements as referring to "perceptions" is a characterization of the language of science and not of its subject matter, he often seems to confuse the two factors; surely, it is misleading to talk as if statements about the world before man referred to "complexes of perceptions." One has the feeling, with due respect to Mach and to Frank's interpretation of Mach, that Frank himself has not worked sufficiently clear of the difficulties and ambiguities of Mach's own sensationalistic or phenomenalistic terminology.

But this is a topic that would lead into the center of contemporary discussion. It is sufficient to say that the appearance of this volume should be welcomed by those who are interested in one of the most important contemporary movements in the analysis of science. This book will orient the reader in both the historical development and the analytic contributions of logical empiricism. The scientist will find no better guide.

CHARLES MORRIS

University of Chicago

Three Copernican Treatises: The "Commentariolus" of Copernicus; The "Letter against Werner"; The "Narratio prima" of Rheticus. Translated with Introduction and Notes by EDWARD ROSEN. New York: Columbia University Press, 1939. Pp. xi+211; 26 figs. Cloth, $3.00.

This valuable volume constitutes No. 30 of the "Records of Civilization," a collection of source books and studies edited under the auspices of the department of history, Columbia University. It is of interest to astronomers as well as to historians of science; the

three treatises, offered here for the first time in an English translation, with abundant commentaries and a fifty-page introduction, constitute a series of prolegomena to the magnum opus of Copernicus, the *De revolutionibus orbium coelestium* (Nuremberg, 1543). Few modern readers will have the courage to celebrate the quatercentenary of the publication of *De revolutionibus* by reading the work itself; they could, however, understand some of the aspects of the sixteenth-century revolution in the European Weltanschauung by working their way through these short treatises, guided by Rosen's Introduction and his six hundred footnotes. The reading of the *Three Copernican Treatises* is both educational and enjoyable.

The *Commentariolus* of Copernicus, a brief sketch representing a first stage in the development of the heliocentric theory of the canon of the Cathedral of Frauenburg, circulated in a number of handwritten copies among the contemporaries of Copernicus, was known to Tycho Brahe and then disappeared from the records of civilization for more than a quarter of a millennium. A manuscript of the *Commentariolus*, discovered in Vienna, was published by M. Curtze in 1878; a second manuscript was found in Stockholm and was published by A. Lindhagen in 1881. The first English translation, based on L. Prowe's critical edition of the text (1884), was prepared by E. Rosen and published, with annotations, in Vol. 3 of *Osiris* (1937); the book under review offers this translation, with certain revisions and with a considerably expanded commentary. One of the essential features of the heliocentric system of the *Commentariolus* consists in the use of two epicycles upon a deferent which is concentric with the great circle ("concentrobiepicyclic" arrangement), whereas in the *De revolutionibus* this device is replaced, for the three superior planets, by a single epicycle upon an eccentric deferent ("eccentrepicyclic" arrangement).

The *Letter against Werner*, dated June 3, 1524, and addressed by Copernicus to Bernard Wapowski, a canon at Cracow who had been his fellow-student at the University of Cracow, is a criticism of Johann Werner's *De motu octavae sphaerae tractatus primus* (Nuremberg, 1522). Handwritten copies of this Copernican *opus minor* circulated among his contemporaries; Tycho Brahe had a copy in his possession; the *Letter* was first published in Jan Baranowski's edition of *De revolutionibus* (Warsaw, 1854) from a manuscript preserved in Berlin; a second manuscript of the *Letter* was found in Vienna by M. Curtze, who collated both copies and published a critical text; Rosen's translation was made from Curtze's text.

The *Narratio prima*—in the form of a letter addressed by Georgius Joachim Rheticus to his former teacher, Johann Schöner—was first printed in Danzig, in 1540; a second edition, printed in Basel, in 1541, followed. Rheticus, the young Protestant professor of mathematics at Wittenberg who made a pilgrimage, in 1539, to Frauenburg and absorbed the new knowledge at its source, wrote the *Narratio prima* as a survey of the principal features of the new system. He intended, originally, to prepare a sequel, a "Narratio altera," but he had to change his plans: the favorable reception of the Danzig and Basel editions of the *Narratio prima* indicated that the time was ripe for the publication of the great work of Copernicus. In 1543 the world lost Copernicus and received his *De revolutionibus orbium coelestium*. The Basel (1566), Warsaw (1854), and Thorn (1873) editions of *De revolutionibus* contained reprints of the *Narratio prima* of Rheticus; it was also reprinted as a companion piece to the Tübingen (1596) and Frankfurt (1621) editions of Kepler's *Mysterium cosmographicum*. Rosen's translation is based on L. Prowe's edition (1884) of the text of the *Narratio prima*.

An elaborate Index increases the value of Rosen's edition of *Three Copernican Treatises*.

A. Pogo

INDEX TO VOLUME 94

INDEX TO SUBJECTS

INDEX OF AUTHORS